Dissertation zur Erlangung des Doktorgrades

der Fakultät für Chemie und Pharmazie

der Ludwig-Maximilians-Universität München

Design and characterization of photochromic ligands for voltage-gated ion channels

Timm Fehrentz

aus

Heidelberg

2012

This work is dedicated to my parents

Table of Contents

Abstract

Optical control of cellular function with high temporal and spatial precision has been a goal for many years. Neuroscience was especially lacking tools that would allow for detailed noninvasive studies of neuronal communications within networks. At the beginning of this century, the dawn of a field called optogenetics, including optochemical genetics, appeared.[1,2,3] Here genetics, optics and to a certain extent chemistry are combined to generate strategies for the reversible control of ion channels, receptors and neuronal activity with light. This methodology has been received with great attention and already helped to gain numerous insights into scientific and medical questions.[4,5,6,7]

One optogenetic approach takes advantage of the known pharmacology of neuronal transmembrane receptors and ion channels. Here the strategy targets specific receptors with photoswitches that contain an azobenzene, a pharmacophore and a variable group.[2,8] If freely diffusible, these photoswitches are called photochromic ligands (PCLs).[9,10,11,12] Photoswitches possess a *cis* and *trans* state, which can be converted into each other by different wavelengths of light. Both states of a PCL show different efficacies towards its receptor, which allows for a reversible light dependent activation or inactivation of the receptor.[2,8]

The doctoral thesis presented here, discusses a selection of PCLs for voltage-gated sodium (Na_v), calcium (Ca_v) and potassium (K_v) channels.

QAQ, a membrane impermeable photoswitch contains twice the core structure of QX-314, a permanently charged version of the local anesthetic lidocaine.[13] Electrophysiological characterization revealed that the photoswitch blocks the conductance of Na_v, Ca_v and K_v channels from the cytosolic site, in a light dependent manner.[13]
Furthermore, this doubly charged PCL allows for the reversible silencing of neuronal activity, once delivered into neurons. An alternative, noninvasive strategy to load cells with QAQ requires the expression of TRPV1 or $P2X_7$ ion channels. Both

channels enter a dilated pore state after prolonged agonist application, which allows bulky compounds to access the inner cell.[14,15,16,17] Thus, extended agonist and QAQ incubation of HEK293 cells, expressing TRPV1 or P2X$_7$ channels, offers the opportunity to load cells and photoregulate the conductance of voltage-gated ion channels.

Endogenous expression of TRPV1 is mainly limited to specific neurons called nociceptors, which are responsible for the detection of pain.[18] This anatomical condition allows for a selective, non-genetic strategy to load QAQ into nociceptors and to control their activity with light. Thus, QAQ acts as a photoswitchable local anesthetic.[13]

The presence of the TRPV1 dilated pore state under normal physiological conditions in tissues has not been confirmed. Whether pore dilation of TRPV1 takes place in relation to inflammation phenotypes, like in chronic pain, also remains elusive. Quantification of QAQ loading under different conditions into intact DRG could provide empirical information about these questions. Therefore a method was established to record photoswitching with a multi-electrode array of intact dorsal root ganglia, resulting in a proof of principle that the technology could be applied to answer the raised questions.[13]

To extend the applications of QAQ and related PCLs of voltage-gated potassium channels, investigations have been performed to red-shift the action spectrum. QAQ was derivatized, with e.g. dimethoxy-, dimethyl-, dimorpholino and other substituents in its 2,2′ and 6,6′ positions, *ortho* to the diazen unit. Out of six QAQ-derivatives, three allow for light control of Na$_v$ and K$_v$ channel conductance, once applied to the internal side of the channels. One active derivative, 2,2'-dimethoxy-QAQ, shows a red-shifted action spectrum. The *trans* and the *cis* state of the photoswitch can be converted into each other by using blue light or darkness, respectively. The *trans* state of all QAQ-derivatives blocks the channel conductance. Furthermore, neuronal activity of cortical pyramidal neurons can be reversibly silenced by internal 2,2'-dimethoxy-QAQ application.

Studies on PCLs for K$_v$ channels demonstrated how to red-shift the action spectra by substituting the 4 position of azobenzene photoswitches.[11] Diethyl or other

amino functions attached generate push-pull systems that shift the absorption maxima to approximately 470 nm light. Thus, blue light can be used to convert the photoswitch into its *cis* state. In the dark the PCL relaxes rapidly back into the *trans* state. One detailed investigated compound is DENAQ, which acts as *trans* blocker on specific K_v channel subtypes. Compared to QAQ, these PCLs are applied on the external side of cells and reliably allow for the reversible light control of K_v channel conductance.[11]

Another chapter of this thesis describes the efforts to generate photoswitchable L-type calcium channel agonists and antagonists. Based on the agonist FPL-64176 [19] and the 1,4-dihydropyridine antagonist Felodipin,[20] six derivatives were synthesized containing one azobenzene each. Compared to Felodipin, electrophysiological recordings of 1,4-dihydropyridine derivatives revealed no clear antagonistic effect on L-type calcium channels expressed in HEK293T cells. Furthermore, the latter compounds and the FPL-derivative did not allow for light control of L-type calcium channel conductance. The data presented here provide a fundament to launch further investigations to create PCLs for L-type calcium channels.

[1]   K. Deisseroth, *Nat. Methods* **2011**, *8*, 26-29.
[2]   T. Fehrentz, M. Schönberger, D. Trauner, *Angew. Chem. Int. Ed.* **2011**, *50*, 12156-12182.
[3]   F. Zhang, A. M. Aravanis, A. Adamantidis, L. de Lecea, K. Deisseroth, *Nat. Rev. Neurosci.* **2007**, *8*, 577-581.
[4]   C. Wyart, F. Del Bene, E. Warp, E. K. Scott, D. Trauner, H. Baier, E. Y. Isacoff, *Nature* **2009**, *461*, 407-410.
[5]   A. B. Arrenberg, D. Y. Stainier, H. Baier, J. Huisken, *Science* **2010**, *330*, 971-974.
[6]   V. Busskamp, J. Duebel, D. Balya, M. Fradot, T. J. Viney, S. Siegert, A. C. Groner, E. Cabuy, V. Forster, M. Seeliger, M. Biel, P. Humphries, M. Paques, S. Mohand-Said, D. Trono, K. Deisseroth, J. A. Sahel, S. Picaud, B. Roska, *Science* **2010**, *329*, 413-417.
[7]   V. Gradinaru, M. Mogri, K. R. Thompson, J. M. Henderson, K. Deisseroth, *Science* **2009**, *324*, 354-359.
[8]   R. H. Kramer, D. L. Fortin, D. Trauner, *Curr. Opin. Neurobiol.* **2009**, *19*, 544-552.
[9]   M. R. Banghart, A. Mourot, D. L. Fortin, J. Z. Yao, R. H. Kramer, D. Trauner, *Angew. Chem. Int. Ed.* **2009**, *48*, 9097-9101.
[10]   E. Bartels, N. H. Wassermann, B. F. Erlanger, *Proc. Natl. Acad. Sci. USA* **1971**, *68*, 1820-1823.

[11] A. Mourot, M. Kienzler, M. Banghart, T. Fehrentz, F. Huber, M. S., R. H. Kramer, D. Trauner, *ACS. Chem. Neurosci.* **2011**, *2*, 536-543.

[12] M. Volgraf, P. Gorostiza, S. Szobota, M. R. Helix, E. Y. Isacoff, D. Trauner, *J. Am. Chem. Soc.* **2007**, *129*, 260-261.

[13] A. Mourot, T. Fehrentz, Y. Le Feuvre, C. M. Smith, C. Herold, D. Dalkara, F. Nagy, D. Trauner, R. H. Kramer, *Nat. Methods* **2012**, *9*, 396-402.

[14] M. K. Chung, A. D. Guler, M. J. Caterina, *Nat. Neurosci.* **2008**, *11*, 555-564.

[15] C. Virginio, A. MacKenzie, F. A. Rassendren, R. A. North, A. Surprenant, *Nat. Neurosci.* **1999**, *2*, 315-321.

[16] B. S. Khakh, X. R. Bao, C. Labarca, H. A. Lester, *Nat. Neurosci.* **1999**, *2*, 322-330.

[17] A. Surprenant, F. Rassendren, E. Kawashima, R. A. North, G. Buell, *Science* **1996**, *272*, 735-738.

[18] A. I. Basbaum, D. M. Bautista, G. Scherrer, D. Julius, *Cell* **2009**, *139*, 267-284.

[19] S. I. McDonough, Y. Mori, B. P. Bean, *Biophy. J.* **2005**, *88*, 211-223.

[20] S. Yiu, E. E. Knaus, *J. Med. Chem.* **1996**, *39*, 4576-4582.

1) Review: Optochemical genetics

Optochemical genetics

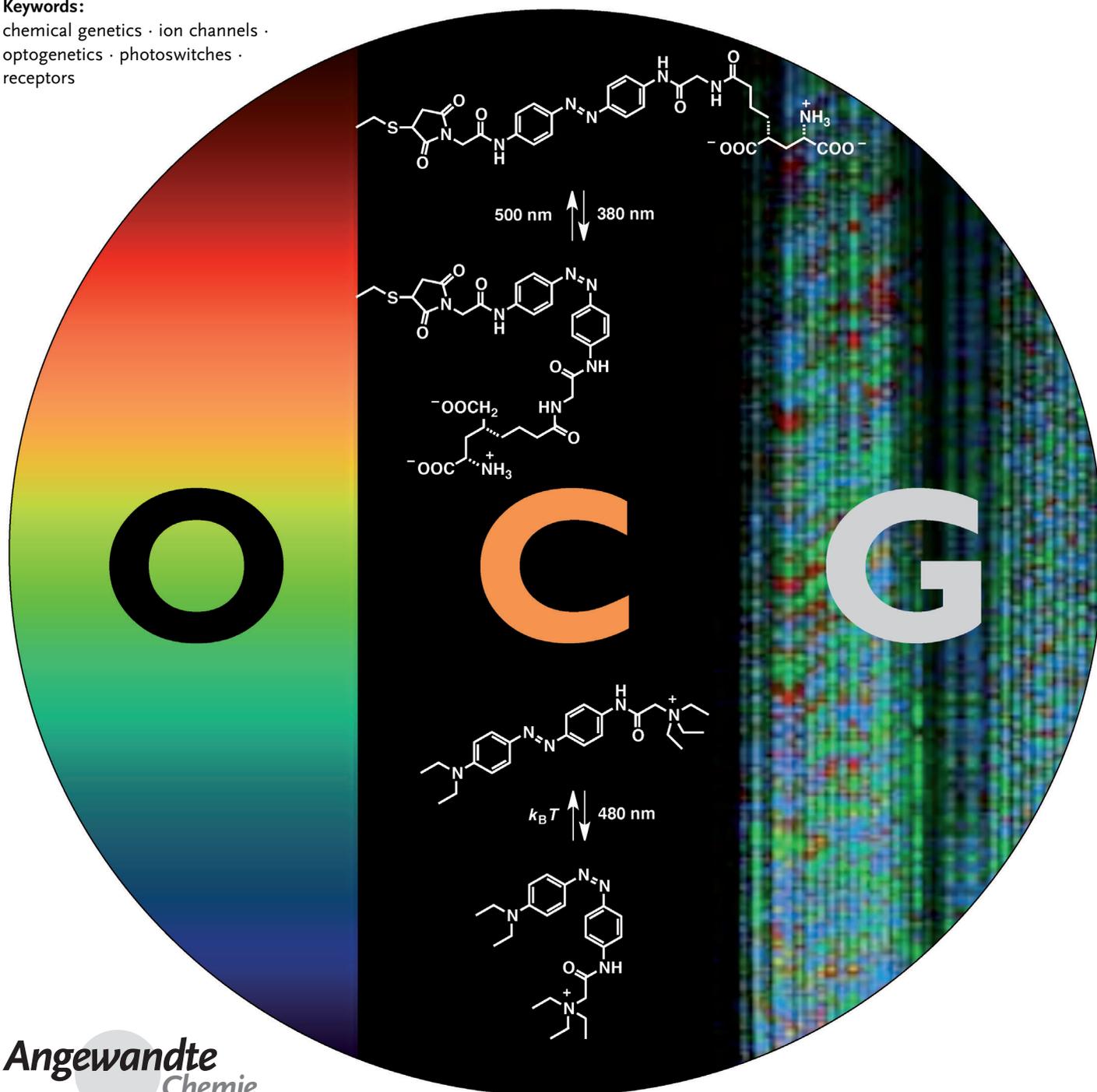**Timm Fehrentz**, Matthias Schönberger, Dirk Trauner

Optochemical Genetics

Timm Fehrentz, Matthias Schönberger, and Dirk Trauner*

Angewandte
Chemie

Transmembrane receptors allow a cell to communicate with its environment in response to a variety of input signals. These can be changes in the concentration of ligands (e.g. hormones or neurotransmitters), temperature, pressure (e.g. acoustic waves or touch), transmembrane potential, or light intensity. Many important receptors have now been characterized in atomic detail and our understanding of their functional properties has markedly increased in recent years. As a consequence, these sophisticated molecular machines can be reprogrammed to respond to unnatural input signals. In this Review, we show how voltage-gated and ligand-gated ion channels can be endowed with synthetic photoswitches, and how the resulting artificial photoreceptors can be used to optically control neurons with exceptional temporal and spatial precision. They work well in animals and might find applications in the restoration of vision and the optical control of other sensations. The combination of synthetic photoswitches and receptor proteins contributes to the field of optogenetics and adds a new functional dimension to chemical genetics. As such, we propose to call it "optochemical genetics".

> *"The trick then is not to use the clumsy and inefficient techniques of classical organic chemistry by themselves but to make use of Nature's tools."*
> Sir Francis Crick, 1999[1]

From the Contents

1. Introduction

Nature's molecular devices are unsurpassed in their beauty, efficiency, and ability to integrate into complex systems. This is not entirely surprising, given that they have evolved over billions of years. Organic chemistry, by contrast, is about two hundred years old. The synthesis of complex molecules is barely a third of that age, and far from being a mature and efficient technique. Nevertheless, synthetic chemistry has made remarkable progress over the last few decades and many molecules have been created that have no structural or functional counterpart in nature.

Still, what we can make today comes nowhere near to what nature can achieve. The drugs we synthesize are comparatively simple molecules and the switches, motors, and machines we forge are conceptually beautiful, but pale in comparison with nature's devices.[2] These have been studied in great detail by using various biophysical methods, and our understanding of how they work has dramatically increased in recent years. Some famous examples of molecular machines that have now been elucidated in atomic detail include ATP synthase,[3] the ribosome,[4] RNA polymerase,[5] various molecular motors,[6] and ion channels that control nervous activity.[7] Although they operate on a scale where the peculiarities of quantum mechanics apply, they can often be described in terms of relatively simple and intuitive mechanical models.

This much-improved understanding of nature's molecular machines opens the door for their functional manipulation using synthetic chemistry. Just as macroscopic engines can be taken apart, "souped up", and fitted with an ignition key, nanomachines can be manipulated and endowed with additional features and control elements. This can be done to a certain extent at a genetic level, that is, through classical protein engineering, but also by adding and attaching synthetic molecules. The trick is then not to use the traditional techniques of synthetic organic chemistry by themselves, but to make use of them in combination with nature's tools. This approach creates hybrid devices that can be controlled with unnatural input signals and can be easily integrated into highly complex biological systems. As such, they not only function in vitro or in single cells, but also in complex cellular networks—even in neural tissues and in living animals.

[*] T. Fehrentz, M. Schönberger, D. Trauner
Department of Chemistry, Ludwig-Maximilians-Universität and Center for Integrated Protein Science
81377 Munich (Germany)
E-mail: dirk.trauner@lmu.de

3

In this Review, we will show how the paradigm—that nature's molecular machines can be harnessed with synthetic chemistry—can be applied to a set of transmembrane proteins that play key roles in neurophysiology. To this end, we will first review some of the elementary machinery that is involved in sensory perception, synaptic transmission, and the generation of action potentials. We will then discuss in general terms how it can be reprogrammed to become sensitive to a very useful stimulus—light—and how the resulting artificial photoreceptors can be used to control and study neural networks. This is also the goal of "optogenetics", a new field of neuroscience that is currently undergoing rapid expansion.[8] We will show how the addition of a chemical component complements and extends optogenetics and how "optochemical genetics" contributes to the dissection and functional enhancement of nervous systems in new and exciting ways.[9]

2. Transmembrane Receptors and Their Role in Neurobiology

Transmembrane receptors underlie cellular communication, including the electrical and chemical communication within and in-between neurons. For the purposes of this Review, we define these receptors as transmembrane proteins that respond to changes in an input signal, be it light intensity, pressure, voltage, temperature, or the concentration of a small ligand. These include ion channels (ionotropic receptors), G-protein-coupled receptors (metabotropic receptors), and receptor-linked enzymes. For many years, these proteins were considered to be very difficult to study by structural methods, particularly by X-ray crystallography. This perception changed in 1998, when MacKinnon and co-workers disclosed the X-ray structure of KcsA, a potassium-selective ion channel sensitive to changes in pH value.[10] Since this groundbreaking study, representatives of several fundamental receptor classes have been characterized in atomic detail, including G-protein-coupled receptors (GPCRs),[11] ionotropic glutamate receptors (iGluRs),[12] trimeric ATP receptors (P2X),[13] voltage-gated ion channels,[14] and pentameric ligand-gated ion channels (pLGICs).[15] For convenience, these receptors are grouped in Figure 1 according to their symmetry. Note that these receptors can exist as homomultimers, but often assemble as heteromultimers composed of several similar, but not identical, subunits.

With the exception of rhodopsin,[11b] none of the receptors shown in Figure 1 are inherently light-sensitive. Three of them, GluA2,[12] P2X$_4$,[13] and the nicotinic acetylcholine receptor,[15a] are ligand-gated ion channels that respond to changes in the concentration of neurotransmitters or extracellular metabolites. Voltage-gated ion channels, such as
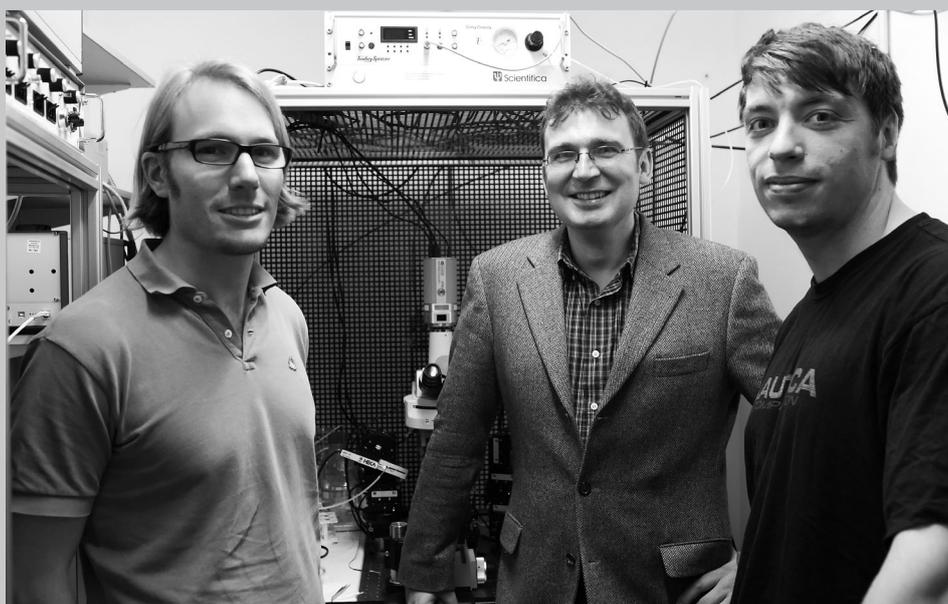
Dirk Trauner (middle) was born in Linz, Austria. After studying biology and then biochemistry at the University of Vienna, he joined the group of J. Mulzer at the Free University of Berlin to pursue natural product synthesis. In the late 1990s, he was a postdoctoral fellow with S. J. Danishefsky at the Memorial Sloan-Kettering Cancer Center in New York City. In 2000, he joined the University of California, Berkeley, where he rose through the ranks to become an Associate Professor of chemistry. In 2008, he moved to the University of Munich, where he is currently a Professor for Chemical Biology and Genetics.

Timm Fehrentz (left) studied chemistry in Konstanz, Uppsala, and Heidelberg and performed his Diploma research at the Max Planck Institute for Medical Research, Heidelberg, under the supervision of P. H. Seeburg and J. Spatz. In 2008, he joined the laboratory of D. Trauner at LMU Munich as a graduate student. Part of his graduate work has been carried out as a visiting researcher with R. H. Kramer at the University of California, Berkeley. His research focuses on new PCL strategies to target different voltage-gated ion channels.

Matthias Schönberger (right) studied biomedicinal chemistry at the University of Mainz and graduated in 2009. His Diploma research was carried out in the Brookhaven National Laboratory under the supervision of J. Fowler and J. Hooker and focused on positron emission tomography. Since 2010, he has been a graduate student with D. Trauner at the LMU Munich, working on optochemical genetics. He is a member of the International Max Planck Research School of Life Science and a recipient of a German National Foundation Graduate Fellowship.
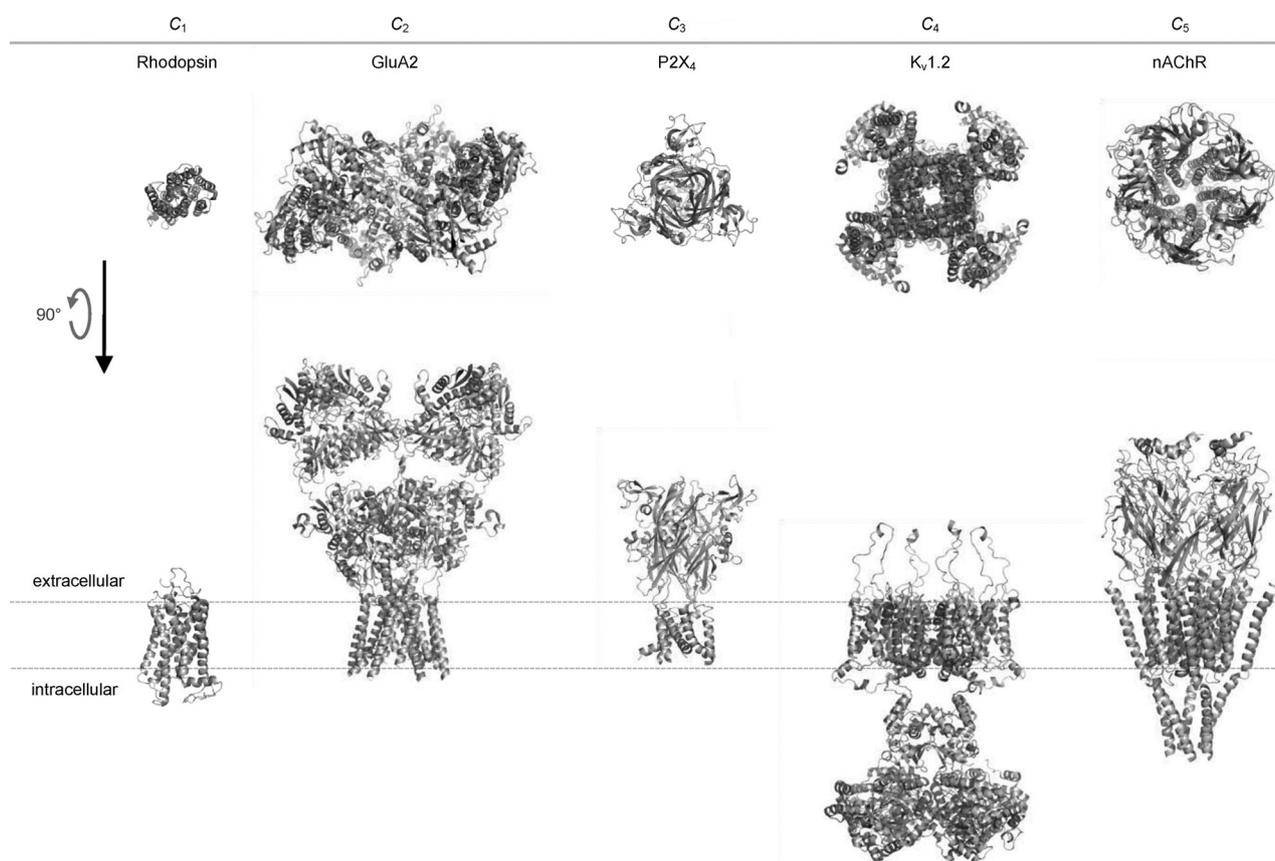
4

Figure 1. Selected transmembrane receptors of different symmetry characterized by X-ray crystallography and electron microscopy. Each receptor is shown in side and top views (from the extracellular side) and fitted to the same scale. Left to right: Rhodopsin, a G-protein-coupled receptor responsible for vision (pdb 1U19); GluA2, a glutamate-gated ion channel involved in excitatory neurotransmission (pdb 2KG2); P2X$_4$, an ATP-gated cation channel that mediates pain sensation (pdb 3H9V); K$_v$1.2, a voltage-gated potassium channel involved in controlling cellular excitability (pdb 2A79); nAChR, a nicotinic acetylcholine receptor that mediates the communication between nerves and muscles (pdb 2BG9). The dotted lines in this and other figures describe the boundaries between the cell interior, the membrane, and the space outside the cell.

K$_v$1.2,[16] are opened and closed by changes in transmembrane potential. However, they can also be influenced by ligands, such as channel blockers. As a consequence, all of the receptors shown in Figure 1 can be regulated in one form or another by a small molecule. Provided this small molecule can be persuaded to change its activity in response to light, the whole receptor–ligand assembly could be transformed into a photoreceptor.

Before we address this topic, however, it may be worthwhile to briefly review how some of these receptors are involved in neurotransmission and the all-important generation of action potentials (APs).[17] These can be studied by electrophysiology, a very powerful technique that allows for microsecond to millisecond resolution. The generalized shape of an AP and a schematic view of a typical neuron are shown in Figure 2. Ligand-gated cationic ion channels, such as ionotropic glutamate receptors (in the human central nervous system) or nicotinic acetylcholine receptors (mostly in the periphery) are responsible for the initial depolarization of the postsynaptic membrane. Binding of the neurotransmitter to its respective channel leads to pore opening, thereby allowing sodium and potassium ions to pass. Given the resting potential of the neuron and the tightly controlled relative concentrations of sodium and potassium on either side of the membrane, this will lead to a net influx of positive charge, which changes the membrane potential (Figure 2). Once a certain value has been reached (typically around -40 mV), voltage-gated sodium channels begin to open. As sodium rushes in, the membrane is further depolarized and the transmembrane potential inverts its sign (up to $+50$ mV). The neuron is quickly repolarized, however, as the voltage-gated sodium channels deactivate, and voltage-sensitive potassium channels begin to open after a brief delay. Once those are deactivated, the cell regains its resting potentials through the action of transporters and pumps, such as Na/K-ATPase.

Ion channels can have both excitatory and inhibitory effects on neurons, depending on whether they make the transmembrane potential less or more negative when opened. This is not only dependent on the charge of the ions they conduct but also on the relative concentration of ions on either side of the membrane. Consequently, at physiological conditions, nonselective cation channels and sodium channels will depolarize, whereas potassium channels hyper- or repolarize cells when opened. Chloride channels, such as GABA$_A$ or glycine receptors are generally inhibitory on AP firing.[17a]
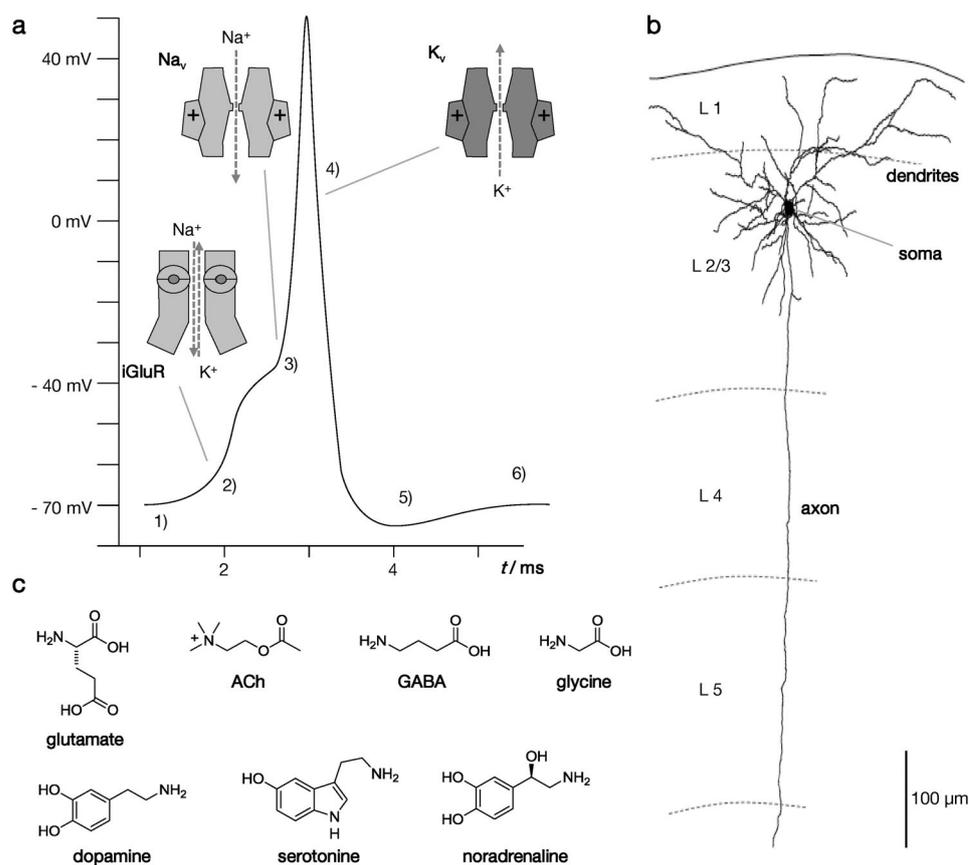
Figure 2. An overview of neurotransmission. a) The action potential: 1) the transmembrane potential of a neuron at rest; 2) a neurotransmitter binds to a ligand-gated ion channel, for example, a glutamate receptor (iGluR), and evokes an excitatory postsynaptic potential; 3) voltage-gated sodium channels (Na$_v$) respond and further depolarize the membrane, but quickly deactivate; 4) voltage-gated potassium channels (K$_v$) follow suit and repolarize the membrane, even beyond its resting potential (5); 6) the undershoot is removed through the concerted action of channels that are open at the resting potential and by ATP-driven ion pumps. b) A representative neuron from the visual cortex. The dendrites, the soma, and the axon are clearly visible. The soma resides in layer 2/3 (L2/3) and is much less extended than the axon, which spans several layers of the cortex. c) The most important neurotransmitters and neuromodulators.

be modulated in its intensity within femtoseconds, can be focused onto very small areas (on the order of its wavelength), and can carry enough energy to trigger larger molecular motions (such as isomerizations). As such, it is unsurpassed in its temporal and spatial precision, as well as in its ability to remote-control molecular devices and systems, including neural systems.

Light has been used for eons to glean information from the environment. Visual systems have emerged at almost all levels in evolution and have been greatly enhanced by human technology, such as microscopy. This is still a highly active area of research, with new imaging technologies continuing to be developed. Recent examples include superresolution microscopy[21] and two-photon imaging.[22] As a consequence of these technical advances, neurons can now be described in incredible detail, action potentials can be visualized with fluorescent calcium sensors, and the activity of many neurons in a network can be monitored simultaneously in live animals.[23]

Light, however, can also be used to put information into systems—provided suitable photoreceptors are present. As in imaging, this can be done with exquisite temporal and spatial precision, and the optical setups needed are largely the same. If the light intensities are not too high and the wavelengths are not too short, it can be done with little damage to the tissues, especially when compared with the invasiveness of multiple electrodes. The usefulness of light as an input signal for neuroscience was realized by none other than Sir Francis Crick, who stated in 1999: "*The ideal signal [to study and control a brain] would be light, probably at an infrared wavelength to allow the light to penetrate far enough. This seems rather far-fetched but it is conceivable that molecular biologists could engineer a particular cell type to be sensitive to light in this way.*"[1]

It did not take long for molecular biologists to take up this challenge, which gave rise to a new field called "optogenetics" (Figure 3).[8a,b] In essence, optogenetics is an effort to control neurons, or other cells of interest, with genetically targeted photoreceptors. As a result of this genetic component, the sensitivity to a stimulus and not the stimulus itself can be precisely located. Therefore, the light beam itself does not need to be spatially controlled with very high resolution, and light scattering is less of an issue than it is in imaging.

The targeting of innately "blind" neurons with genetically encoded photoreceptors has been achieved in several ways. Historically, the first system used was "ChARGe", which

In addition to these primary ion channels, there are receptors that perform a more modulatory role and influence the shape, duration, and frequency of the action potentials. These receptors can also be ion channels (such as KCNQ channels)[18] or, more often, G-protein-coupled receptors (GPCRs).[17a,19] In comparison to ion channels, GPCRs are "slow acting", since their effect is mediated by heterotrimeric G proteins, enzymes, second messengers, and transcription factors. Notably, the same neurotransmitter, for example, glutamate, acetylcholine, or GABA, can act on both the ionotropic receptors and the metabotropic receptors. Even neuromodulators that primarily target metabotropic receptors, such as serotonin, have an occasional ion channel target.[20]

3. Lighting up the Brain

Amongst different input signals that can actuate a receptor, light stands out for a variety of reasons: light can
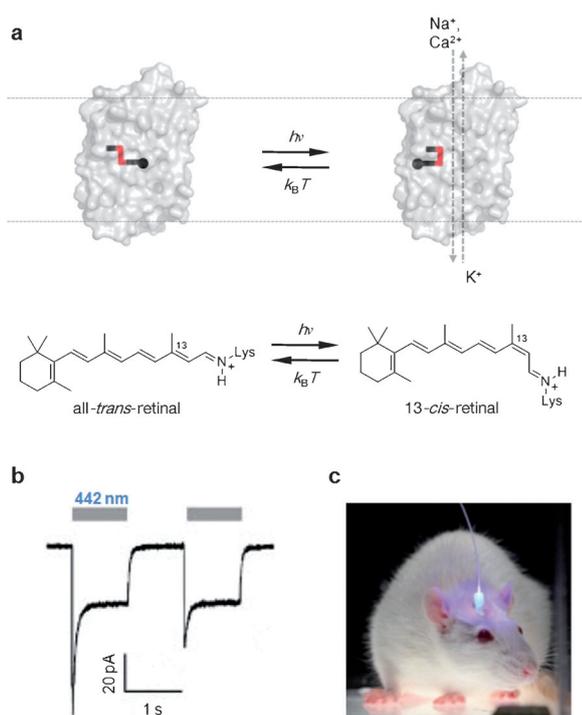
Figure 3. Optogenetics. a) Schematic representation of ChR2, a light-gated ion channel. The chromophore 13-*trans*-retinal (shown here conjugated as a Schiff base) undergoes isomerization with blue light and thermal relaxation, thereby gating the channel. b) Shining blue light on ChR2 triggers depolarization. c) Control of mouse behavior with blue light. Note the glass fiber cable that delivers light deep into the brain.[8b]

essentially consists of the primary components of the *Drosophila* visual cascade (rhodopsin, the associated heterotrimeric G protein, and arrestin).[24] This multicomponent system was shown to trigger APs when heterologously expressed in dissociated hippocampal neurons. This was quickly followed by early optochemical systems, which will be discussed in much more detail below. In 2004, a natural photoreceptor called channelrhodopsin-2 (ChR2) was introduced, which has since established itself as the most practical and popular tool.[25] ChR2 is an excitatory cation channel isolated from the alga *Chlamydomonas reinhardtii*.[25a] It can be activated with blue light and is rapidly deactivated once the light is gone, which allows for the control of AP firing with high precision.[25b] Similar to the rhodopsins, it uses retinal as a photoswitch, but unlike the mammalian visual pigments, the retinal is not excised after photoswitching. Therefore, ChR2 can be repeatedly used to trigger action potentials. As an added advantage, retinal is endogenously produced in many tissues and does not need to be added externally.[26]

Shortly after the excitatory photoreceptor channel ChR2 was identified, an inhibitory counterpart, namely a light-driven chloride pump called *Natromonas pharaonis* halorhodopsin (NpHR) was introduced.[27] NpHR can be activated with bright yellow light and is capable of silencing neurons, also with millisecond resolution. Importantly, as a consequence of little spectral overlap, ChR2 and NpHR can be

expressed and used in the same neuron simultaneously.[8b,27] Variants of ChR2 and NpHR with modified spectral and kinetic features continue to be developed,[28] and other systems, such as light-driven proton pumps, have recently been discovered that can control neuronal activity with light.[29]

Since its inception at the beginning of the new millennium, optogenetics has found many applications in dissecting neuronal circuitries and has helped to answer fundamental questions in neuroscience. As a testament to its enthusiastic reception by the scientific community, it was deemed "Method of the Year" in 2010.[8a,c] In addition to its important role in basic neuroscience, optogenetics has, within the last few years, also found its first applications in clinical research. For example, ChR2 and NpHR have been used to investigate the mechanism of deep-brain stimulation, which ameliorates the symptoms of Parkinson disease.[30] A second study was aimed at Retinitis pigmentosa, a condition which involves the loss of photoreceptor cells. Here, the light sensitivity of the retina could be restored by expressing NpHR, which resulted in visually guided behavior in previously blind mice.[31] In another application of ChR2 and NpHR, cardiac pacemaker cells of zebrafish could be optically stimulated or inhibited, thus enabling the control of heart beat patterns.[32]

4. Optochemical Genetics

Given that the molecular tools used in optogenetics are mostly derived from bacteria and protozoa, they work amazingly well in the neurons of worms, flies, and furry animals. These neurons, however, express numerous receptors on their own that are easily accessible on their extracellular side but are not inherently photosensitive. The challenge then is to persuade endogenous receptors to become sensitive toward light.

Three general strategies have emerged to do just that by using small synthetic molecules (Figure 4). The simplest and oldest approach employs caged ligands (CLs).[33] Here, a ligand is endowed with a protecting group that renders it pharmacologically ineffective. This protecting group is rarely a true molecular cage (in the sense a chemist would use this term), but typically a photolabile moiety that masks a functional group crucial to the ligand–receptor interaction. Photochemical cleavage of the protecting group then sets the active ligand free and triggers the desired biological effect.

Caged ligands have indeed been applied to great effect in neuroscience. Caged glutamate, for example, has been very useful for unraveling neural systems, and two-photon cages have enabled the stimulation of single synapses through the spatial precision that can be achieved with two-photon techniques.[34] The photosensitization of P2X$_2$ receptors and TRPV1 channels with caged ATP and capsaicin, respectively, was the first approach shown to work in living animals (in this case decapitated fruit flies, to ensure that the visual system was inactivated).[35]

There are, however, certain functional disadvantages associated with caged ligands. Uncaging is an irreversible process and it is difficult, if not impossible, to "stuff the beast
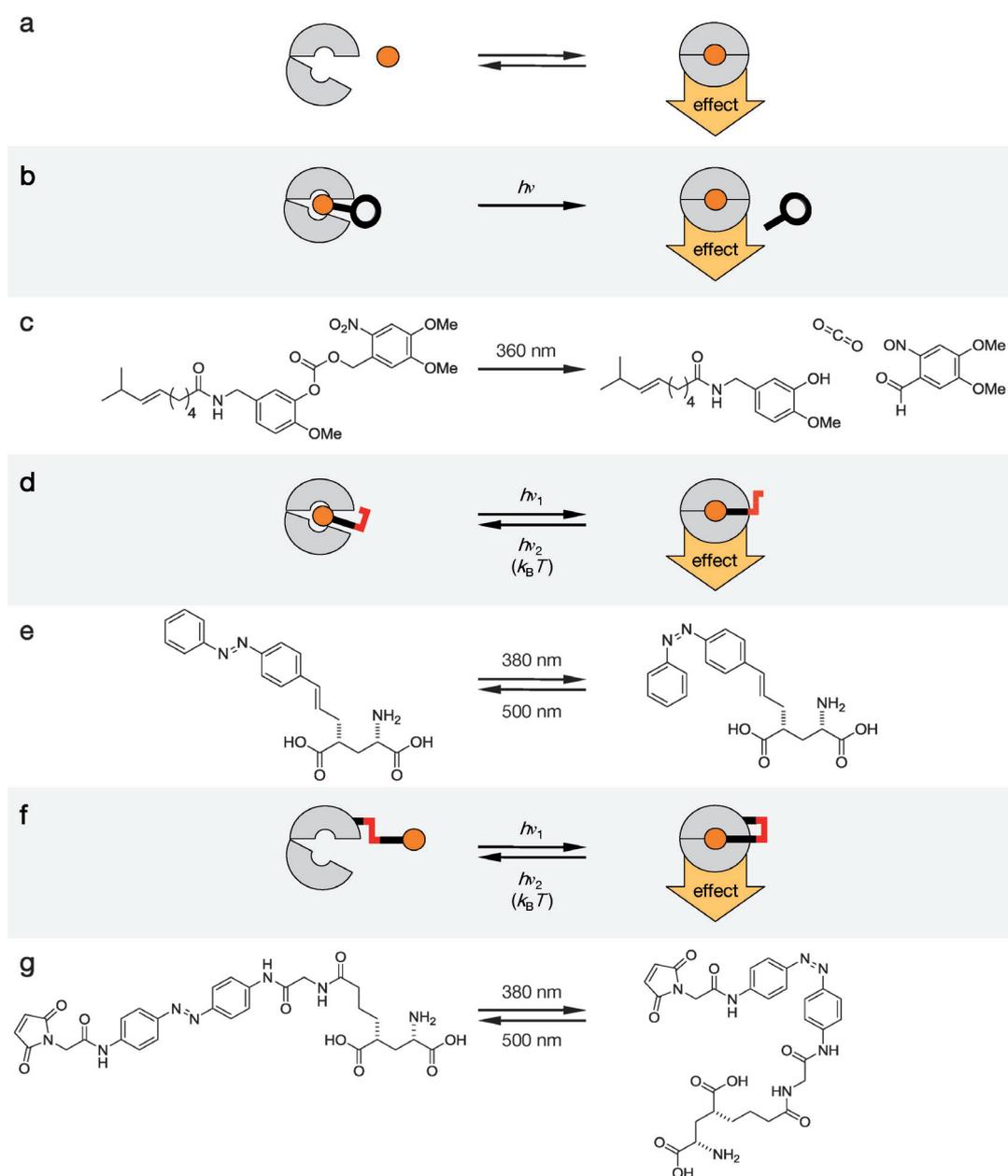
Figure 4. Three strategies used in optochemical genetics. a) A ligand binds to a generic receptor (not necessarily the clamshell-like receptor domain shown here), triggering a biological response. b) A caged ligand (CL) is broken apart with light, thus releasing its active form. c) Caged capsaicin, used to stimulate TRPV1 channels. d) A photochromic ligand (PCL) reversibly acts on a receptor. e) 4-GluAzo, a PCL that functions as "reversibly caged glutamate". f) A covalently attached photoswitchable tethered ligand (PTL) can optically regulate a receptor. g) MAG-1, a typical PTL in its unconjugated form.

back into the cage". Unless one is interested in tonic effects, such as a sustained receptor activation or inhibition, one can only hope that the ligand leaves the active zone as quickly as possible or is cleared by either a reuptake pump or a deactivating enzyme. The former exists for glutamate itself but not for more-selective synthetic agonists and antagonists. In addition, uncaging produces by-products, that is, the remnants of the protecting group, which can be toxic. The background release of the neurotransmitter, for example, through thermal hydrolysis, can also be a problem, as can be

the fact that some caged compounds have off-target effects, for example as antagonists to other receptors.

Some of these shortcomings can be overcome with a second approach called the photochromic ligand (PCL) approach. Here, the ligand carries a photoswitchable side chain that can be switched between two configurations. As the photoswitch toggles between these states, the efficacy of the ligand changes, thereby triggering the desired biological effect in a reversible fashion. The ligand can change its efficacy upon photoswitching and could even be an agonist in one form and an antagonist in the other.

8

PCLs have all the advantages of small-molecule drugs, including their ease of application and fast distribution in tissues. As with drugs, selectivity between receptor subtypes can be a challenge, but this can often be overcome through systematic variation of the molecule. In addition, one could be concerned that their photoisomers show relatively small differences in efficacy. However, in our experience PCLs work remarkably well in complex systems that have nonlinear responses, particularly in neural networks. Here, it is often the case that small changes in the activity of a modulator have dramatic effects on the output. Since the AP is an "all or nothing" response that is triggered only when a certain threshold is reached after a complex cellular integration, compounds that subtly influence this integration can have pronounced effects.

Of course, there are situations where receptor-subtype selectivity and cellular targeting is highly desirable. In this case, a third approach, which we call the photoswitched tethered ligand approach (PTL approach), can be employed. Here, the ligand is covalently attached to its receptor through a tether that contains a photoswitch. As the photoswitch toggles between long and short forms, the local concentration and/or efficacy of the ligand changes, thereby triggering a biological response in a reversible fashion. Importantly, PTLs can be genetically encoded, since the point of attachment is an engineered cysteine residue or any other encodable chemical motif that allows for specific bioconjugation. Since the PTL is covalently tethered, its local concentration at the site of attachment is very high in the active form of the photoswitch, which means that the affinity of the ligand is not a major concern. In fact, low-affinity ligands are usually preferred to ensure that photoswitching removes the ligand from the binding site.

The PTL approach is essentially a variant of optogenetics, since it combines a genetically encodable receptor with light to precisely control neural activity. In contrast to "classical" optogenetics, a synthetic component, that is, a reactive chemical, is needed, which is not endogenously produced, but needs to be synthesized and supplied by a chemist. The PCL and the CL strategies, on the other hand, are more akin to "chemical genetics".[36] Chemical genetics aims to address every protein target with a selective small-molecule ligand. Although such pharmacological control has a rapid onset, it is still not fast enough for many applications in neuroscience, where millisecond precision is required. This limitation can be overcome by optically controlling the small molecules that function as ligands.

Taken together, the CL, PCL, and PTL approaches provide the basis for what we call "optochemical genetics". It is an effort to control neural activity (or any network activity) with light and light-responsive synthetic molecules, with or without a genetically determined component. It shares with chemical genetics a certain desire to overcome the limitations of conventional genetic manipulation, but it also acknowledges that the targeted expression of proteins can be very powerful.

Which variant is used depends on the exact application. For therapeutic applications, where a certain lack of selectivity can be tolerated or is even desirable,[37] the PCL approach

may be more suitable. On the other hand, in the analysis of functional pathways, for example, in neural circuitry mapping, the genetically targeted transfection of a specific cell is clearly advantageous. In addition, PTLs could be extremely useful in the functional dissection of closely related receptor subtypes, since selectivity can be achieved through covalent attachment to genetically engineered isoforms (Figure 5). Following
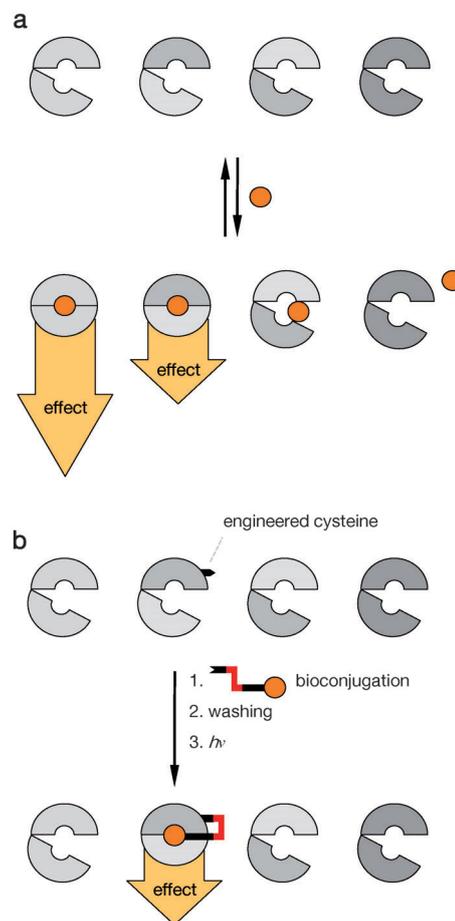

Figure 5. The PTL approach to selective pharmacology. a) Chemical genetics and pharmacology generally aim at individually targeting receptors and receptor isoforms. This requires ligands that bind with high affinity and selectivity. b) In optochemical genetics, selectivity can be achieved through genetic engineering of a bioconjugation site. In addition, the photoactivatable ligand can have low affinity to the receptor subtype.

conjugation, tonic activation or inhibition of the receptor can be prevented through action of the photoswitch. Overall, this PTL approach to selective pharmacology bears a certain resemblance to the "bump-hole" technique, which has been used so successfully in dissecting the human kinome, that is, the total of all human kinases.[38] In both cases, engineered proteins and unnatural ligands are needed. The PTL approach, however, not only provides a precise answer to the question "who", but also to "when" and "where".

Caged ligands have been mostly developed by other research groups and have been extensively reviewed elsewhere,[33] which is why our discussion here will focus on

9

synthetic photoswitches, that is, on PTLs and PCLs. Of the different photoswitch architectures investigated, azobenzenes have so far proven to be the most versatile and reliable ones.[39] This is due to several distinguishing functional features (Figure 6). For example, their geometries in their
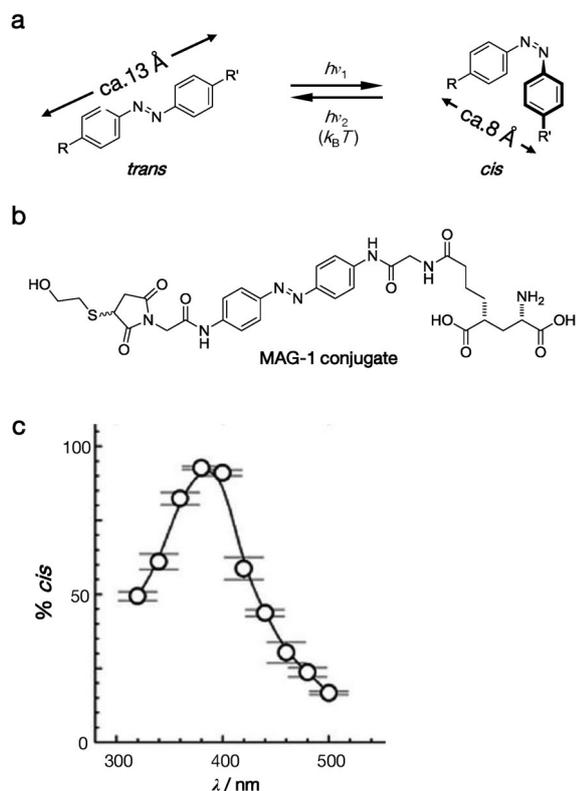

Figure 6. The logic of azobenzene photoswitches. a) Azobenzenes change their configuration and length upon irradiation with light of different wavelengths. They revert thermally or photochemically to their thermodynamically more stable state, which is usually the *trans* state. b) The mercaptoethanol conjugate of MAG-1, a model for the tethered PTL. c) The photostationary *cis/trans* ratio of the MAG-1 conjugate as a function of wavelength.

cis and *trans* states are well defined and the conformational space that can be mapped by both isomers has relatively little overlap. Substituents in the 4- and 4′-positions are substantially closer in their *cis* form than in their *trans* form, an effect that can be amplified further by appropriate substitution. Although azobenzenes are helically chiral in their *cis* form, which is not planar, they are typically not optically active because of facile racemization, and they do not generate stereocenters upon switching between a long and short form.

Azobenzenes often display high extinction coefficients and quantum yields, which mean that light of relatively low intensity can be used for photoisomerization. In addition, azobenzenes undergo photoswitching at very fast rates, which prevents intersystem crossing and the formation of triplet diradicals. These would react with triplet oxygen to generate singlet oxygen, a highly reactive and cytotoxic species, which is also damaging to the chromophore itself. Consequently, azobenzenes are relatively photostable and can be switched over many cycles. Their spectral tuning through substitution is straightforward and follows well-established rules. While

most azobenzenes used to date are isomerized to their *cis* form with UV-A or deeply violet light (315–380 nm), red-shifted versions that are less harmful upon prolonged application to tissue are also known (see Section 6). Finally, azobenzenes are relatively easy to synthesize and modify, as several synthetic strategies are available, including diazonium coupling, Mills reactions, and transition-metal-catalyzed cross-coupling strategies.[40] One potential disadvantage is their comparatively low solubility, but this can usually be overcome with appropriate functional groups, in particular with charged substituents.

Notably, azobenzene photoswitches are marked by photostationary states that are a function of the wavelength. While they can exist 100% in the thermodynamically more stable *trans* form (also the dark-adapted form) and their photostationary *cis/trans* ratios can exceed 9:1 at short wavelengths (Figure 6),[41] it is practically impossible to push them fully into the *cis* state through irradiation. Therefore, the background activity of the remaining *trans* isomer is a concern, but for the reasons stated above this is often not a problem in neural networks. In fact, the dependence of the photostationary ratio on the wavelength also offers an opportunity to tune the response by gradually tuning the color. The thermal bistability of photoswitches can be further influenced through appropriate substitution. PTLs wherein one end of the *cis*-azobenzene interacts with the protein covalently and the other noncovalently show slow thermal relaxation, at least on a neurobiological time scale. On the other hand, certain red-shifted azobenzene PCLs can revert to their dark-adapted state within milliseconds.[42]

Once a photoswitch has been chosen, the design of PTLs and PCLs is straightforward, provided both the structural coordinates for the receptor and extensive structure–activity relationship data for the ligands are available. The latter is often the case, since neuropharmacology is a well-developed field. Today, one cannot complain about a lack of the former either, since relevant structures appear in the literature almost every week.

The design of PCLs and PTLs is closely intertwined. It typically starts out with a structure of a ligand, gleaned from the crystal structure or from the pharmacology literature. From this, it is often immediately clear where and how to attach the photoswitch to the ligand and which stereochemistry to choose at the point of attachment. In an intermediate stage, a so-called "tether model" is sometimes synthesized, which retains one phenyl ring of an azobenzene. This is then extended to a full-blown PCL that contains the entire chromophore and, finally, after addition of an electrophilic functional group, to the corresponding PTL. In general, extensive structure–activity data are sufficient to design a PCL with a reasonable chance of success, whereas X-ray structures are normally needed for a PTL. The latter requires cysteine sites for covalent attachment, and choosing those can be difficult without structural coordinates. Increasingly, sophisticated computational tools are used for that purpose.

Since most PTLs that have been used to date are cysteine-reactive compounds, unspecific labeling of the cell-surface might be a concern. However, one has to bear in mind that reduced, accessible cysteine residues are rare on the surface

of cells and the bioconjugation typically proceeds through affinity labeling. This means that the noncovalent interaction of the PTL with its ligand-binding site precedes formation of the covalent bond, thereby enhancing the rate and selectivity of the labeling, which will also depend on the state of the photoswitch. In addition, cells seem to be remarkably tolerant toward molecules attached to their surface, as long as they do not interfere with vital cell–cell interactions.[43]

The design of suitable PTLs and PCLs also goes hand in hand with their syntheses. These can present considerable challenges since the chemistry of photoswitches needs to interface with the chemistry of polar and charged ligands, which requires intricate protecting-group operations. In the case of PTLs, this is acerbated by the presence of an electrophile, which should be introduced into the molecule as late as possible. The syntheses have to be practical and efficient enough to support a sustained biology program that includes in vivo investigations and, eventually, behavioral studies in animals.

In the following sections we will show how optochemical genetics can be applied to some of the most basic molecular machines involved in synaptic transmission: voltage-gated potassium channels and ionotropic glutamate receptors. To this end, we will first discuss their innate functions and systemic roles in some detail and then show how they can be converted into hybrid photoreceptors through covalent or noncovalent attachment of azobenzene photoswitches. Afterwards, we will address other targets, such as the nicotinic acetylcholine receptor (nAChR) or the P2X$_4$ receptor, where this has been previously studied to a limited extent. Finally, we will address a few receptors that have not yet been converted into photoreceptors, but which are "sitting ducks" for the optochemical approach.

5. Voltage-Gated Potassium Channels

Together with voltage-gated sodium channels (Na$_v$), voltage-gated potassium channels (K$_v$) modulate cellular excitability and play a key role in the generation of action potentials.[17c] K$_v$ channels are transmembrane proteins that assemble as tetramers from four single polypeptide chains that are

known as α subunits.[4] In humans, 40 genes encode 12 α-subunit families (K$_v$1–K$_v$12).[44] Within each subfamily, different genes exist, as indicated by an additional number, for example, K$_v$1.2. This diversity is further increased by heterotetrameric assembly of the α subunits, which results in a very large number of potential combinations. K$_v$1 channels additionally interact with intracellular tetrameric β subunits that alter the gating behavior.[45]

To date, several potassium channels have been elucidated in atomic detail by X-ray crystallography. The first structure to be reported was that of KcsA, a simple bacterial channel from *Streptomyces lividans*. Its disclosure in 1998 stands as a milestone in biophysics.[10] Subsequently, the structures of a calcium-gated potassium channel (MthK),[46] several inward-rectifier potassium channels (e.g. K$_{ir}$3.1),[47] a sodium- and potassium-conducting channel (NaK),[48] and several prokaryotic and eukaryotic voltage-gated potassium channels have been reported.[14b, 16] The structure of K$_v$1.2, a mammalian voltage-gated ion channel that modulates the electric excitability of neurons, in its open form is shown in Figure 7.[14b] In this representative structure, the voltage sensors, the pore, and both the inner cavity and outer vestibule of the channel are clearly visible (the β subunit is removed here, but present in Figure 1). Each single subunit contains an intracellular
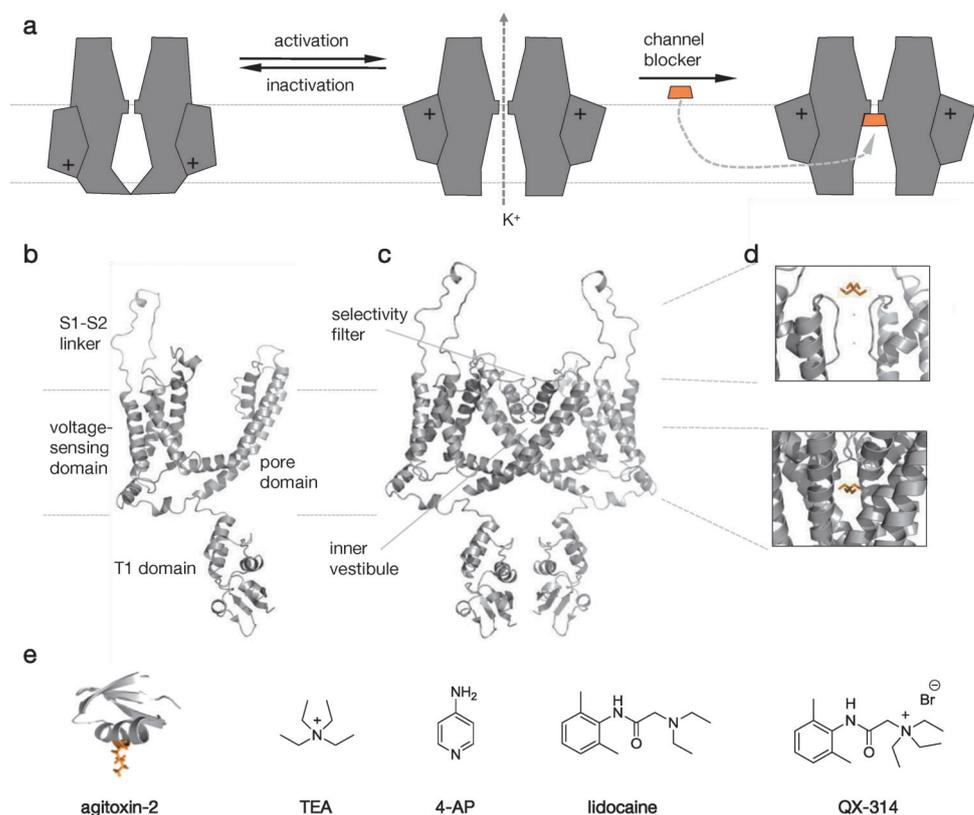

Figure 7. Structure and function of voltage-gated potassium channels. a) A highly schematic representation of K$_v$ channels illustrating their functional cycle and channel blocking. b) A single K$_v$1.2 subunit showing the extracellular S1-S2 linker, the voltage-sensing domain, the pore domain embedded in the membrane, and the intracellular T1 domain (pdb 3LUT). The β subunit has been removed and the ball peptide is not resolved in this structure. c) Two of the four subunits, indicating the architecture of the selectivity filter and the inner vestibule. d) Expanded view of the TEA binding sites in the inner and outer vestibules (pdb 2BOB and 2BOC). e) Chemical structures of extracellular and intracellular potassium channel blockers.

tetramerization domain, a voltage sensor domain (with helices S1–S4), and a pore domain (containing helix S5, a short pore helix, a pore loop, and the C-terminal helix S6).[44] Both the N and the C termini are located in the cytosol, but the N-terminal domain is not resolved in the structure.

Like most ion channels, K_v channels have three elementary functions that are physically represented by their protein domains and their movements: 1) an "activation gate" that interacts with the input signal (i.e. voltage) and opens the channel, 2) a "selectivity filter", which determines which ions can pass through the channel, and 3) an "inactivation gate", which is responsible for their desensitization. Activation is initiated by the voltage sensor once the membrane potential reaches −40 mV. The S4 helix of the voltage sensor domain in each subunit contains several positively charged residues, usually arginines, that move across the membrane as the cell depolarizes. This movement is mechanically coupled with a hinged motion of the inner helix bundle (S6) of the pore domain, which opens a gate through which the ions can pass.[7,44,45] Driven by the electrochemical gradient, the ions then permeate the selectivity filter, thereby generating a current that is specific for K_v channels. The selectivity filter is essentially a stack of backbone carbonyl groups that compensate for the hydration sphere of the cation as it passes through. This compensation is energetically more favorable for potassium ions than sodium ions.[7]

There are two native mechanisms of inactivation of K_v channels: N-type and C-type inactivation. N-type inactivation is mediated by the positively charged intracellular N terminus, which functions like a "ball" (or plug) on a chain. Once the voltage gate is opened, the N terminus follows the outward K^+ current. This pushes the "ball" into the inner vestibule of the channel and blocks further ion conduction.[49] In comparison, slow or C-type inactivation depends on permeant ions and blockers, and is believed to occur through a conformational change near the extracellular pore region.[48a,49] In a physiological context, fast inactivation of the sodium channels and currents through the K_v channel repolarize the neurons after an AP and determine the duration and frequency of the APs.[51]

K_v channels can be blocked by Cs^+ ions, small organic cations, and venom peptides. Venom peptides, such as agitoxin-2, are produced by some of the most dangerous animals known, for example, the death-stalker scorpion, certain sea anemones, and the green mamba.[45,52] These peptides bind to the outer vestibule of the channel and literally plug its pore from the extracellular side, usually with a protonated lysine side chain. Typical small organic K_v channel blockers are quaternary ammonium ions, such as tetraethylammonium (TEA) and 4-aminopyridine (4-AP; Figure 7).[17c,53]

Interestingly, K_v channels feature both an internal and external binding site for quaternary ammonium ions.[54] External TEA mimics the protonated lysine side chain that functions as the plug in agitoxin-2, whereas internally applied TEA acts similar to the positively charged ball peptide involved in N-type inactivation. This blockade requires opening of the activation gate. Therefore, charged blockers that act from the internal side are called "open-channel blockers" or "use-dependent blockers."[17c] The KcsA structure was also solved in the presence of analogues of TEA, which helped to exactly locate its intracellular and extracellular binding sites.[54]

6. Photosensitizing Voltage-Gated Potassium Channels

With their structures elucidated and their functions reasonably well understood, voltage-gated potassium channels have become prime targets for optochemical genetics. The first system to emerge was the "synthetic photoisomerizable azobenzene-regulated K^+ channel" (SPARK), which is an example of the PTL approach (Figure 8).[55] As a consequence of its hyperpolarizing effect, it was later renamed H-SPARK. H-SPARK consists of the channel blocker MAQ (maleimide/azobenzene/quaternary/ammonium) covalently attached to a genetically introduced cysteine residue on an extracellular loop of a K_v1-type channel. The location of this cysteine residue (E422C) could be determined on the basis of existing X-ray structures and previous experiments with "molecular tape measures."[56] Once attached, MAQ essentially functions as TEA on a leash that can be lengthened or shortened with light. MAQ was designed to block the channel in its elongated *trans* state, that is, at 500 nm or in the dark, whereas the blockage would be lifted in the *cis* state of the photoswitch, that is, at 380 nm. Slow and fast inactivation of the channel had to be prevented by using genetic engineering to make H-SPARK an effective modulator of membrane potential. The activation voltage was shifted from −35 to −70 mV through another point mutation (L366A), which led to a constantly open channel before conjugation of *trans* MAQ. As a result, the potassium channel is blocked in the dark or under 500 nm light. Illumination with light of wavelength 380 nm unblocks the pore and the resulting outward current leads to re- or hyperpolarization of the membrane. To our amazement, SPARK not only worked in excised patches from Xenopus oocytes but also in excitable cells, such as dissociated hippocampal neurons.[55] Indeed, when SPARK was introduced in 2004, it was the first system that allowed for optical silencing of neuronal activity.

As a complement to the silencing H-SPARK, a depolarizing version, termed D-SPARK, was engineered.[57] A single additional mutation (V443Q) was sufficient to convert the potassium selective H-SPARK into a nonselective cation channel. With this mutation in the selectivity filter, the permeability ratio of the K^+/Na^+ ions changes to 0.7:1, and Na^+ influx into the cell dominates the net effect on the membrane potential. After covalent attachment of MAQ, the channel depolarizes the membrane upon UV illumination instead of hyperpolarizing it, thus allowing for AP firing rather than silencing. This is a nice case of "sign inversion," which is often encountered in neuroscience.

The diversity of K^+ channels, the lack of selective pharmacology, and the success of H*b*-SPARK provided the motivation to extend the PTL strategy to other members of the family.[58] K_v1.3, which is involved in membrane repolarization after AP firing of neurons and has immunosuppres-
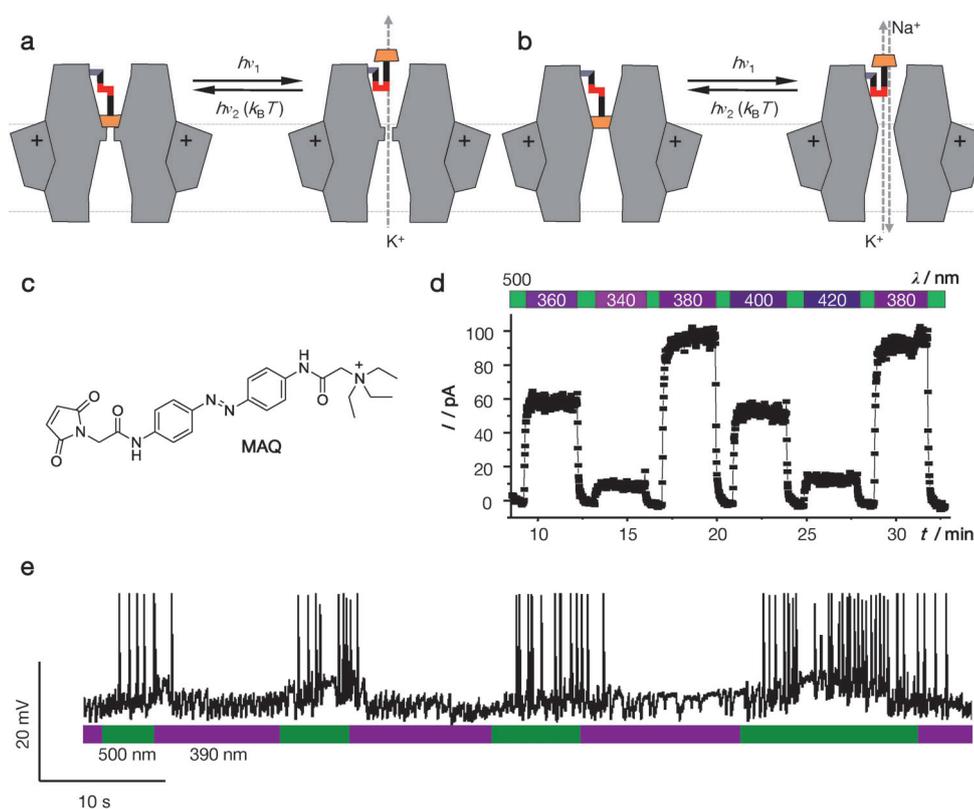
12166 www.angewandte.org

© 2011 Wiley-VCH Verlag GmbH & Co. KGaA, Weinheim

Angew. Chem. Int. Ed. **2011**, *50*, 12156 – 12182

Figure 8. SPARK, the light-sensitive potassium channel. a) A highly schematic representation of H-SPARK, the hyperpolarizing channel. b) A schematic representation of D-SPARK, the depolarizing variant. c) The chemical structure of MAQ, the PTL used for SPARK. d) Reversible light control of potassium currents by H-SPARK. Irradiation in the UV range unblocks channels, while 500 nm light induces blocking. By convention, outward currents are plotted upwards. e) Light-dependent induction of AP firing by H-SPARK expressed in neurons. This is the original recording of the first experiment where neuronal activity was controlled reversibly by a PTL.

native channels, as initially hypothesized. To reach the inner vestibule, the amphiphilic XAQs have to cross the membrane or they can be added to the cytosol through a patch pipette. External application of AAQ and BzAQ to cells or tissues blocks K_v channels in the *trans* state of the photoswitch, that is, in the dark or under 500 nm irradiation, while 380 nm light relieves the block. Interestingly, PrAQ preferentially blocks in its *cis* state (i.e. at 380 nm), which is another example of sign inversion.[59a]

Structurally, as well as functionally, XAQs resemble the well-known analgesic lidocaine or its permanently charged derivative QX-314, with the important difference that their efficacy is light-dependent. Similar to lidocaine, XAQs can be simply added to nervous tissues, which make them very attractive for therapeutic applications. After a brief waiting period, they reliably control action potential firing (Figure 9). When added to cerebellar slices, AAQ controls the activity of Purkinje neurons, mostly through its effect on inhibitory interneurons known as basket neurons.[59b] AAQ also has effects on the heartbeat of the medicinal leech *Hirudo medicinalis*.[59b] In this animal, central pattern generator interneurons (co-called HN cells) control the frequency of heart contractions. Earlier studies indicated that K^+ channels play a crucial role in burst firing of these HN cell. After application of AAQ, the activity of HN neurons could be modulated with light. Interestingly, burst periods decreased under 380 nm light illumination, whereas 500 nm light extended the period.

A major goal of our research program is to shift the absorption and action spectra of PTLs and PCLs toward the red, which would allow for deeper tissue penetration and would diminish the phototoxicity. This can easily be done through chemical derivatization of the azobenzene chromophore. For example, the introduction of an electron-donating substituent yielded XAQs that can be isomerized to their *cis* isomers with blue light. As an added advantage, these compounds revert to their *trans* form in the dark within milliseconds, effectively turning themselves off (Figure 10). Therefore, it is not necessary to toggle between two different wavelengths. An example of this type of compound is DENAQ, whose action spectrum reaches a maximum at
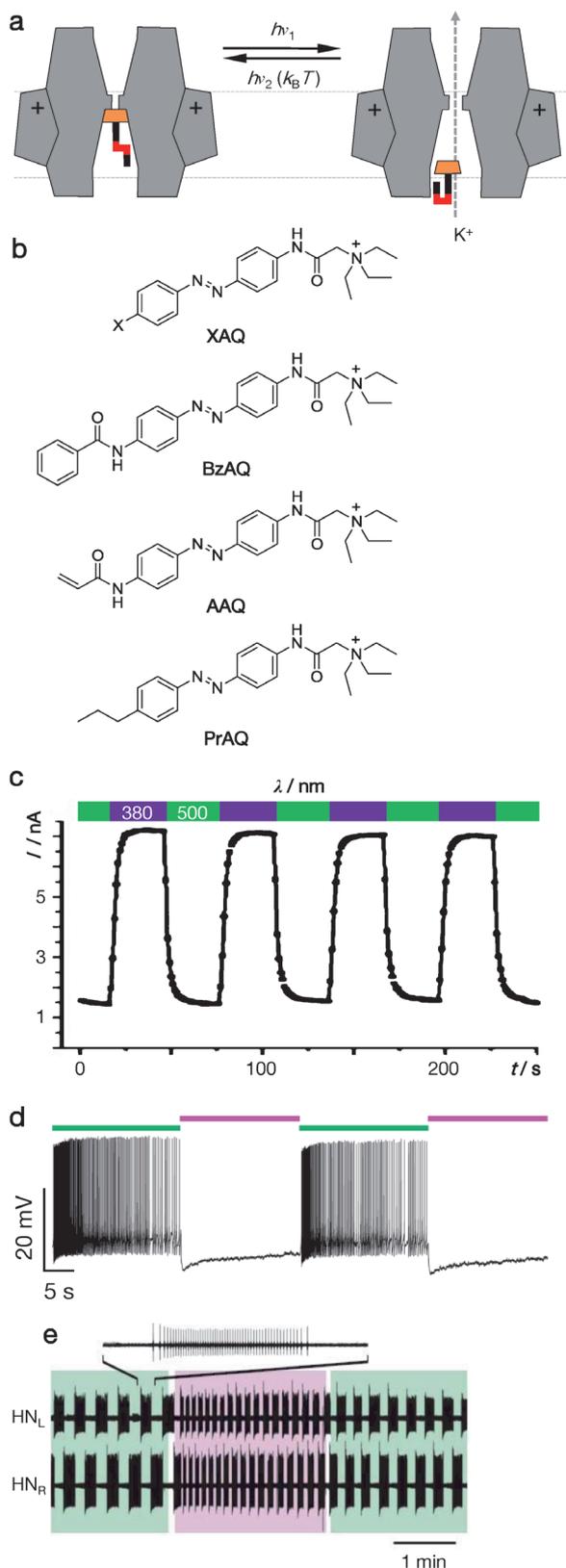
sive effects when blocked, became the next channel to be rendered light-sensitive by attachment of MAQ. Its very low affinity for TEA could be overcome by introducing a point mutation (H401Y). Both $K_v3.1$ and $K_v7.1$ could be converted into photoreceptors in a similar fashion. As a consequence of their fast deactivation, $K_v3.1$ channels play an important role in generating high-frequency APs, which occur in neurons of the auditory brainstem and the cerebellum. Finally, the PTL concept could be applied to the small conductance Ca^{2+}-activated K^+ channel 2 (SK2), a channel that is naturally sensitive to voltage and an intracellular ligand.[58] Taken together, these studies provide a first example for the PTL-driven selective pharmacology discussed in Figure 5.

As an alternative to PTLs, PCLs offer a way to control native K_v channels and neuronal activity with light. For this purpose, the cysteine-reactive maleimide group of MAQ was replaced with various moieties. This yielded a series of photochromic blockers, termed XAQs, which display different pharmacological and photophysical properties.[59] These compounds include the benzoate BzAQ, the propyl derivative PrAQ, and the acrylamide AAQ (Figure 9). Detailed investigations showed that the XAQs act as use-dependent, photochromic open-channel blockers.[59a] This also applies to AAQ, which does not react with the extracellular surface of
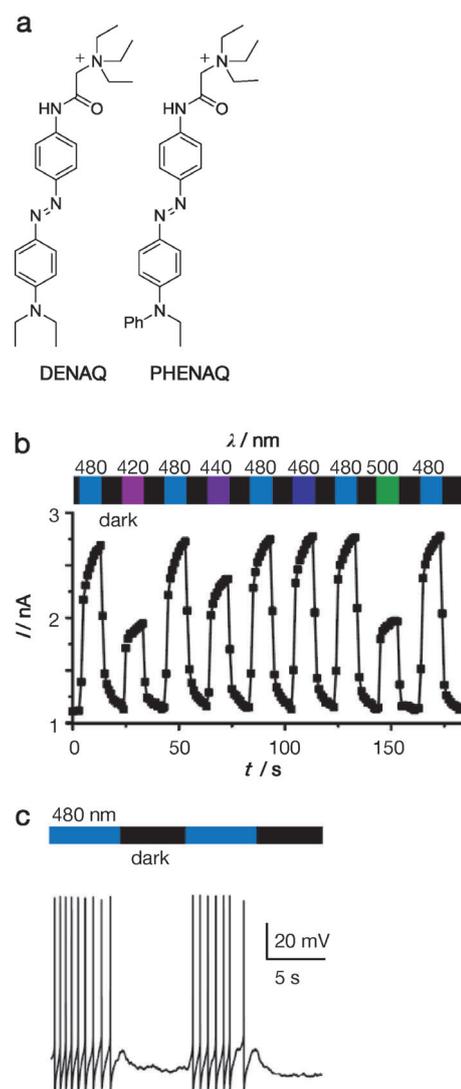
13

Figure 10. Red-shifted photochromic blockers. a) The chemical structures of DENAQ and PhENAQ, two red-shifted XAQs. b) Action spectrum of DENAQ. c) Controlling neuronal firing with PhENAQ.

480 nm. Interestingly, its analogue PhENAQ does not act as a blocker in the *trans* state but rather in the *cis* state (another case of sign inversion). It can also be switched to the blocking state with blue light and reverts to the inactive state automatically. Therefore, neuronal firing could be triggered with irradiation and quickly silenced by turning the light off.[42]

7. Ionotropic Glutamate Receptors

Ionotropic glutamate receptors (iGluRs) play a central role in synaptic transmission.[17a, 50, 60] Located primarily in postsynaptic membranes, these ligand-gated ion channels respond to the neurotransmitter glutamate released from vesicles on the presynaptic side. Upon glutamate binding, iGluRs generate a depolarizing current, which results in an excitatory postsynaptic potential (EPSP). With their fundamental involvement in neuronal communication, iGluRs are

Figure 9. PCLs for voltage-gated ion channels. a) A schematic depiction of a XAQ that functions as a photochromic open-channel blocker of K_v channels. b) The chemical structures of BzAQ, AAQ, and PrAQ, three typical XAQ PCLs for potassium channels. c) AAQ reversibly blocks potassium currents of a Kv1 family channel. d) AP firing of hippocampal neurons controlled by AAQ. e) Controlling the heart beat of a leech with AAQ.

Figure 11. Ionotropic glutamate receptors. a) A highly schematic illustration of glutamate receptor gating. b) X-ray structure of a single GluA2 subunit, indicating the TMD (including M1–4), the extracellular LBD, and TMD. c) The fully functional tetrameric GluA2 channel cocrystallized with an antagonist (yellow; pdb 3KG2). d) Expanded view of a GluA2 LBD cocrystallized with glutamate, emphasizing the clamshell (pdb 1FTJ). e) The chemical structures of various agonists and antagonists for iGluRs.

associated with a wide variety of neurological diseases, including Alzheimer's disease, epilepsy, and neuronal damage from stroke, and have therefore been very important neuropharmacological targets.[61]

All ionotropic glutamate receptors in higher animals assemble as tetramers and allow the permeation of monovalent cations with little selectivity (Figure 11). Some are also permeable to calcium. On the basis of functional differences and their response to synthetic ligands, they can be classified into *N*-methyl-D-aspartate (NMDA) receptors and non-NMDA receptors. The latter can be divided into three subgroups, namely so-called AMPA, kainite, and δ receptors.[51,62]

AMPA receptors, named after a selective agonist, form homo- and heteromeric channels composed of GluA1–GluA4 subunits.[51,62] They mediate postsynaptic depolarization after release of glutamate from the presynaptic side and exhibit fast activation and deactivation kinetics (within a few milliseconds). This feature makes them the principle molecular component of fast excitatory synaptic transmission.[51,62]

By contrast, kainate receptors play a role in the modulation of neuronal excitability rather than in fast excitatory transmission.[62,63] Their mode of action, however, is not as well understood as in the case of AMPA receptors. Homo- and heteromeric channels assemble from so-called GluK1–GluK5 subunits. δ Receptors assemble as homomeric receptors of GluD1 or GluD2 subunits. The function of these receptors, however, remains largely unknown.[62]

NMDA receptors assemble as obligate heterotetramers from a pool of seven subunits. Activation requires not only the simultaneous binding of glutamate and glycine (or D-serine), but also an elevated membrane potential of greater than −30 mV. This renders NMDA receptors coincidence detectors, since they are sensitive to both the release of ligands by the presynaptic neuron (and from glial cells)[51,62] and changes in voltage on the postsynaptic side. In addition, NMDA receptors are not only permeable for Na^+ and K^+, but also for Ca^{2+} ions. These activate various intracellular targets, such as the Ca^{2+}/calmoduline-dependent protein kinase II (CamKII). As such, NMDA receptors are involved in the

15

strengthening of synapses, which is believed to underlie learning and memory.[51, 64]

A single iGluR subunit contains an extracellular amino-terminal domain (NTD), a ligand-binding domain (LBD), a transmembrane domain (TMD), and an intracellular carboxy-terminal domain (CTD). The NTD is involved in subtype-specific assembly and modulation of the receptor, while the LBD provides a binding site for agonists (and antagonists). Two subdomains called D1 and D2 form the LBD in a clamshell-like arrangement. The TMD is composed of three transmembrane helices (M1, M3, M4) and a pore helix (M2). The CTD plays a role in channel localization, stabilization, and targeting for degradation.[51, 62]

X-ray crystallographic studies on GluRs began with soluble versions of LBD clamshells carved out of the full-length receptors through clever protein engineering.[63] These structures were obtained in conjunction with various ligands and proved to be remarkably insightful, since they could explain the activity of agonists, antagonists, and modifiers that affect desensitization.[63] For example, they showed that the binding mode of glutamate to the LBD clamshell is highly conserved in glutamate receptors and that the degree of closure of the clamshell is roughly correlated with the activity of a partial or full agonist.[62, 65] In line with this logic, antagonists, such as DNQX, bind to the clamshell but do not allow it to close tight enough to trigger the biological effect.[61] This "foot-in-the-door" mechanism of antagonism also explains why relatively small changes in the molecular structure can turn an agonist into an antagonist.

In a recent breakthrough in structural biology, the first crystal structure of a full-length homomeric GluA2 receptor was determined at 3.6 Å resolution (Figure 11 b).[12] This AMPA receptor was cocrystallized with a strong competitive antagonist, thus resulting in a closed, nonconducting state of the receptor. The structure confirmed that the subunits arrange as a dimer of dimers with an overall C_2 symmetry. The TMD architecture resembles an "inverted" K^+ channel, which is linked to a ligand sensor (the LBD) instead of a voltage sensor.

The activation cycle of glutamate receptors can be divided into an inactive resting state, an active nondesensitized state, and an inactive desensitized state. The LBDs of the four subunits are arranged in such a way that two clamshells on either side of the C_2 axis are sitting back to back. The binding of glutamate to the LBD of the inactive receptor initiates closure of the clamshell cleft. The movement of the lower lobe of the clamshell (D2) during this event rearranges the connector between the LBD and the TMD, which exerts a mechanical force that opens the channel. However, this active non-desensitized state creates tension at the LBD interface. This tension can be lifted by dissociation of the agonist or by rearrangement at the LBD dimer interface to give a closed, desensitized state.[62]

8. Photosensitizing Ionotropic Glutamate Receptors

Just as the outer vestibule of K_v channels had provided a suitable platform for the attachment of MAQ, the structurally well-characterized extracellular clamshell of glutamate receptors presented an opportunity to explore tethered ligands (i.e. PTLs). In this case, we opted for an agonist, instead of a blocker or antagonist. This approach yielded LiGluR, the "light-gated ionotropic glutamate receptor," which combines a genetically engineered kainate receptor (GluK2) with a PTL called MAG-1 (Figure 12).[66] MAG-1 consists of a maleimide for covalent attachment, an azobenzene photoswitch, and a substituted glutamate as the ligand. Once MAG-1 is attached to a cysteine residue at the LBD of GluK2 (L439C), light-induced *cis* and *trans* isomerization of the azobenzene moiety results in reversible binding of the tethered agonist, which translates into opening and closing of the channel.

The design of LiGluR was based on the crystal structure of a closed GluK2-LBD containing the agonist (2*S*,4*R*)-4-methylglutamate (pdb 1SD3).[63] This structure suggested the existence of a small "exit tunnel" from the bound ligand to the surface of the closed clamshell. It was, therefore, hypothesized that a tethered glutamate with this stereochemistry could bind to the LBD and still activate the receptor as an agonist or at least a partial agonist. A so-called tether model (T-Mod) was synthesized to support this hypothesis. It could be shown by calcium imaging in HEK293 cells that the tether model, and later MAG-1, indeed act as agonists.[66] Other crystal structures, such as the one of the partial agonist domoic acid bound to GluK2 (pdb 1YAE) also facilitated the design of suitable PTLs.[67]

Once the tether model was found to work, the molecule was extended to MAG-1 by installing the azobenzene photoswitch and adding a maleimide as an electrophile for cysteine conjugation. Several cysteine mutants of GluK2 were generated by site-directed mutagenesis to find a suitable attachment site for this maleimide. After screening about a dozen mutants, L439C turned out to be the best position for MAG-1 attachment and light-dependent activation of the channel.[66]

Since it was not clear whether and how the attachment of the PTL to the protein would affect the photophysics of its azobenzene moiety, the optimal wavelength for activation and inactivation was determined experimentally (Figure 12).[66] It was found that 380 nm light gave the maximum current, whereas 500 nm led to the fastest channel closure. Interestingly, this observation corresponds very well to the photostationary states of MAG-1 in solution (Figure 12). In addition, the thermal relaxation of *cis*-MAG-1 bound to the channel was found to be much slower than in solution, probably because of the noncovalent interaction of the glutamate ligand with the clamshell, which stabilizes the *cis* configuration.[41]

When expressed in neurons, which contain the full machinery to generate APs, LiGluR allows for the optical control of neuronal firing with millisecond resolution.[68] Brief light pulses (1–5 ms) alternating between 380 nm and 500 nm are sufficient to generate reproducible patterns of APs. APs can be induced in dissociated hippocampal neurons with a frequency of up to 50 Hz without missing a beat (Figure 12).[68] The *cis* stability of MAG means that it is possible to induce constant AP firing for seconds following a single flash of 380 nm light that lasts only a few milliseconds.
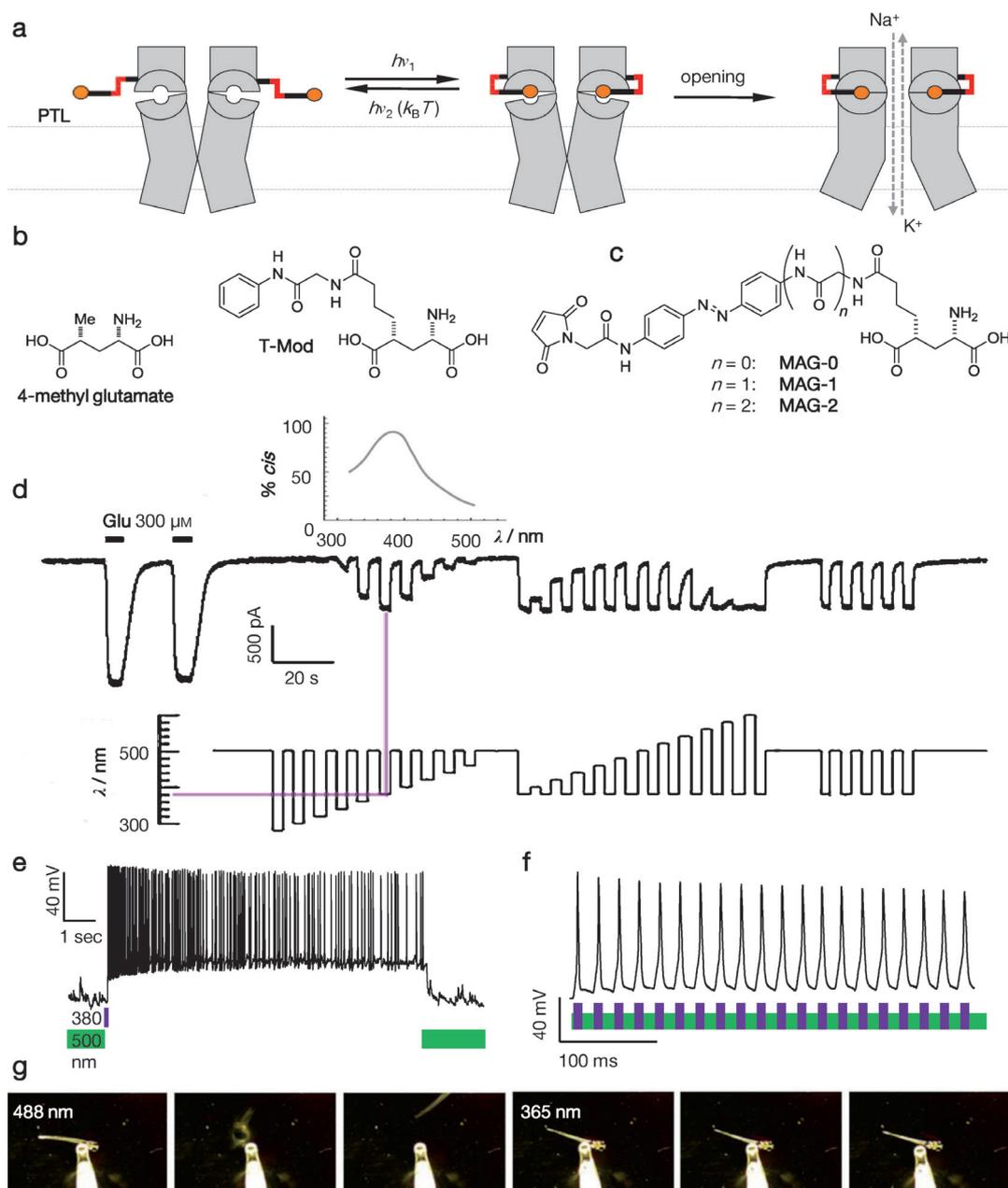
Figure 12. The light-gated glutamate receptor LiGluR. a) A highly schematic illustration of LiGluR. b) The chemical structure of 4-methylglutamate and the "tether model" (T-Mod), two important milestones on the way to LiGuR. c) The chemical structure of MAG-0, MAG-1, and MAG-2. d) The action spectrum of LiGluR. By convention, inward currents are plotted downwards. The phototunability of the system is apparent. e) LiGluR controls AP firing with millisecond precision. A very brief UV flash induces a train of APs, thus demonstrating the *cis* stability of the system. f) LiGluR enables AP firing of up to 50 Hz. g) Controlling the escape reflex in zebrafish.

Thus, long illumination periods leading to toxic side effects can be avoided.[68,69]

LiGluR shows some fundamental functional differences compared with SPARK. Both irradiation and depolarization are needed to open the SPARK channel (corresponding to a logic AND gate). By contrast, in LiGluR, either soluble glutamate or light is sufficient to allow ions to flow along their electrochemical gradient (corresponding to a logic OR gate). LiGluR is a light-powered molecular machine, since the energy of the photoisomerization translates into the free energy released upon ligand binding, triggering clamshell-

closure and channel opening. It can be reset through slow thermal isomerization or active photoswitching with a longer wavelength. SPARK, on the other hand, is a more passive system, since the tethered blocker functions as an extracellular gatekeeper but does not trigger large molecular motions itself. These need to be generated by membrane depolarization, which moves the voltage sensor and opens the voltage gate.

One of the hallmarks of our systems in general, and LiGluR in particular, is their remarkable flexibility and tunability. This is evident at the level of the photoswitches and

also at the level of the protein. In addition to MAG-1, further derivatives called MAG-0 and MAG-2 with different lengths and stiffnesses were synthesized, and additional attachment sites were generated by site-directed mutagenesis. This "mix and match" approach led to some interesting results. For example, MAG-0 anchored at L439C provided the biggest change in the effective concentration in competition with the antagonist DNQX. In comparison, MAG-1, our original PTL, and MAG-2 are less effective.[69]

In another case of "sign inversion," we found that the point of attachment can determine whether a PTL activates the channel in the *cis* or in the *trans* form of the photoswitch (Figure 13).[69] MAG-0 bound to L439C, our original attach-
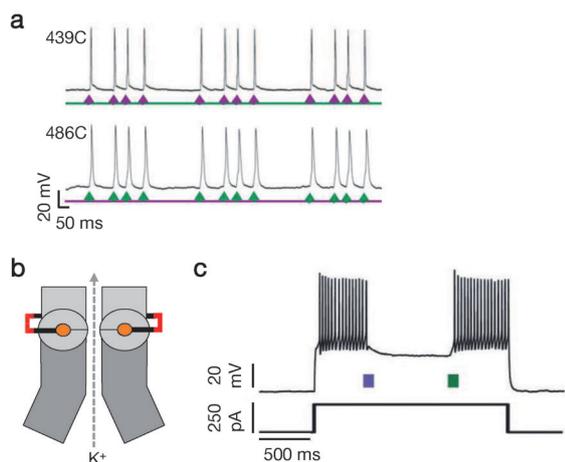
Figure 13. Sign inversion through variation of LiGluR. a) MAG-0 attached to mutant 439C activates at 380 nm, whereas MAG-0 attached to mutant 486C induces neuronal firing at 500 nm. b) Schematic representation of HyLighter, a hyperpolarizing light-gated glutamate receptor. c) HyLighter can be used to silence neurons. Evoked AP firing can be stopped and re-induced by light pulses at 380 nm and 500 nm, respectively, thus demonstrating the bistability of the system.

ment site, acts as a *cis* agonist but becomes a *trans* agonist when attached to L486C. This is somewhat surprising given that these two sites are only a few Ångstroms apart in the X-ray structures of GluK2. As a consequence of this inverted wavelength sensitivity, the transfection of neurons with L486C followed by MAG-0 attachment triggers AP firing at 500 nm and not at 380 nm, as previously observed.

Just as H-SPARK could be converted into D-SPARK, LiGluR, a light-gated depolarizing ion channel, could be converted into a hyperpolarizing ion channel, called HyLighter.[70] As before, this could be achieved by changing the ion selectivity of the transmembrane domain through genetic manipulation. However, in the case of HyLighter, not a single point mutation, but the exchange of a whole protein domain was necessary. HyLighter combines the GluK2-derived photosensitive LBD of LiGluR with the potassium-selective TMD of the prokaryotic glutamate receptor SGluR0, which contains the signature GYG motif of K^+ channels.[71] Expression of HyLighter in hippocampal neurons showed that inhibition of neuronal firing can be reversibly turned on and off by irradiation with 380 nm and 500 nm light, respectively (Figure 13). The main advantage of HyLighter in

comparison to fully genetically encoded hyperpolarizing systems is the thermal stability of *cis*-MAG-1 bound to the LBD. Therefore, in analogy to LiGluR, a single flash of 380 nm light of a few milliseconds is sufficient to prevent neurons from firing for seconds to minutes.

One of the big surprises in the development of optochemical systems was how quickly they could be transferred to animals and could be used to dissect behavior.[68, 70] The first in vivo experiments with LiGluR were performed in zebrafish larvae.[68] Zebrafish at this stage of development are fully transparent, which is a necessary requirement for reaching neuronal circuits with light. To implement LiGluR, iGluK2-L439C was genetically encoded in small subsets of neurons which are involved in touch sensation and located at the head and trunk of the animals. For the delivery of the photoswitch to the tissue of interest, it was enough to bath the larvae in a solution containing MAG-1. Following this treatment, an escape reflex initiated by touching the trunk with a pipette tip could be controlled by optical activation of LiGluR. This reflex could be suppressed by brief illumination with 365 nm light and restored with 488 nm light.[68] HyLighter could be applied to zebrafish larvae in a similar way.[70]

In more sophisticated subsequent studies, LiGluR was genetically targeted to a single type of cell and used to elucidate the functional role of so-called Kolmer–Agduhr neurons—a mystery unsolved for 75 years. They turned out to be the central pattern generators of locomotion in the early development of vertebrates.[72]

In addition to PTLs, PCLs also turned out to be applicable to glutamate receptors (Figure 14). Their design was based on
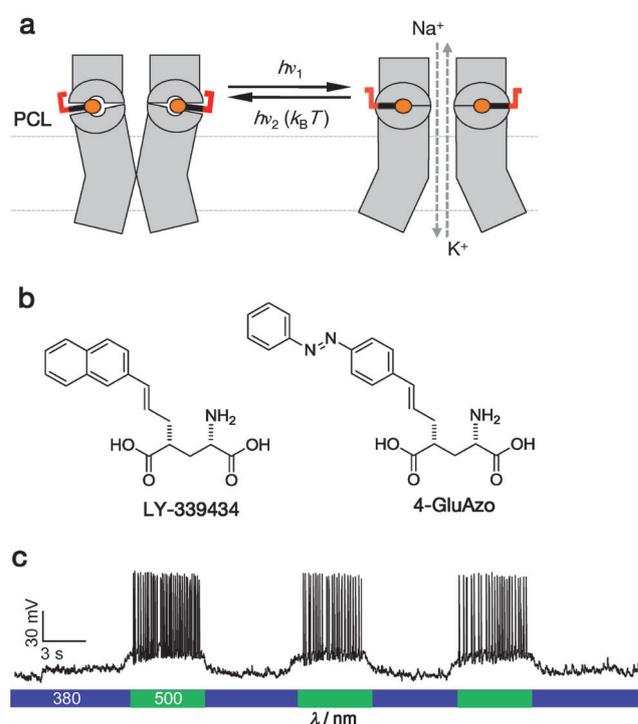

Figure 14. The PCL logic applied to ionotropic glutamate receptors. a) Schematic view of a PCL operating on LiGluR. b) The structures of LY-339434 and its derivative 4-GluAzo, a PCL that targets kainate receptors. c) Controlling the AP firing of hippocampal neurons with 4-GluAzo.

12172 www.angewandte.org

© 2011 Wiley-VCH Verlag GmbH & Co. KGaA, Weinheim

Angew. Chem. Int. Ed. **2011**, *50*, 12156–12182

18

the extensive pharmacology of iGluR agonists, antagonists, and blockers, but was also supported by the LBD X-ray structures. Replacement of the naphthyl moiety of LY339434, a know agonist of GluK1 and GluK2, with an azobenzene moiety gave 4-GluAzo. This compound turned out to be a highly effective photochromic agonist of certain kainate receptors.[73] Its application to GluK1 and GluK2 channels expressed in HEK293 cells demonstrated the reversible control of inward currents in a light-dependent manner. In this case, the *trans* state of the azobenzene preferentially activates the receptors, and 4-GluAzo showed a slightly higher selectivity for GluK1 than for GluK2. When applied to dissociated rat hippocampal neurons, 4-GluAzo functioned as "reversibly caged" glutamate.[73] Action potential firing could be triggered by changing from 380 to 500 nm light and stopped by switching back to the lower wavelength. In subsequent studies, the burst firing of cerebellar Purkinje neurons could be effectively controlled with 4-GluAzo.[74]

Detailed biophysical studies will be needed to understand how 4-GluAzo and other PCLs work. In particular, it would be interesting to know whether the photoisomerization can take place while they are attached to their binding sites or whether have to dissociate before switching can occur. X-ray crystallographic studies could also provide important insights into the binding modes of PCLs (and PTLs) and guide their further development.

9. Pentameric Ligand-Gated Ion Channels

Pentameric ligand-gated ion channels (pLGICs) also play important roles in synaptic transmission.[51] In contrast to mammalian glutamate receptors, they can have both excitatory and inhibitory effects on the postsynaptic cell, which can be a neuron or a muscle cell. The superfamily of pLGICs includes nicotinic acetylcholine receptors (nAChR), γ-aminobutyric acid receptors (GABA$_A$ and GABA$_C$), 5-hydroxytryptamine receptors (5-HT$_3$), and glycine receptors (GlyRs).[75] They are sometimes also called Cys-loop receptors because of the fact that all pLGICs subunits feature an extracellular disulfide bond in a conserved region. GABA$_A$ and GABA$_C$ are chloride-selective ion channels that mediate fast inhibition of neuronal activity in the brain and the retina.[76] The serotonin receptor 5-HT$_3$ is an excitatory cation channel that modulates neurotransmitter release. Similar to GABA$_A$ receptors, GlyRs have an inhibitory effect on neuronal communication. They are ligand-gated chloride channels that are mostly expressed in the spinal cord and the brain stem (Figure 15).[77]

Nicotinic acetylcholine receptors are excitatory cation channels that are expressed throughout the mammalian nervous system and at the neuromuscular junction.[78] Five classes of subunits exist for the muscle-type receptor nAChR: α_1, β_1, γ, ϵ, and δ.[51, 78b] Together, they form a cation-selective pentameric ion channel with $(\alpha_1)_2\beta_1\gamma\delta$ stoichiometry. In contrast, the neuronal types are composed of α_2–α_{10} and β_2–β_4 subunits and can form both heteromeric (e.g. $(\alpha_4)_2(\beta_2)_3$) and homomeric (e.g $(\alpha_7)_5$) pentamers. Notably, only α_7, α_8, and α_9 form homomers when expressed heterologously.[78b, 79]

Each subunit of the nAChR is divided into an extracellular, N-terminal ligand-binding domain, a transmembrane region with four transmembrane spanning helices, and an intracellular region (Figure 15). Both the N and C terminus are located in the extracellular space. The transmembrane helices of five single subunits line up to form the pore of the ion channel. The $(\alpha_1)_2\beta_1\gamma\delta$ receptor at the neuromuscular end plate has two ligand-binding sites located between the α–γ and α–δ subunits, which have distinct affinities for the neurotransmitter acetylcholine (Ach). Both binding sites must be occupied to open the channel pore.[51, 78b]

The structural biology of nAChR has a long history, since it was accessible from the electric organ of the ray *Torpedo californica* well before the advent of molecular cloning and heterologous expression.[17c, 51] By using electron microscopy, a structural model of the *Torpedo* nAChR could be gradually built and ultimately refined to 4 Å resolution.[15a, 80] More recently, X-ray structures of the two bacterial homologues ELIC and GLIC were solved in their closed and open states, respectively, which provided a detailed view of the pentameric assembly and shed some light on channel gating.[15b,c] Unfortunately, none of the abovementioned receptors were crystallized and elucidated in conjunction with agonists or antagonists.

The X-ray structure of two acetylcholine-binding proteins, isolated from the sea snails *Limnia stagnalis* (L-AChBP) and *Aplysia californica* (A-AChBP) provided more insight into the interaction of pLGICs with their ligands.[81] These soluble proteins are homologous to the extracellular ligand-binding domain of pLGICs, but lack their transmembrane domain. Sequence alignment of L-AChBP with various pLGICs gave a 20–24% match with the nAChR subunits and a 15–18% match to the 5-HT$_3$, GABA$_A$, GABA$_C$, and glycine receptor subunits.[81b] The X-ray structures of L-AChBP cocrystallized with the agonists nicotine and carbachol showed that the cationic ligands bind at the interface between two subunits in an "aromatic box" made up mostly of tyrosine and tryptophan side chains. This confirmed the importance of cation–π interactions that had been previously proposed on the basis of intricate biophysical studies with labeled amino acids.[81c] One side of the binding site is covered by the so-called C loop, which closes like a flap upon binding of the agonist. This flexible C loop also carries a cysteine disulfide at its tip but is not to be confused with the Cys loop, which is located closer to the membrane.

Subsequently, other ligands for pLGICs, such as epibatidine (an agonist for nAChR),[81d] lobeline (a mixed agonist/antagonist for nAChR),[81d] methyllycaconitine (an antagonist for nAChR),[81d] as well as strychnine (an antagonist for GlyR),[82] were cocrystallized with A-AChBP. These structures showed that the C loop indeed acts as an induced-fit sensor for ligands, and that the degree of C-loop closure correlates with the agonist versus antagonist activity. How this movement is mechanically linked with the opening of the channel is still a matter of debate.
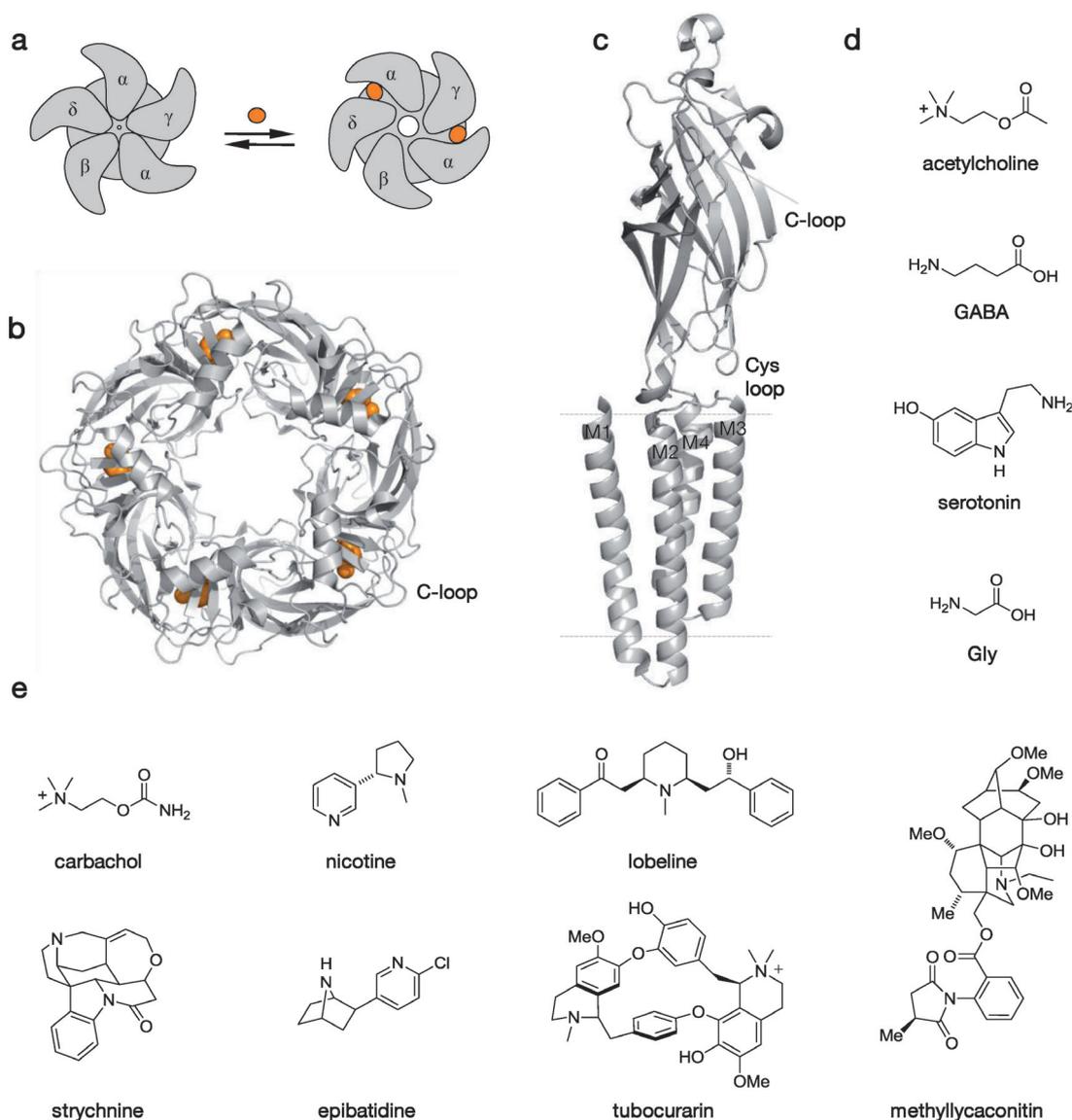
Figure 15. Pentameric ligand-gated ion channels (pLGICs). a) A highly schematic view of nAChR gating. b) Crystal structure of the acetylcholine-binding protein (AChBP) cocrystallized with nicotine (pdb 1UW6). c) A single subunit of a pLGIC, showing the transmembrane domain, the extracellular ligand-binding domain, and the Cys loop (pdb 3P4W). d) Endogenous ligands that gate pLGICs. e) Other well-known ligands of pentameric ligand-gated ion channels that have been cocrystallized with the AChBP.

10. Photosensitizing Pentameric Ligand-Gated Ion Channels

The nicotinic acetylcholine receptor has been studied for many decades, since it was the first ligand-gated ion channel to be isolated and characterized as a protein.[17c] It occurs in high concentrations in the electric organs of certain fish, such as the ray *Torpedo electroplax* and the eel *Electrophorus electricus*, which is why it could be investigated with biophysical methods that were not applicable to other types of receptors at the time. This may be the reason why the nAChR was also the first receptor to be photosensitized, both with a PCL and a PTL.[83] Amazingly, this was done in the early 1970s, well before the advent of molecular cloning, heterologous expression, modern structural biology, and patch-clamp

electrophysiology. It took more than three decades to repeat this achievement with other types of receptors!

The PCL used in this case was an azobenzene unit called Bis-Q, which bears a quaternary ammonium ion (Q) on both sides of the chromophore. This simple, symmetric molecule functions as a photoswitchable version of the natural agonist acetylcholine.[83] Whereas *trans*-Bis-Q activated nAChRs in *Electrophorus electricus*, the corresponding *cis* isomer was found to be less active. The activity of the two isomers was assayed by measuring the transmembrane potential of *Electrophorus* electroplaques, which are specialized cells from its electric organ. The system was later used to determine the opening and closing rates of nAChRs.[84]

The corresponding PTL system was based on careful reasoning and a bit of luck, since the native receptor could be used without genetic manipulation. It turns out that nAChRs

12174 www.angewandte.org

© 2011 Wiley-VCH Verlag GmbH & Co. KGaA, Weinheim

Angew. Chem. Int. Ed. **2011**, *50*, 12156 – 12182
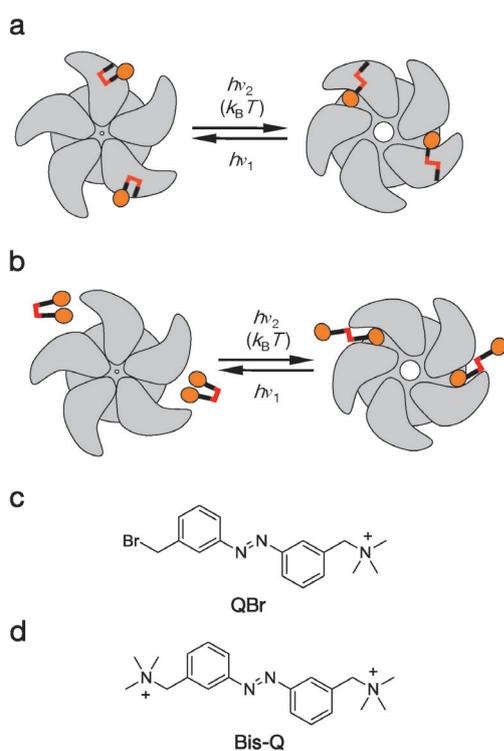
Figure 16. Photosensitizing the nicotinic acetylcholine receptor. A highly schematic depiction of a) a PTL reversibly acting on a nAChR, and b) a PCL controlling the nAChRs. c) The structure of QBr, a PTL, and d) BisQ, a PCL.

possess a disulfide bond on the tip of their C loops in the α subunits, in proximity to the ligand-binding site (Figure 16). This disulfide could be reduced without greatly affecting the function of the receptor, thereby providing a reactive thiol for the covalent attachment of a PTL.[83] The PTL was a benzylic bromide, called QBr, which also carried the requisite quaternary ammonium ion for activation of the receptor. Conveniently, QBr could be obtained through a slight modification of the synthetic protocol used to make Bis-Q. Once attached to nAChRs, QBr could be used to reversibly stimulate *Electrophorus* electroplaques, frog muscles, and rat myoballs with light.[85]

Of course, in the 1970s and 1980s the light-activated nAChR could not be heterologously expressed and genetically targeted, and it was, therefore, never used to control AP firing. Similarly, Bis-Q was mostly seen as a tool to study the innate function of nAChRs and not as a practical way to optically control nervous systems or animal behavior. However, with detailed structures and the modern tools of molecular biology now available, it is highly likely that light-gated nAChRs will soon resurface and be used in optochemical genetics. In addition, PCLs and PTLs for other pLGICs are bound to be developed.

11. An Abundance of Targets

From the preceding paragraphs it is clear that a variety of receptors from different structural classes can be rendered photosensitive by using synthetic PTLs and PCLs. However, the vast majority of potential candidates with sufficient structural and pharmacological data have not yet been investigated, and opportunities abound to explore the optochemical genetics of these targets. For example, given the many structural and functional similarities between voltage-gated potassium (K_v), sodium (Na_v), and calcium channels (Ca_v), the photochromic open-channel blockers discussed above could be applied to the latter as well. In addition, Na_v and Ca_v channels have extensive pharmacology of their own, which could be exploited to design more selective PCLs. The long-awaited X-ray structure of a Na_v channel has just been reported and should greatly facilitate the design of the corresponding PTLs.[86]

Even if one were confined to clamshell-bearing receptors, there would be a large number of interesting targets to work on. Clamshell-like ligand-binding domains appeared early in evolution and are a prime example of how a successful structural motif has been used again and again in different functional contexts.[87]

Originally evolved as bacterial periplasmic binding proteins (such as the well-known maltose-binding protein or amino acid binding proteins), clamshells have subsequently been integrated as functional and structural domains into prokaryotic and eukaryotic transmembrane proteins. Apparently, they were first captured by bacterial ABC transporters that initially interacted with soluble periplasmic binding proteins in a noncovalent fashion. At some point, they made their way into ion channels, such as ionotropic glutamate receptors. These include several prokaryotic glutamate-gated channels,[71] a plant receptor,[88] and one that was recently found in a comparatively simple eukaryotic rotifer.[89] As discussed in Section 7, glutamate-gated ion channels have assumed a major role in the fast synaptic transmission of higher animals. However, glutamate-binding clamshells can also be found in metabotropic glutamate receptors (mGluRs), which are family C GPCRs.[90] This large and important class also includes $GABA_B$ receptors[91] and T1R taste receptors,[92] and is found in many places in neurophysiology. The clamshell of several of these mGluRs has been characterized by X-ray crystallography in atomic detail and their pharmacology is very well developed (Figure 17).[93] Therefore, they are logical next targets for manipulation with PTLs or PCLs. Finally, clamshell-like ligand binding domains have been found in certain receptor-linked enzymes, which represent the third major class of receptors involved in signal transduction, in addition to ion channels and GPCRs. An example is the ANP receptor, the clamshell-dimer of which has been crystallized bound to the atrial natriuretic peptide (Figure 17).[94] Clamshell-containing receptor tyrosine kinases have also been recently described.[95]

The X-ray structure of a full-length GPCR of family C that includes the transmembrane domain has not yet been reported. In contrast, several GPCRs belonging to family A have been recently elucidated by X-ray crystallography (Figure 18). These receptors comprise the largest class of GPCRs and have a ligand-binding site that is embedded more- or less-deeply within the membrane. They include such
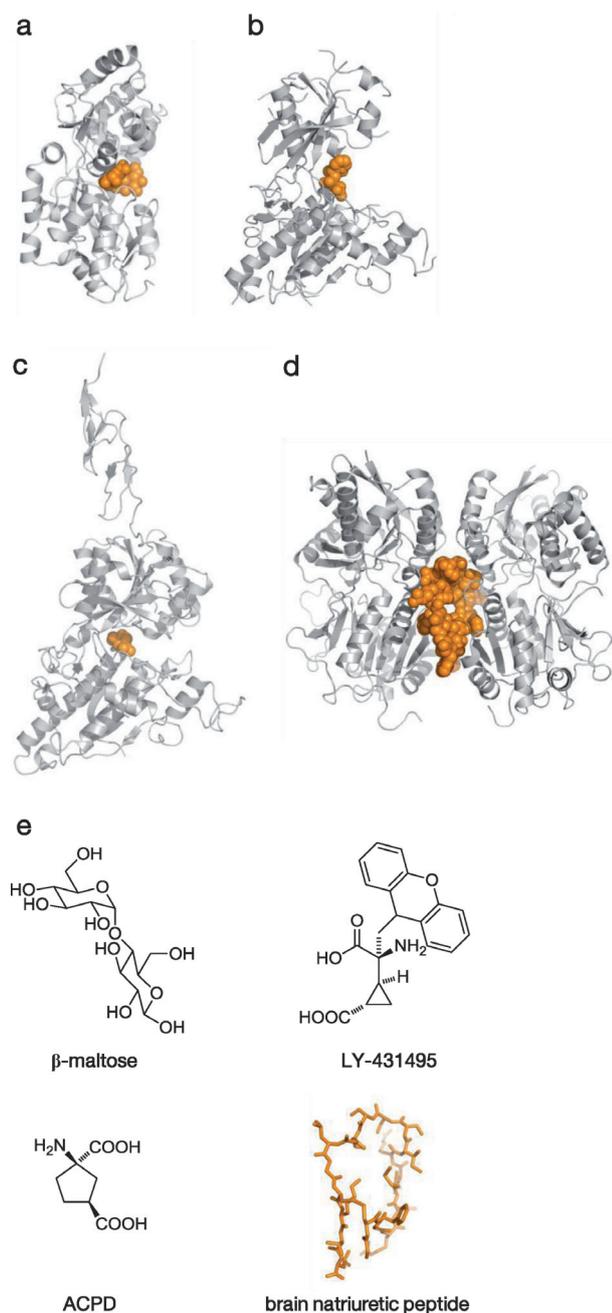
Figure 17. Clamshell-like LBDs as potential targets for optochemical genetics. a) The maltose-binding protein, a typical periplasmic binding protein (pdb 1ANF). b) The extracellular clamshell of mGluR3 with an agonist (pdb 2E4X). c) The extracellular clamshell of mGluR1 with an antagonist (pdb 3KS9). d) The clamshell dimer of the ANP receptor, a receptor-linked enzyme (pdb 1YK0). e) The chemical structures of ligands for clamshell-containing receptors.

important pharmacological targets as adrenergic receptors (e.g. β2A),[96] adenosine receptors (e.g. A$_{2A}$, which is a target of the antagonist caffeine),[11c] and dopamine receptors (e.g. D3).[11d] Rhodopsin, the photoreceptor used in animal vision, also belongs to this category.[11b] In this case, however, the photoswitch retinal is covalently bound in an inactive form (11-*cis*) and undergoes photoisomerization to the active form (all-*trans*), followed by hydrolysis and recycling, instead of

reversible binding. As such, it resembles a PTL to a certain extent. Given this analogy, it is entirely conceivable that well-characterized ligands for other class A GPCRs could be replaced with PTLs and PCLs, thus turning them into photoreceptors.

Trimeric ion channels are also interesting targets, since they have recently been structurally characterized in atomic detail and have good pharmacology (Figure 19). They include purinergic receptors (P2X receptors), acid-sensing ion channels (ASICs), and epithelial sodium channels (ENaCs). The ionotropic P2X receptors are nonselective cation channels that are activated by extracellular adenosine 5′-triphosphate (ATP). They are widely expressed in the nervous and immune system, and are involved in numerous neurological functions, such as pain sensation.[97]

The first X-ray crystal structure of a P2X receptor, the zebrafish P2X$_4$ receptor, was solved in its closed state at 3.1 Å resolution.[13] The structure confirmed the trimeric channel architecture and provided important insights into the ion-conducting pore. The position of the ATP binding site was proposed to be located between each subunit at the outer extracellular surface of the receptor. However, the P2X$_4$ structure was solved without ATP or an antagonist bound (e.g. the azobenzene PPADS), thus leaving the exact binding mode of ligands undefined.

One particular P2X receptor, P2X$_2$, holds a special place in the development of optochemical genetics. After heterologous expression, this cationic channel could be optically stimulated with caged ATP. This system was reported in 2003, and was one of the first systems to work in neurons. Since ATP is hydrolyzed rapidly, even in the extracellular space, photostimulation could be carried out repeatedly and with relatively good temporal resolution. Incidentally, caged ATP is also one of the first caged ligands, if not the first.[35]

ASIC channels belong to the degenerin/epithelial sodium channel (DEG/ENaC) family. They are ligand-gated trimeric cation channels that are activated by extracellular protons and favor Na$^+$ over K$^+$ ions by a factor of ten. Isoforms of ASICs are distributed throughout the mammalian central and peripheral nervous system. They play important physiological roles, for example, in the detection of tissue acidosis during ischemia.[98] Two crystal structures of homotrimeric ASIC channels have been reported recently.[99]

Unfortunately, this is not yet the case for ENaC, a heterotrimeric channel that is constitutively open and is extremely selective for sodium. It plays a key role in sodium reabsorption and the perception of salt taste, and is the target of widely used diuretics, such as Amiloride.[100]

Transient-receptor potential channels (TRP channels) have been identified as major molecular players in sensory perception.[101] They are tetrameric cation channels that are polymodal and sensitive to a wide variety of input signals, including temperature, small molecules, and ligands. One famous member of this large superfamily is TRPV1, which is activated upon heating, but also responds to capsaicin, the active component of chili peppers.[102] Therefore, on a molecular level, "hot" as in "hotplate" and "red-hot chili peppers" are really the same thing. In one of the first applications of optochemical genetics, TRPV1 was hetero-

12176 www.angewandte.org

© 2011 Wiley-VCH Verlag GmbH & Co. KGaA, Weinheim

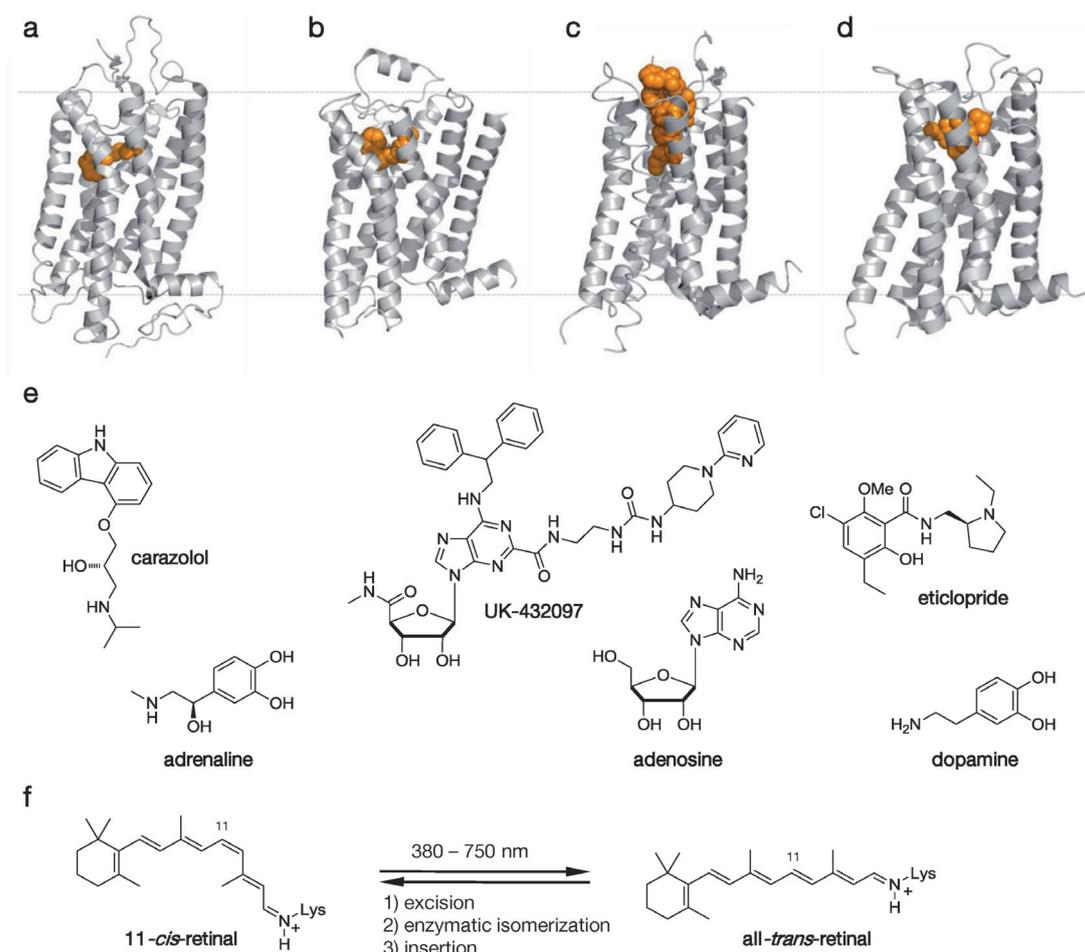*Angew. Chem. Int. Ed.* **2011**, *50*, 12156 – 12182

Figure 18. Family A GPCRs as potential targets of optochemical genetics. a) Rhodopsin, a natural photoreceptor with a covalently attached photoswitch (pdb 1U19). b) The β2 adrenergic receptor bound to the inverse agonist carazolol (pdb 2RH1). c) The A$_{2A}$ adenosine receptor bound to the agonist UK-432097 (pdb 3QAK). d) The D3 dopamine receptor bound to the antagonist eticlopride (pdb 3PBL). Protein domains used to facilitate the crystallization have been cut off. e) Chemical structures of the cocrystallized and endogenous ligands for the receptors depicted above. f) Isomerization of 11-*cis*-retinal to all-*trans*-retinal in rhodopsin.

logously expressed in neurons and stimulated with caged capsaicin and light (Figure 4 b,c).[35]

TRP channels are not only responsible for sensing heat and coldness but may also play a role in sensing pressure.[101] As such, they could have physiological roles in mechanoreception (touch), balance, pain, the regulation of blood flow, and hearing.[103] The regulation of pressure sensors with light would indeed be a very interesting exercise. This has not yet been done with a TRP channel, but proof of principle has been given with a comparatively simple bacterial mechanoreceptor isolated from *Mycobacterium tuberculosis* (Figure 20).[104] This homopentameric channel, called MscL, was crystallized in its closed form and its structure was elucidated by X-ray crystallography.[105] If the tension of the membrane in which it is embedded exceeds a certain value, it opens to form a very large pore, thus functioning like a valve that relieves osmotic pressure in the bacterium. The closed gate of the channel is formed by a ring of five hydrophobic residues that prevent ions and other solutes from passing through. Detailed biophysical investigations had shown that replacement of these hydrophobic residues with charged

amino acids leads to a constitutively open channel, presumably as a result of electrostatic repulsion.[106]

In a first approach toward the photosensitization of MscL, a caged carboxylic acid was covalently attached to a cysteine residue to replace the hydrophobic residues at the gate. Upon irradiation with UV light, the cages were cleaved and the resulting negative charges triggered the opening of the channel. In a second step, the caged acids were replaced with a covalently attached spiropyran/merocyanine (SP/MC) photoswitch. Switching from the comparatively nonpolar SP state to the highly polar MC state resulted in the opening of the valve. This process was reversible over a few cycles.[104] Although this system was developed as a "nanovalve" for drug delivery and may never find its way into neurobiology, it is nevertheless a very nice example of the optical control of channel activity and it involves both cages and photoswitches. Interestingly, photoswitchable lipids have also been used to change the membrane tension with light and reversibly activate MscL.[107] Indeed, photoswitchable lipids may provide yet another general way to influence the function of transmembrane proteins and cells with light.
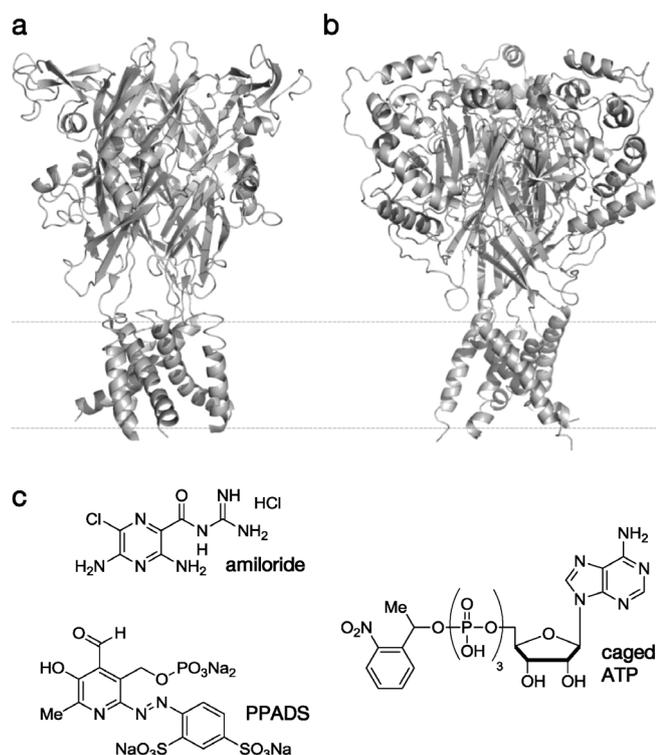
Figure 19. Trimeric ion channels as potential targets for optochemical genetics. a) The ASIC1 channel (pdb 3HGC). b) The P2X$_4$ receptor (pdb 3H9V). c) Chemicals acting on trimeric ion channels. Amiloride: a blocker for ASIC and ENaC channels. PPADS: an antagonist of purinergic receptors. Caged ATP: a CL for P2X$_2$ receptors.
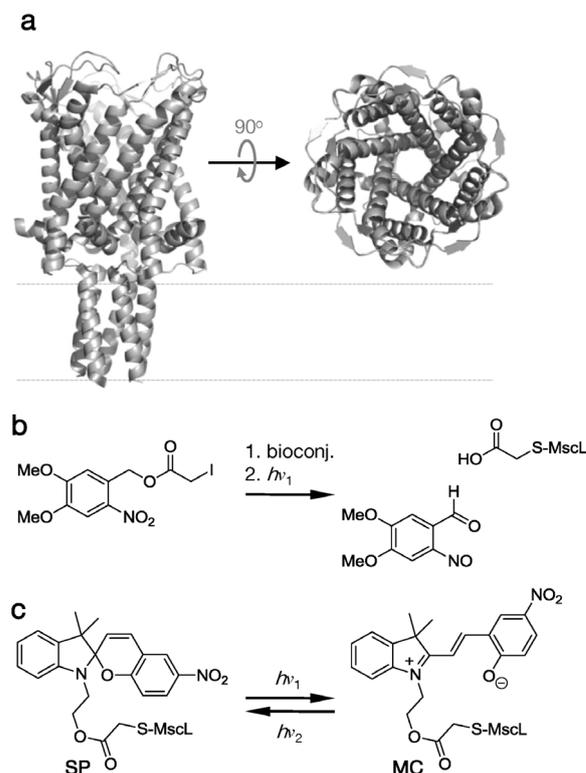

Figure 20. Photosensitization of a bacterial mechanosensitive ion channel. a) The structure of MsCl in its closed form: side and top view (pdb 2OAR). b) A caged acid used to trigger MscL opening. c) The SP and MC forms of a photoswitch used to reversibly gate MscL.

12. Summary and Outlook

As outlined above, there is certainly no shortage of protein targets that could be addressed with optochemical genetics. These include naturally occurring photoreceptors, such as the channelrhodopsins, which could be fitted with synthetic switches to tune their spectral properties. However, many variants of synthetic molecules attached to naturally blind receptors are also conceivable. For example, all of the PTLs and PCLs presented herein are either agonists or blockers, but it should be possible to turn them into antagonists or find photochromic molecules that function as channel openers. In addition, photoswitchable cross-linkers could be developed that could be hooked up to two cysteine residues.[108] These have been used with great success to control the helical content of peptides,[108b,109] and they have already found applications in governing the activity of proteins.[110] It is entirely possible that this approach could be extended to transmembrane receptors, thereby providing yet another way to control neural activity with light.

Other types of photoswitches, such as hemthioindigos or SPMCs, could be systematically explored and applied in regard to neurobiologically relevant receptors. However, much could be done even if one sticks with azobenzenes, since azobenzenes can be easily tuned toward specific photophysical and thermal requirements. For example, the red-shifted variants that operate far in the visible range of the spectrum and turn themselves off in the dark need to be further developed. Perhaps, one could even push the spectral sensitivity of azobenzenes into the near-infrared, in keeping with the grand challenge of Sir Francis Crick. Even if it is not possible to develop single-photon switches that respond to these wavelengths, one could explore two-photon photoswitches that would also allow for the precise activation of PCLs in very small volumes. These could be used, for example, to photochemically stimulate a single dendritic spine, which can be simultaneously monitored with two-photon fluorescence imaging.

Light, however, is not the only "unnatural" input signal that could be considered. For example, one could reprogram a ligand-gated ion channel to respond to an orthogonal ligand, that is, a molecule that does not interact with native receptors. This strategy has already been achieved with much success with kinases and GPCRs, and it should be possible to extend this approach to other types of receptors.[111] One could even speculate about sensitizing ion channels to signals that can penetrate deep into tissues, such as radiofrequency electromagnetic fields or static magnetic fields.

Yet, as tempting as these speculations are, light is, and will remain, the most interesting input signal for neuroscience. The technology needed to quickly modulate its wavelength and intensity is highly developed and new ways to deliver light with spatiotemporal control and deep within tissues continue to emerge. These include digital micromirror arrays[112] and fiber-optic microendoscopy.[113] At the same time, genetic targeting through viral transfection is becoming increasingly

12178 www.angewandte.org

© 2011 Wiley-VCH Verlag GmbH & Co. KGaA, Weinheim

Angew. Chem. Int. Ed. **2011**, *50*, 12156–12182

24

precise and effective, and the application of synthetic photo-switches will certainly benefit from new drug-delivery techniques. Thus, we expect that many neurobiological questions will be tackled with optochemical genetics in the future.

Much could be learned, for example, about the innate function of receptors and their many isoforms, since the optical control of genetically defined receptor subtypes could clarify their individual contributions to various physiological processes (see Figure 5). So far, this has been carried out with a variety of K_v channels (see Section 6), but we anticipate that the optochemical genetic approach can be applied more broadly. Simple pharmacological approaches frequently fail because of a lack of selectivity, and genetic knock-out strategies are often inconclusive because of compensatory effects. Therefore, a knock-in animal, wherein the receptor of interest is substituted with a simple cysteine mutation for PTL attachment and can be conditionally activated and deactivated with light could be very useful.

In addition to basic neuroscience research, where the goal is to understand existing systems through systematic perturbation, one could apply optochemical genetics to what could be called "synthetic neurobiology". Here, the emphasis lies on rewiring nervous systems and altering their components to create new forms of neural processing or sensory perception. For example, the receptors that underlie our sense of temperature or mediate pain sensation could be reprogrammed to become photoreceptors. The mechanoreceptors responsible for our sense of hearing and balance could be engineered in a similar fashion. Perhaps, the day is not far away where taste receptors and odorant receptors can be stimulated with light!

This may sound a bit outlandish, but such a philosophy may actually lead to useful human therapies. A premier therapeutic target would be the retina, which can be easily reached with light, viruses, and small molecules. In many forms of blindness, such as retinitis pigmentosa, the natural photoreceptor cells of the retina, that is, the rods and cones, have been destroyed, but its remaining layers are largely intact. Their neurons express numerous receptors that could be persuaded to become light-sensitive by using PTLs or PCLs. Indeed, the first attempts to use optochemical genetics to restore vision are very promising (Figure 21). In a recent study, LiGluR was expressed in the retinal ganglion cells of blind mice after transfection with adeno-associated virus (AAV). Following injection of MAG-0 into the vitreous body, the retinal ganglion cells, which communicate directly with the brain trough the optical nerve, responded to stimulation with light. This information was relayed to the visual cortex and, as a consequence, the pupillary reflex as well as natural light-avoidance behavior of the animals was restored.[114] The first experiences with PCLs have also been promising and bode well for applications of synthetic photoswitches in human therapy.

For us, it is simply amazing that our attempts to teach old receptors new tricks have gone from a proof of principle to studies of vision restoration within seven years. This pace is likely to increase, as numerous new targets are on the horizon and a growing number of neurobiologists, biophysicists, and chemists are drawn into the field. We are convinced that these highly collaborative efforts will yield many useful techniques
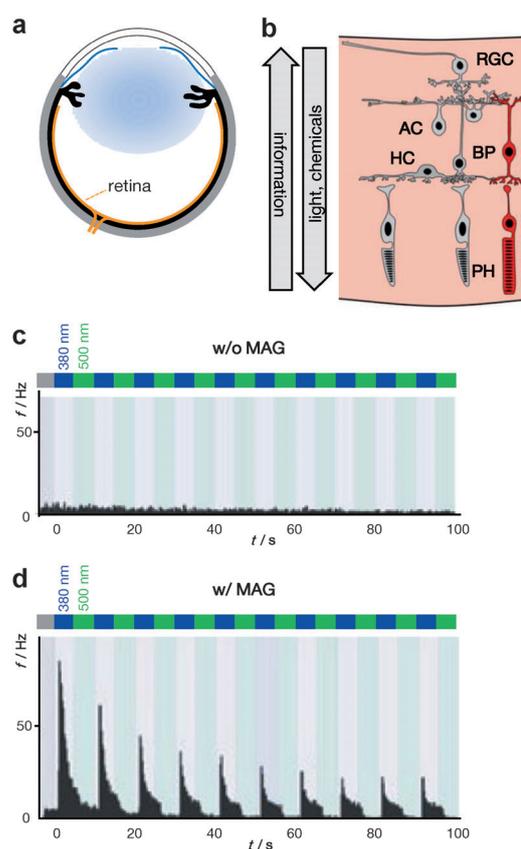
Figure 21. Restoring visual responses with synthetic photoswitches. a) Cross-section of a mouse eye with the retina shown in orange. b) A schematic diagram of the retina, showing its layered architecture. RGC: retinal ganglion cell, AC: amacrine cell, BP: bipolar cell, HC: horizontal cell, PH: photoreceptor cells (rods and cones). c), d) Electrical activity of RGCs expressing LiGluR before (c) and after addition of MAG (d).

with which to study neural networks or treat disorders of the nervous system. But usefulness aside, optochemical genetics will always remain an incredibly rewarding intellectual exercise and a nice demonstration that the complexities of
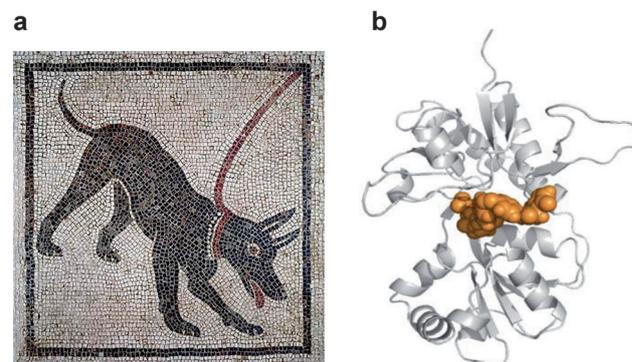
Figure 22. Harnessing the complexities of life. a) A dog (a natural creature slightly modified through breeding) with a leash (a crude device used to control its behavior, with mixed success). b) LiGluR (a complex receptor slightly modified through genetic engineering) on a comparatively simple synthetic leash.

life can be harnessed with comparatively simple synthetic chemistry (Figure 22).

13. Addendum (10. November 2011)

Orthogonal ligands, mentioned in Section 12, have recently been developed for pentameric ligand-gated ion channels.[115]

14. Abbreviations

AMPA	2-amino-3-hydroxy-5-methyl-4-isoxazole-propionic acid
AP	action potential
Ca_v	voltage-gated calcium channel
CL	caged ligand
GABA	γ-aminobutyric acid
GPCR	G-protein-coupled receptor
K_v	voltage-gated potassium channel
MscL	large-conductance mechanosensitive channel from *M. tuberculosis*
Na_v	voltage-gated sodium channel
NMDA	methyl-D-aspartate
pLGIC	pentameric ligand-gated ion channel
PTL	photoswitchable tethered ligand
PCL	photochromic ligand
SPMC	spiropyran/merocyanine photoswitch
TEA	tetraethylammonium ion
TRPV1	transient receptor potential channel, for example, subtype V1

[1] F. Crick, *Philos. Trans. R. Soc. London Ser. B* **1999**, *354*, 2021–2025.

[2] a) B. Feringa, *Molecular Switches, Vol. 1*, Wiley-VCH, Weinheim, **2001**; b) V. Balzani, M. Venturi, A. Credi, *Molecular Devices and Machines: A Journey into the Nanoworld, 2 ed.*, Wiley-VCH, Weinheim, **2008**.

[3] M. Yoshida, E. Muneyuki, T. Hisabori, *Nat. Rev. Mol. Cell Biol.* **2001**, *2*, 669–667.

[4] T. A. Steitz, *Nat. Rev. Mol. Cell Biol.* **2008**, *9*, 242–253.

[5] a) P. Cramer, E. Arnold, *Curr. Opin. Struct. Biol.* **2009**, *19*, 680–682; b) G. Orphanides, D. Reinberg, *Nature* **2000**, *407*, 471–475.

[6] J. R. Kardon, R. D. Vale, *Nat. Rev. Mol. Cell Biol.* **2009**, *10*, 854–865.

[7] S. Choe, *Nat. Rev. Neurosci.* **2002**, *3*, 115–121.

[8] a) K. Deisseroth, *Nat. Methods* **2011**, *8*, 26–29; b) S. Peron, K. Svoboda, *Nat. Methods* **2011**, *8*, 30–34; c) L. Sjulson, G. Miesenböck, *Chem. Rev.* **2008**, *108*, 1588–1602; d) F. Zhang, A. M. Aravanis, A. Adamantidis, L. de Lecea, K. Deisseroth, *Nat. Rev. Neurosci.* **2007**, *8*, 577–581.

[9] a) P. Gorostiza, E. Y. Isacoff, *Science* **2008**, *322*, 395–399; b) R. H. Kramer, D. L. Fortin, D. Trauner, *Curr. Opin. Neurobiol.* **2009**, *19*, 544–552.

[10] D. A. Doyle, J. Morais Cabral, R. A. Pfuetzner, A. Kuo, J. M. Gulbis, S. L. Cohen, B. T. Chait, R. MacKinnon, *Science* **1998**, *280*, 69–77.

[11] a) D. M. Rosenbaum, C. Zhang, J. A. Lyons, R. Holl, D. Aragao, D. H. Arlow, S. G. Rasmussen, H. J. Choi, B. T. Devree, R. K. Sunahara, P. S. Chae, S. H. Gellman, R. O. Dror, D. E. Shaw, W. I. Weis, M. Caffrey, P. Gmeiner, B. K. Kobilka, *Nature* **2011**, *469*, 236–240; b) T. Okada, M. Sugihara, A. N. Bondar, M. Elstner, P. Entel, V. Buss, *J. Mol. Biol.* **2004**, *342*, 571–583; c) F. Xu, H. Wu, V. Katritch, G. W. Han, K. A. Jacobson, Z. G. Gao, V. Cherezov, R. C. Stevens, *Science* **2011**, *332*, 322–327; d) E. Y. Chien, W. Liu, Q. Zhao, V. Katritch, G. W. Han, M. A. Hanson, L. Shi, A. H. Newman, J. A. Javitch, V. Cherezov, R. C. Stevens, *Science* **2010**, *330*, 1091–1095.

[12] A. I. Sobolevsky, M. P. Rosconi, E. Gouaux, *Nature* **2009**, *462*, 745–756.

[13] T. Kawate, J. C. Michel, W. T. Birdsong, E. Gouaux, *Nature* **2009**, *460*, 592–598.

[14] a) Y. Jiang, A. Lee, J. Chen, V. Ruta, M. Cadene, B. T. Chait, R. MacKinnon, *Nature* **2003**, *423*, 33–41; b) S. B. Long, E. B. Campbell, R. Mackinnon, *Science* **2005**, *309*, 897–903.

[15] a) N. Unwin, *J. Mol. Biol.* **2005**, *346*, 967–989; b) R. J. Hilf, R. Dutzler, *Nature* **2008**, *452*, 375–379; c) R. J. Hilf, R. Dutzler, *Nature* **2009**, *457*, 115–118.

[16] X. Chen, Q. Wang, F. Ni, J. Ma, *Proc. Natl. Acad. Sci. USA* **2010**, *107*, 11352–11357.

[17] a) E. R. Kandel, J. Schwartz, T. Jessell, *Principles of Neural Science, 4 ed.*, Elsevier, Dordrecht, **2000**; b) B. P. Bean, *Nat. Rev. Neurosci.* **2007**, *8*, 451–465; c) B. Hille, *Ionic Channels of Excitable Membranes, 3 ed.*, Sinauer, Sunderland, **2001**.

[18] C. Yue, Y. Yaari, *J. Neurosci.* **2004**, *24*, 4614–4624.

[19] W. M. Oldham, H. E. Hamm, *Nat. Rev. Mol. Cell Biol.* **2008**, *9*, 60–71.

[20] D. E. Nichols, C. D. Nichols, *Chem. Rev.* **2008**, *108*, 1614–1641.

[21] S. W. Hell, *Nat. Methods* **2009**, *6*, 24–32.

[22] W. Denk, J. H. Strickler, W. W. Webb, *Science* **1990**, *248*, 73–76.

[23] J. N. Kerr, W. Denk, *Nat. Rev. Neurosci.* **2008**, *9*, 195–205.

[24] B. V. Zemelman, G. A. Lee, M. Ng, G. Miesenböck, *Neuron* **2002**, *33*, 15–22.

[25] a) G. Nagel, T. Szellas, W. Huhn, S. Kateriya, N. Adeishvili, P. Berthold, D. Ollig, P. Hegemann, E. Bamberg, *Proc. Natl. Acad. Sci. USA* **2003**, *100*, 13940–13945; b) E. S. Boyden, F. Zhang, E. Bamberg, G. Nagel, K. Deisseroth, *Nat. Neurosci.* **2005**, *8*, 1263–1268.

[26] E. S. Boyden, F. Zhang, E. Bamberg, G. Nagel, K. Deisseroth, *Nat. Neurosci.* **2005**, *8*, 1263–1268.

[27] F. Zhang, L. P. Wang, M. Brauner, J. F. Liewald, K. Kay, N. Watzke, P. G. Wood, E. Bamberg, G. Nagel, A. Gottschalk, K. Deisseroth, *Nature* **2007**, *446*, 633–639.

[28] a) A. Berndt, P. Schoenenberger, J. Mattis, K. M. Tye, K. Deisseroth, P. Hegemann, T. G. Oertner, *Proc. Natl. Acad. Sci. USA* **2011**, *108*, 7595–7600; b) V. Gradinaru, F. Zhang, C. Ramakrishnan, J. Mattis, R. Prakash, I. Diester, I. Goshen, K. R. Thompson, K. Deisseroth, *Cell* **2010**, *141*, 154–165; c) L. A. Gunaydin, O. Yizhar, A. Berndt, V. S. Sohal, K. Deisseroth, P. Hegemann, *Nat. Neurosci.* **2010**, *13*, 387–392;

d) A. Berndt, O. Yizhar, L. A. Gunaydin, P. Hegemann, K. Deisseroth, *Nat. Neurosci.* **2009**, *12*, 229 – 234; e) F. Zhang, M. Prigge, F. Beyriere, S. P. Tsunoda, J. Mattis, O. Yizhar, P. Hegemann, K. Deisseroth, *Nat. Neurosci.* **2008**, *11*, 631 – 633.

[29] B. Y. Chow, X. Han, A. S. Dobry, X. Qian, A. S. Chuong, M. Li, M. A. Henninger, G. M. Belfort, Y. Lin, P. E. Monahan, E. S. Boyden, *Nature* **2010**, *463*, 98 – 102.

[30] V. Gradinaru, M. Mogri, K. R. Thompson, J. M. Henderson, K. Deisseroth, *Science* **2009**, *324*, 354 – 359.

[31] V. Busskamp, J. Duebel, D. Balya, M. Fradot, T. J. Viney, S. Siegert, A. C. Groner, E. Cabuy, V. Forster, M. Seeliger, M. Biel, P. Humphries, M. Paques, S. Mohand-Said, D. Trono, K. Deisseroth, J. A. Sahel, S. Picaud, B. Roska, *Science* **2010**, *329*, 413 – 417.

[32] A. B. Arrenberg, D. Y. Stainier, H. Baier, J. Huisken, *Science* **2010**, *330*, 971 – 974.

[33] G. C. Ellis-Davies, *Nat. Methods* **2007**, *4*, 619 – 628.

[34] J. Noguchi, A. Nagaoka, S. Watanabe, G. C. Ellis-Davies, K. Kitamura, M. Kano, M. Matsuzaki, H. Kasai, *J. Physiol.* **2011**, *589*, 2447 – 2457.

[35] B. V. Zemelman, N. Nesnas, G. A. Lee, G. Miesenböck, *Proc. Natl. Acad. Sci. USA* **2003**, *100*, 1352 – 1357.

[36] a) P. J. Alaimo, M. A. Shogren-Knaak, K. M. Shokat, *Curr. Opin. Chem. Biol.* **2001**, *5*, 360 – 367; b) S. L. Schreiber, *Bioorg. Med. Chem.* **1998**, *6*, 1127 – 1152; c) B. R. Stockwell, *Nat. Rev. Genet.* **2000**, *1*, 116 – 125.

[37] M. J. Keiser, V. Setola, J. J. Irwin, C. Laggner, A. I. Abbas, S. J. Hufeisen, N. H. Jensen, M. B. Kuijer, R. C. Matos, T. B. Tran, R. Whaley, R. A. Glennon, J. Hert, K. L. Thomas, D. D. Edwards, B. K. Shoichet, B. L. Roth, *Nature* **2009**, *462*, 175 – 181.

[38] a) M. E. Hahn, T. W. Muir, *Trends Biochem. Sci.* **2005**, *30*, 26 – 34; b) M. E. Hahn, T. W. Muir, *Trends. Biochem. Sci.* **2005**, *30*, 26 – 34; c) M. A. Shogren-Knaak, P. J. Alaimo, K. M. Shokat, *Annu. Rev. Cell Biol.* **2001**, *17*, 405 – 433.

[39] M. R. Banghart, M. Volgraf, D. Trauner, *Biochemistry* **2006**, *45*, 15129 – 15141.

[40] F. Hamon, F. Djedaini-Pilard, F. Barbot, C. Len, *Tetrahedron* **2009**, *65*, 10105 – 10123.

[41] P. Gorostiza, M. Volgraf, R. Numano, S. Szobota, D. Trauner, E. Y. Isacoff, *Proc. Natl. Acad. Sci. USA* **2007**, *104*, 10865 – 10870.

[42] A. Mourot, M. Kienzler, M. Banghart, T. Fehrentz, F. Huber, M. Stein, R. H. Kramer, D. Trauner, *ACS. Chem. Neurosci.* **2011**, *2*, 536 – 543.

[43] a) P. V. Chang, J. A. Prescher, M. J. Hangauer, C. R. Bertozzi, *J. Am. Chem. Soc.* **2007**, *129*, 8400 – 8401; b) J. A. Prescher, C. R. Bertozzi, *Nat. Chem. Biol.* **2005**, *1*, 13 – 21; c) J. A. Prescher, D. H. Dube, C. R. Bertozzi, *Nature* **2004**, *430*, 873 – 877.

[44] F. Tombola, M. M. Pathak, E. Y. Isacoff, *Annu. Rev. Cell Dev. Biol.* **2006**, *22*, 23 – 52.

[45] H. Wulff, N. A. Castle, L. A. Pardo, *Nat. Rev. Drug Discovery* **2009**, *8*, 982 – 1001.

[46] Y. Jiang, A. Lee, J. Chen, M. Cadene, B. T. Chait, R. MacKinnon, *Nature* **2002**, *417*, 515 – 522.

[47] a) M. Nishida, M. Cadene, B. T. Chait, R. MacKinnon, *EMBO J.* **2007**, *26*, 4005 – 4015; b) M. Nishida, R. MacKinnon, *Cell* **2002**, *111*, 957 – 965; c) S. Pegan, C. Arrabit, W. Zhou, W. Kwiatkowski, A. Collins, P. A. Slesinger, S. Choe, *Nat. Neurosci.* **2005**, *8*, 279 – 287.

[48] N. Shi, S. Ye, A. Alam, L. Chen, Y. Jiang, *Nature* **2006**, *440*, 570 – 574.

[49] a) T. Hoshi, W. N. Zagotta, R. W. Aldrich, *Science* **1990**, *250*, 533 – 538; b) W. N. Zagotta, T. Hoshi, R. W. Aldrich, *Science* **1990**, *250*, 568 – 571.

[50] a) L. G. Cuello, V. Jogini, D. M. Cortes, A. C. Pan, D. G. Gagnon, O. Dalmas, J. F. Cordero-Morales, S. Chakrapani, B. Roux, E. Perozo, *Nature* **2010**, *466*, 272 – 275; b) L. G. Cuello, V. Jogini, D. M. Cortes, E. Perozo, *Nature* **2010**, *466*, 203 – 208; c) L. Kiss, S. J. Korn, *Biophys. J.* **1998**, *74*, 1840 – 1849.

[51] C. Hammond, *Cellular and Molecular Neurophysiology*, 3 ed., Elsevier Science, Dordrecht, **2008**.

[52] a) K. G. Chandy, M. Cahalan, M. Pennington, R. S. Norton, H. Wulff, G. A. Gutman, *Toxicon* **2001**, *39*, 1269 – 1276; b) M. A. Eriksson, B. Roux, *Biophys. J.* **2002**, *83*, 2595 – 2609.

[53] C. M. Armstrong, *J. Gen. Physiol.* **1971**, *58*, 413 – 437.

[54] M. J. Lenaeus, M. Vamvouka, P. J. Focia, A. Gross, *Nat. Struct. Mol. Biol.* **2005**, *12*, 454 – 459.

[55] M. Banghart, K. Borges, E. Isacoff, D. Trauner, R. H. Kramer, *Nat. Neurosci.* **2004**, *7*, 1381 – 1386.

[56] a) R. O. Blaustein, *J. Gen. Physiol.* **2002**, *120*, 203 – 216; b) R. O. Blaustein, P. A. Cole, C. Williams, C. Miller, *Nat. Struct. Mol. Biol.* **2000**, *7*, 309 – 311.

[57] J. J. Chambers, M. R. Banghart, D. Trauner, R. H. Kramer, *J. Neurophysiol.* **2006**, *96*, 2792 – 2796.

[58] D. L. Fortin, T. W. Dunn, A. Fedorchak, D. Allen, R. Montpetit, M. R. Banghart, D. Trauner, J. P. Adelman, R. H. Kramer, *J. Neurophysiol.* **2011**, *106*, 488 – 496.

[59] a) M. R. Banghart, A. Mourot, D. L. Fortin, J. Z. Yao, R. H. Kramer, D. Trauner, *Angew. Chem.* **2009**, *121*, 9261 – 9265; *Angew. Chem. Int. Ed.* **2009**, *48*, 9097 – 9101; b) D. L. Fortin, M. R. Banghart, T. W. Dunn, K. Borges, D. A. Wagenaar, Q. Gaudry, M. H. Karakossian, T. S. Otis, W. B. Kristan, D. Trauner, R. H. Kramer, *Nat. Methods* **2008**, *5*, 331 – 338.

[60] R. W. Gereau, G. T. Swanson, *The Glutamate Receptors*, Humana Press, New York, **2008**.

[61] a) G. N. Barnes, J. T. Slevin, *Curr. Med. Chem.* **2003**, *10*, 2059 – 2072; b) M. R. Farlow, *Geriatrics* **2004**, *59*, 22 – 27.

[62] S. F. Traynelis, L. P. Wollmuth, C. J. McBain, F. S. Menniti, K. M. Vance, K. K. Ogden, K. B. Hansen, H. Yuan, S. J. Myers, R. Dingledine, *Pharmacol. Rev.* **2010**, *62*, 405 – 496.

[63] M. L. Mayer, *Neuron* **2005**, *45*, 539 – 552.

[64] a) G. L. Collingridge, J. T. Isaac, Y. T. Wang, *Nat. Rev. Neurosci.* **2004**, *5*, 952 – 962; b) C. G. Lau, R. S. Zukin, *Nat. Rev. Neurosci.* **2007**, *8*, 413 – 426.

[65] P. Stawski, H. Janovjak, D. Trauner, *Bioorg. Med. Chem.* **2010**, *18*, 7759 – 7772.

[66] M. Volgraf, P. Gorostiza, R. Numano, R. H. Kramer, E. Y. Isacoff, D. Trauner, *Nat. Chem. Biol.* **2006**, *2*, 47 – 52.

[67] M. H. Nanao, T. Green, Y. Stern-Bach, S. F. Heinemann, S. Choe, *Proc. Natl. Acad. Sci. USA* **2005**, *102*, 1708 – 1713.

[68] S. Szobota, P. Gorostiza, F. Del Bene, C. Wyart, D. L. Fortin, K. D. Kolstad, O. Tulyathan, M. Volgraf, R. Numano, H. L. Aaron, E. K. Scott, R. H. Kramer, J. Flannery, H. Baier, D. Trauner, E. Y. Isacoff, *Neuron* **2007**, *54*, 535 – 545.

[69] R. Numano, S. Szobota, A. Y. Lau, P. Gorostiza, M. Volgraf, B. Roux, D. Trauner, E. Y. Isacoff, *Proc. Natl. Acad. Sci. USA* **2009**, *106*, 6814 – 6819.

[70] H. Janovjak, S. Szobota, C. Wyart, D. Trauner, E. Y. Isacoff, *Nat. Neurosci.* **2010**, *13*, 1027 – 1032.

[71] G. Q. Chen, C. Cui, M. L. Mayer, E. Gouaux, *Nature* **1999**, *402*, 817 – 821.

[72] C. Wyart, F. Del Bene, E. Warp, E. K. Scott, D. Trauner, H. Baier, E. Y. Isacoff, *Nature* **2009**, *461*, 407 – 410.

[73] M. Volgraf, P. Gorostiza, S. Szobota, M. R. Helix, E. Y. Isacoff, D. Trauner, *J. Am. Chem. Soc.* **2007**, *129*, 260 – 261.

[74] Z. R. Abrams, A. Warrier, D. Trauner, X. Zhang, *Front Neural Circuits* **2010**, *4*, 13.

[75] M. O. Ortells, G. G. Lunt, *Trends Neurosci.* **1995**, *18*, 121 – 127.

[76] a) J. Bormann, A. Feigenspan, *Trends Neurosci.* **1995**, *18*, 515 – 519; b) U. Rudolph, H. Mohler, *Annu. Rev. Pharm. Toxicol.* **2004**, *44*, 475 – 498; c) W. Sieghart, G. Sperk, *Curr. Top. Med. Chem.* **2002**, *2*, 795 – 816.

27

[77] a) C. M. Becker, *Neuroscientist* **1995**, *1*, 130–141; b) E. Y. Kim, N. Schrader, B. Smolinsky, C. Bedet, C. Vannier, G. Schwarz, H. Schindelin, *EMBO J.* **2006**, *25*, 1385–1395.

[78] a) P. J. Corringer, N. Le Novere, J. P. Changeux, *Annu. Rev. Pharm. Toxicol.* **2000**, *40*, 431–458; b) A. Karlin, *Nat. Rev. Neurosci.* **2002**, *3*, 102–114.

[79] D. Paterson, A. Nordberg, *Prog. Neurobiol.* **2000**, *61*, 75–111.

[80] N. Unwin, *FEBS Lett.* **2003**, *555*, 91–95.

[81] a) Y. Bourne, T. T. Talley, S. B. Hansen, P. Taylor, P. Marchot, *EMBO J.* **2005**, *24*, 1512–1522; b) K. Brejc, W. J. van Dijk, R. V. Klaassen, M. Schuurmans, J. van Der Oost, A. B. Smit, T. K. Sixma, *Nature* **2001**, *411*, 269–276; c) P. H. Celie, S. E. van Rossum-Fikkert, W. J. van Dijk, K. Brejc, A. B. Smit, T. K. Sixma, *Neuron* **2004**, *41*, 907–914; d) S. B. Hansen, G. Sulzenbacher, T. Huxford, P. Marchot, P. Taylor, Y. Bourne, *EMBO J.* **2005**, *24*, 3635–3646.

[82] M. Brams, A. Pandya, D. Kuzmin, R. van Elk, L. Krijnen, J. L. Yakel, V. Tsetlin, A. B. Smit, C. Ulens, *PLoS. Biol.* **2011**, *9*, e1001034.

[83] E. Bartels, N. H. Wassermann, B. F. Erlanger, *Proc. Natl. Acad. Sci. USA* **1971**, *68*, 1820–1823.

[84] H. A. Lester, H. W. Chang, *Nature* **1977**, *266*, 373–374.

[85] a) L. D. Chabala, H. A. Lester, *J. Physiol.* **1986**, *379*, 83–108; b) H. A. Lester, M. E. Krouse, M. M. Nass, N. H. Wassermann, B. F. Erlanger, *J. Gen. Physiol.* **1980**, *75*, 207–232.

[86] J. Payandeh, T. Scheuer, N. Zheng, W. A. Catterall, *Nature* **2011**, *465*, 353–358.

[87] C. B. Felder, R. C. Graul, A. Y. Lee, H. P. Merkle, W. Sadee, *AAPS PharmSci* **1999**, *1*, 7–26.

[88] E. Michard, P. T. Lima, F. Borges, A. C. Silva, M. T. Portes, J. E. Carvalho, M. Gilliham, L. H. Liu, G. Obermeyer, J. A. Feijo, *Science* **2011**, *332*, 434–437.

[89] H. Janovjak, G. Sandoz, E. Y. Isacoff, *Nat. Commun.* **2011**, *2*, 232.

[90] H. Brauner-Osborne, P. Wellendorph, A. A. Jensen, *Curr. Drug. Targets* **2007**, *8*, 169–184.

[91] J. P. Pin, J. Kniazeff, V. Binet, J. Liu, D. Maurel, T. Galvez, B. Duthey, M. Havlickova, J. Blahos, L. Prezeau, P. Rondard, *Biochem. Pharmacol.* **2004**, *68*, 1565–1572.

[92] a) M. Behrens, W. Meyerhof, C. Hellfritsch, T. Hofmann, *Angew. Chem.* **2011**, *123*, 2268–2291; *Angew. Chem. Int. Ed.* **2011**, *50*, 2220–2242; b) G. Q. Zhao, Y. Zhang, M. A. Hoon, J. Chandrashekar, I. Erlenbach, N. J. Ryba, C. S. Zuker, *Cell* **2003**, *115*, 255–266.

[93] T. Muto, D. Tsuchiya, K. Morikawa, H. Jingami, *Proc. Natl. Acad. Sci. USA* **2007**, *104*, 3759–3764.

[94] X. L. He, A. Dukkipati, K. C. Garcia, *J. Mol. Biol.* **2006**, *361*, 698–714.

[95] J. Vicogne, J. P. Pin, V. Lardans, M. Capron, C. Noel, C. Dissous, *Mol. Biochem. Parasitol.* **2003**, *126*, 51–62.

[96] V. Cherezov, D. M. Rosenbaum, M. A. Hanson, S. G. Rasmussen, F. S. Thian, T. S. Kobilka, H. J. Choi, P. Kuhn, W. I. Weis, B. K. Kobilka, R. C. Stevens, *Science* **2007**, *318*, 1258–1265.

[97] B. S. Khakh, *Nat. Rev. Neurosci.* **2001**, *2*, 165–174.

[98] Y. Yu, Z. Chen, W. G. Li, H. Cao, E. G. Feng, F. Yu, H. Liu, H. Jiang, T. L. Xu, *Neuron* **2010**, *68*, 61–72.

[99] a) E. B. Gonzales, T. Kawate, E. Gouaux, *Nature* **2009**, *460*, 599–604; b) J. Jasti, H. Furukawa, E. B. Gonzales, E. Gouaux, *Nature* **2007**, *449*, 316–323.

[100] L. Schild, *Biochim. Biophys. Acta Mol. Basis Dis.* **2010**, *1802*, 1159–1165.

[101] A. I. Basbaum, D. M. Bautista, G. Scherrer, D. Julius, *Cell* **2009**, *139*, 267–284.

[102] M. J. Caterina, M. A. Schumacher, M. Tominaga, T. A. Rosen, J. D. Levine, D. Julius, *Nature* **1997**, *389*, 816–824.

[103] A. P. Christensen, D. P. Corey, *Nat. Rev. Neurosci.* **2007**, *8*, 510–521.

[104] A. Kocer, M. Walko, W. Meijberg, B. L. Feringa, *Science* **2005**, *309*, 755–758.

[105] G. Chang, R. H. Spencer, A. T. Lee, M. T. Barclay, D. C. Rees, *Science* **1998**, *282*, 2220–2226.

[106] a) K. Yoshimura, A. Batiza, C. Kung, *Biophys. J.* **2001**, *80*, 2198–2206; b) K. Yoshimura, A. Batiza, M. Schröder, P. Blount, C. Kung, *Biophys. J.* **1999**, *77*, 1960–1972.

[107] J. H. Folgering, J. M. Kuiper, A. H. de Vries, J. B. Engberts, B. Poolman, *Langmuir* **2004**, *20*, 6985–6987.

[108] A. A. Beharry, L. Wong, V. Tropepe, G. A. Woolley, *Angew. Chem.* **2011**, *123*, 1361–1363; *Angew. Chem. Int. Ed.* **2011**, *50*, 1325–1327.

[109] J. A. Ihalainen, B. Paoli, S. Muff, E. H. Backus, J. Bredenbeck, G. A. Woolley, A. Caflisch, P. Hamm, *Proc. Natl. Acad. Sci. USA* **2008**, *105*, 9588–9593.

[110] F. Bonardi, G. London, N. Nouwen, B. L. Feringa, A. J. Driessen, *Angew. Chem.* **2010**, *122*, 7392–7396; *Angew. Chem. Int. Ed.* **2010**, *49*, 7234–7238.

[111] a) B. N. Armbruster, X. Li, M. H. Pausch, S. Herlitze, B. L. Roth, *Proc. Natl. Acad. Sci. USA* **2007**, *104*, 5163–5168; b) B. R. Conklin, E. C. Hsiao, S. Claeysen, A. Dumuis, S. Srinivasan, J. R. Forsayeth, J. M. Guettier, W. C. Chang, Y. Pei, K. D. McCarthy, R. A. Nissenson, J. Wess, J. Bockaert, B. L. Roth, *Nat. Methods* **2008**, *5*, 673–678.

[112] S. Wang, S. Szobota, Y. Wang, M. Volgraf, Z. Liu, C. Sun, D. Trauner, E. Y. Isacoff, X. Zhang, *Nano Lett.* **2007**, *7*, 3859–3863.

[113] a) K. Deisseroth, G. Feng, A. K. Majewska, G. Miesenböck, A. Ting, M. J. Schnitzer, *J. Neurosci.* **2006**, *26*, 10380–10386; b) B. A. Wilt, L. D. Burns, E. T. Wei Ho, K. K. Ghosh, E. A. Mukamel, M. J. Schnitzer, *Annu. Rev. Neurosci.* **2009**, *32*, 435–506.

[114] N. Caporale, K. D. Kolstad, T. Lee, I. Tochitshy, D. Dalkara, D. Trauner, R. H. Kramer, Y. Dan, E. Y. Isacoff, J. C. Flannery, *Mol. Ther.* **2011**, *19*, 1212–1219.

[115] C. J. Magnus, P. H. Lee, D. Atasoy, H. H. Su, L. L. Looger, S. M. Sternson, *Science* **2011**, *333*, 1292–1296.

28

2) Rapid optical control of nociception with an ion-channel photoswitch

2.1) Introduction

Local and general anesthetics have a long history in the suppression of pain and perception.[1] Both pharmaceutical strategies play an important role during therapeutic interventions like surgery and exhibit distinct mode of actions.

General anesthetics, including propofol (**1**) and isoflurane (**2**) produce anesthesia, unconsciousness, analgesia and immobility (Fig. 1).[1] Little is known about the molecular and cellular targets. Recently $GABA_A$ receptors have been identified as molecular targets of several general anesthetics. New evidence suggest that several brain areas are involved in procedure of establishing the typical symptoms of general anesthetics.[1]

Local anesthetics play, besides their role in surgery, a fundamental role in the treatment of acute and chronic pain. Famous pharmacological representatives are lidocaine (**3**), its permanently charged derivative QX-314 (**4**), procaine (**5**) and tetracaine (**6**) (Fig. 1). They typically silence neuronal activity by blocking voltage-gated sodium (Na_v) channels and thus prevent the initiation of action potentials.[2] The prevention of Na_v channel conductance follows the principle of use-dependent block.[3] Here the channel has to be opened first by a depolarization of the membrane before the local anesthetic can block the channel.

The class of neurons that are responsible for sensing acute pain and represent the main cellular target of local anesthetics are called nociceptors (Fig. 1).[4] Cell bodies of nociceptors are located in dorsal root ganglia throughout the body, whereas in the head they innervate the trigeminal ganglion.[4] The branches of nociceptors project from the epidermis to the dorsal horn of the spinal cord. From there on information is processed into hierarchically higher regions of the brain, like the brainstem and the somatosensory cortex.[4]

Different nociceptors types can be divided into myelinated Aδ afferents and unmyelinated C fibers. Distinct subclasses of the Aδ afferents and C fibers are responsible for the detection of noxious temperatures or violent pressure. Type II nociceptors, which belong to the Aδ afferents, have a high mechanical threshold and are responsible for the detection of temperature induced acute pain. Silent nociceptors, a subclass of C fibers, are responsible for the slow temperature induced pain.[4]
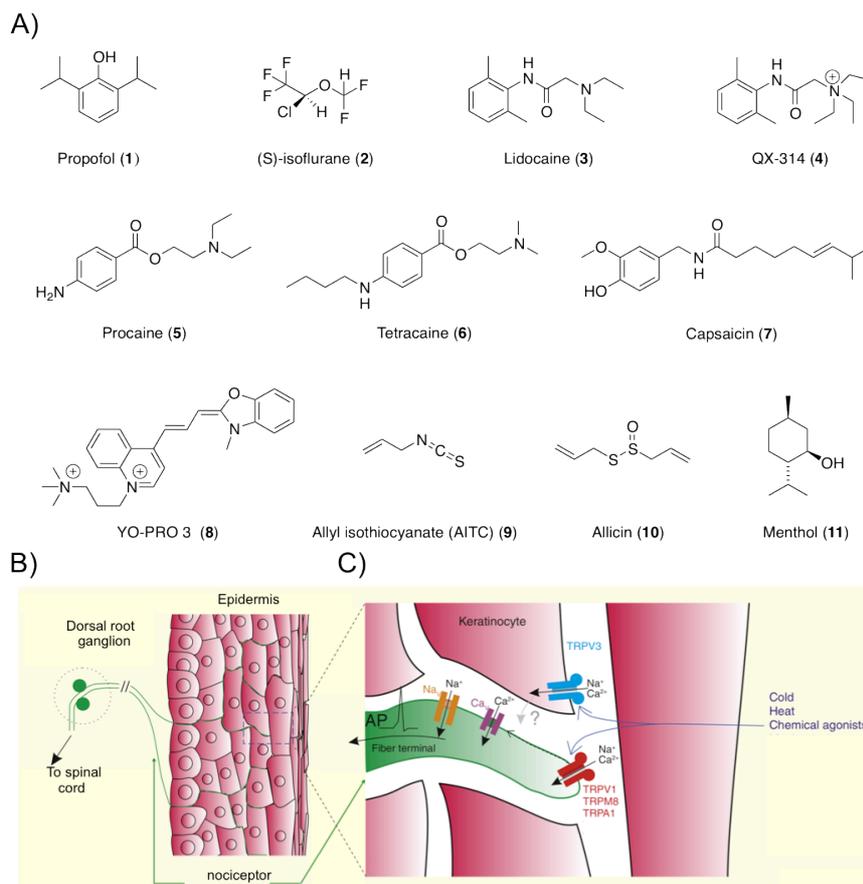
Figure 1. A) Chemical structures of general anesthetics, local anesthetics, dyes and TRP channel agonists. **B**) Schematic depiction of sensory neurons (nociceptors), projecting from the spinal cord into the skin. **C**) TRP channels responsible for the detection of cold, heat and chemical irritants expressed in nociceptors and keratinocytes (modified from publication[5]).

In recent years several ion channels that detect the physical and chemical stimuli of heat, chemical irritants and pressure have been found and characterized.[4,6,7,8,9,10,11,12,13,14,15] Detection of heat and cold is associated with the transient receptor potential (TRP) ion channel family, including the cation selective channels TRPV1, TRPV3, TRPM8, TRPM3.[4,6,7,8,9,10,11,12,13,14,15] TRPV1 and TRPA1 are

mainly expressed in nociceptors.[9,16] Activation of TRPV1 and TRPA1 leads to membrane depolarization, triggering action potential firing and thus pain sensation. TRPV1 opens at temperatures above 37 °C and is also activated by the hot chili ingredient capsaicin (**7**) or by acidic pH.[4,8,9] The tetrameric structure of the channel shares similarities with K_v channels. Prolonged capsaicin (**7**) stimulation of TRPV1 leads to a dilation of the channel pore, which allows huge dyes like YO-PRO 3 (**8**) to enter the cell.[17] Currently the question whether the process of pore dilation occurs under normal physiological tissue conditions or in pain states remains unanswered. TRPA1 represents a cation selective ion channel that is activated by chemical irritants such as allyl isothiocyanate (AITC) (**9**) and allicin (**10**).[6,18,19] Both TRPA1 and TRPV1 share the phenomena of pore dilation, which is initiated for TRPA1 after prolonged AITC (**9**) application.[20] In contrast, the cold sensing ion channel TRPM8 that is activated by menthol (**11**) does not show any agonist induced pore dilation.[20]

Application of lidocaine (**3**) to prevent pain usually affects other neurons in proximity to the treated tissue region, which is due to the membrane permeability of the drug. Thus, patients treated with lidocaine (**3**) suffer from paralysis due to block of motor axons, block of autonomic fibers and numbness from the block of low-threshold pressure receptors. The discovery of the TRPV1 pore dilation provided the opportunity to deliver drugs through this conduit selectively into nociceptors.[21] The coapplication of QX-314 (**4**) and capsaicin (**7**) on inflamed animal tissue resulted in a strong reduction of the side effects providing a potential new strategy in pain treatment.[21]

In the attached paper a PCL called QAQ is described, which contains twice the QX-314 (**4**) structure.[22] The photoswitch allows to reversibly light control the conductance of voltage-gated sodium (Na_v), calcium (Ca_v) and potassium (K_v) channels from the internal site. Under 500 nm light or in the dark, QAQ rests in its *trans* state and blocks voltage-gated ion channels. Illumination with 380 nm light converts QAQ into its *cis* state and releases channel block. QAQ is membrane impermeable and acts as a reversible neuronal silencer once introduced into neurons. Based on the limited expression of TRPV1 to nociceptors and the agonist induced pore dilation of TRPV1,[17] QAQ can be selectively loaded into these neurons

allowing for reversible control of neuronal activity. Thus, QAQ acts as a light regulated local anesthetic.[22]

[1]   H. C. Hemmings, Jr., M. H. Akabas, P. A. Goldstein, J. R. Trudell, B. A. Orser, N. L. Harrison, *Trend. Pharma.Sci.* **2005**, *26*, 503-510.
[2]   A. Scholz, *British journal of anaesthesia* **2002**, *89*, 52-61.
[3]   B. Hille, *Ionic channels of excitable membranes*, 3 ed., Sinauer Associates, Inc., **2001**.
[4]   A. I. Basbaum, D. M. Bautista, G. Scherrer, D. Julius, *Cell* **2009**, *139*, 267-284.
[5]   N. Damann, T. Voets, B. Nilius, *Curr. Bio. : CB* **2008**, *18*, R880-889.
[6]   D. M. Bautista, S. E. Jordt, T. Nikai, P. R. Tsuruda, A. J. Read, J. Poblete, E. N. Yamoah, A. I. Basbaum, D. Julius, *Cell* **2006**, *124*, 1269-1282.
[7]   D. M. Bautista, J. Siemens, J. M. Glazer, P. R. Tsuruda, A. I. Basbaum, C. L. Stucky, S. E. Jordt, D. Julius, *Nature* **2007**, *448*, 204-208.
[8]   M. J. Caterina, T. A. Rosen, M. Tominaga, A. J. Brake, D. Julius, *Nature* **1999**, *398*, 436-441.
[9]   M. J. Caterina, M. A. Schumacher, M. Tominaga, T. A. Rosen, J. D. Levine, D. Julius, *Nature* **1997**, *389*, 816-824.
[10]   B. Coste, J. Mathur, M. Schmidt, T. J. Earley, S. Ranade, M. J. Petrus, A. E. Dubin, A. Patapoutian, *Science* **2010**, *330*, 55-60.
[11]   B. Coste, B. Xiao, J. S. Santos, R. Syeda, J. Grandl, K. S. Spencer, S. E. Kim, M. Schmidt, J. Mathur, A. E. Dubin, M. Montal, A. Patapoutian, *Nature* **2012**, *483*, 176-181.
[12]   A. M. Peier, A. J. Reeve, D. A. Andersson, A. Moqrich, T. J. Earley, A. C. Hergarden, G. M. Story, S. Colley, J. B. Hogenesch, P. McIntyre, S. Bevan, A. Patapoutian, *Science* **2002**, *296*, 2046-2049.
[13]   G. M. Story, A. M. Peier, A. J. Reeve, S. R. Eid, J. Mosbacher, T. R. Hricik, T. J. Earley, A. C. Hergarden, D. A. Andersson, S. W. Hwang, P. McIntyre, T. Jegla, S. Bevan, A. Patapoutian, *Cell* **2003**, *112*, 819-829.
[14]   J. Vriens, G. Owsianik, T. Hofmann, S. E. Philipp, J. Stab, X. Chen, M. Benoit, F. Xue, A. Janssens, S. Kerselaers, J. Oberwinkler, R. Vennekens, T. Gudermann, B. Nilius, T. Voets, *Neuron* **2011**, *70*, 482-494.
[15]   H. Xu, I. S. Ramsey, S. A. Kotecha, M. M. Moran, J. A. Chong, D. Lawson, P. Ge, J. Lilly, I. Silos-Santiago, Y. Xie, P. S. DiStefano, R. Curtis, D. E. Clapham, *Nature* **2002**, *418*, 181-186.
[16]   D. M. Bautista, P. Movahed, A. Hinman, H. E. Axelsson, O. Sterner, E. D. Hogestatt, D. Julius, S. E. Jordt, P. M. Zygmunt, *Proc. Natl. Acad. Sci. USA* **2005**, *102*, 12248-12248.
[17]   M. K. Chung, A. D. Guler, M. J. Caterina, *Nat. Neurosci.* **2008**, *11*, 555-564.
[18]   L. J. Macpherson, A. E. Dubin, M. J. Evans, F. Marr, P. G. Schultz, B. F. Cravatt, A. Patapoutian, *Nature* **2007**, *445*, 541-545.
[19]   A. Hinman, H. H. Chuang, D. M. Bautista, D. Julius, *Proc. Natl. Acad. Sci. USA* **2006**, *103*, 19564-19568.
[20]   J. Chen, D. Kim, B. R. Bianchi, E. J. Cavanaugh, C. R. Faltynek, P. R. Kym, R. M. Reilly, *Molecular pain* **2009**, *5*, 3.
[21]   A. M. Binshtok, B. P. Bean, C. J. Woolf, *Nature* **2007**, *449*, 607-610.
[22]   A. Mourot, T. Fehrentz, Y. Le Feuvre, C. M. Smith, C. Herold, D. Dalkara, F. Nagy, D. Trauner, R. H. Kramer, *Nat. Methods* **2012**, *9*, 396-402.

2.2) Publication

Rapid optical control of nociception with an ion-channel

photoswitch

Alexandre Mourot[*], **Timm Fehrentz**[*], Yves Le Feuvre, Caleb S. Smith, Christian

Herold, Deniz Dalkara, Frédéric Nagy, Dirk Trauner and Richard H. Kramer

Nature methods **2012**, *9*, 396-402.[1]

[*] authors contributed equally.

Rapid optical control of nociception with an ion-channel photoswitch

Alexandre Mourot[1,6], Timm Fehrentz[1,2,6], Yves Le Feuvre[3,4], Caleb M Smith[1], Christian Herold[1], Deniz Dalkara[5], Frédéric Nagy[3,4], Dirk Trauner[2] & Richard H Kramer[1]

Local anesthetics effectively suppress pain sensation, but most of these compounds act nonselectively, inhibiting activity of all neurons. Moreover, their actions abate slowly, preventing precise spatial and temporal control of nociception. We developed a photoisomerizable molecule, quaternary ammonium–azobenzene–quaternary ammonium (QAQ), that enables rapid and selective optical control of nociception. QAQ is membrane-impermeant and has no effect on most cells, but it infiltrates pain-sensing neurons through endogenous ion channels that are activated by noxious stimuli, primarily TRPV1. After QAQ accumulates intracellularly, it blocks voltage-gated ion channels in the *trans* form but not the *cis* form. QAQ enables reversible optical silencing of mouse nociceptive neuron firing without exogenous gene expression and can serve as a light-sensitive analgesic in rats *in vivo*. Because intracellular QAQ accumulation is a consequence of nociceptive ion-channel activity, QAQ-mediated photosensitization is a platform for understanding signaling mechanisms in acute and chronic pain.

Optogenetic tools enable photoregulation of action potential firing in neurons both *in vitro* and *in vivo*[1] through the introduction of exogenous genes. In contrast, small-molecule photoswitches enable optical control of neuronal excitability without genetic manipulation[2,3]. Photoswitch molecules confer light-sensitivity on the intrinsic excitability of neurons within minutes[4–6]. However, unlike optogenetic tools that can be promoter-targeted for expression in particular types of neurons, photoswitches act nonselectively on all neurons that are exposed to the molecule. Depending on the scientific or biomedical application, it could be a benefit or even a requirement to target photosensitivity to a particular type of neuron.

Here we used a non-genetic strategy to target a photoswitch molecule to pain-sensing (nociceptive) neurons. Nociceptive neurons have been particularly inaccessible to selective electrophysiological manipulation because both their peripheral sensory endings and central synaptic terminals are quite small, either embedded in the skin or interspersed with other neurons in the spinal cord. Nociceptors are unique in possessing a high density of ion channels that respond directly or indirectly to noxious stimuli[7]. For example, the capsaicin receptor TRPV1, which is sensitive to noxious heat, protons and mediators of inflammation, is expressed in nociceptive neurons, but it is very sparsely expressed elsewhere in the nervous system[8]. TRPV1 enters into a pore-dilated state upon prolonged agonist activation, allowing permeation of relatively large cations[9]. This property has been exploited to deliver into nociceptors a membrane-impermeant derivative of the local anesthetic lidocaine, QX-314 (ref. 10). The selective entry and silencing of nociceptors by QX-314 gives this molecule potential as a pain-selective local anesthetic[10]. However, once QX-314 enters cells, it cannot escape, and silencing persists for many hours[11]. The irreversibility of QX-314 precludes temporally precise regulation of nociceptor activity.

Here we describe QAQ, a photoisomerizable molecule that confers reversible light-sensitivity selectively onto neurons involved in pain signaling, enabling rapid optical control of nociception without genetic manipulation.

RESULTS
QAQ photosensitized voltage-gated ion channels
We developed QAQ, a photoswitch that reversibly suppresses neuronal excitability by optically regulating voltage-gated Na^+, Ca^{2+} and K^+ channels. QAQ has a central photoisomerizable azobenzene coupled on both sides to quaternary ammonium groups (**Fig. 1a**). Upon illumination with 380-nm light, the elongated *trans*-QAQ converts to the bent *cis* form (**Supplementary Fig. 1a**). *Cis*-QAQ spontaneously reverts to the *trans* form slowly in the dark (**Supplementary Fig. 1b**), but this transition occurs quickly (within milliseconds) in 500-nm light.

QAQ resembles lidocaine and its derivative QX-314 (**Fig. 1b,c**), local anesthetics that block voltage-gated Na^+, K^+ and Ca^{2+} channels from the cytoplasmic side[12,13]. Lidocaine is a tertiary amine that crosses the membrane in an uncharged state and blocks ion channels after becoming protonated in the cytoplasm.

[1]Department of Molecular and Cell Biology, University of California Berkeley, Berkeley, California, USA. [2]Department of Chemistry, University of Munich, Munich, Germany. [3]Centre National de la Recherche Scientifique, Interdisciplinary Institute for Neuroscience, Unité Mixte de Recherche 5297 'Central Mechanisms of Pain Sensitization', Bordeaux, France. [4]Université de Bordeaux, Bordeaux, France. [5]Department of Chemical Engineering and Department of Bioengineering and The Helen Wills Neuroscience Institute, University of California, Berkeley, California, USA. [6]These authors contributed equally to this work. Correspondence should be addressed to R.H.K. (rhkramer@berkeley.edu) or D.T. (dirk.trauner@cup.uni-muenchen.de).

Figure 1 | Intracellular QAQ photosensitized voltage-gated ion channels. (**a**–**c**) Chemical structures of *cis* and *trans* QAQ (**a**), lidocaine (**b**) and QX-314 (**c**). k_BT, thermal energy of relaxation, with k_B denoting the Boltzman constant and T, the temperature. (**d**) Na^+ current in cells with intracellular QAQ (100 µM). Depolarization was from −70 mV to −10 mV. Photoswitching, as defined by (current $(I)_{380\ nm} - I_{500\ nm})/I_{380\ nm}$, was 60.5 ± 5.8% (n = 4 cells) (**e**) Na^+ current in cells with extracellular QAQ (1 mM). Photoswitching was 1.4 ± 1.3% (n = 7 cells). (**f**) Current versus membrane voltage (Vm) of peak Na^+ current. (**g**) Na^+ current in cells with intracellular QAQ (100 µM) and repetitive depolarizing pulses (1 Hz). Control with no QAQ is shown. (**h**) Reversibility of Na^+ current photoswitching. (**i**) $Ca_v2.2$ current using intracellular QAQ (100 µM). Depolarizing pulse was from −60 mV to +10 mV. Photoswitching was 60.5 ± 10.5% (n = 3 cells). (**j**) Shaker K^+ channel current using intracellular QAQ (100 µM). Depolarizing pulse was from −70 mV to +40

mV. Photoswitching was 60.3 ± 8.6% (n = 4 cells). (**k**) Percentage photoswitching of currents through voltage-gated Na^+ (Na_v), voltage-gated Ca^{2+} (Ca_v) and voltage-gated K^+ (K_v) channels. 'Neuronal', Na^+ channels from NG108-15 cells; 'sensory', Na^+ channels from rat trigeminal ganglion neurons; TTX^R, tetrodotoxin-resistant; L-type, voltage-gated channels from GH3 cells; $Ca_v2.2$, $K_v2.1$, $K_v3.1$ and $K_v4.2$ were expressed in HEK-293 cells; 'hippocampal', K^+ channels from primary hippocampal cultures (n = 3–13 cells, error bars, s.e.m.). NG108-15 cells were examined in **d**–**h**, and HEK-293 cells in **i**,**j**.
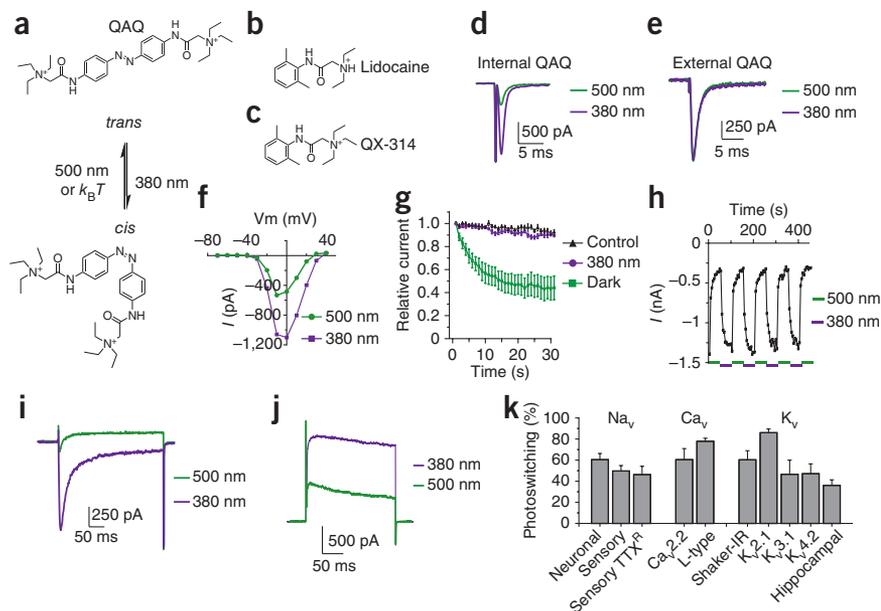
QX-314 contains a permanently charged quaternary ammonium, preventing it from crossing the membrane. However, QX-314 is a potent blocker of activity when introduced through a patch pipette into the cytoplasm[14].

To test whether QAQ can act like a photoregulated ion-channel blocker, we made whole-cell recordings from NG108-15 cells, a mouse neuroblastoma and rat glioma hybrid cell line that expresses neuronal voltage-gated Na^+ (Na_v) channels[15]. When we delivered QAQ into the cytoplasm through the patch pipette, it blocked most of the Na^+ current in the *trans* configuration, but blockade was removed in 380-nm light (**Fig. 1d**). In contrast, bath application of QAQ did not block (**Supplementary Fig. 2**) or photosensitize the Na^+ current (**Fig. 1e**), indicating that QAQ is membrane-impermeant like QX-314 (ref. 10). Light-sensitive block of the Na^+ current occurred at all membrane potentials tested (**Fig. 1f**). We quantified block of *trans*-QAQ versus *cis*-QAQ by examining Na^+ current during a train of depolarizing stimuli. In the *trans* form, the amount of QAQ blockade is use-dependent, becoming more complete with increasing duration or frequency of depolarization (56% ± 10% block after 30 s, n = 7 cells, **Fig. 1g**). In contrast, *cis*-QAQ decreased the current by 9.6% ± 0.1% (n = 7 cells), indistinguishable from control experiments with no QAQ (8.3% ± 0.1%, n = 5 cells, P = 0.52 Student's *t*-test). Photocontrol of Na^+ current could be elicited repeatedly and rapidly without decrement over many minutes (**Fig. 1h** and **Supplementary Fig. 3**).

Local anesthetics are used to silence the activity of sensory neurons, which have a variety of voltage-gated Na^+ channels, including tetrodotoxin-sensitive and -resistant types[7]. Whole-cell recordings from rat trigeminal ganglion neurons showed that both channel types could be photoregulated by intracellular QAQ (**Supplementary Fig. 4**).

QAQ also photoregulated voltage-gated Ca^{2+} channels. We recorded from HEK-293 cells stably expressing voltage-gated

Ca^{2+} channel $Ca_v2.2$ and from GH3 cells, a rat pituitary tumor cell line expressing L-type calcium channels[16]. In both cell types, internal *trans*-QAQ blocked the Ca^{2+} current, but blockade was removed in 380-nm light (**Fig. 1i** and **Supplementary Fig. 5a**). Photoregulation of both Ca^{2+} channels was rapid, occurred at all voltages tested and exhibited little decrement over time (**Supplementary Fig. 5b–f**).

Voltage-gated K^+ channels were also sensitive to QAQ. We recorded from HEK-293 cells expressing the inactivation-removed Shaker K^+ channel[17] and again observed robust photoregulation, with current blocked by *trans*-QAQ and unblocked by converting the molecule to the *cis* form (**Fig. 1j**). QAQ block at 500 nm was voltage-dependent, increasing with depolarization, as observed with other quaternary ammonium molecules[5] (**Supplementary Fig. 6a**). QAQ photosensitized other voltage-gated K^+ channels exogenously expressed in HEK-293 cells as well as native K^+ current in hippocampal neurons (**Supplementary Fig. 6b–j**). Photoregulation of K^+ channels occurred rapidly and without decrement over time (**Supplementary Fig. 6k,l**).

Hence whereas QAQ was normally membrane-impermeant, it photosensitized current flowing through voltage-gated Na^+, Ca^{2+} and K^+ channels when introduced into the cell (**Fig. 1k**). Intracellular QAQ photosensitized many but not all K^+ channels; inward-rectifier (K_{ir}) and hyperpolarization-activated cyclic nucleotide–gated (HCN) channels were unaffected by QAQ (**Supplementary Fig. 7**). Intracellular QAQ did not photoregulate current through *N*-methyl-D-aspartic acid (NMDA) and non-NMDA receptors (**Supplementary Fig. 8**).

QAQ enabled photocontrol of neuronal excitability
Because it imparted light-sensitive block on voltage-gated Na^+, K^+ and Ca^{2+} channels, QAQ should have a strong influence on the electrical excitability of neurons. To examine the net effect of

Figure 2 | Intracellular QAQ as a photoswitchable inhibitor of neuronal activity. (**a**) Action potential (AP) firing in dissociated rat hippocampal neurons with 100 μM QAQ in the patch pipette under illumination with 380-nm or 500-nm light. Firing was elicited with current injections ($I_{inj.}$) of increasing amplitude (35-pA steps). (**b**) Number of action potentials elicited by incremental current injections at indicated wavelengths. (**c**) Action potential shape in 380-nm and 500-nm light. (**d**) Input resistance directly after (0 min; $P = 0.86$) and ~15 min after establishing whole-cell mode, in 380-nm and 500-nm light ($P = 0.93$). (**e**) Resting membrane potential at 0 min ($P = 0.47$) and ~15 min after establishing whole-cell mode in 380-nm and 500-nm light ($P = 0.47$). (**f**) Firing threshold ~15 min after establishing whole-cell mode in 380-nm and 500-nm light ($P = 0.5$). All error bars, s.e.m.; Student t-test; $n = 4$–6 cells.
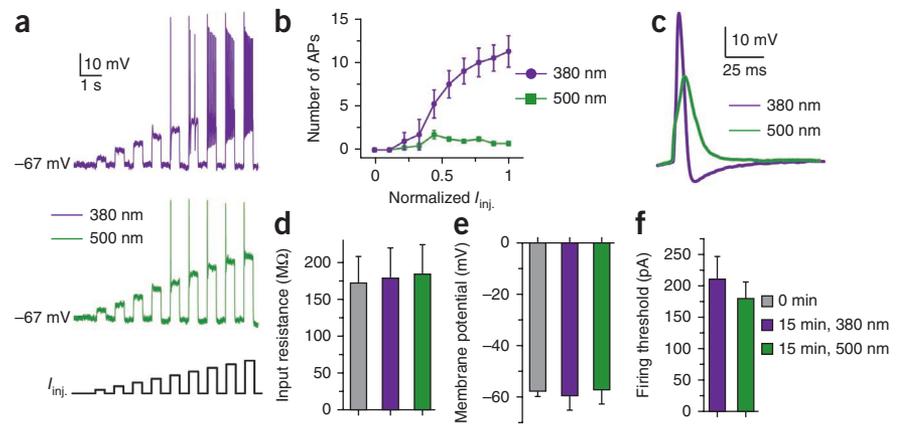
internal QAQ on action-potential firing we carried out current clamp recordings from dissociated rat hippocampal neurons in culture. Current pulses of increasing amplitude elicited a progressive increase in the number of action potentials when QAQ was in the *cis* configuration (**Fig. 2a**). However, when QAQ was converted to the *trans* form, neurons fired a single spike at the onset of stimulation, but did not fire additional spikes even with the largest current pulse tested, consistent with use-dependent blockade of Na^+ channels (**Fig. 2a,b**). The amplitude of the first spike decreased and its half-width increased when we switched from 380 nm to 500 nm light, in agreement with both Na^+ and K^+ channels being blocked (**Fig. 2c**). Higher internal concentration of QAQ (≥200 μM) eliminated all spikes at 500 nm (data not shown).

QAQ affected spiking but had little or no effect on the resting properties of these neurons. Neither the input resistance nor the membrane potential changed over time as QAQ diffused into the neuron (**Fig. 2d,e**). Moreover, light had no effect on these parameters, in agreement with QAQ not affecting K_{ir} and HCN channels, two channels that have a role in setting the resting membrane potential of neurons. Firing threshold in these neurons was the same with (195 pA ± 31 pA; ± s.e.m.) and without (161 pA ± 12 pA, $P = 0.44$ Student t-test) QAQ in the pipette and was not affected by changing the wavelength of light (**Fig. 2f**).

QAQ entered cells through nociceptive ion channels

QAQ is normally membrane impermeant, so it does not photosensitize most cells. However, we asked whether QAQ could be delivered into cells without requiring dialysis through a patch electrode. This strategy involves using nociceptive pore channels as a conduit for QAQ entry. We transfected HEK-293 cells with the gene encoding the Shaker K^+ channel, which we used as an indicator of intracellular QAQ accumulation. We first used TRPV1, a channel whose pore dilates after exposure to its agonist capsaicin[9]. Control cells treated with capsaicin showed no QAQ-mediated photosensitization (**Fig. 3a**). However, cells expressing TRPV1 showed photosensitization of Shaker current, but only when we applied QAQ on the cells in conjunction with capsaicin. We then tested two other TRP channels, TRPA1 and TRPM8, but found no significant loading through either TRPA1 (7.3% ± 4.0%; s.e.m., $n = 11$ cells, $P = 0.39$, Student t-test) or TRPM8

(−0.3% ± 1.4%; s.e.m., $n = 3$ cells, $P = 0.81$, Student t-test) channels after these channels were activated with allyl isothiocyanate (30 μM) or menthol (30 μM), respectively (data not shown).

Some ionotropic receptors for ATP (P2X receptors) also exhibit pore dilation upon prolonged activation[18,19]. Therefore we tested whether $P2X_7$ channels could be used as a conduit for QAQ entry. Control HEK-293 cells treated with ATP showed no QAQ-mediated photosensitization (**Fig. 3b**). However, cells expressing $P2X_7$ receptors showed photosensitization of Shaker current, but only when we applied QAQ on the cells in conjunction with ATP. The amount of K^+ channel photosensitization was nearly the same 5 min and 30 min after ATP application, suggesting that QAQ equilibrated quickly in the cell.

To test whether QAQ can enter into neurons through dilating pore channels, we recorded from cultured rat hippocampal neurons. QAQ alone had no effect on endogenous voltage-gated K^+ current (**Fig. 3c**). However, we could bestow light-sensitivity to neurons that exogenously expressed $P2X_7$ receptors, by treating them with QAQ and ATP. A cell death assay showed that there was no toxicity resulting from this treatment (**Supplementary Fig. 9**).
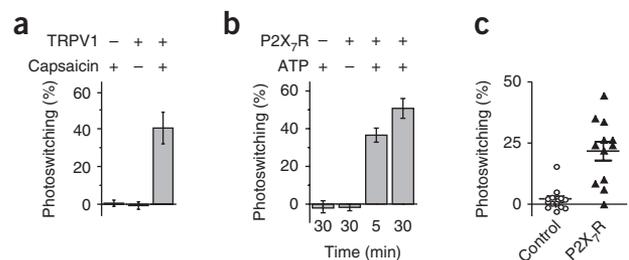
Figure 3 | TRPV1 channels and $P2X_7$ receptors as a conduit for QAQ entry into cells. (**a**) Percentage photoswitching of Shaker K^+ channels in cells expressing (+) or not expressing (−) TRPV1 channels and treated with or without capsaicin (1 μM) in conjunction with QAQ (30 min, 1 mM); $n = 10$ cells for each condition. (**b**) Same experiment as in **a** using $P2X_7$ receptors ($P2X_7$R) instead of TRPV1 channels. ATP (1 mM) was applied for 5 min or 30 min to activate the $P2X_7$ receptors during QAQ loading; $n = 3$–5 cells for each condition. (**c**) Percentage photoswitching of native K^+ channels in hippocampal neurons. Control neurons or neurons expressing $P2X_7$R were treated for 30 min with QAQ (100 μM) plus ATP (2.5 mM). Error bars, ± s.e.m. ($n = 12$ cells).

Figure 4 | Photosensitization of intact DRGs recorded with a three-dimensional multielectrode array (MEA). (**a**) Experimental setup. (**b**) Mouse DRG placed onto the MEA (scale bar, 200 μm). Extracellular recordings are shown superimposed on each electrode. (**c**) Signals recorded from one electrode (under 380-nm and 500-nm light) after 30-min treatment with 1 mM QAQ. (**d**) For simultaneous recording of 24 units, shown are a raster plot of spiking under 10-Hz stimulation (top) and average firing rate (bottom; 100 ms time bins). (**e**) Signals from a single electrode during a train of 50 stimuli (stim; 10 Hz). The first response is shown in black; the last in violet or green. The signal was integrated over a poststimulus time window represented by the colored box. (**f**) Average integrated signal over five light cycles, from a DRG treated with 1 mM QAQ for 30 min or 0.3 mM QAQ for 5 min. (**g**) Quantification of photosensitization with the following treatment conditions, normalized to photosensitization with QAQ alone (0.3 mM for 5 min, dotted line): BCTC (1 μM), 22 ± 18%, $P = 0.03$; $Trpv1^{-/-}$ mice, 34 ± 8% photosensitization, $P = 0.005$; ruthenium red (RR, 10 μM), 7 ± 18% photosensitization, $P = 0.006$; capsaicin (1 μM), 172 ± 30% photosensitization, $P = 0.05$; Bradykinin (BK; 1 μM), 192 ± 30% photosensitization, $P = 0.02$; and electrical stimulation (stim.: 5-s trains of 1-ms stimuli at 10 Hz, repeated every 30 s for 5 min), 138 ± 21% photosensitization, $P = 0.02$. Error bars ± s.e.m.; Mann-Whitney U test ($n = 3$–5 DRGs).
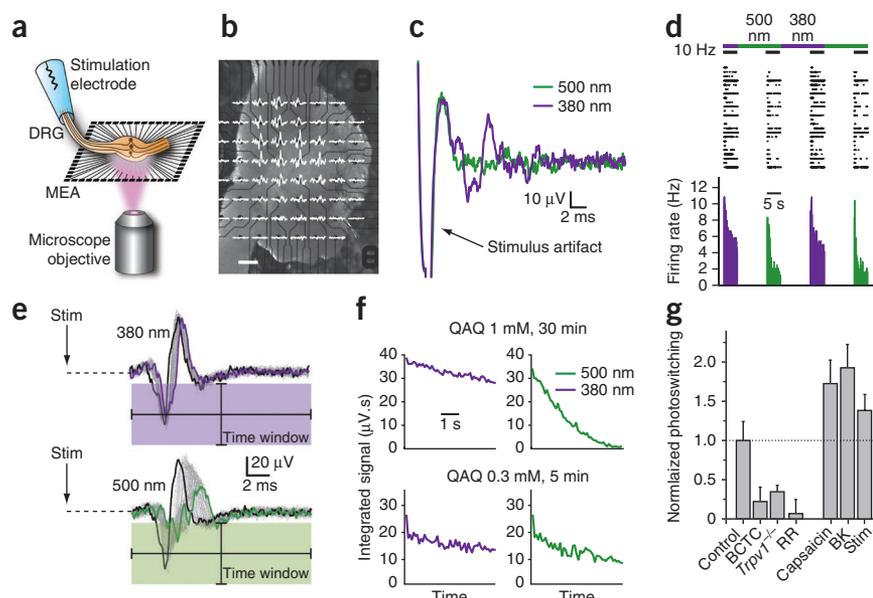
TRPV1 channels are crucial for nociception in peripheral sensory neurons[7,8]. The presence of endogenous TRPV1 channels suggests that QAQ might enter nociceptive neurons without requiring exogenous gene expression. We examined the effect of QAQ on three different parts of nociceptive neurons; their cell bodies, located in the dorsal root ganglion (DRG), their synaptic terminals, located in the spinal cord, and their sensory nerve endings, located in the periphery.

Photosensitization of neurons in intact DRGs

We developed a system to record and analyze many mouse DRG neurons at once while simultaneously photoregulating their electrical activity (**Fig. 4a** and Online Methods). We used a three-dimensional multielectrode array containing 60 pin-shaped electrodes. We controlled the isomeric state of QAQ with a light source positioned under the multielectrode array; the array was transparent to 380-nm and 500-nm light. We positioned a suction electrode on the peripheral nerve of the DRG and used an external stimulation unit to elicit action potentials, which could be recorded as extracellular signals by electrodes of the multielectrode array (**Fig. 4b**). We focused on action potentials resulting from slowly conducting C fibers (<2.5 m s^{-1}), which specifically belong to nociceptive neurons. With the stimulating electrode 10–15 mm from the recording electrodes, spikes attributable to these neurons appeared >4 ms after the onset of the stimulus.

After treatment with QAQ, individual electrodes recorded spikes that could be silenced by switching from 380-nm to 500-nm light, consistent with QAQ photosensitization (**Fig. 4c**). This suggests that there must be some basal activity of QAQ-permeant channels in DRG neurons. We plotted the activity of 24 neurons on a raster plot (**Fig. 4d**). Trains of stimuli at 10 Hz elicited trains of action potentials, which could be photoregulated by switching from 380-nm to 500-nm light. At both

wavelengths, the number of spikes diminished within a train of stimuli, but the extent of spike-train accommodation was much greater in 500-nm light.

Principal component analysis is a common method in multielectrode array recordings for sorting spikes belonging to different neurons, depending on their stereotypical spike waveforms. However, QAQ modulated voltage-gated channels underlying action potentials, changing the spike waveform as a consequence of photoswitching (**Fig. 4e**). Therefore, instead of assigning spikes to different units, which could be particularly error-prone in this circumstance, we devised an analytical method that involves integrating the signal over a 'poststimulus' time window (**Fig. 4e** and Online Methods).

After treating the DRG with a high concentration of QAQ (1 mM for 30 min), we observed a dramatic decrease in the integrated signal upon switching from 380-nm to 500-nm light (**Fig. 4f**). At a lower concentration of QAQ (0.3 mM for 5 min), the integrated signal decreased to a lesser extent upon switching to 500-nm light. The weak photoswitching imparted on the DRG neurons by mild QAQ treatment suggests that little QAQ accumulated in the cells.

If the TRPV1 channel is the main conduit for QAQ entry, blocking or eliminating TRPV1 channels should reduce QAQ loading and consequently the amount of photosensitization. Consistent with this, we found that N-(4-tertiarybutylphenyl)-4-(3-cholorphyridin-2-yl)-tetrahydro-pyrazine1(2H)-carboxamide (BCTC), a TRPV1 antagonist that inhibits acid- and capsaicin-induced activation, considerably reduced DRG photosensitization (**Fig. 4g**). In $Trpv1^{-/-}$ mice, photosensitization was also strongly reduced but not completely abolished. Ruthenium red, a nonselective TRP channel pore blocker, entirely prevented photosensitization. Taken together, these data suggest that TRPV1 channels are the main entry route for QAQ into DRGs.

37

Figure 5 | Photosensitization of spinal cord slices. (**a**) Schematic of a spinal cord slice with a whole-cell patch recording from neurons either in lamina II or laminae III–IV and using electrical stimulation of the dorsal root (stim.). (**b**,**c**) Postsynaptic responses recorded in a lamina II (**b**) and a laminae III–IV neuron (**c**), in response to single stimuli to the dorsal root. (**d**) Percentage photoswitching of the integrated current exhibited by inputs to laminae II ($35 \pm 9\%$, $n = 8$ cells) and III–IV neurons ($-1.5 \pm 9.4\%$, $n = 10$ cells, *$P = 0.01$). (**e**,**f**) Cumulative probability distributions of EPSC amplitude (**e**) and frequency (**f**) recorded in a lamina II neuron in 380-nm and 500-nm light. (**g**) Average light-elicited EPSC frequency in 380-nm, 500-nm and again in 380-nm light ($37.5 \pm 11.3\%$ photoswitching, $n = 8$ cells).

(**h**) Polysynaptic responses recorded from a lamina II neuron in response to a 20 Hz train of stimuli to the dorsal root. (**i**) Quantification of average responses to train stimulation (50 Hz for 500 µs) in 11 neurons in 380-nm, 500-nm and again in 380-nm light. Synaptic responses after the stimulus train were integrated and normalized to the initial amplitude in 380-nm light ($n = 11$ cells). In all experiments described in this figure, slices were treated with 1 mM QAQ for 20 min before recording. Error bars, $\pm$ s.e.m.; Student t-test.
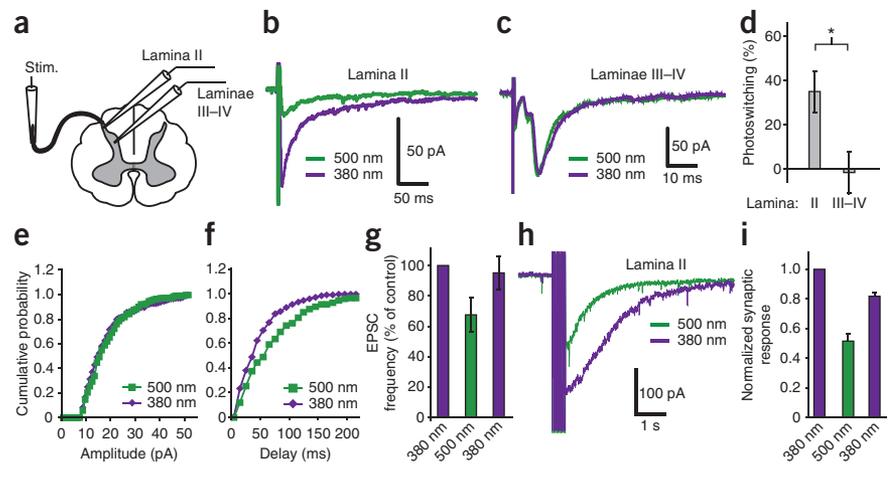
This system can be used as a platform for assessing the activity of TRP channels in the intact DRG in response to various stimuli. We treated the ganglia with capsaicin during QAQ loading, followed by thorough washing with normal saline. Capsaicin is a selective agonist of TRPV1, and as expected, it increased QAQ loading and therefore photosensitization (**Fig. 4g**). Bradykinin is a neuropeptide that promotes pain hypersensitivity and inflammation[20]. We found that Bradykinin also promoted QAQ-mediated DRG photosensitization, consistent with a signaling cascade that leads to activation of TRP channels[21].

Direct electrical stimulation of sensory neuron axons in the peripheral nerve also promoted DRG photosensitization (**Fig. 4g**), indicating enhanced QAQ entry during the stimulation period. Action potential firing may directly promote QAQ entry into TRPV1-containing neurons, but TRPV1 channels are only weakly voltage-sensitive[22]. In addition, action potential firing may promote DRG somata to release neuro-inflammatory transmitters, and these may indirectly lead to activation of nociceptive channels, a positive feedback mechanism that could contribute to prolonged hypersensitivity and chronic pain.

Photosensitization of neurons in spinal cord slices

TRPV1 is abundantly expressed throughout the entire length of nociceptive neurons, including the central terminals in the spinal cord, but it is thought to be largely absent from non-nociceptive sensory neurons[7]. The central terminals of nociceptive neurons are located in laminae I–II of the dorsal horn of the spinal cord, whereas the terminals of non-nociceptive neurons are located in laminae III–IV (ref. 7). If QAQ loading is selective for nociceptors, it should photosensitize only the subset of sensory neurons that terminate in laminae I–II.

We treated spinal cord slices with QAQ and recorded synaptic responses in dorsal horn neurons triggered by electrical stimulation of the dorsal root (**Fig. 5a**). In lamina II, the average excitatory postsynaptic current (EPSC) amplitude was reduced by switching from 380-nm to 500-nm light, whereas light had no effect for EPSCs recorded in laminae III–IV (**Fig. 5b,c**).

These results are consistent with preferential photosensitization of nociceptive neurons by QAQ (**Fig. 5d**).

To distinguish between a pre- versus postsynaptic effect of QAQ, we recorded spontaneous EPSCs in lamina II neurons and analyzed the cumulative distribution of amplitudes and inter-event intervals. The amplitude of these EPSCs was unaffected by the wavelength of light but the frequency of these EPSCs was decreased by 500-nm light (**Fig. 5e–g**) in six of eight cells. A change in EPSC amplitude indicates a postsynaptic alteration in neurotransmitter receptor function, whereas a change in frequency usually indicates a change in presynaptic neurotransmitter release.

QAQ-mediated photosensitization also impacted polysynaptic pathways on the spinal cord. Trains of stimuli generated a strong inward current that persisted for several seconds after the monosynaptic EPSCs should have decayed (**Fig. 5h**). Switching from 380-nm to 500-nm light caused a dramatic reduction in the amplitude of this current. Switching back to 380-nm light largely restored the initial amplitude of the response (**Fig. 5i**).

In some, but not all lamina II neurons, QAQ photosensitized not only the presynaptic inputs but also intrinsic voltage-gated channels K^+ currents (**Supplementary Fig. 10a**). In contrast, there was little photosensitization of K^+ channels in lamina III–IV neurons. Photosensitization of lamina II neurons was eliminated by BCTC (**Supplementary Fig. 10b**). These results suggest that TRPV1 channels enabling QAQ entry are present and active in lamina II neurons to a much greater extent than in lamina III–IV neurons.

In vivo photoregulation of peripheral nerve endings

If QAQ effectively photosensitizes nociceptive neurons, exposure to light should alter pain sensation *in vivo*. We explored this possibility by testing the pain-avoidance (nocifensive) blinking response that is elicited by mechanical stimulation of the cornea in rats using the von Frey hair test[23] (Online Methods). The cornea is densely innervated with nociceptors[24] that mediate the blink response[23]. Free nerve endings are only a few micrometers below the surface, and the cornea is transparent, facilitating optical control. To enable QAQ entry into nociceptor nerve endings, we topically applied
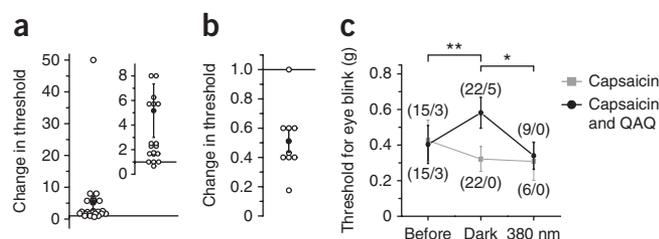
Figure 6 | QAQ optically regulated nociception *in vivo*, in live rats. (**a**) Change in blink threshold in the eye treated with capsaicin (10 µM) plus QAQ (20 mM), normalized to the contralateral eye treated with capsaicin alone. Experiments were performed in ambient light. Average increase was 5.1-fold (black dot; n = 22 rats, P = 0.007). (**b**) Change in blink threshold in the eye treated with capsaicin (10 µM) plus QAQ (20 mM) after illumination with 380-nm light. Average decrease was to 0.5 the value in the dark (black dot; n = 9 rats, P = 0.03). (**c**) Group data for eye-blink threshold experiments. Numbers in parentheses indicate the total number of rats together with number of rats that did not respond to the maximum force applied (1 g). Error bars, ± s.e.m.; Student t-test; *P < 0.05; **P < 0.01.

QAQ with capsaicin in one eye and capsaicin alone in the contralateral eye. We immobilized the rats by mild sedation with xylazine and ketamine at low doses that do not interfere with nocifensive blinking[25]. The von Frey hair test in ambient light showed that the normalized blink threshold was about fivefold higher in the eye treated with QAQ plus capsaicin compared to the eye treated with capsaicin alone (**Fig. 6a**). Moreover, 380-nm light decreased the normalized blink threshold in the eye treated with QAQ plus capsaicin (**Fig. 6b**). The decrease in blink sensitivity caused by QAQ was completely removed by exposure to 380-nm light (**Fig. 6c**). Taken together, these results show that QAQ can serve as a local anesthetic that can be turned off with light.

DISCUSSION

Microbial light-sensitive ion transporters, including halorhodopsin[26] and archaerhodopsin-3 (ref. 27), have been used as optogenetic inhibitors of neuronal activity. Genes encoding these proteins can be promoter-targeted to subpopulations of neurons[1]. However, for several reasons, nongenetic optical control of nociception with QAQ may be preferable to optogenetic methods.

Unlike optogenetic tools that overpower the natural activity of cells, QAQ acts on endogenous ion channels that underlie initiation and propagation of action potentials. Hence QAQ suppresses electrical excitability at its source. Because the ion-transport rate of transporters is much slower than ion flux through channels, optical silencing with halorhodopsin and archaerhodopsin-3 requires very high expression[1]. Exogenous expression can be achieved by injecting viral vectors into the appropriate part of the nervous system[1], but expression requires days to weeks and is restricted to neurons that are exposed to an adequate titer of virus. Optogenetic expression can result in permanent genetic alteration of neurons, which may not be necessary or desirable for the acute regulation of pain signaling, either for scientific or biomedical applications. In contrast, QAQ-mediated photosensitization occurs within minutes and persists only until the molecule dissipates, either by being metabolized inside the cell or diffusing away from targeted neurons. Because QAQ is a small molecule, it diffuses readily through tissue and presumably gains access to all neurons that have ion channels that permit its entry into the cytoplasm.

QAQ has potential value as both a scientific and a clinical tool for controlling nociception. Because it selectively accumulates in nociceptors, QAQ could selectively inhibit pain signaling while sparing other sensory modalities and therefore could function as a targeted analgesic. This is similar to the recently proposed therapeutic use of QX-314 (ref. 10). However, QAQ has the added feature of being rapidly controllable with light. *In vivo* photocontrol would require delivery of sufficient QAQ and projection of sufficient light onto target neuronal tissues. Because it is doubly charged, QAQ is unlikely to cross the blood-brain barrier. But our results show that QAQ penetrates into spinal cord slices and intact DRGs, so if injected, QAQ should have access to other neural structures. Implanted fiber-optic systems such as those developed for deep brain photocontrol of neurons expressing optogenetic tools[28] could be adapted for controlling QAQ administered to internal neural structures (for example, spinal roots or DRGs). QAQ might also be controlled by an external light source after topical administration (for example, for treating corneal pain).

QAQ-mediated photosensitization could facilitate mapping of nociceptive circuit connections mediated by fast conventional synapses or by slow neuromodulatory neurotransmitters that may contribute to central sensitization and pain hypersensitivity[20]. Our synaptic studies in spinal cord were limited to full-field regulation of presynaptic activity, but higher-resolution photocontrol should be possible by projecting through a microscope small spots or patterns of light, for example, to target presynaptic axons or terminals.

Finally QAQ provides insight into the activity status of ion channels implicated in pain and inflammation. Previously, the activity of nociceptive ion channels has been studied almost exclusively in isolated neurons that had been enzymatically and mechanically dissociated from DRGs[21]. This disruptive procedure could alter the activity and expression of these channels[29]. QAQ enabled investigation of nociceptive ion-channel activity in undisrupted neural structures. Moreover, QAQ photosensitized regions of a nociceptor that are largely inaccessible to electrodes. Hyperalgesia in both inflammatory and neuropathic pain is associated with upregulation of TRP channel gene expression in peripheral nociceptors[7], but the activation status of these channels in chronic pain is unknown. Because QAQ-mediated photosensitivity is a consequence of the cumulative activity of nociceptive channels, it serves as an ultrasensitive reporter that provides new insights about when and where these channels are active, in both physiological and pathological conditions.

METHODS

Methods and any associated references are available in the online version of the paper at http://www.nature.com/naturemethods/.

Note: Supplementary information is available on the Nature Methods website.

1. Yizhar, O., Fenno, L.E., Davidson, T.J., Mogri, M. & Deisseroth, K. Optogenetics in neural systems. *Neuron* **71**, 9–34 (2011).
2. Kramer, R.H., Fortin, D. & Trauner, D. New photochemical tools for controlling neuronal activity. *Curr. Opin. Neurobiol.* **19**, 544–552 (2009).
3. Fehrentz, T., Schönberger, M. & Trauner, D. Optochemical genetics. *Angew. Chem. Int. Edn.* **50**, 12156–12182 (2011).
4. Fortin, D. *et al.* Photochemical control of endogenous ion channels and cellular excitability. *Nat. Methods* **5**, 331–338 (2008).
5. Banghart, M.R. *et al.* Photochromic blockers of voltage-gated potassium channels. *Angew. Chem. Int. Ed.* **48**, 9097–9101 (2009).
6. Mourot, A. *et al.* Tuning photochromic ion channel blockers. *ACS Chem. Neurosci.* **2**, 536–543 (2011).
7. Basbaum, A.I., Bautista, D.M., Scherrer, G. & Julius, D. Cellular and molecular mechanisms of pain. *Cell* **139**, 267–284 (2009).
8. Cavanaugh, D.J. *et al.* Trpv1 reporter mice reveal highly restricted brain distribution and functional expression in arteriolar smooth muscle cells. *J. Neurosci.* **31**, 5067–5077 (2011).
9. Chung, M.-K., Güler, A.D. & Caterina, M.J. TRPV1 shows dynamic ionic selectivity during agonist stimulation. *Nat. Neurosci.* **11**, 555–564 (2008).
10. Binshtok, A.M., Bean, B.P. & Woolf, C.J. Inhibition of nociceptors by TRPV1-mediated entry of impermeant sodium channel blockers. *Nature* **449**, 607–610 (2007).
11. Binshtok, A.M. *et al.* Coapplication of lidocaine and the permanently charged sodium channel blocker QX-314 produces a long-lasting nociceptive blockade in rodents. *Anesthesiology* **111**, 127–137 (2009).
12. Scholz, A. Mechanisms of (local) anaesthetics on voltage-gated sodium and other ion channels. *Br. J. Anaesth.* **89**, 52–61 (2002).
13. Hille, B. *Ion Channels of Excitable Membranes* 3rd edn. (Sinauer Associates, 2001).
14. Strichartz, G.R. The inhibition of sodium currents in myelinated nerve by quaternary derivatives of lidocaine. *J. Gen. Physiol.* **62**, 37–57 (1973).
15. Kawaguchi, A. *et al.* Enhancement of sodium current in NG108–15 cells during neural differentiation is mainly due to an increase in NaV1.7 expression. *Neurochem. Res.* **32**, 1469–1475 (2007).
16. Rogawski, M.A., Inoue, K., Suzuki, S. & Barker, J.L. A slow calcium-dependent chloride conductance in clonal anterior pituitary cells. *J. Neurophysiol.* **59**, 1854–1870 (1988).
17. Hoshi, T., Zagotta, W.N. & Aldrich, R.W. Biophysical and molecular mechanisms of Shaker potassium channel inactivation. *Science* **250**, 533–538 (1990).
18. Khakh, B.S., Bao, X.R., Labarca, C. & Lester, H.A. Neuronal P2X transmitter-gated cation channels change their ion selectivity in seconds. *Nat. Neurosci.* **2**, 322–330 (1999).
19. Virginio, C., MacKenzie, A., Rassendren, F.A., North, R.A. & Surprenant, A. Pore dilation of neuronal P2X receptor channels. *Nat. Neurosci.* **2**, 315–321 (1999).
20. Wang, H. *et al.* Bradykinin produces pain hypersensitivity by potentiating spinal cord glutamatergic synaptic transmission. *J. Neurosci.* **25**, 7986–7992 (2005).
21. Bautista, D.M. *et al.* TRPA1 mediates the inflammatory actions of environmental irritants and proalgesic agents. *Cell* **124**, 1269–1282 (2006).
22. Voets, T. *et al.* The principle of temperature-dependent gating in cold- and heat-sensitive TRP channels. *Nature* **430**, 748–754 (2004).
23. de Castro, F., Silos-Santiago, I., López de Armentia, M., Barbacid, M. & Belmonte, C. Corneal innervation and sensitivity to noxious stimuli in trkA knockout mice. *Eur. J. Neurosci.* **10**, 146–152 (1998).
24. Rózsa, A.J. & Beuerman, R.W. Density and organization of free nerve endings in the corneal epithelium of the rabbit. *Pain* **14**, 105–120 (1982).
25. Wenk, H.N. & Honda, C.N. Silver nitrate cauterization: characterization of a new model of corneal inflammation and hyperalgesia in rat. *Pain* **105**, 393–401 (2003).
26. Zhang, F. *et al.* Multimodal fast optical interrogation of neural circuitry. *Nature* **446**, 633–639 (2007).
27. Chow, B.Y. *et al.* High-performance genetically targetable optical neural silencing by light-driven proton pumps. *Nature* **463**, 98–102 (2010).
28. Zhang, F., Aravanis, A.M., Adamantidis, A.R., de Lecea, L. & Deisseroth, K. Circuit-breakers: optical technologies for probing neural signals and systems. *Nat. Rev. Neurosci.* **8**, 577–581 (2007).
29. Malin, S.A., Davis, B.M. & Molliver, D.C. Production of dissociated sensory neuron cultures and considerations for their use in studying neuronal function and plasticity. *Nat. Protoc.* **2**, 152–160 (2007).

ONLINE METHODS

General. All animals were housed in the centralized animal facilities as assigned by the University of California Berkeley and were provided food and water ad libitum. Animal care and experimental protocols were approved by the University of California Berkeley Animal Care and Use Committee. All chemicals were purchased from Sigma-Aldrich, except BCTC (*N*-(4-tertiarybutylphenyl)-4(3-cholorphyridin-2-yl)-tetrahydro-pyrazine1(2H)-carboxamide) and AITC (allyl isothiocyanate) that were purchased from Tocris.

QAQ synthesis and spectroscopic characterization. QAQ was synthetized as previously described[5]. UV-vis spectra of QAQ were measured using a smartSpec Plus spectrophotometer (Bio-Rad) in combination with illumination using the Polychrome V (Till Photonics), through an optic fiber positioned perpendicular to the detection beam of the spectrophotometer.

Cell culture. HEK-293 cells were cultured under standard conditions (Dulbecco's modified Eagle medium (DMEM) containing 10% FBS). We grew GH3 cells in F-12K medium containing 15% horse serum and 2.5% FBS. NG108-15 cell medium contained 95% DMEM mixed with HAT (0.1 mM hypoxanthine, 400 nM aminopterin and 0.016 mM thymidine) and 5% FBS. Cells were plated on poly(L-lysine) (0.1 mg/ml) treated coverlips in a density of 12,000 cells per cm^2 for electrophysiological measurements. Dissociated hippocampal neuronal preparations were performed from neonatal Sprague-Dawley rats according to standard procedures[4]. Hippocampi were dissected, dissociated and cells were plated on poly(L-lysine)-coated coverslips at a density of $100,000/cm^2$. We grew hippocampal neurons in minimum essential medium containing 5% FBS, 20 mM glucose, B27 (Invitrogen), glutamine and Mito+ Serum Extender (BD Biosciences). Trigeminal ganglion (TG) neurons from neonatal rats were prepared as previously described[30]. TGs were dissected and neurons were dissociated (with collagenase and trypsin) and plated on poly(L-lysine)-coated coverslips. We grew TG neurons in minimum essential medium containing 5% horse serum, MEM vitamins (Invitrogen), glutamine and penicillin-streptomycin. HEK-293 cells were transfected using calcium phosphate precipitation and measured after 24–48 h (ref. 4). GH3 and NG108-15 cells were recorded 24 h after plating. Hippocampal neurons were transfected 7 d after plating and measured 10–14 d after plating. TG cells were measured 12–48 h after plating.

Dorsal root ganglia (DRG) preparation. Mice, C57/BL6 wild type or *Trpv1*$^{-/-}$ aged 1–6 months of either sex, were deeply anesthetized with isoflurane and killed by cervical dislocation. The spinal column and surrounding muscle, from the sacral to cervical regions, was removed from the mouse and dissected in cold (4 °C) artificial cerebral spinal fluid (ACSF) (124 mM NaCl, 4 mM KCl, 2 mM $MgCl_2$, 2 mM $CaCl_2$, 26 mM $NaHCO_3$, 20 mM glucose, 2 mM sodium pyruvate and 0.4 mM ascorbic acid, pH 7.3) equilibrated with 95% O_2 and 5% CO_2. A laminectomy was performed from the thorax to the sacrum, and the spinal cord was gently removed, exposing the DRGs. The DRGs and attached nerves (10–20 mm long) were removed from the lumbar region and incubated for at least 30 min at room temperature

(18–22 °C) in an oxygenation chamber on a nitrocellulose membrane (Sartorius Stedim Biotech) moistened with ACSF.

Spinal cord slice preparation. C57/BL6 mice were deeply anesthetized with isoflurane and quickly beheaded. The spinal column and surrounding muscles were removed and dissected in ice-cold oxygenated low calcium, low magnesium ACSF (101 mM NaCl, 3.8 mM KCl, 18.7 mM $MgCl_2$, 1.3 mM $MgSO_4$, 1.2 mM KH_2PO_4, 10 mM HEPES, 1 mM $CaCl_2$ and 1 mM glucose). After laminectomy, the spinal roots were cut, the spinal cord was gently removed, and its lumbar part was placed into a small agarose block. We prepared 300-μm-thick slices using a Leica VTS 1000 vibratome. The slices were then transferred in warm (31 °C) ASCF equilibrated with 95% O_2 and 5% CO_2 for at least 1 h before starting patch-clamp recordings.

Whole-cell electrophysiology. Patch clamp recordings of mammalian cells were performed at room temperature. Bath solution for K^+ current contained 138 mM NaCl, 1.5 mM KCl, 1.2 mM $MgCl_2$, 2.5 mM $CaCl_2$, 1 μM tetrodotoxin (for hippocampal neurons only), 5 mM HEPES and 10 mM glucose. Bath solution for Na^+ current contained NaCl 145 mM, $CdCl_2$ 0.5 mM, $CaCl_2$ 2 mM, HEPES 5 mM and glucose 5 mM. Bath solution for Ca^{2+} current contained NaCl 138 mM, KCl 5.4 mM, $MgCl_2$ 0.8 mM, $BaCl_2$ 20 mM, tetrodotoxin 1 μM (for GH3 cells only), HEPES 10 mM and glucose 5 mM. Bath solution for current clamp experiments contained NaCl 138 mM, KCl 1.5 mM, $MgCl_2$ 1.2 mM, $CaCl_2$ 2.5 mM, HEPES 5 mM and glucose 10 mM. Pipette solution for K^+ current contained NaCl 10 mM, K^+ gluconate 135 mM, HEPES 10 mM, $MgCl_2$ 2 mM, MgATP 2 mM, EGTA 1 mM. Pipette solution for Na^+ current contained NaCl 30 mM, CsCl 100 mM, HEPES 10 mM, $MgCl_2$ 2 mM, $CaCl_2$ 1 mM, MgATP 2 mM, NaGTP 0.05 mM, EGTA 10 mM and glucose 5 mM. Pipette solution for Ca^{2+} current contained CsCl 120 mM, HEPES 20 mM, $CaCl_2$ 1 mM, MgATP 2 mM, EGTA 11 mM and glucose 5 mM. Pipette solution for current clamp experiments contained NaCl 38 mM, potassium gluconate 97 mM, HEPES 20 mM, MgATP 4 mM, NaGTP 0.35 mM and EGTA 0.35 mM. All solutions were adjusted to pH 7.4. Electrophysiological measurements were performed with an Axopatch 200A (Molecular Devices) or a Patch-Clamp PC505B (Warner) amplifier. Patch pipettes resistances were 2–4 MΩ. Sodium channel currents in NG108-15 cells and calcium channel currents in GH3 cells were corrected by P/N leak subtraction. pClampex 8.2 software (Molecular Devices) in combination with a Digidata 1200 interface (Molecular Devices) were used to create and apply pulse protocols. Voltage clamp recordings were low-pass–filtered at 2 kHz and current clamp measurements were low-pass filtered at 5 kHz. Illumination of cells was based on a xenon lamp either in combination with narrow band-pass filters or with a monochromator Polychrome V, as described previously[5]. For direct internal application through the patch pipette, QAQ was dissolved to a final concentration of 100 μM. Measurements were started after 5–10 min of equilibration time for HEK-293, NG108-15, GH3 cells and TG neurons, and after 15–20 min for hippocampal neurons. For bath incubation, cells were incubated with QAQ (classically 1 mM) in the presence or absence of agonist (1–2.5 mM ATP or 1 μM capsaicin) at 37 °C in the dark. Loading solution is similar to K^+ current recording solution but with no calcium.

Treated coverslips were rinsed with regular calcium-containing recording solution before measurement.

For spinal slice electrophysiology, slices were placed in a recoding chamber bathed with warmed (31 °C) ACSF (NaCl 130.5 mM; KCl 2.4 mM, CaCl$_2$ 2.4 mM, NaHCO$_3$ 19.5 mM, MgSO$_4$ 1.3 mM, KH$_2$PO$_4$ 1.2 mM, HEPES 1.25 mM and glucose 10 mM, pH 7.4) equilibrated with 95% O$_2$ and 5% CO$_2$. Electrophysiological measurements were performed under the control of an Olympus BX51 microscope using an Axoclamp 2B (Molecular devices). Patch pipettes (7–11 MΩ) were filled with appropriate pipette solution (potassium gluconate 120 mM, KCl 20 mM, CaCl$_2$ 0.1 mM, MgCl$_2$ 1.3 mM, EGTA 1 mM, HEPES 10 mM, GTP 0.1 mM, cAMP 0.2 mM, leupeptin 0.1 mM, Na$_2$ATP 3 mM and D-manitol 77 mM, pH 7.3). Illumination of preparations was performed using two different wavelength diodes (380 nm and 500 nm) controlled by transistor-transistor logic (TTL) pulses. A glass suction electrode connected to Master-8 (A.M.P.I.) stimulator was used to stimulate dorsal roots. Non-nociceptive primary afferent fibers were specifically recruited using low-threshold stimulations (50 μs, less than 100 μA), whereas nociceptive fibers were recruited using high-intensity stimulations (500 μs, more than 250 μA).

Multielectrode array recordings. A DRG was placed onto a three-dimensional multielectrode array (MEA) chip (MEA60 200 3D GND, Ayanda Biosystems) and secured in place with a 'harp' made from dialysis membrane stretched over thick platinum wire and bonded with super glue; the wire was U-shaped to allow the nerve to exit without being crushed. The MEA chip was mounted on an MEA1060-Up amplifier (Multi Channel Systems) and placed on the stage of an IX71 inverted microscope (Olympus). The nerve was led into a manipulator-mounted glass suction electrode of appropriate size driven by a DS2 stimulus isolator (Digitimer) triggered by pClamp v10.0 software through a Digidata 1440A data acquisition system (Molecular Devices). Except during drug incubations, the MEA chamber was continuously perfused with oxygenated ACSF at ~2 ml/min. Recordings were performed at ~30 °C.

Before the drug incubation, the DRG was checked for response to stimulation at 1 Hz. If the signal was acceptable, the MEA chamber solution was replaced with oxygenated ACSF containing QAQ with or without other drugs and incubated for 5 min. When using blockers, the DRG was preincubated with the blocker for 5 min before the application of QAQ with the blocker. The DRG was then washed with ACSF for 10 min before performing the experiment.

Recordings were done at a stimulation rate of 10 Hz while illuminating the DRG with 380-nm or 500-nm light. Each experiment consisted of 5 cycles of 30 s under 380-nm light followed by 30 s under 500-nm light. The DRG was stimulated with 1-ms pulses at 10 Hz for the last 5 s under each wavelength of light, allowing 25 s to recover from adaptation in between stimulation episodes. Illumination was provided by a U-LH100HGAPO mercury lamp (Olympus) through a 4× objective, resulting in intensities of 17–28 mW/mm^2. Filters for 380 nm and 500 nm were switched by a Lambda 10-3 system (Sutter Instrument Company) under the control of Metamorph v7.5.3.0 software (Molecular Devices). Evoked responses were recorded at 20 kHz with MC_Rack v4.0 software (Multi Channel Systems). Pictures were taken using Metamorph with a CoolSNAP HQ2 camera (Photometric) connected to the microscope.

Multielectrode array data analysis. Data were recorded in 40-ms-long sweeps synced to stimulation pulses, so that the stimulation produced an artifact at the beginning of the sweeps. Evoked spikes were detected by a negative threshold manually set beyond the noise level. For each detected spike, the first millisecond before the peak and the two milliseconds after were extracted into text files by MC_DataTool software (Multi Channel Systems), for processing with a custom Matlab (MathWorks) program.

Our custom Matlab program calculated the area under each spike to the threshold level. A region of interest (ROI) was also set manually for each recording to exclude the stimulus artifact. The total integrated area of all spikes was calculated for each sweep, and averaged over the five cycles in each wavelength (**Fig. 4e,f**). This averaged area per sweep was summated over the 5 s of stimulation to quantify the total evoked response in each wavelength of light. For each active channel, the normalized photosensitization was calculated as (area$_{380nm}$ – area$_{500nm}$) / (area$_{380nm}$ + area$_{500nm}$). Channels with excessively small and/or irregular signals were conservatively culled. The per-channel photosensitization values, generated from at least three separate DRGs per drug condition, were pooled by condition and compared for significance using a Mann-Whitney U test (5% significance level).

Cornea-evoked reflex blinks. Sprague-Dawley rats (3–6 weeks old of either sex) were sedated using intraperitoneal injection of xylazine (9 mg/kg) and ketamine (60 mg/kg). We placed rats on a warming pad, and we intiated behavioral testing when rat spontaneous movements ceased but while pinching the rat's paw with a pair of forceps elicited a brisk withdrawal reflex. We used a series of von Frey hairs, nylon fibers of increasing diameter, which we pressed against the cornea to impart increasing force with high accuracy. We held von Frey hairs perpendicular to the cornea for ~2 s, or until a blink initiated, using progressive increase in force from 8 mg to a maximal value of 1 g. Stimuli were presented three times for each stiffness, at intervals of several seconds. Both eyes were tested, and a positive response was noted if the rat blinked two or three times for a given force. Capsaicin (10 μM) was then topically applied on one cornea using a pipette (10 μl volume), and the contralateral cornea was treated with a mixture of capsaicin (10 μM) and QAQ (20 mM). Von Frey testing was done again 10–15 min after drug application. Immediately after von Frey testing, light was applied using an LED (Prizmatix, λmax = 385 nm, 30 mW/cm^2) for 1 min and von Frey testing was done again.

Statistical analysis. Unless otherwise noted, all data are presented as ± s.e.m. and statistics were analyzed using a Student t-test.

30. McKemy, D.D., Neuhausser, W.M. & Julius, D. Identification of a cold receptor reveals a general role for TRP channels in thermosensation. *Nature* **416**, 52–58 (2002).

Supplementary Files

Supplementary File	Title
Supplementary Figure 1	Photochemical properties of QAQ.
Supplementary Figure 2	External QAQ does not block voltage-gated Na^+ channels.
Supplementary Figure 3	Intracellular QAQ quickly blocks and unblocks Na^+ channels.
Supplementary Figure 4	QAQ photosensitizes voltage-gated Na^+ channels from sensory TG neurons.
Supplementary Figure 5	QAQ photosensitizes various voltage-gated Ca^{2+} channels.
Supplementary Figure 6	QAQ photosensitizes various voltage-gated K^+ channels.
Supplementary Figure 7	QAQ does not photosensitize K_{ir} or HCN channels.
Supplementary Figure 8	QAQ does not photosensitize glutamate receptors.
Supplementary Figure 9	Neuronal survival after ATP and QAQ treatment.
Supplementary Figure 10	QAQ photosensitizes second order neurons in spinal cord slices.

Supplementary Figure 1: Photochemical properties of QAQ.
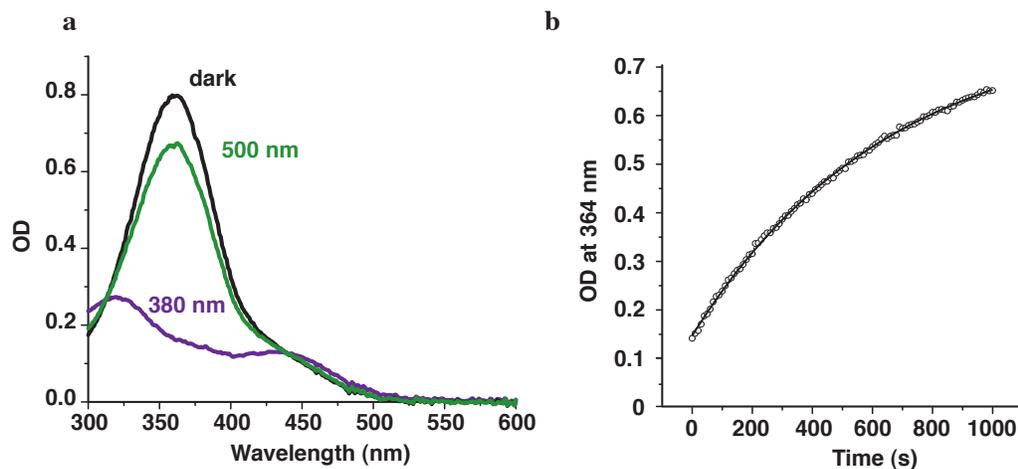
(**a**) UV-Vis spectrum of QAQ in solution (10 mM PBS, pH 7.4) either in the dark, or under illumination with 500 nm or 380 nm light. (**b**) Thermal relaxation of QAQ from *cis* to *trans* in the dark. Data was fitted using a mono-exponential decay ($t_{1/2}$ = 449 +/- 5 s).

Supplementary Figure 2: External QAQ does not block voltage-gated Na$^+$ channels.
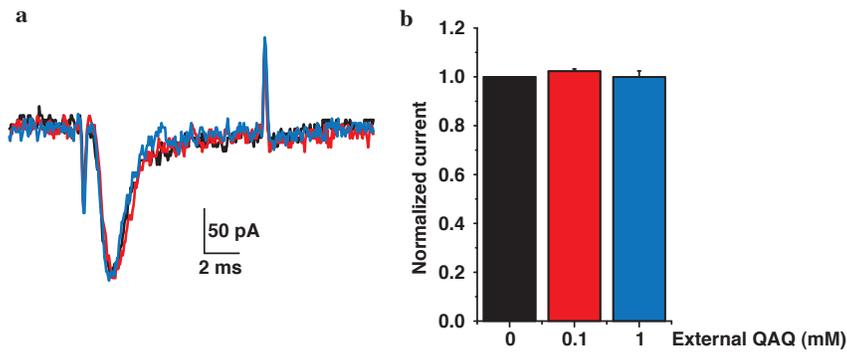
(**a**) Na$^+$ current recorded from an NG108-15 cell upon depolarization from -70 to -10 mV. Perfusion with QAQ 100 μM (red) or 1 mM (blue) did not alter Na$^+$ current (black). (**b**) Normalized current (0.1 ± 2.5 % block ± s.e.m., n = 3 cells, p = 0.97 Student t-test).

Supplementary Figure 3: Intracellular QAQ quickly blocks and unblocks Na$^+$ channels.
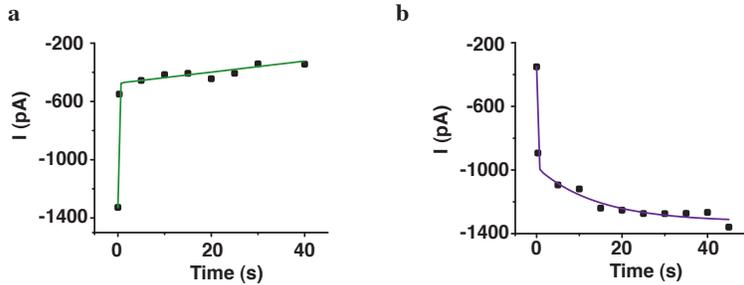
(**a**) Onset of block after switching light to 500 nm. Current was fitted with a bi-exponential decay equation. The fast process ($t_{1/2}$ = 88 ± 5 ms, n = 3 cells) reflects block of Na$^+$ channels, whereas the slow process may reflect slow inactivation of Na$^+$ channels. (**b**) Kinetics of unblock after switching light to 380 nm. Current was fitted with a bi-exponential decay equation, with $t_{1/2}$ = 58 ± 30 ms (n = 3 cells). The slow process may reflect slow recovery from inactivation of Na$^+$ channels.

Supplementary Figure 4: QAQ photosensitizes voltage-gated Na⁺ channels from sensory TG neurons.
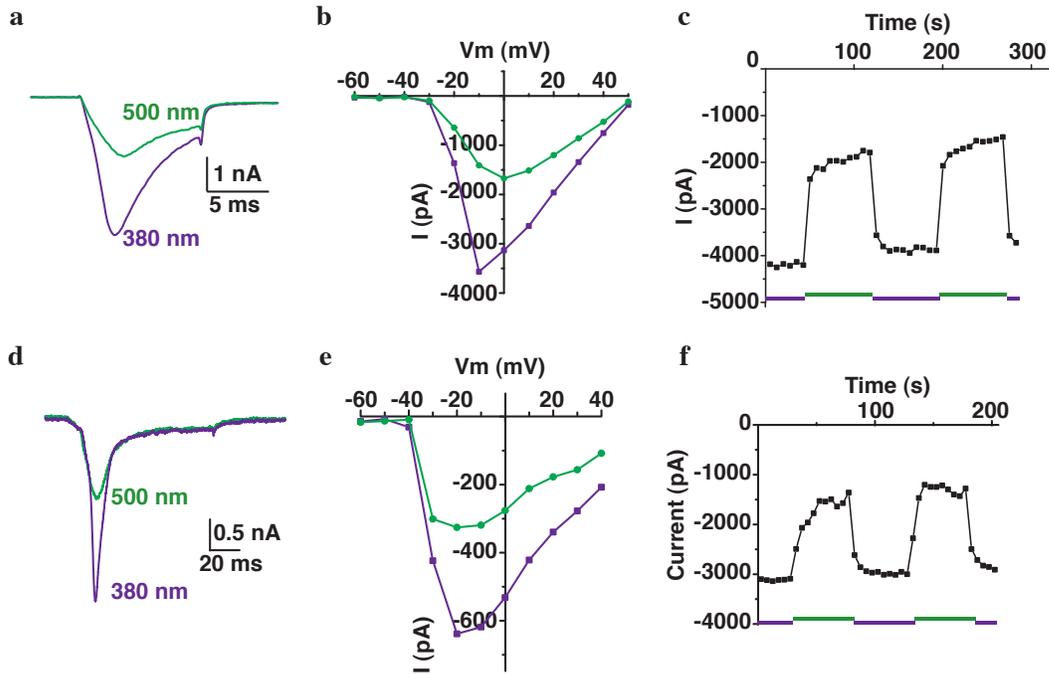
(**a**) Na⁺ current recorded from a TG neuron upon depolarization from -70 to -10 mV, using 100 μM QAQ in the pipette and under both wavelengths of light (49.7 ± 5.2 % photoswitching ± s.e.m., n = 6 cells). (**b**) I/V dependency of block and unblock. (**c**) Reversibility of block and unblock. (**d**) TTX-resistant Na⁺ current recorded from a TG neuron upon depolarization from -70 to -10 mV, using 100 μM QAQ in the pipette, 0.5 μM TTX in the bath, and under both wavelengths of light (46.3 ± 7.9 % photoswitching ± s.e.m., n = 4 cells). (**e**) I/V dependency of block and unblock. (**f**) Reversibility of block and unblock under both wavelength of light.

Supplementary Figure 5: QAQ photosensitizes various voltage-gated Ca^{2+} channels.
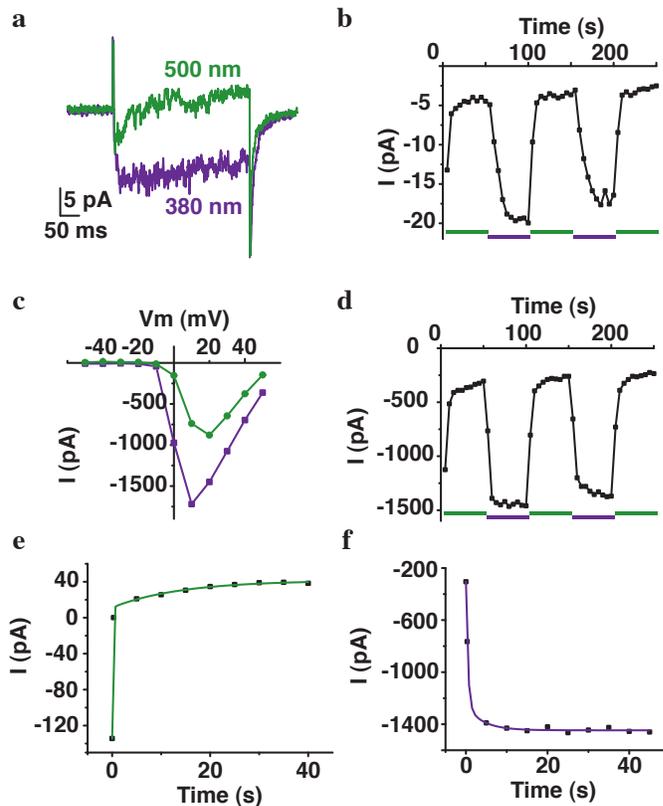
Whole-cell calcium current recording from GH3 cells, using 100 μM QAQ in the pipette, showing (**a**) raw current traces (77.9 ± 2.9 % photoswitching ± s.e.m., n = 5 cells) and (**b**) reversibility of block and unblock under both wavelength of light. Depolarization to +10 mV. Whole cell calcium current recording from HEK-293 cells stably expressing Ca$_v$2.2, using 100 μM QAQ in the pipette, showing (**c**) I/V dependency and (**d**) reversibility of block and unblock. Depolarization to +10 mV. For both voltage-gated Ca^{2+} channels currents were measured using barium instead of calcium, to limit fast inactivation of the current. (**e**) Onset of block on Ca$_v$2.2 after switching light to 500 nm. Current was fitted with a bi-exponential decay equation. For the fast process t$_{1/2}$ = 187 ± 57 ms (n = 3 cells). (**f**) Kinetics of unblock on Ca$_v$2.2 after switching light to 380 nm. Current was fitted with a bi-exponential decay equation. For the fast process t$_{1/2}$ = 270 ± 30 ms (n = 3 cells).

Supplementary Figure 6: QAQ photosensitizes various voltage-gated K⁺ channels.
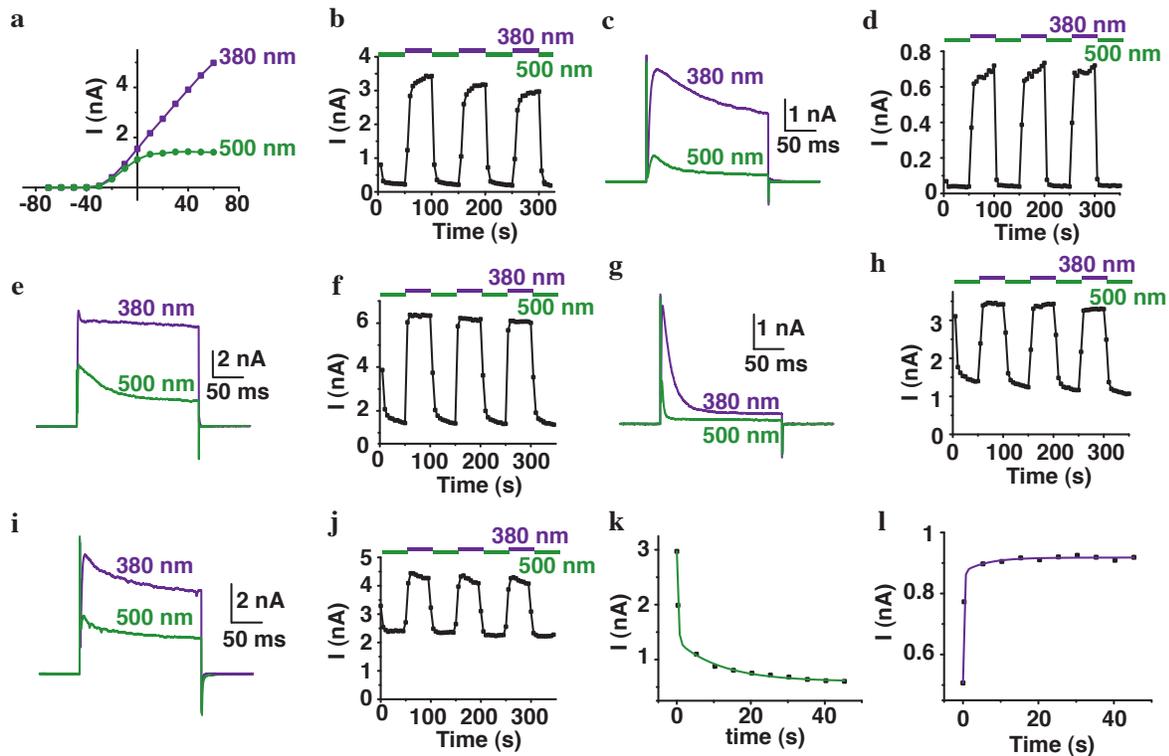
(**a**) I/V relationship for Shaker steady-state current under 380 and 500 nm light illumination, using 100 μM QAQ in the patch pipette. (**b**) Reversibility of QAQ block for Shaker current, using 100 μM QAQ in the pipette. (**c**), (**e**), (**g**) Whole cell current from HEK-293 cells transfected with $K_v2.1$ (86.0 ± 3.5 % photoswitching ± s.e.m., n = 4 cells), $K_v3.1$ (46.6 ± 13.4 % photoswitching s.e.m., n = 4 cells) and $K_v4.2$ (47.1 ± 9.4 % photoswitching s.e.m., n = 4 cells), respectively. (**d**), (**f**), (**h**) Reversibility of QAQ block on $K_v2.1$, $K_v3.1$ and $K_v4.2$, respectively. (**i**) Whole cell potassium current from a hippocampal neuron using 100 μM QAQ in the patch pipette (36.0 ± 5.3 % photoswitching ± s.e.m., n = 13 cells). (**j**) Reversibility of QAQ block in a hippocampal neuron. For all recordings: depolarization from -70 to +40 mV. (**k**) Onset of block on Shaker after switching light to 500 nm. Current was fitted with a bi-exponential decay equation. For the fast process $t_{1/2}$ = 201 ± 20 ms (n = 3 cells). (**l**) Kinetics of unblock on Shaker-IR after switching light to 380 nm. Current was fitted with a bi-exponential decay equation. For the fast process $t_{1/2}$ = 164 ± 15 ms (n = 3 cells).

Supplementary Figure 7: QAQ does not photosensitize K$_{ir}$ or HCN channels.
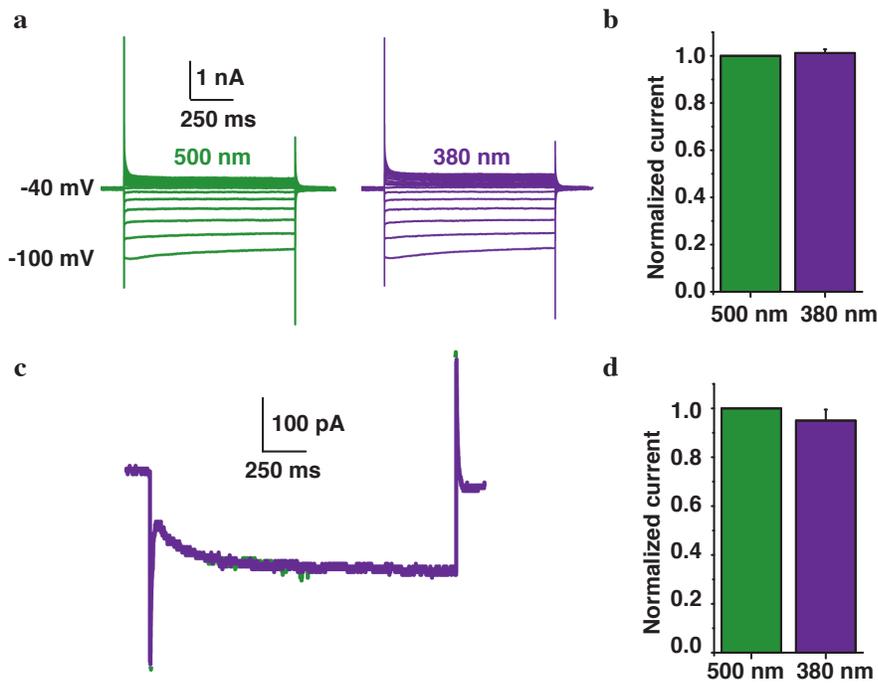
(**a**) K$_{ir}$ currents were measured from HEK-293 cells transfected with K$_{ir}$ 2.1. Currents were elicited by voltage steps from -40 to -100 mV, in 10 mV increments, under illumination with 380 or 500 nm light. (**b**) Normalized current measured at -100 mV under both wavelengths of light (1.2 ± 1.5 % photoswitching, n = 5 cells, p > 0.05). (**c**) HCN currents were measured from acutely dissociated TG neurons upon hyperpolarization to -100 mV under 380 and 500 nm light. (**d**) Normalized current under both wavelengths of light (-5.2 ± 4.7 % photoswitching, n = 3 cells, p > 0.05). Error bars ± s.e.m.; Student t-test.

Supplementary Figure 8: QAQ does not photosensitize glutamate receptors.
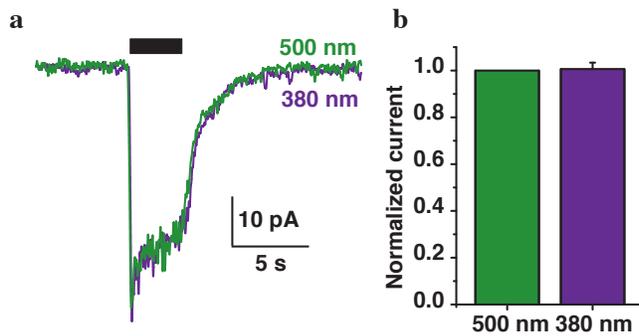
(**a**) Glutamate receptor currents were measured from hippocampal neurons in culture two days after plating. Extracellular solution is similar to K^+ current recording solution without Mg^{2+}. The black bar represents perfusion of extracellular solution containing 100 μM glutamate and 10 μM glycine. Currents were measured under illumination with 380 or 500 nm light. (**b**) Normalized glutamate current under both wavelengths (0.6 ± 2.6 % photoswitching, n = 3 cells, p > 0.05 Student t-test). Error bars ± s.e.m.

Supplementary Figure 9: Neuronal survival after ATP and QAQ treatment.
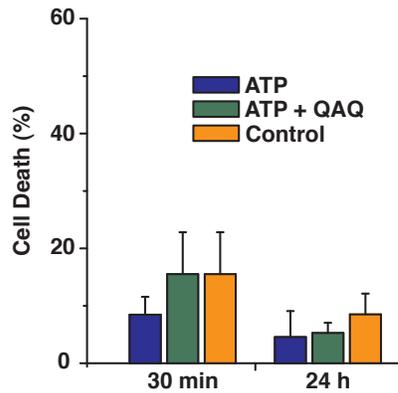
The Live/Dead assay was performed as described by Invitrogen (L-7013). Only dead cells were quantified by using DEAD Red. P2X$_7$ and GFP co-transfected hippocampal neurons were identified by green fluorescence. Cultured hippocampal neurons were transfected with P2X$_7$ (d7) and treated for 30 min with ATP (2.5 mM) +/- QAQ (100 μM), without external calcium, at d9-10. A Live/Dead Assay (Molecular Probes) was used to quantify cell survival among transfected cells, 30 minutes or 24 h after treatment. Both treatments did not cause toxicity compared to control (n = 11-18 fields of view, each field of view containing approximately 1-10 transfected cells; error bars ± s.e.m.).

Supplementary Figure 10: QAQ photosensitizes second order neurons in spinal cord slices.
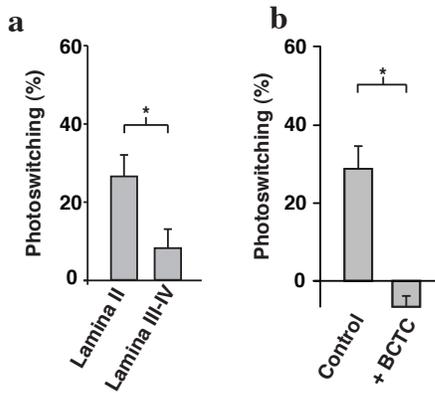
(**a**) Percent photoswitching for laminae II (26.5 ± 5.0 % photoswitching, n = 22 cells) and III-IV neurons (8.2 ± 4.9 % photoswitching, n = 11 cells, p<0.05). (**b**) Percent photoswitching for lamina II neurons with (6.6 ± 3.0 % photosensitization, n = 6 cells) and without 10 μM BCTC (26.5 ± 5.0 % photoswitching, n = 22 cells, p < 0.05). Error bars ± s.e.m.; Student t-test.

3) Exploring the Pharmacology and Action-Spectra of Photochromic Open Channel Blockers & Tuning Photochromic Ion Channel Blockers

3.1) Introduction

The originally introduced PCL and PTL approaches, unifies the fact that all photoswitches are based on a bis-acylated azodianiline core.[1,2,3,4,5,6,7] Here 380 nm and 500 nm light are best suited for converting the trans and *cis* states into each other, respectively. In principle, photoswitches with a red-shifted absorption spectrum could be controlled independently of traditional PCLs and PTLs, creating an orthogonal system, which would broaden possibilities to study neuronal networks. A second feature that increases the need for PCLs and PTLs lies in the application of photoswitches in deeper tissue regions. UV-A light does not penetrate into these regions, preventing the use of traditional PCLs and PTLs.[4] Ideally, the absorption maximum of photoswitches should be around 650-700 nm light.

Similar considerations have lead to the development of VChR1,[8] a microbial rhodopsin from Volvox carteri, which represents a red-shifted ChR2 analogon. Once expressed in neurons, this cation selective channelrhodopsin is activated by 589 nm light, resulting in a membrane depolarization.[9] The disadvantage of VChR1 lies in the incorrect light induced neuronal spike initiation, at frequencies above 5-10 Hz.[8,10]

In the first paper attached in this chapter, the light regulated local anesthetic QAQ, which photocontrols Na_v, Ca_v and K_v channels, has been derivatized to red-shift its action spectrum. Here, at the 2,2' and 6,6' positions of the bis-acylated azodianiline core, different substituents were attached, an approach that has been described before.[11,12] Six derivatives were characterized on K_v channels. 2,2′-dimethoxy-QAQ, 2,6-dimethyl-QAQ and 2,2′,6,6′-tetramethyl-QAQ allow for light control of K_v and Na_v channel current and thereby for light control of neuronal activity. Among the

successful candidates, 2,2′-dimethoxy-QAQ exhibits a red-shifted action spectrum, which allows to use 420 nm light and darkness to switch between the *cis* and *trans* state.[8,10]

In the second paper presented in this chapter, several red-shifted K_v channel PCLs have been synthesized and characterized.[13] Here, one acyl group of the bis-acylated azodianiline core was replaced by amino functions, generating push-pull systems with red-shifted absorption spectra. Among the synthesized compounds, DENAQ and PhENAQ turned out to be most applicable. These compounds can be converted into their *cis* state by 470 nm light and quickly relax back into their *trans* state in the dark.

[1] M. Banghart, K. Borges, E. Isacoff, D. Trauner, R. H. Kramer, *Nat. Neurosci.* **2004**, *7*, 1381-1386.
[2] M. R. Banghart, A. Mourot, D. L. Fortin, J. Z. Yao, R. H. Kramer, D. Trauner, *Angew. Chem. Int. Ed.* **2009**, *48*, 9097-9101.
[3] M. R. Banghart, M. Volgraf, D. Trauner, *Biochemistry* **2006**, *45*, 15129-15141.
[4] T. Fehrentz, M. Schönberger, D. Trauner, *Angew. Chem. Int. Ed.* **2011**, *50*, 12156-12182.
[5] D. L. Fortin, M. R. Banghart, T. W. Dunn, K. Borges, D. A. Wagenaar, Q. Gaudry, M. H. Karakossian, T. S. Otis, W. B. Kristan, D. Trauner, R. H. Kramer, *Nat. Methods* **2008**, *5*, 331-338.
[6] M. Volgraf, P. Gorostiza, R. Numano, R. H. Kramer, E. Y. Isacoff, D. Trauner, *Nat. Chem. Biol.* **2006**, *2*, 47-52.
[7] M. Volgraf, P. Gorostiza, S. Szobota, M. R. Helix, E. Y. Isacoff, D. Trauner, *J. Am.Chem. Soc.* **2007**, *129*, 260-261.
[8] F. Zhang, M. Prigge, F. Beyriere, S. P. Tsunoda, J. Mattis, O. Yizhar, P. Hegemann, K. Deisseroth, *Nat. Neurosci.* **2008**, *11*, 631-633.
[9] F. Zhang, A. M. Aravanis, A. Adamantidis, L. de Lecea, K. Deisseroth, *Nat. Rev. Neurosci.* **2007**, *8*, 577-581.
[10] L. A. Gunaydin, O. Yizhar, A. Berndt, V. S. Sohal, K. Deisseroth, P. Hegemann, *Nat. Neurosci.* **2010**, *13*, 387-392.
[11] A. A. Beharry, O. Sadovski, G. A. Woolley, *J. Am. Chem. Soc.* **2011**, *133*, 19684-19687.
[12] O. Sadovski, A. A. Beharry, F. Zhang, G. A. Woolley, *Angew. Chem. Int. Ed.* **2009**, *48*, 1484-1486.
[13] A. Mourot, M. Kienzler, M. Banghart, T. Fehrentz, F. Huber, M. S., R. H. Kramer, D. Trauner, *ACS. Chem. Neurosci.* **2011**,*2*, 536-543 .

3.2) Publication

Exploring the Pharmacology and Action-Spectra of Photochromic

Open Channel Blockers

Timm Fehrentz[*], Christian A. Kuttruff[*], Florian M. E. Huber, Michael A. Kienzler,

Peter Mayer and Dirk Trauner

Under revision.[1]

[*] authors contributed equally.

---

[1] Experiments were designed by T. Fehrentz and D. Trauner. Electrophysiological characterization of QAQ-derivatives was carried out by T. Fehrentz. Synthesis of 2,2´-dimethoxy-QAQ, 2,2´-dimorpholino-QAQ and 2,2´-di-methylpiperazin-QAQ was performed by C. A. Kutruff. Synthesis of dimethylamino-QAQ was carried out by T. Fehrentz and F. M. E. Huber. Synthesis of 2,6-dimethyl-QAQ and 2,2´,6,6´-tetramethyl-QAQ was performed by M. A. Kienzler.

Exploring the Pharmacology and Action-Spectra
of Photochromic Open Channel Blockers

Timm Fehrentz[a], Christian A. Kuttruff[a], Florian M. E. Huber, Michael A. Kienzler,

Peter Mayer and Dirk Trauner*

Department of Chemistry, University of Munich and Center for Integrated Protein Science (CIPSM), 81377 Munich, Germany

[a] these authors contributed equally to this work.

* corresponding author

E-mail: dirk.trauner@cup.uni-muenchen.de

Photochromic ligands (PCLs) act as light-dependent agonists or antagonists of receptors that allow for the control of neuronal activity with high temporal and spatial precision.[1] An important subclass of PCLs is formed by photochromic ion channel blockers, which have been successfully applied on voltage-gated potassium (K_V) and sodium (Na_V) channels.[2] These channels are evolutionarily related and share similar overall architectures despite marked differences in ion-permeability and subunit stoichiometry.[3] Ions enter or leave the channels through a selectivity filter on the extracellular side, which is connected to a water-filled inner cavity. The path from this inner cavity to the intracellular milieu is controlled by a voltage-gate, which opens and closes in response to changes in the membrane potential. Local anesthetics such as lidocaine or procaine bind in the inner cavity below the selectivity filter, preventing the permeation of cations along their electrochemical gradients.[4] Since the voltage-gate has to open before these molecules can reach the inner cavity, they are often referred as "use-dependent" or "open channel blockers".[4-5]

Recently, we introduced a family of azobenzenes that are essentially photochromic versions of lidocaine.[5b] One of our most effective compounds is a simple symmetric molecule termed QAQ, which functions as a light dependent blocker of a wide variety of K_V and Na_V channels (Figure 1).[2c] Structurally, QAQ consists of two quaternary ammonium ions derived from glycine, which are linked to a 4,4'-azodianiline core *via* two amide bonds. Due to its twofold charge, QAQ is membrane-impermeant and only infiltrates pain-sensing neurons that express endogenous import channels.[2c, 6] Other

cells can be loaded with QAQ more invasively *via* a patch pipette. QAQ blocks voltage-gated Na_V and K_V channels in the *trans* form but not the *cis* form of its azobenzene photoswitch. These channels underlie the initiation and propagation of action potentials (APs).[3a, 4a, 7] Thus, QAQ enables reversible optical silencing of neuronal activity and acts as a light-sensitive analgesic once applied to neural tissues. As such, it is a useful tool for studying signaling mechanisms in acute and chronic pain.[2c]

While QAQ proved to be an effective tool for the control of neuronal activity, its photophysical properties needed to be optimized. As a diacyl derivative of azodianiline, QAQ can be best switched to its *cis* form with 380 nm light and back to its *trans* form with 500 nm light. The short wavelengths used to deactivate it, however, are not ideal for physiological applications, where tissue penetration and associated phototoxicity is a primary concern. Woolley has recently introduced a class of azobenzene photoswitches that are substituted in the 2,2' and 6,6' position with electron-donating substituents and show red-shifted spectra with respect to their unsubstituted analogues.[8] Trying to maintain the symmetrical nature of QAQ, we decided to modulate these substitutions in order to red-shift the action spectrum of the photochromic blocker. The question was whether these structural changes at the azobenzene core would be tolerated by the confined inner cavity of the channel protein, while allowing the use of longer-wavelength light to actuate the switch.

To address this question, we synthesized four QAQ derivatives bearing electron donating substituents in the indicated positions: 2,2′-dimethoxy-QAQ (**1**), 2,2′-dimethylamino-QAQ (**2**), 2,2′-dimorpholino-QAQ (**3**) and 2,2′-N-dimethylpiperazine-QAQ (**4**) (Figure 1). To better discriminate steric from electronic influences, we also synthesized methyl substituted derivatives 2,2′-dimethyl-QAQ (**5**) and 2,2′,6,6′-tetramethyl-QAQ (**6**). The synthesis of these compounds was achieved using short sequences that involved diazonium coupling or oxidative coupling to generate the azobenzene core, followed by amide bond formation (see Supporting Information).

With compounds **1**-**6** in hand, we first characterized their ability to induce light dependent block of the inactivation-removed Shaker K^+ channel (Shaker-IR),[9] a voltage-gated K^+ channel (Figure 2). Compounds were loaded *via* patch pipette into

HEK293 cells expressing Shaker-IR. Measurements were performed after a short equilibration period of the cytosol and pipette solution.

Application of compounds **1**, **5** and **6** permitted the reversible light control of Shaker-IR K$^+$ current (Figure 2). Derivatives **1**, **5** and **6** resulted in 31.8% ± 5,7% (350 μM, n = 3 cells), 64.7% ± 5,5% (100 μM, n = 3 cells) and 67.8% ± 4,8% (100 μM, n = 5 cells) light induced voltage dependent block of the channel current, respectively (Figure 2 and 3). The *trans* state of all active compounds induced block, whereas the *cis* state reversed the effect. Derivatives **5** and **6** were converted into their *cis* and *trans* states with 380 nm and 500 nm light, respectively.

Compound **1** represents a red-shifted azobenzene PCL[8a] with an absorption maximum λ_{max} = 416 nm light. Irradiation with 420 nm light was used to convert the thermally stable *trans* form into the *cis* state. Thermal relaxation in the dark was used to revert compound **1** into its *trans* state. Here, the relative channel current follows the equation: $y_0 + A_1 \exp(-x/\tau_1) + A_2 \exp(-x/\tau_2)$, y_0 = 0.649 ± 0.02, A_1 = 0.190 ± 0.010, A_2 = 0.160 ± 0.014, τ_1 = 1.948 ± 0.226 s, τ_2 = 39.454 ± 10.8 s (see Supporting Information). In contrast, thermal relaxation of compound **1** in DMSO shows slower kinetics, whereat data were fitted to the equation: $y_0 + A \exp(-x/\tau)$, y_0 = 0.006 ± 0.002, A = 0.978 ± 0.004, τ = 4.61 ± 0.40 min (see Supporting Information). The action spectrum of compound **1** indicates that wavelengths between 350 nm - 500 nm allow for *trans* to *cis* conversion (see Supporting Information). Compounds **2**, **3** and **4** showed no voltage dependent block and thus no photoregulation of the Shaker-IR current.

The finding that QAQ acts on both Na$_v$ and K$_v$ channels[2c] prompted us to investigate, whether QAQ derivatives also block Na$_v$ channels. We tested compounds **1**, **5** and **6** on NG108-15 cells, a mouse neuroblastoma cell line that endogenously expresses Na$_v$ channel subtypes Na$_v$1.1-1.4, 1.6 and 1.7.[10] After delivery through the patch pipette into cells, all three compounds reversibly blocked voltage induced Na$^+$ current in a light dependent manner (Figure 4). As for the case with Shaker-IR, block was induced by the *trans* state of all three QAQ derivatives. Compounds **1**, **5** and **6** resulted in 38,6% ± 6,5% (1 mM, n = 4 cells), 75.5% ± 1,8% (50 μM, n = 3 cells) and 46.3% ± 4,7% (100 μM, n = 4 cells) photoregulation of Na$^+$ peak current, respectively.

Na_v and K_v channels play a crucial role in the initiation and propagation of APs in neurons.[4a, 7] Application of compounds **1, 5** and **6** *via* the patch pipette into cortical CA1 neurons of mouse slices allowed, after injection of a depolarizing current pulse, modulation of AP firing in a light dependent manner (Figure 4). The *trans* state of all three compounds silenced neuronal excitability, whereas the *cis* state unblocked Na_v and K_v channels, restoring AP firing. A single spike remained under *trans* recording conditions, which can be explained by the principle of open-channel block, i.e. the delay between channel opening and blocker accumulation within the pore that is sufficient to trigger a single AP.[2c]

In summary, we have shown that the useful photochromic channel blocker QAQ can be further substituted at its azobenzene core. Its derivatives **1**, **5** and **6** allowed for the rapid reversible control of Na_V and K_V channel conductance, whereas larger substituents showed no block of channel current. Of the three blockers identified, only compound **1** shows a red-shifted action spectrum. Our data indicates, that either the inner vestibule, or the open gate leading into the inner vestibule of the Shaker-IR and Na_v channels do not tolerate QAQ derivatives bearing substituents larger than a methoxy group in 2,2'-*ortho* positions. The higher concentration of compound **1** needed to elicit photoswitching can be interpreted as lower efficacy of the compound towards the channel, which may be a consequence of its increased size. Our study has provided three new photochromic blockers of voltage-gated channels, which may help to probe the influence of Na_v and K_v channels on dendritic signaling in neurons.[11] Moreover, they could serve as tools to unravel molecular mechanisms of pain.[2c, 12]
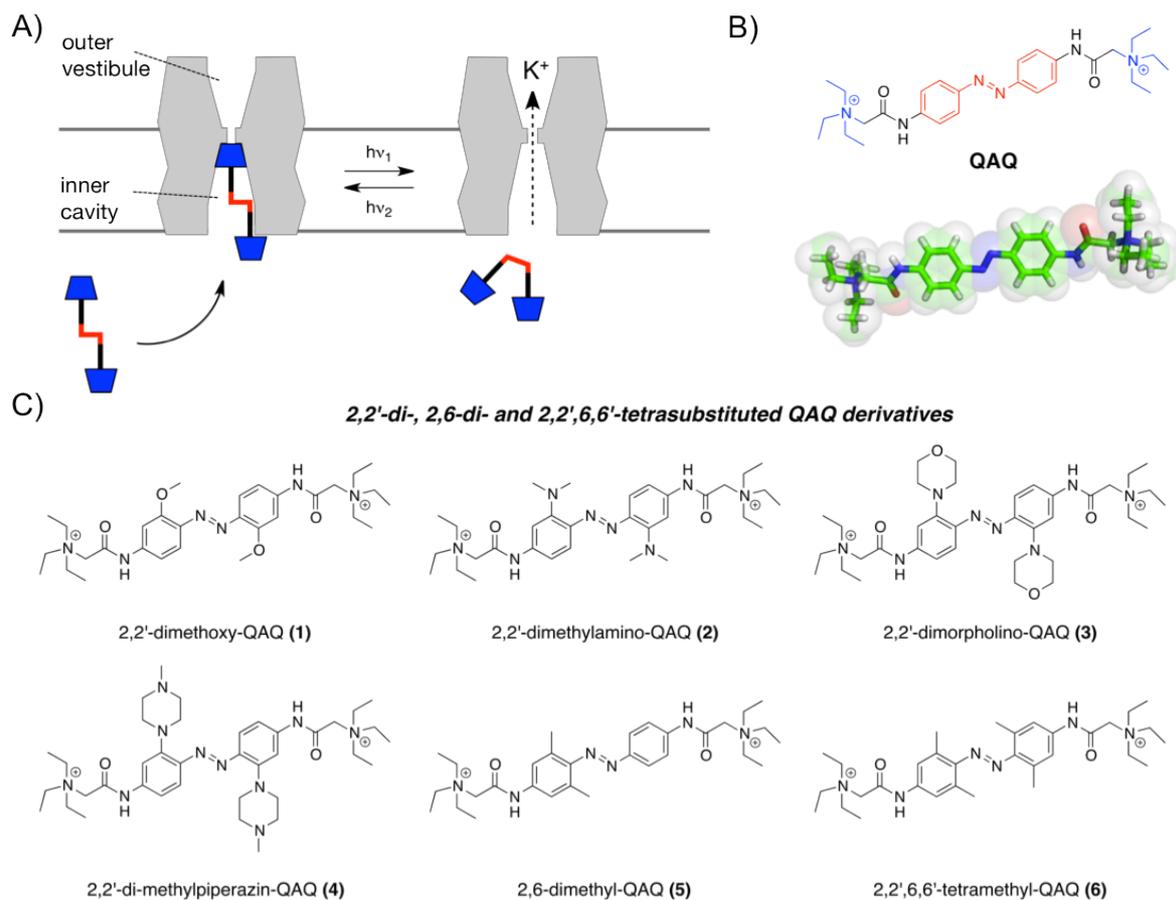
Figure 1. A) QAQ and derivatives act as light controlled open channel blockers. Schematic depiction of light induced *trans* block and *cis* unblock of QAQ derivatives on voltage-gated ion channels. The *trans* state of the photoswitch prevents ionic current, whereas the *cis* state restores ionic conductance. B) Chemical and crystal structure of the parent molecule QAQ. The distance between the quaternary ammonium groups is approximately 18,9 Å. C) QAQ derivatives introduced in this study.
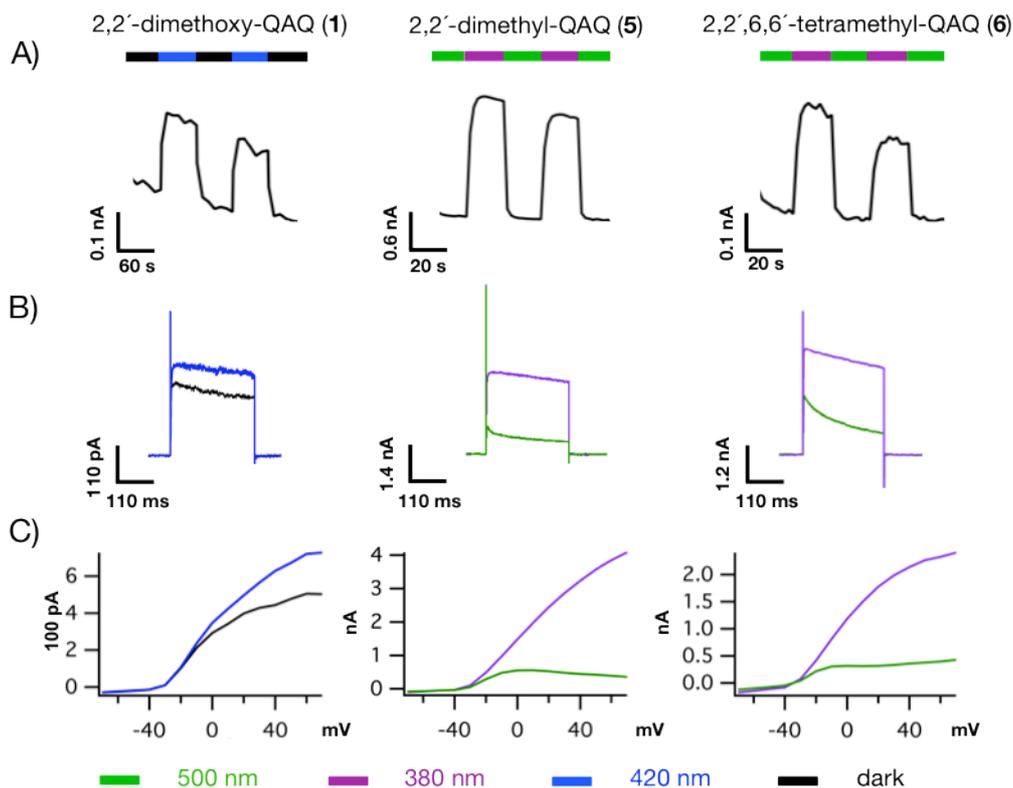
Figure 2. Application of QAQ derivatives on the internal side of a K_v channel subtype. from left to right: compound **1** (350 µM), **5** (100 µM) and **6** (100 µM); purple, green, blue and dark lines indicate irradiation of 380 nm light, 500 nm light, 420 nm light and darkness, respectively.

A) Reversible photosensitizing of Shaker-IR K^+ current. Individual amplitudes of voltage-clamp recordings, under different irradiation wavelengths, are connected by a line. B) Comparison of single Shaker current traces under indicated wavelength, elicited by a depolarizing pulse from a holding potential of -70 mV to +40 mV for 250 ms. C) Current-voltage dependent *trans* block and *cis* unblock under indicated wavelengths from -50 mV to +70 mV.
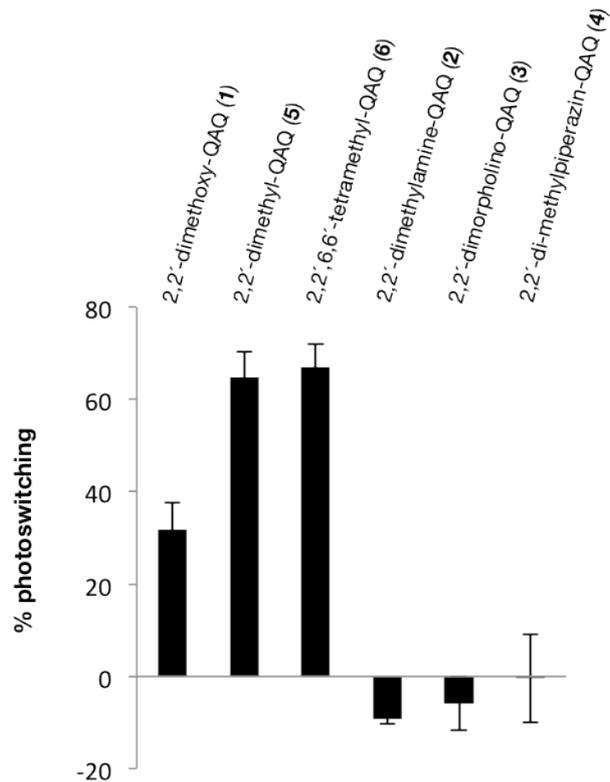
Figure 3. Quantification of QAQ derivative photoswitching on Shaker-IR. Percent photoswitching is defined as $I_{500nm(30sec)} - I_{300(30sec)}/I_{380(30sec)}$. Derivative **1** resulted in 31.8% ± 5,7% (350 μM, n = 3 cells), derivative **5** in 64.7% ± 5,5% (100 μM, n = 3 cells), derivative **6** in 67.8% ± 4,8% (100 μM, n = 5 cells), derivative **2** resulted in -9,3% ± 1% (500 μM, n = 3 cells), derivative **3** in -5,8% ± 5,8% (500 μM, n = 4 cells) and derivative **4** in -0,4% ± 9,8% (500 μM, n = 4 cells) photoswitching, respectively. Negative photoswitching is due to a recording artefact of current rundown.
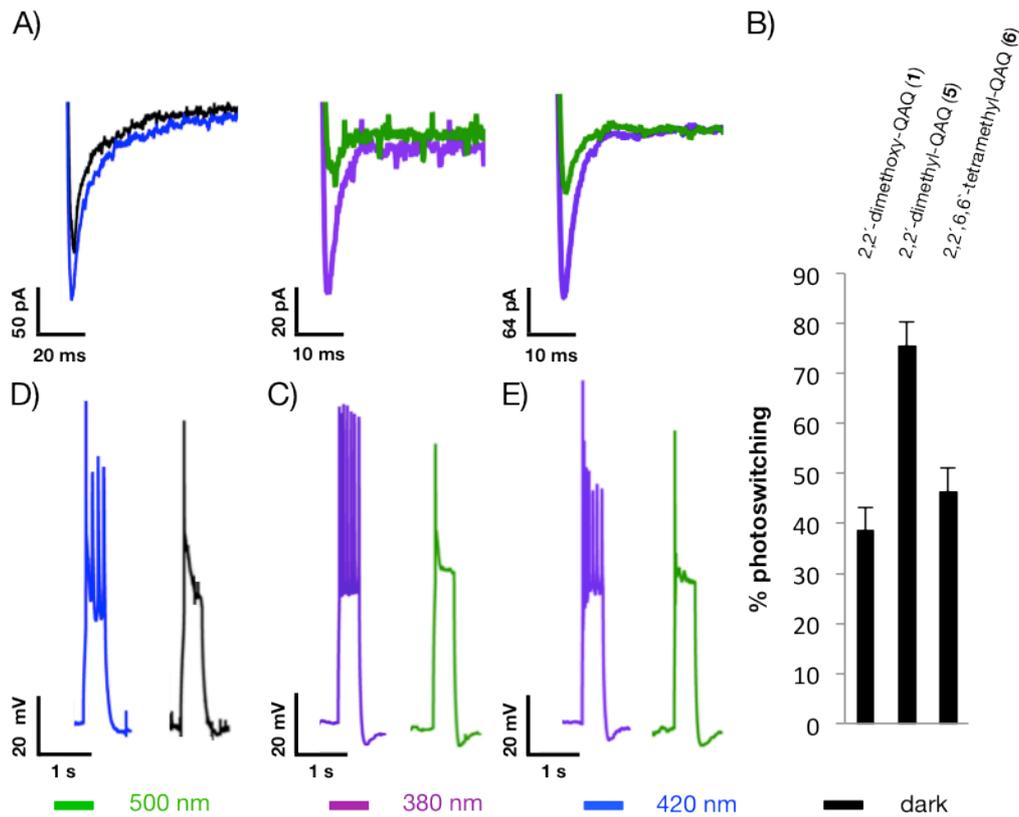
Figure 4. QAQ derivatives act as reversible internal Na_v channel bockers and control activity of cortical pyramidal neurons. Recording artefacts have been removed for clarity A) from left to right: 1 mM compound **1**, 50 µM compound **5**, 100 µM compound **6** induce light dependent Na_v current block of NG108-15 cells. B) Quantification of QAQ derivatives induced photoswitching. Amount of photosensitization of Na_v current is defined as $I_{peak\_current\_380nm(10sec)} - I_{peak\_current\_500nm(10sec)})/I_{peak\_current\_380nm(10sec)}$. C-E) Reversible silencing of neuronal AP trains, evoked by current injection of approximately 150 pA (400 ms). C) 1 mM of derivative **1**. D) 50 µM of derivative **5**. E) 100 µM of derivative **6**. Resting potentials of all neurons measured were about -75 - -80 mV.

[1]   a) E. Bartels, N. H. Wassermann, B. F. Erlanger, *Proc. Natl. Acad. Sci. USA* **1971**, *68*, 1820-1823; b) T. Fehrentz, M. Schönberger, D. Trauner, *Angew. Chem. Int. Ed.* **2011**, *50*, 12156-12182; c) M. Volgraf, P. Gorostiza, S. Szobota, M. R. Helix, E. Y. Isacoff, D. Trauner, *J. Am. Chem. Soc.* **2007**, *129*, 260-261.

[2]   a) M. R. Banghart, A. Mourot, D. L. Fortin, J. Z. Yao, R. H. Kramer, D. Trauner, *Angew. Chem. Int. Ed.* **2009**, *48*, 9097-9101; b) D. L. Fortin, M. R. Banghart, T. W. Dunn, K. Borges, D. A. Wagenaar, Q. Gaudry, M. H. Karakossian, T. S. Otis, W. B. Kristan, D. Trauner, R. H. Kramer, *Nat. Methods* **2008**, *5*, 331-338; c) A. Mourot, T. Fehrentz, Y. Le Feuvre, C. M. Smith, C. Herold, D. Dalkara, F. Nagy, D. Trauner, R. H. Kramer, *Nat. Methods* **2012**, 9, 396-402; d) A. Mourot, M. Kienzler, M. Banghart, T. Fehrentz, F. M. S. Huber, R. H. Kramer, D. Trauner, *ACS. Chem. Neurosci.* **2011**, *2*, 536-543.

[3]   a) C. Hammond, *Cellular and molecular neurophysiology*, 3 ed., Elsevier Science, **2008**; b) F. H. Yu, V. Yarov-Yarovoy, G. A. Gutman, W. A. Catterall, *Pharmacol. Rev.* **2005**, *57*, 387-395.

[4]   a) B. Hille, *Ionic channels of excitable membranes*, 3 ed., Sinauer Associates, Inc., **2001**; b) G. R. Strichartz, *J. Gen. Physiol.* **1973**, *62*, 37-57.

[5]   a) C. M. Armstrong, *J. Gen. Physiol.* **1969**, *54*, 553-575; b) A. Scholz, *Br. J. Anaesth.* **2002**, *89*, 52-61.

[6]   A. M. Binshtok, B. P. Bean, C. J. Woolf, *Nature* **2007**, *449*, 607-610.

[7]   B. P. Bean, *Nat. Rev. Neurosci.* **2007**, *8*, 451-465.

[8]   a) A. A. Beharry, O. Sadovski, G. A. Woolley, *J. Am. Chem. Soc.* **2011**, *133*, 19684-19687; b) O. Sadovski, A. A. Beharry, F. Zhang, G. A. Woolley, *Angew. Chem. Int. Ed.* **2009**, *48*, 1484-1486.

[9]   T. Hoshi, W. N. Zagotta, R. W. Aldrich, *Science* **1990**, *250*, 533-538.

[10]   A. Kawaguchi, H. Asano, K. Matsushima, T. Wada, S. Yoshida, S. Ichida, *Neurochem. Res.* **2007**, *32*, 1469-1475.

[11]   A. Losonczy, J. K. Makara, J. C. Magee, *Nature* **2008**, *452*, 436-441.

[12]   A. I. Basbaum, D. M. Bautista, G. Scherrer, D. Julius, *Cell* **2009**, *139*, 267-284.

Exploring the Pharmacology and Action-Spectra of
Photochromic Open Channel Blockers

Timm Fehrentz[a], Christian A. Kuttruff[a], Florian M. E. Huber, Michael A. Kienzler,

Peter Mayer and Dirk Trauner*

Department of Chemistry, University of Munich and Center for Integrated Protein Science (CIPSM), 81377 Munich, Germany

[a] these authors contributed equally to this work.

* corresponding author

  E-mail: dirk.trauner@cup.uni-muenchen.de

Supplementary Information

Index:

General Experimental Details. Unless stated otherwise, all reactions were performed in oven-dried or flame-dried glassware under a positive pressure of nitrogen. Commercial reagents and solvents were used as received with the following exceptions. Tetrahydrofuran

(THF) was distilled from benzophenone and sodium immediately prior to use. Triethylamine, diisopropylamine and diisopropylethylamine were distilled over calcium hydride immediately before use. Reactions were magnetically stirred and monitored by NMR spectroscopy or analytical thin-layer chromatography (TLC) using E. Merck 0.25 mm silica gel 60 F_{254} precoated glass plates. TLC plates were visualized by exposure to ultraviolet light (UV, 254 nm) and/or exposure to an aqueous solution of ceric ammoniummolybdate (CAM), an aqueous solution of potassium permanganate (KMnO$_4$), an acidic solution of vanillin or a solution of ninhydrin in ethanol followed by heating with a heat gun. Flash column chromatography was performed as described by Still *et al.* employing silica gel (60 Å, 40-63 µm, Merck) and a forced flow of eluant at 1.3-1.5 bar pressure.[2] Reversed phase column chromatography was carried out with Waters Prep C$_{18}$ (55–105 µm, 125 Å) silica gel. Yields refer to chromatographically and spectroscopically (^{1}H and ^{13}C NMR) pure material.

Instrumentation. Proton nuclear magnetic resonance (^{1}H NMR) spectra were recorded on Varian VNMRS 300, VNMRS 400, INOVA 400 or VNMRS 600 spectrometers. Proton chemical shifts are expressed in parts per million (δ scale) and are calibrated using residual undeuterated solvent as an internal reference (CDCl$_3$: δ 7.26, DMSO-d_6: δ 2.50, CD$_3$OD: δ 3.31). Data for ^{1}H NMR spectra are reported as follows: chemical shift (δ ppm) (multiplicity, coupling constant (Hz), integration). Multiplicities are reported as follows: s = singlet, d = doublet, t = triplet, q = quartet, m = multiplet, *br* = broad, app = apparent, or combinations thereof. Carbon nuclear magnetic resonance (^{13}C NMR) spectra were recorded on Varian VNMRS 300, VNMRS 400, INOVA 400 or VNMRS 600 spectrometers. Carbon chemical shifts are expressed in parts per million (δ scale) and are referenced to the carbon resonances of the solvent (CDCl$_3$: δ 77.0, DMSO-d_6: δ 39.5, CD$_3$OD: δ 49.0). Infrared (IR) spectra were recorded on a Perkin Elmer Spectrum BX II (FTIR System). IR data is reported in frequency of absorption (cm^{-1}). Mass spectroscopy (MS) experiments were performed on a Thermo Finnigan MAT 95 (EI), a Thermo Finnigan LTQ FT (ESI) or a JEOL JMS-700 (FAB) instrument. UV/Visible spectra were recorded on a Varian Cary 50 Scan UV-Visible Spectrophotometer using STARNA 29/B/12 quartz cuvettes with 10 mm section thickness.

---

[2] Still, W. C.; Kahn, M.; Mitra, A. *J. Org. Chem.* **1978**, *43*, 2923–2925.

Electrophysiology and cell culture. HEK293 and NG108-15 cells haven been cultured and cortical slice preparation was performed as described before.[3,4]

Patch clamp recordings and analysis have been performed with a standard electrophysiological setup, including an HEKA Patch Clamp EPC10 USB amplifier and patch master software. Measurements were recorded in whole cell mode. Pipette (Science Products GB200-F-8P with filament) resistance varied between 4-6 MΩ. Irradiation of samples have been performed with a TILL Photonics Polychrome 5000 monochromator, through a Nicon Fluor 60x/1.00w objective.[2]

Extracellular potassium current recording solution contained in mM: 138 NaCl, 1.5 KCl, 1.2 $MgCl_2$, 2.5 $CaCl_2$, 5 HEPES free acid, 10 glucose and pH was adjusted to 7.4. Extracellular sodium current recording solution contained in mM: 145 NaCl, 0.5 $CdCl_2$, 2 $CaCl_2$, 5 HEPES free acid, 5 glucose and pH was adjusted to 7.4. Internal potassium current recording solution contained in mM: 10 NaCl, 135 K gluconate, 10 HEPES free acid, 2 $MgCl_2$, 2 MgATP, 1 EGTA and pH was adjusted to 7.4. Internal sodium current recording solution contained in mM: 30 NaCl, 100 CsCl, 10 HEPES free acid, 2 $MgCl_2$, 1 $CaCl_2$, 2 MgATP 0.05 GTP, 10 EGTA, 5 glucose and pH was adjusted (CsOH) to 7.3. Ringer solution contained in mM: 96 NaCl, 2 KCl, 1 $MgCl_2$, 1.8 $CaCl_2$, 5 HEPES free acid and pH was adjusted to 7.4.

Photoswitches were dissolved in internal solution to give the final working concentrations. DMSO concentration in internal solutions was below 0.1%. After patching cells, internal solution and cytosol were allowed to equilibrate for about 2–3 min. A typical voltage clamp protocol to record Shaker-IR current depolarized, in a looped manner, the membrane from its holding potential of -70 mV to +40 mV for 250 ms. The protocol was applied with a frequency of 0.5 Hz and the depolarization was initiated 250 ms after protocol started. Recordings were accompanied by illumination at a defined wavelength, which was changed every 30 cycles. To record current-voltage (IV) curves of Shaker-IR, a protocol hold the cell at -70 mV and depolarized the cell in a loop sequence to values between -50 mV and +70 mV, in 10 mV intervals. Illumination wavelengths were changed for each IV protocol.

The voltage clamp protocol to record Na_v channel current, hold the cell at -100 mV and depolarized the cell, for 250 ms, to -10 mV. The depolarisation was initiated 250 ms after the beginning of the protocol, which was applied at a frequency of 0.5 Hz. Recordings were accompanied by changing irradiation wavelength every 10 cycles. Recording of APs was performed in current clamp mode. Single current pulses with the same strength were injected

---

[3] Mourot, A.; Fehrentz, T.; Le Feuvre, Y.; Smith, C. M.; Herold, C.; Dalkara, F.; Nagy, F.; Trauner, D.; Kramer, R. H. *Nat. Methods* **2012**, Article *ASAP.*

[4] Bischofberger, J.; Engel, D.; Li, L.; Geiger, J. R. P.; Jonas, P. *Nat. Prot.* **2006**, *1*, 2075–2081.

into cortical pyramidal neurons to elicit robust AP firing in the presence of QAQ derivatives in the *cis* state but not in the *trans* state. All data presented have been analyzed as averages ± s.e.m.

Synthesis of 2,2'-Dimethylamino-QAQ (2), 2,2'-Dimorpholino-QAQ (3) and 2,2'-Dimethylpiperazine-QAQ (4)

Compounds **2**, **3** and **4** were synthesized from the corresponding bisacetamides **S2**, **S3** and **S4**, whose syntheses were described previously.[5]
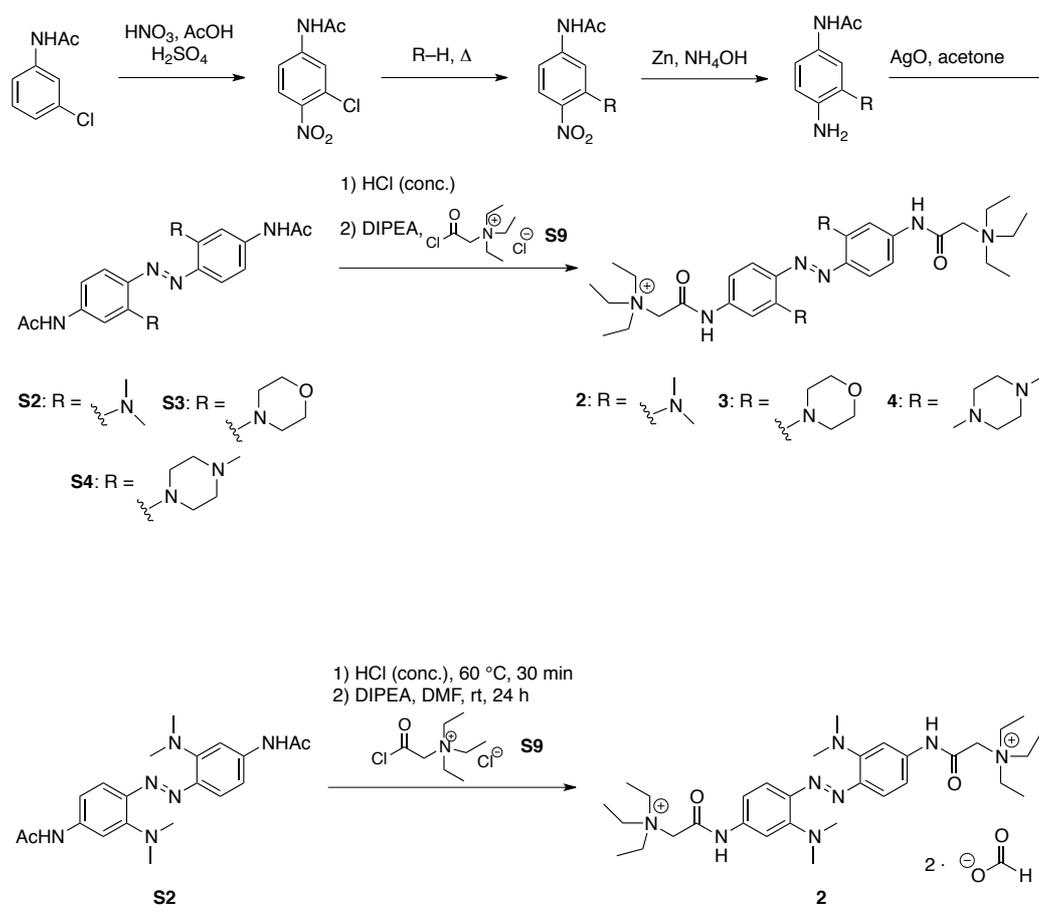
2,2'-Dimethylamino-QAQ (2):

Diazene **S2** (32 mg, 0.8 µmol, 1.0 equiv.) was dissolved in conc. HCl (1.0 mL) and the dark red reaction mixture was heated to 60 °C for 30 min. The reaction mixture was cooled to rt and the solvent removed under high vacuum. The residue was dissolved in dry DMF (1.0 mL) and DIPEA (0.3 mL, 8.0 mmol, 10.0 equiv.) was added dropwise. The solution was cooled to 0 °C and a solution of **S9** (130 mg, 8.0 µmol, 10 equiv.) in dry DMF (1.0 mL) was added dropwise. The reaction mixture was allowed to warm to rt, stirred overnight and DMF was subsequently removed under high vacuum. The crude product was purified by reversed phase

[5] Sadovski, O.; Beharry, A. A.; Zhang, F.; Woolley, G. A. *Angew. Chem. Int. Ed.* **2009**, *48*, 1484–1486.

column chromatography (gradient: MeOH/H$_2$O/HCOOH = 0:1:1·10^{-3} → 2:8:8·10^{-3}) to afford dimethylamino-QAQ formate salt **2** (12 mg, 17.8 µmol, 21%) as a dark red solid.

^{1}H NMR (600 MHz, CD$_3$OD) δ: 8.41 (*br* s, 2 H), 7.65 (d, *J* = 8.8 Hz, 2 H), 7.54 (d, *J* = 1.9 Hz, 2 H), 7.12 (dd, *J* = 8.8, 1.9 Hz, 2 H), 4.19 (s, 4 H), 3.68 (q, *J* = 7.2 Hz, 12 H), 3.06 (s, 12 H), 1.40 (t, *J* = 7.2 Hz, 18 H).

^{13}C NMR (150 MHz, CD$_3$OD) δ: 163.1, 152.8, 142.5, 141.6, 118.9, 113.6, 110.2, 103.3, 57.6, 55.8, 45.5, 8.0.

IR (Diamond-ATR, neat) $\tilde{v}$: 3255, 2987, 2948, 2780, 2683, 1685, 1659, 1579, 1477, 1456, 1404, 1371, 1342, 1307, 1250, 1200, 1173, 1157, 1115, 1051, 1007, 950, 857, 790, 774, 765, 718 cm^{-1}.

HRMS (FAB) calcd for C$_{32}$H$_{54}$O$_2$N$_8$ [M]$^{+\bullet}$: 582.4359; found: 582.4368.

UV-Vis (DPBS, pH = 7.4): λ_{max} = 430 nm.
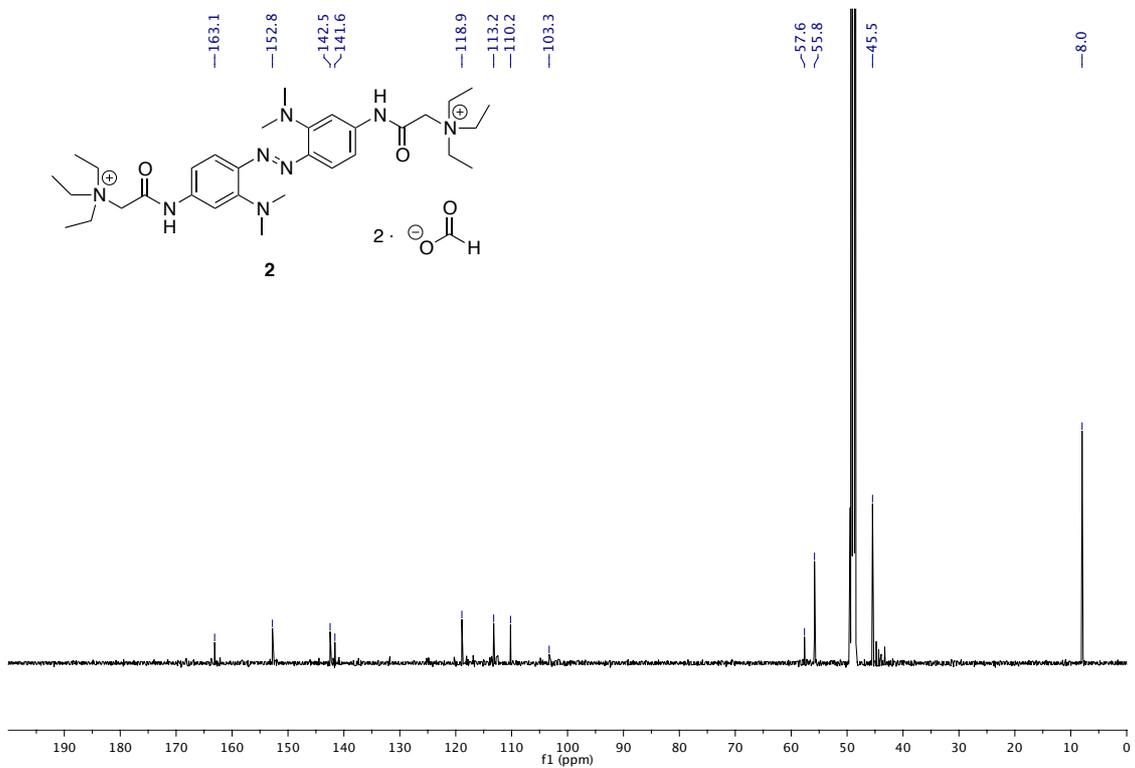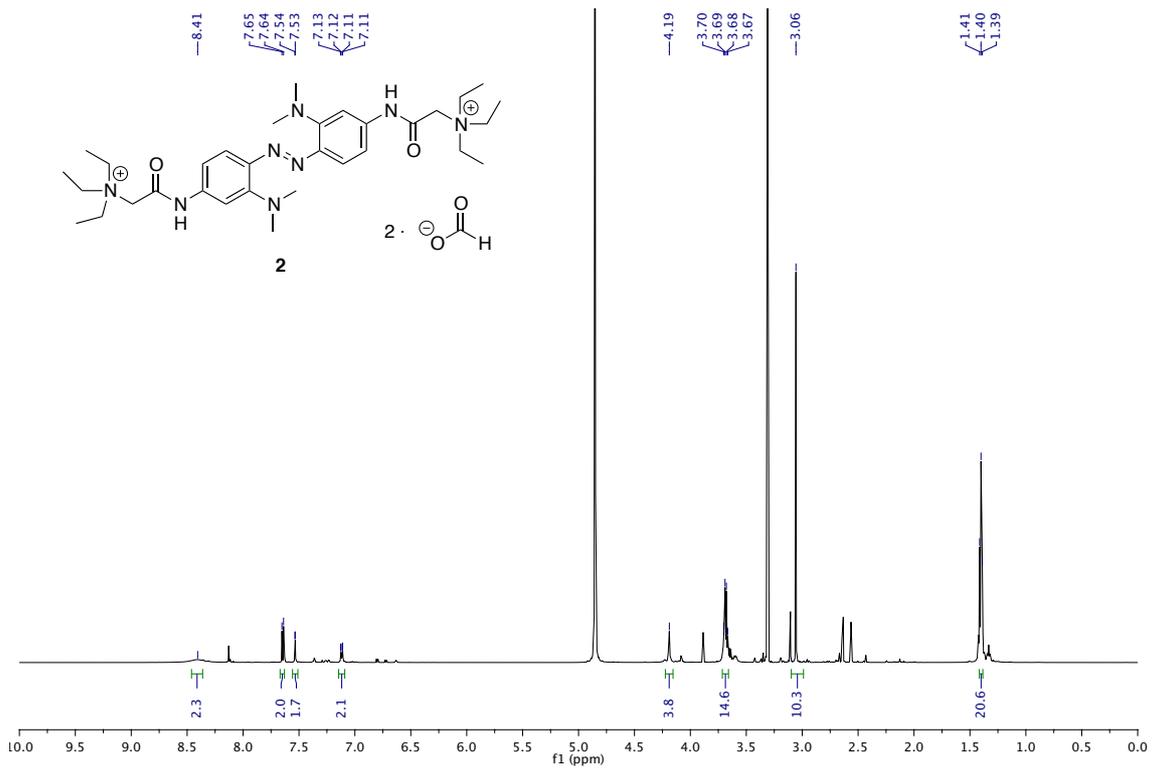
UV/VIS spectra of compounds 1-6

All UV/VIS spectra of compounds **1-6** were recorded in PBS solution. Compound **1** was additional recorded in DMSO.

2,2'-Dimorpholino-QAQ (**3**)

2,2'-Di-metylpiperazin-QAQ (**4**)

2,6-Dimethyl-QAQ (**5**)

extinction (a.u.) vs wavelength (nm)

Dark — 360 nm

2,2',6,6'-Tetramethyl-QAQ (**6**)

extinction (a.u.) vs wavelength (nm)

Dark — 360 nm
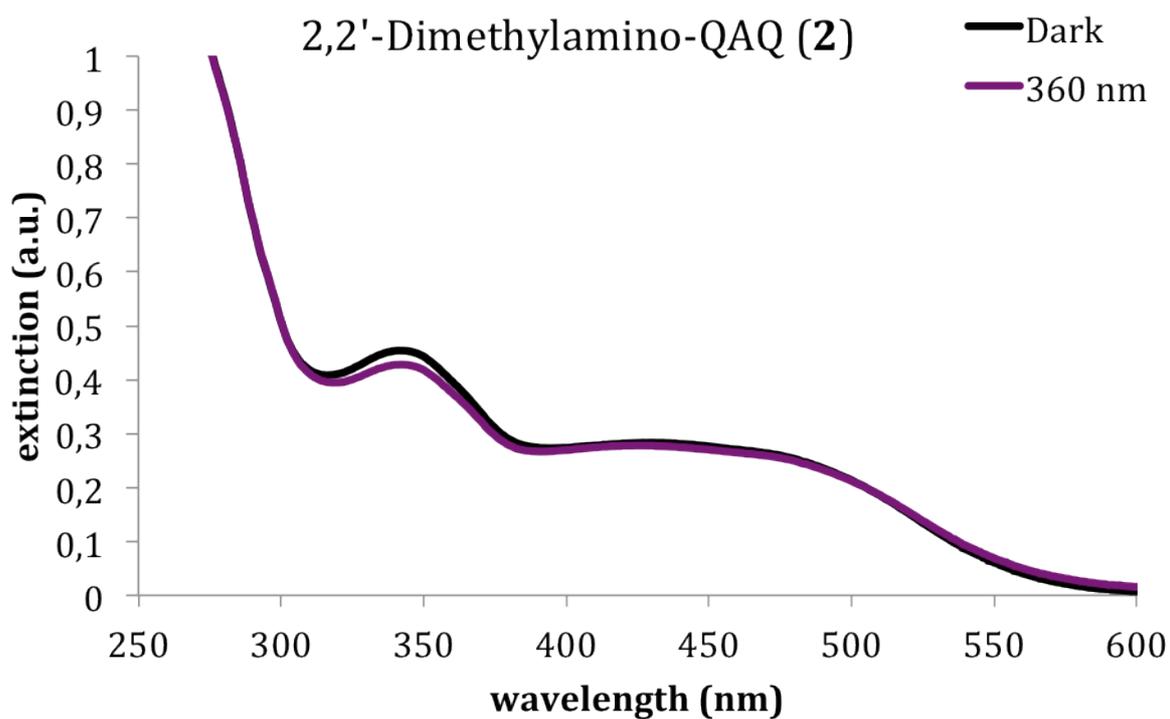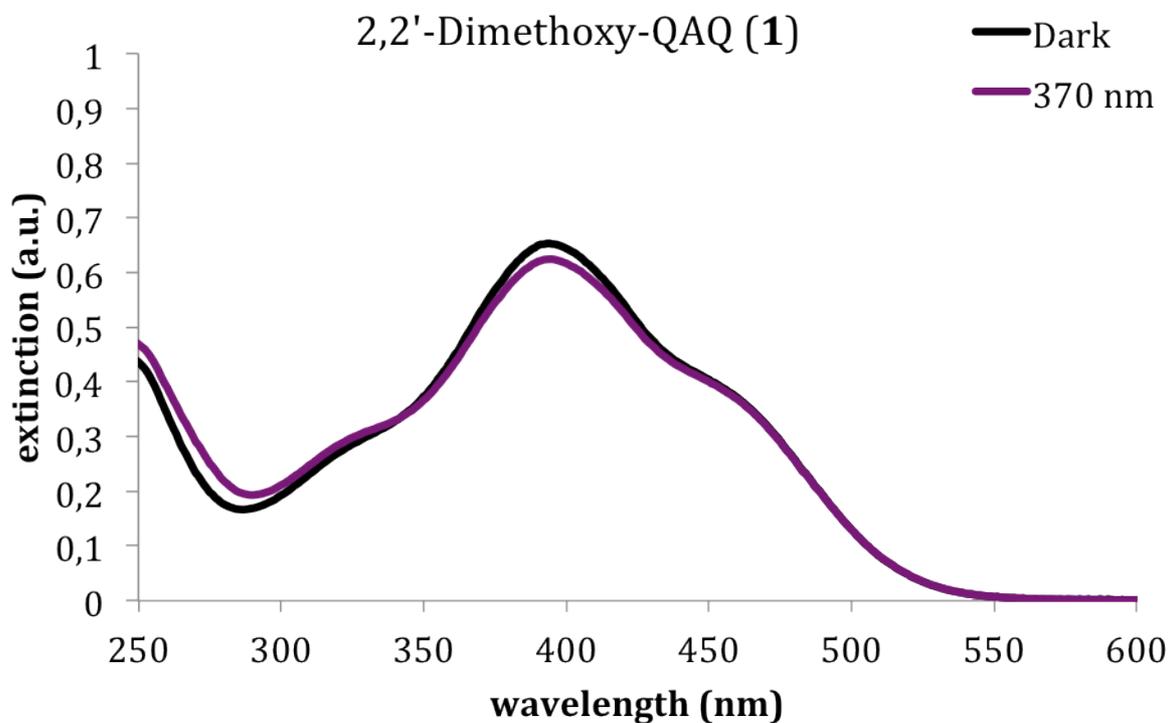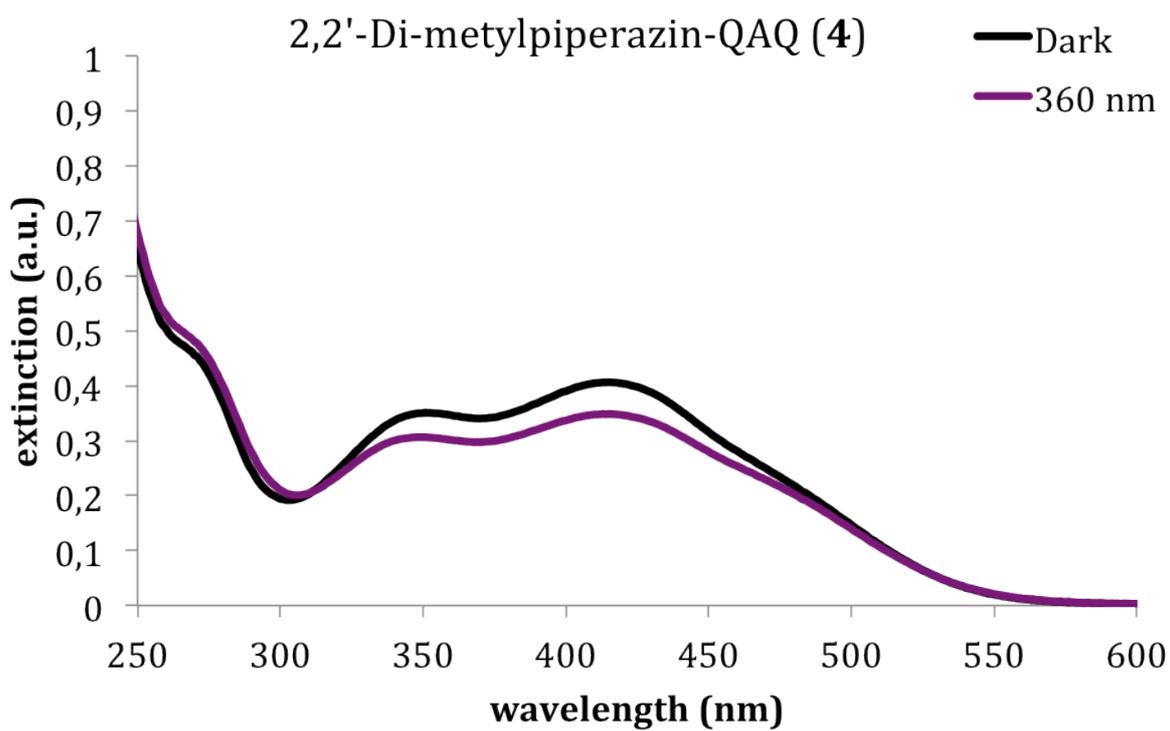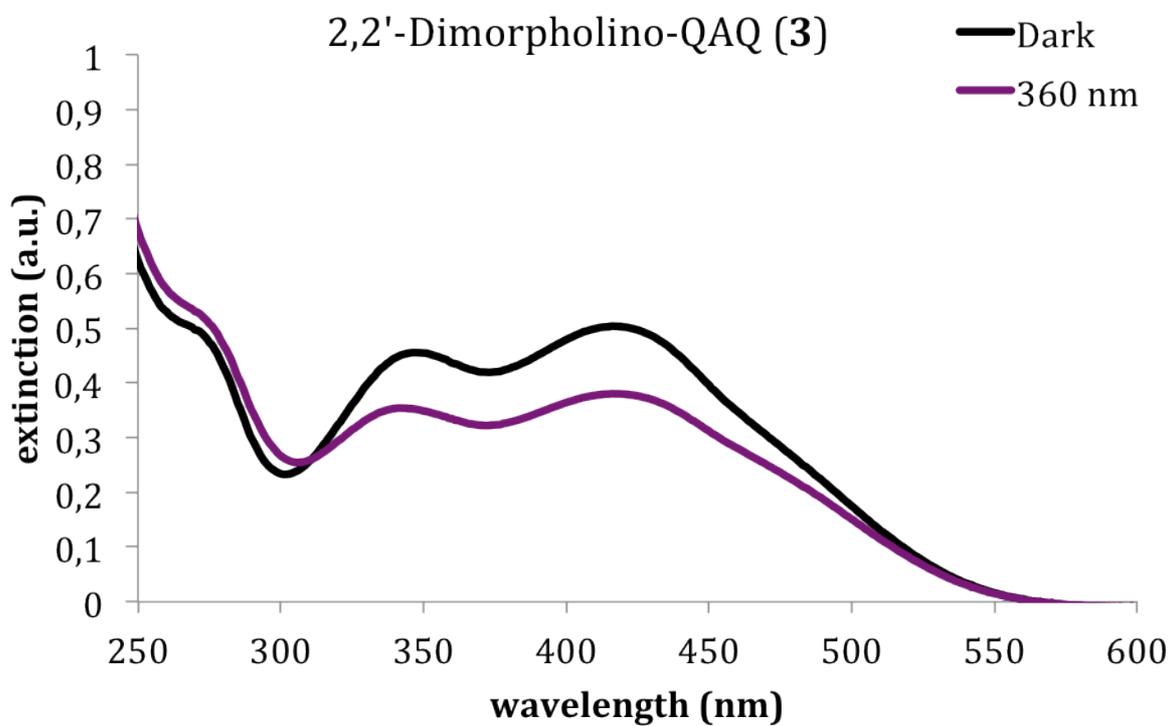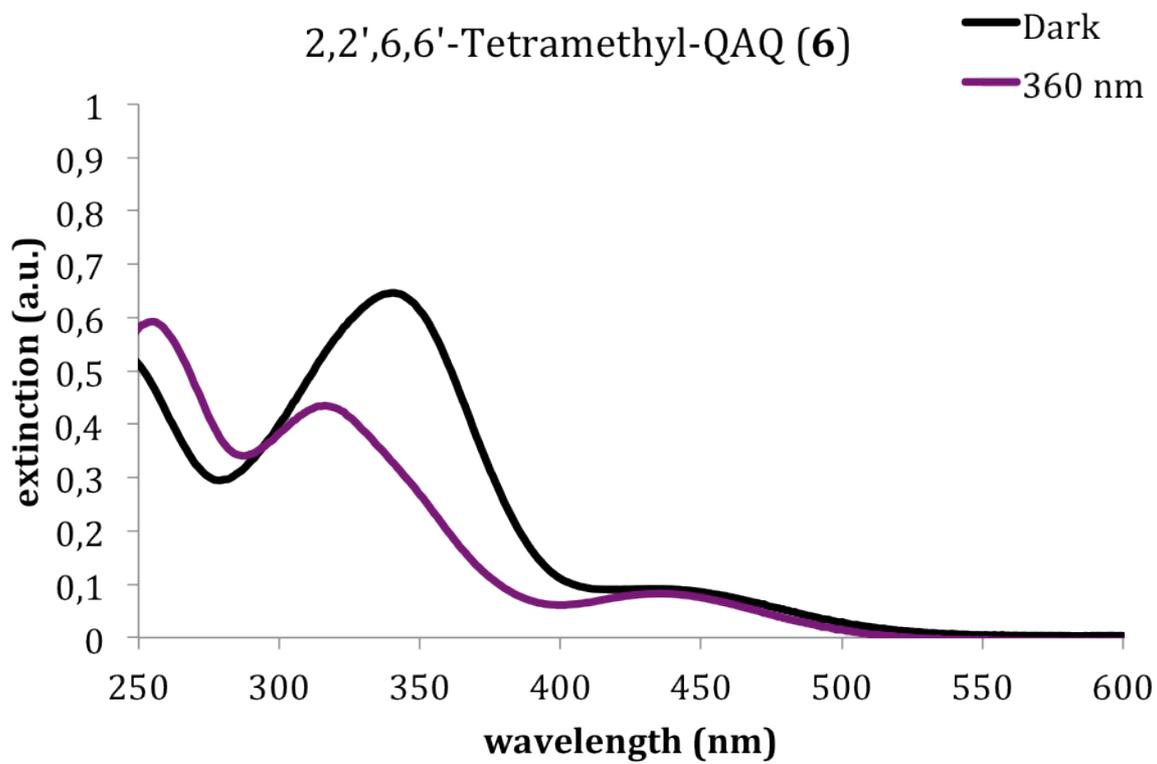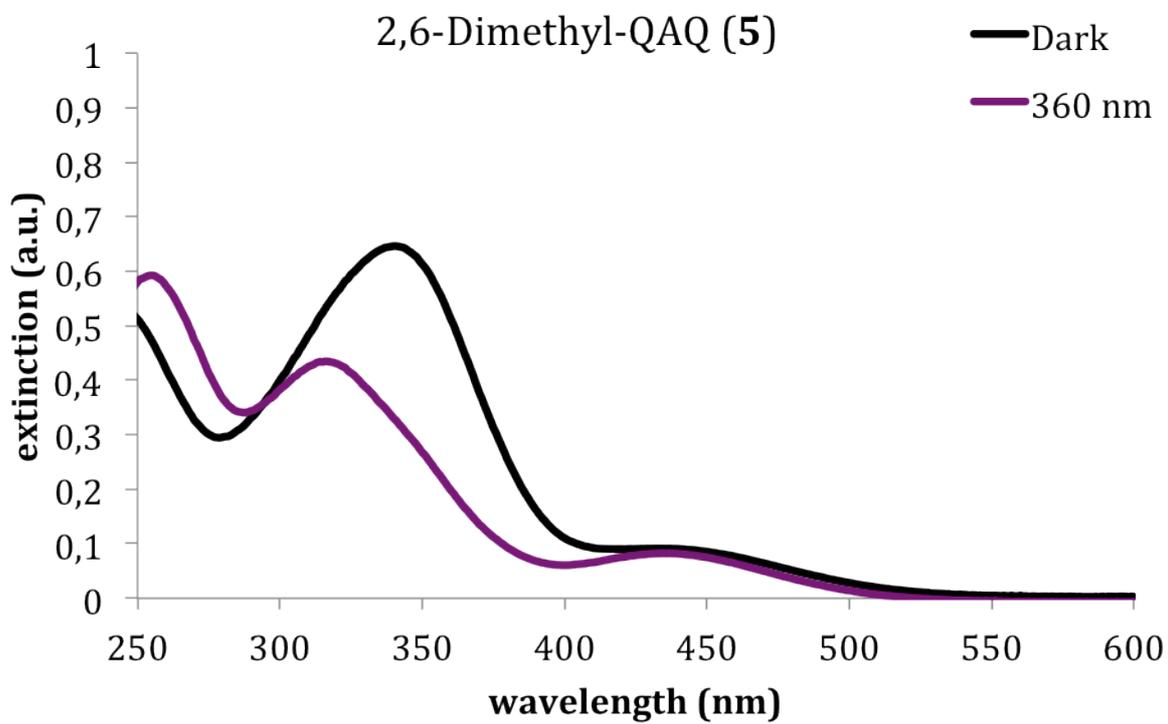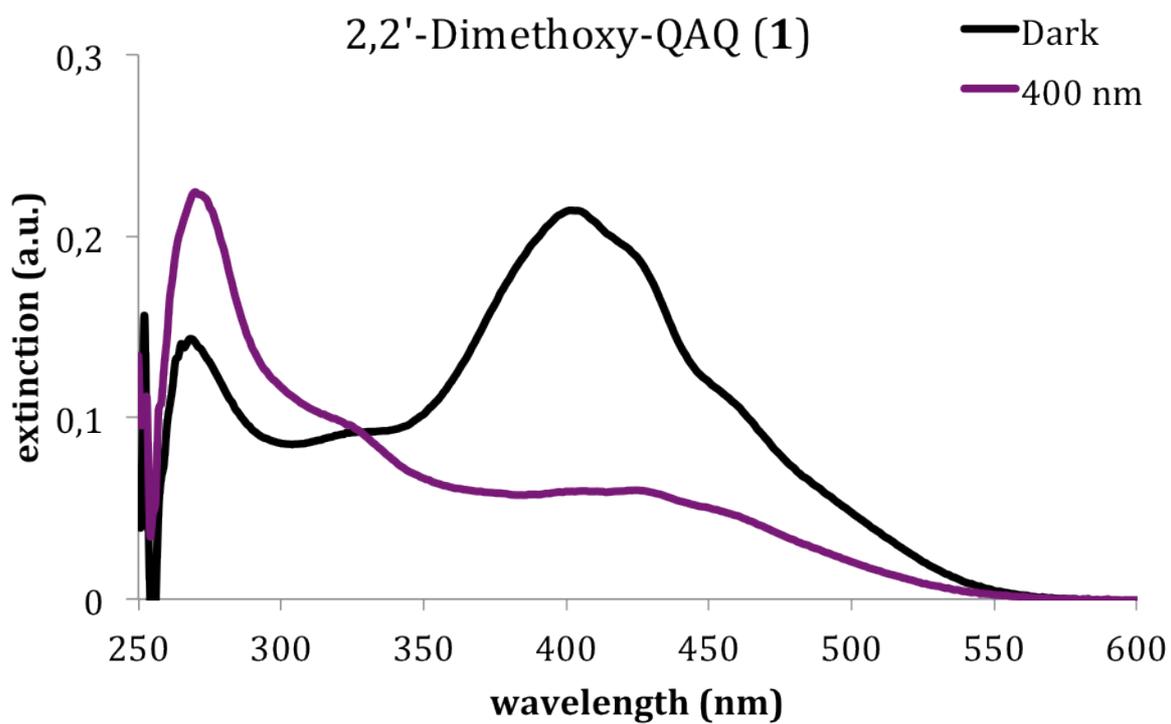
2,2'-Dimethoxy-QAQ (**1**)

To determine the thermal relaxation of compound **1**, the spectrum above was recorded in DMSO.

Thermal relaxation of 2,6-dimethoxy-QAQ 1 in DMSO
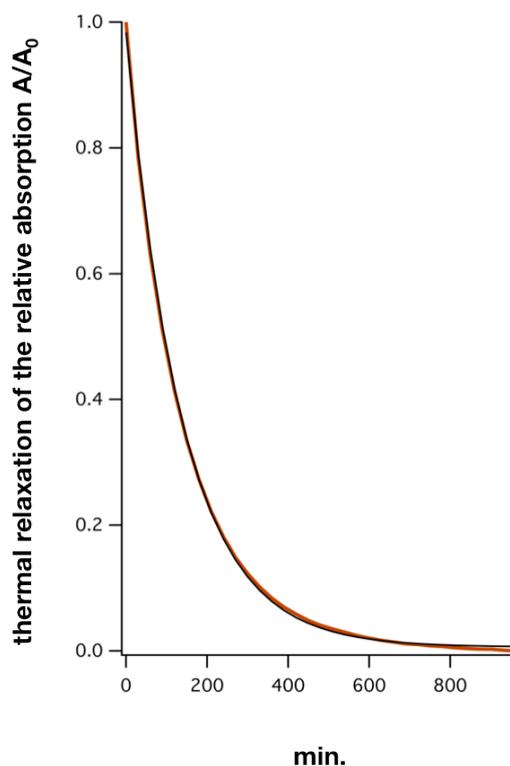
Thermal relaxation of 2,6-dimethoxy-QAQ **1**, measured by an UV-Visible Spectrophotometer in DMSO. Measurement was performed after irradiation with 400 nm. The relative absorption A/A_0 at 403 nm light, is plotted against time. Orange trace represents the recorded absorption. Black trace indicates the course of the fitted exponential function:

$y_0 + A \exp(-x/\tau)$, $y_0 = 0.006 \pm 0.002$, $A = 0.978 \pm 0.004$, $\tau = 4.61 \pm 0.04$ min. Statistics on coefficient values are presented as $\pm$ one standard deviation.

Thermal relaxation of 2,6-dimethoxy-QAQ recorded on Shaker-IR channel
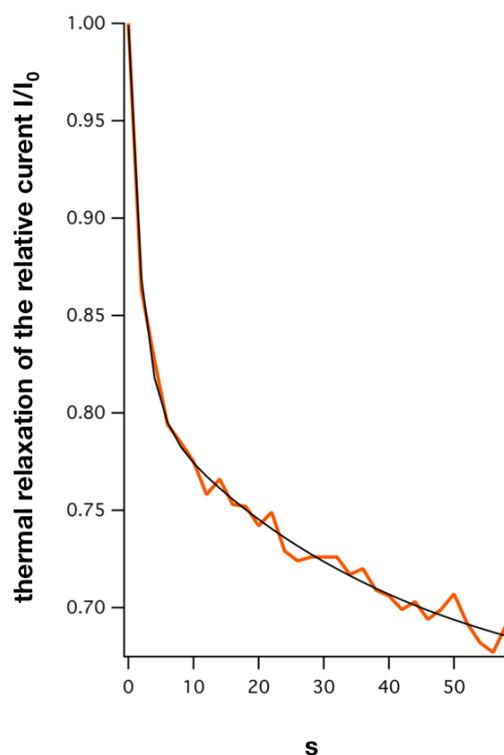
Thermal relaxation of 2,6-dimethoxy-QAQ **1** recorded in voltage clamp mode, in the dark. Measurement was performed after irradiation with 420 nm. The relative Shaker-IR current I/I_0 (n = 4 cycles) is plotted against time. Orange trace represents the average of four cycles. Black trace indicates the course of the fitted biexponential function: $y_0 + A_1 \exp(-x/\tau_1) + A_2 \exp(-x/\tau_2)$, $y_0 = 0.649 \pm 0.02$, $A_1 = 0.190 \pm 0.010$, $A_2 = 0.160 \pm 0.014$, $\tau_1 = 1.948 \pm 0.226$ s, $\tau_2 = 39.454 \pm 10.8$ s. Statistics on coefficient values are presented as $\pm$ one standard deviation.

Action spectrum of 2,6-dimethoxy-QAQ recorded on Shaker-IR
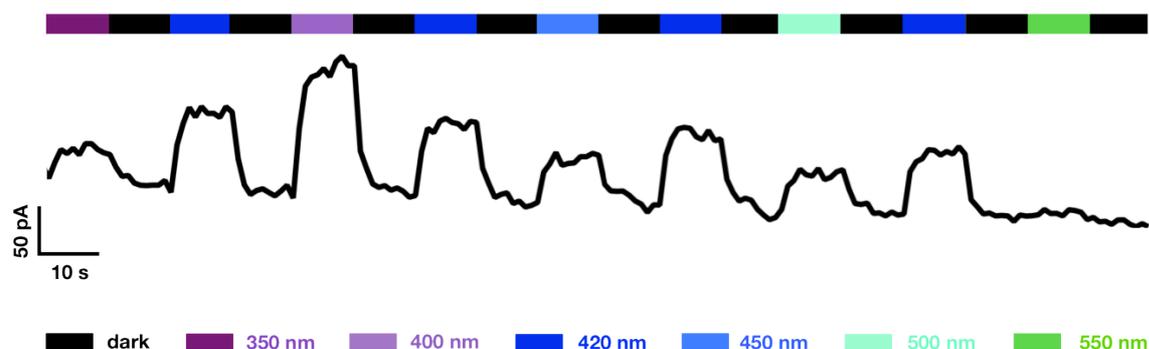
Action spectrum of 2,6-dimethoxy-QAQ (**1**) recorded on Shaker-IR channels. The protocol applied depolarized the cell from - 70 mV to + 40 mV, for 250 ms at 1 Hz. After the first 250 ms of the protocol, depolarization was initiated. The voltage clamp measurements were accompanied with changing illumination, after 10 protocol cycles. Irradiation was varied between 350 nm - 550 nm light. The maximum induced current unblock is detected at 400 nm light. Wavelength higher than 500 nm light, did not unblock Shaker-IR channels. Power output of the Polychrom 5000 has not been considered.[6]

[6] Stawski, P.; Sumser, M.; Trauner, D. *Angew. Chem . Int. Ed.* **2012**, *DOI*: 10.1002/anie.201109265

3.3) Publication

Tuning Photochromic Ion Channel Blockers

Alexandre Mourot[*], Michael A. Kienzler[*], Matthew R. Banghart, **Timm Fehrentz**,

Florian M. E. Huber, Marco Stein, Richard H. Kramer, and Dirk Trauner

[*] authors contributed equally.

Tuning Photochromic Ion Channel Blockers

Alexandre Mourot,[†,∥] Michael A. Kienzler,[‡,§,∥] Matthew R. Banghart,[‡] Timm Fehrentz,[§] Florian M. E. Huber,[§] Marco Stein,[§] Richard H. Kramer,[†] and Dirk Trauner*[,§]

[†]Department of Molecular and Cell Biology and [‡]Department of Chemistry, University of California, Berkeley, California 94720, United States

[§]Department of Chemistry and Pharmacology, Ludwig-Maximilians-Universität, München, and Center for Integrated Protein Science, 81377 Munich, Germany

S *Supporting Information*

ABSTRACT: Photochromic channel blockers provide a conceptually simple and convenient way to modulate neuronal activity with light. We have recently described a family of azobenzenes that function as tonic blockers of K_v channels but require UV-A light to unblock and need to be actively switched by toggling between two different wavelengths. We now introduce red-shifted compounds that fully operate in the visible region of the spectrum and quickly turn themselves off in the dark. Furthermore, we have developed a version that does not block effectively in the dark-adapted state, can be switched to a blocking state with blue light, and reverts to the inactive state automatically. Photochromic blockers of this type could be useful for the photopharmacological control of neuronal activity under mild conditions.

KEYWORDS: photopharmacology, ion channel blockers, voltage-gated potassium channels, photochromic molecules, azobenzenes
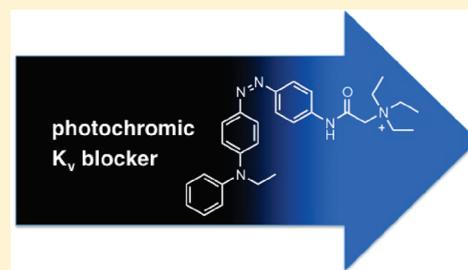
The merger of artificial photoswitches with natural receptor proteins has proven to be an effective way to control neural activity with light.[1−4] This approach combines the virtually limitless repertoire of synthetic chemistry with a detailed understanding of the transmembrane proteins that underlie the generation and modulation of action potentials. As such, it provides a useful alternative to naturally occurring light-gated ion channels and light-powered pumps, which are currently driving the field of optogenetics.[5] Most of these are based on a single photoswitch, retinal, which is often endogenously produced and does not need to be added externally. While this provides advantages in terms of practicality, it confines the tuning of these systems to mutations in the protein surrounding the chromophore.[6] By contrast, a combination of synthetic photoswitches and natural receptors should allow for more flexibility, since both components can be manipulated through chemistry and genetic engineering, respectively.

Artificial photoswitches can be combined with endogenous neural receptors through covalent or noncovalent bonding.[7] So-called photochromic ligands (PCLs) bind noncovalently and contain a photoswitchable moiety whose configuration can be changed upon irradiation.[7−10] As such, they change their efficacy in a light-dependent way and essentially function as photochromic neurotransmitters or neuromodulators. Since they are distributed like small-molecule drugs, they are able to photosensitize naïve tissues within minutes, as opposed to days in the case of optogenetic probes. PCLs can be rapidly switched by using two

different wavelengths of light that greatly favor one isomer or the other. Alternatively, one could use photoswitches that are actively switched to one isomer with light but thermally revert to the more stable form in the dark. This obviates the need to work with two different wavelengths but requires switches that turn themselves off at appropriate rates.

Recently, we introduced a family of simple azobenzene derivatives that function as PCLs for tetrameric voltage-gated ion channels, in particular potassium channels.[7,9] These molecules, represented by AAQ and BzAQ (Figure 1), operate as photochromic open channel blockers, that bind in a light-dependent manner to the tetraethylammonium (TEA) binding site located in the inner cavity of potassium channels.[7] In their extended *trans* form, AAQ and BzAQ fit into this cavity, but in their bent *cis* form their apparent affinity drops sharply. To reach their binding site, these amphiphilic molecules can either partition into the membrane or they can be imported through a patch pipet, whose content can rapidly exchange with the cytosol. Although many details of this reversible molecular encapsulation of azobenzenes by channel proteins remain to be clarified, they have already proven themselves as effective modulators of neural activity. For instance, Purkinje neurons and pacemaker neurons in the heart
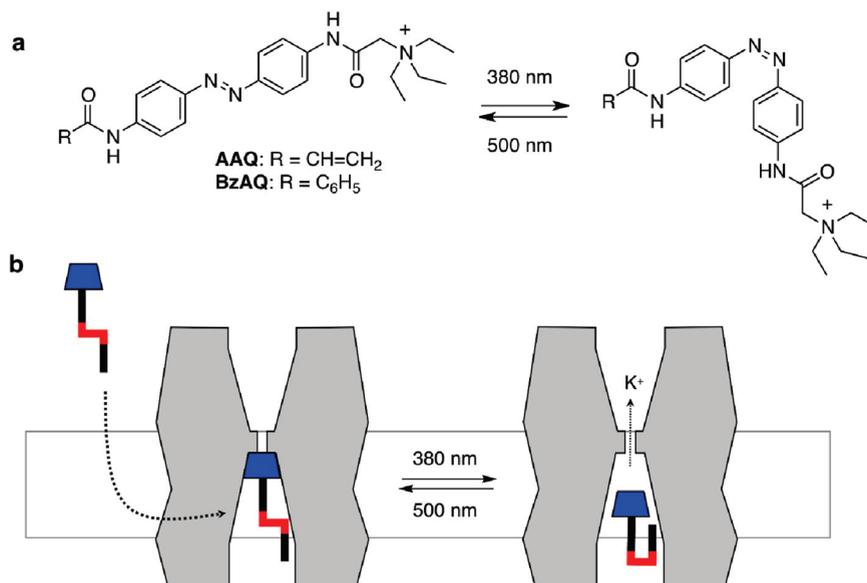
Figure 1. (a) Molecular structures of AAQ and BzAQ, two PCLs for K_v channels; (b) AAQ, BzAQ, and related PCLs are membrane permeable and function as photochromic open-channel blockers.
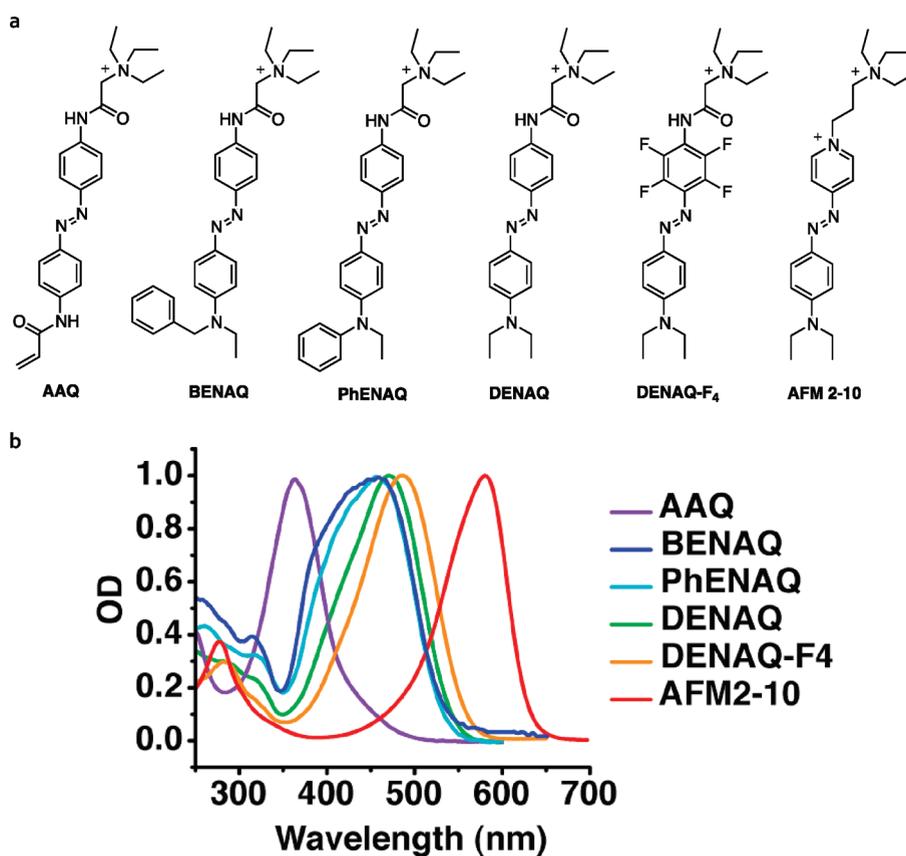
Figure 2. (a) Potential photochromic K_v blockers investigated in this study. (b) UV/Vis spectra of the azobenzenes investigated. Spectra were recorded at room temperature in phosphate buffered saline solution at pH 7.4.

of *Hirudo medicinalis* could be controlled with photochromic neuromodulators of this type.[9]

One of the greatest advantages of azobenzene photoswitches is the well-understood effect of substitutions and molecular extensions on their photophysical properties and thermal stability.[11] So-called "regular azobenzenes", represented by the parent molecule, as well as the bis-acylated azodianilines AAQ and BzAQ, are thermodynamically more stable in their

Scheme 1. Synthesis of BENAQ, PhENAQ, DENAQ, DENAQ-F4, and AFM 2-10[a]
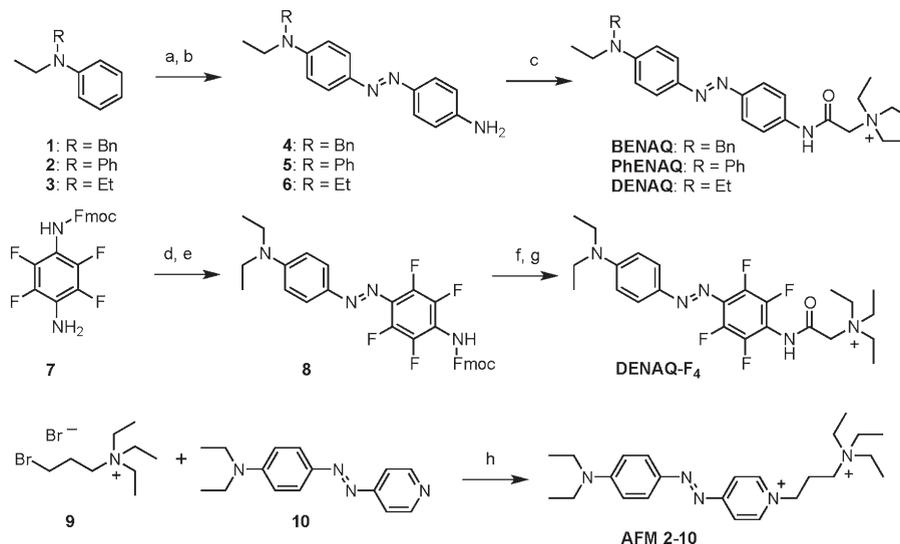
[a] Reagents and conditions: (a) 4-nitroaniline, isoamylnitrite, HCl, MeOH (87% for **1**, 79% for **2**, 62% for **3**); (b) Na$_2$S, H$_2$O, 1,4-dioxane, 90 °C (88% for **4**, 42% for **5**, 88% for **6**); (c) 2-triethylammonium acetic acid chloride, DIPEA, DMF, 0 °C to RT (67% for BENAQ, 66% for PhENAQ, 92% for DENAQ); (d) BF$_3$ Et$_2$O, isoamylnitrite, THF −40 to −5 °C; (e) diethylaniline, NaOAc, 0 °C to RT (36% over two steps); (f) piperidine, Et$_2$O, 0 °C to RT (85%); (g) 2-triethylammonium acetic acid chloride, DIPEA, DMF, 0 °C to RT (38%); (h) DMF, 80 °C (92%).

trans-configuration, which completely predominates in the dark-adapted state. Their photostationary *cis/trans* ratios (PSRs) assume their maximum values in the UV-A region of the electromagnetic spectrum (315−380 nm). At these wavelengths, *cis/trans* ratios exceeding 9:1 can be observed.[12] Once the light is turned off, the *cis*-isomers of regular azobenzenes are thermally relatively stable. The half-life of AAQ in physiological solution at room temperature, for instance, is 7−8 min.

Azobenzenes with strongly electron-donating substituents on both rings are known to absorb at increased wavelengths and have an increased rate of thermal back-isomerization from *cis* to *trans*.[11,13] In addition to these, one could use azobenzenes that feature an electron-donating substituent on one end and an electron-withdrawing one on the other. These "push−pull" azobenzenes, which are also referred to as "pseudo-stilbenes", are marked by greatly red-shifted absorption spectra. They are also thermally instable in their *cis* form and revert at room temperature to the thermodynamically more stable *trans* form on a millisecond to second time scale. The rate of this reversal is greatly dependent on the solvent, with polar protic solvents promoting very fast isomerization.[14] As such, push−pull azobenzenes are ideally suited as photochromic ion channel blockers that can be activated with visible light and turn themselves off once the light intensity drops below a certain level. Studies using red-shifted blockers would generally benefit from the deeper tissue penetration of light with longer wavelength. Since longer wavelengths are also associated with less phototoxicity, photochromic compounds of this type would be particularly useful in chemical approaches toward restoring vision.

■ RESULTS AND DISCUSSION

We now present a family of push−pull azobenzenes that have red-shifted action spectra and decreased thermal stability and function as photochromic blockers of voltage-gated ion channels (Figure 2). These molecules feature a strongly electron-donating

dialkylamino or aryl alkylamino group on one side and a mildly electron-withdrawing acylamino moiety that terminates in a quaternary ammonium ion on the other side of the azobenzene. This positively charged "head group" interacts with the TEA binding site in the inner lumen of the channel, which blocks the flow of ions. The "tail" of the molecules, that is, the electron-donating substituent, determines the spectral properties of the photoswitch as well as the thermal stability of the *cis*-isomer.

Spectroscopic Characterization of Red-Shifted PCLs. AAQ, a representative of our original type, which is marked by a bis-acylated azodianiline core, serves as a point of reference (Figure 2). Spectroscopically, it can be classified as a "regular azobenzene" with a strong $\pi-\pi^*$ band at 362 nm in water (*trans* isomer). Replacement of the lower acylamino group with an alkylamino group increases the electron density of one side and shifts the absorption spectrum of the *trans*-isomer toward the red. For instance, the absorption spectrum of *trans*-PhENAQ, which bears a phenylethylamino group, is shifted to 456 nm in phosphate buffered saline solution. BENAQ, which bears a benzylethylamino substituent, has a similar absorption spectrum peaking at 459 nm. The diethylamino derivative DENAQ is shifted to an larger extent, as its absorption spectrum peaks at 470 nm. To increase the push−pull effect without significantly altering the sterics of the azobenzene moiety, we also explored fluorinated derivatives, such as DENAQ-F4. This compound shows a relatively small bathochromic shift with respect to DENAQ (484 nm). Our most red-shifted compound, AFM2-10, which peaks at 580 nm, is in essence an azobenzene version of the well-known fluorescent styrene dye FM2-10. The synthesis of these compounds follows standard protocols and is summarized in Scheme 1 (for further details see the Supporting Information).

In general, the absorption spectra of the *trans*-isomers of azobenzenes are correlated with their PSRs at different wavelengths. Hence, red-shifting of the absorption maximum of their *trans* isomer through appropriate substitutions should also red-shift
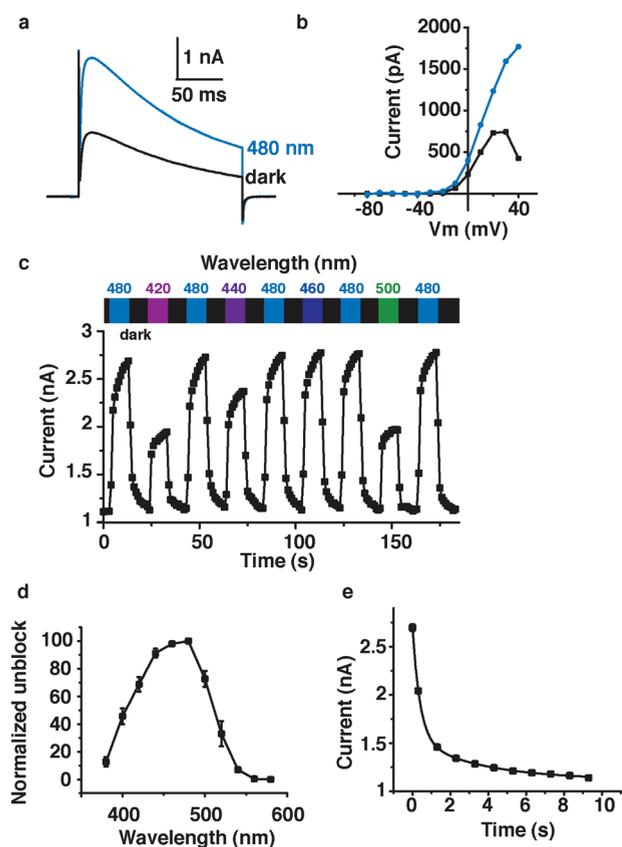
Figure 3. Effect of DENAQ on $K_v3.1$ expressed in HEK293 cells. (a) Cells were treated with 100 μM DENAQ. K_v current was measured in whole cell mode using a 200 ms depolarization from -60 to $+40$ mV, in the dark and under 480 nm light. Capacitive currents have been cut off for clarity. (b) Membrane-voltage dependence of block and unblock. Steady-state current (at the end of the 200 ms depolarization) is plotted as a function of membrane potential. (c) Reversibility of photoswitching and action spectrum of DENAQ on $K_v3.1$. Potassium current was measured using the protocol described in (a) looped at 1 Hz. Peak current is plotted as a function of time. Cycles of dark and illumination (420–500 nm) are indicated. (d) Unblock as a function of wavelength. Unblock was normalized to 100% for 480 nm light ($n = 3$–4 cells). (e) Apparent thermal relaxation rate of DENAQ measured by electrophysiology. $K_v3.1$ peak current is plotted as function of time after light is switched off. Four light-dark cycles are averaged for this single cell. Data points were fitted with a biexponential decay equation: $y = y_0 + A_1 \exp(-x/\tau_1) + A_2 \exp(-x/\tau_2)$ with $y_0 = 1122 \pm 23$ pA, $A_1 = 1148 \pm 59$ pA, $\tau_1 = 392 \pm 37$ ms, $A_2 = 422 \pm 39$ pA, and $\tau_2 = 3.5 \pm 0.8$ s.

the PSR maximum as a function of the wavelength. This is difficult to measure with our push–pull azobenzenes because their thermal relaxation is too fast to enrich the *cis* isomer in aqueous solution for detection by standard spectrophotometric methods.[15] Similar observations were made by Uyeda et al.[16] who investigated structurally related azobenzenes that bore a dimethylamino substituent on one side and acylamino substituents on the other. In this case, thermal *cis*- to *trans*-isomerization was very fast in aqueous solution and only detectable by flash laser photolysis. By contrast, the thermal isomerization was found to be relatively slow in dimethyl sulfoxide (DMSO), and PSRs up to 78% *cis* could be observed in this solvent. Nevertheless, these photoswitches performed well in aqueous solution when incorporated in DNA.[17] Preliminary experiments with our compounds show
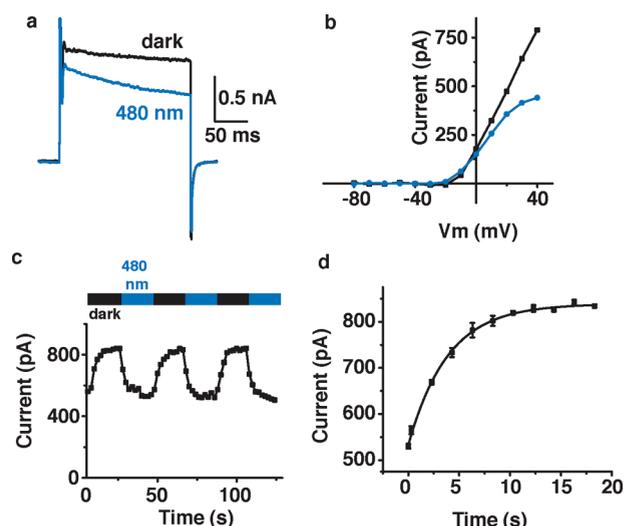
Figure 4. Effects of PhENAQ on Shaker-IR expressed in HEK 293 cells. Cells were treated with 50 μM PhENAQ. (a) K_v current was measured using a 200 ms depolarization from -60 to $+40$ mV, in the dark and under 480 nm light. (b) Current versus voltage dependence of block and unblock, under 480 nm light and in the dark, respectively. Steady state current was plotted as a function of membrane potential. (c) Reversibility of PhENAQ using cycles of 480 nm light and dark. Peak current was measured using the protocol described in (a) looped at 0.5 Hz. (d) Apparent thermal relaxation rate of PhENAQ measured by electrophysiology. Shaker-IR peak current is plotted as a function of time after the light is switched off. Three light/dark cycles are averaged for this single cell. Data points were fitted with a monoexponential decay equation: $y = y_0 + A \exp(-x/\tau)$ with $y_0 = 838 \pm 3$ pA, $A = -306 \pm 5$ pA, and $\tau = 3.9 \pm 0.2$ s.

similar PSRs in DMSO (see Supporting Information Figure 1), but it is difficult to extrapolate this to aqueous buffer solutions.

Electrophysiological Characterization of Red-Shifted PCLs. The electrophysiological action spectrum of photochromic channel blockers should mirror their absorption spectra and PSRs in solution, provided the interaction with the channel protein does not greatly influence these. Push–pull azobenzenes, such as DENAQ or PhENAQ, with their red-shifted absorption spectra, are therefore expected to show a red-shifted action spectrum and fully operate in the visible region of the electromagnetic spectrum. This is indeed the case. Figure 3 shows the effects of 100 μM DENAQ on the conductance of a voltage-gated potassium channel at different wavelengths. Recordings were performed in HEK 293 cells transiently expressing $K_v3.1$ in whole-cell voltage clamp mode after transient treatment with the PCL. Our data show that DENAQ is a much better blocker in the dark adapted-state than at 480 nm (Figure 3a), which is true at all membrane potentials tested (Figure 3b). Unblock could be achieved at all wavelengths between 380 and 540 nm, with maximum unblock observed around 480 nm (Figure 3c and d). At this wavelength, percent photoswitching, as determined by the difference between the maximum current under irradiation and in the dark, divided by the maximum current under irradiation, is $63.2 \pm 7.2\%$ ($n = 5$ cells). Thus, the action spectrum of DENAQ is shifted by ca. 100 nm with respect to AAQ and BzAQ. Remarkably, the blocking effect of *trans*-DENAQ is restored within seconds once the light is turned off ($t_{1/2} = 305 \pm 57$ ms, averaged over $n = 4$ cells, Figure 3e). DENAQ is therefore a *trans*-blocker with a strongly

539

83

dx.doi.org/10.1021/cn200037p |*ACS Chem. Neurosci.* 2011, 2, 536–543
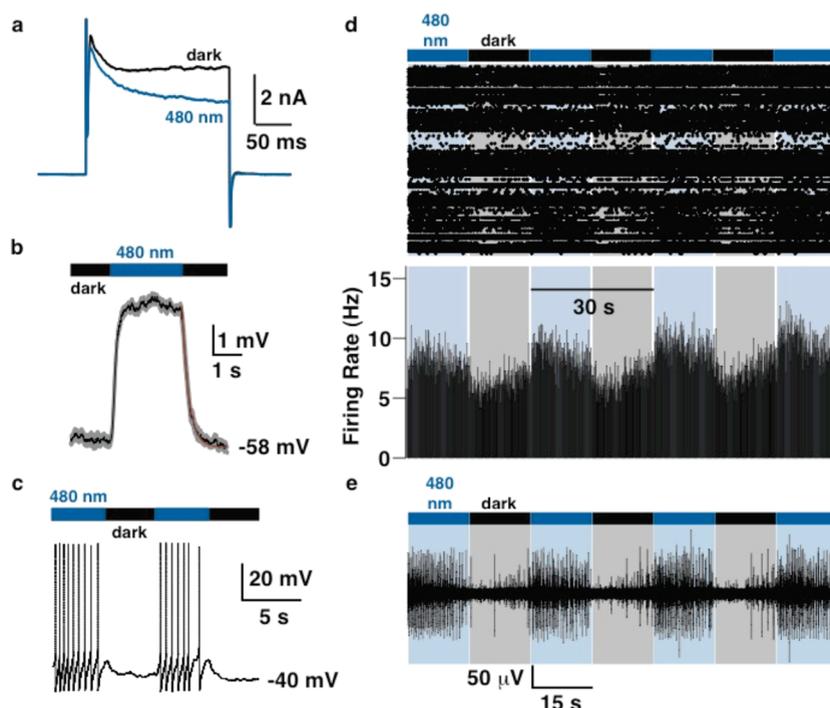
Figure 5. Effect of PhENAQ on neuronal firing. (a) Voltage-clamp recording from a hippocampal neuron treated with 50 μM PhENAQ. Voltage-gated potassium current was elicited using a 200 ms depolarization from -60 to $+40$ mV, under 480 nm light irradiation or in the dark. (b) Reproducibility of light-evoked membrane depolarization in neurons. Current clamp recordings were made from a hippocampal neuron treated with 50 μM PhENAQ. Average trace (black) and standard deviation (gray) of four light cycles are shown. Apparent thermal relaxation rate was fitted with a monoexponential decay equation (red): $y = y_0 + A \exp(-x/\tau)$ with $y_0 = -46.78 \pm 0.01$ mV, $A = 3.86 \pm 0.02$ mV, and $\tau = 237 \pm 3$ ms. (c) Optical regulation of action potential firing. (d) Multielectrode array recording from an acute rat cerebellar slice. Top, raster plot of spiking; bottom, average firing rate calculated in 100 ms time bins. (e) Extracellular recording from a single cell using the multielectrode array. Color bars represent illumination with 480 nm (blue) or periods of darkness (black).

red-shifted action spectrum and decreased thermal stability with respect to AAQ and BzAQ.

The compound PhENAQ has similar spectral properties but shows a key difference in terms of its blocking state. It is a red-shifted azobenzene that preferentially blocks in its thermodynamically less stable *cis*-form, that is, at 480 nm (Figure 4a). In this case, electrophysiological recordings were performed in HEK 293 cells transiently expressing Shaker-IR in whole-cell voltage clamp mode. Percent photoswitching, as determined by the difference between the steady-state current in the dark and in 480 nm light, divided by the current in the dark, was found to be $29.4 \pm 4.8\%$ ($n = 3$ cells). *cis*-Block occurred at all membrane potentials tested (Figure 4b) and was fully reversible over many cycles (Figure 4c). Once the light is turned off, PhENAQ quickly reverts to the less blocking *trans* state ($t_{1/2} = 2.6 \pm 0.1$ s, averaged for $n = 3$ cells) (Figure 4d). Thus, PhENAQ has little effect when added in the dark (or at longer wavelengths) but becomes an efficient blocker when irradiated with blue light.

In comparison, DENAQ and PhENAQ show some key differences, beyond their *trans* versus *cis* activity. Structurally, they are only distinguished by the presence of an ethyl and phenyl substituent, respectively. However, DENAQ does not appear to affect Shaker-IR channels, which we routinely use in our investigations on photochromic K_v blockers, yet it cleanly blocks K_v3.1 channels. By contrast, PhENAQ blocks Shaker-IR and a range of other K_v channels (not shown). Why it does so preferentially in its *cis*-form remains an open question. It could be due to an attractive interaction of the phenyl ring with an amino acid

residue lining the inner lumen of the channel, which can only take effect when the azobenzene is *cis*-configured. Also noticeable is the difference in the rate of thermal relaxation ($t_{1/2} = 305 \pm 57$ ms vs 2.6 ± 0.1 s). This could reflect either differences in the dissociation from the channel protein as the rate-determining step or different rates of the thermal isomerization in solution. Detailed structural and kinetic investigations will be needed to clarify these points.

The remaining azobenzenes shown in Figure 2 were tested on HEK cells expressing various channels but failed to show functional features that significantly go beyond DENAQ or PhENAQ. Despite its seemingly small chemical modification, DENAQ-F$_4$ proved too to toxic to be viable as a photochromic blocker. AFM2-10 had virtually no effect on the conductance of potassium channels, even at very high concentrations (500 μM). It appears that subtle changes in the composition the molecules influence not only the photophysical and thermal but also the pharmacological properties of our photochromic blockers.

Optical Regulation of Neuronal Excitability. *cis*-Blockers, such as PhENAQ, have the inherent advantage that they have little effect on ion channels in their thermodynamically more stable, dark-adapted state, which should make them less toxic to excitable cells. We therefore decided to focus on PhENAQ and investigate its effect on neuronal firing patterns. In accordance with its effect on Shaker-IR in HEK 293 cells, PhENAQ behaves as a *cis*-blocker of voltage-gated potassium channels endogenously expressed in hippocampal neurons (percent photoswitching = $24.5 \pm 4.5\%$, $n = 3$ cells, Figure 5a). To look at optical

modulation of membrane potential, we performed current clamp experiments. When the membrane potential of the cell was close to the resting potential, PhENAQ rapidly and reliably elicited membrane depolarization upon 480 nm light irradiation ($\Delta = 6.0 \pm 0.4$ mV, $n = 4$ cells) without inducing cell firing (Figure 5b). When switched back to the dark, repolarization occurred within a second ($t_{1/2} = 163 \pm 2$ ms, $n = 4$ cells). When current was injected to bring the cell closer to threshold for firing, light-induced depolarization triggered action potential firing, which ceased rapidly when the light was switched off (Figure 5c).

The depolarization required to induce spiking depends not only on the various ion channels expressed in a given type of cell but also on the strength and variability of its synaptic input. To test whether PhENAQ can modulate action potential firing of cells that are not artificially depolarized, we recorded extracellularly from cerebellar slices using a multielectrode array (MEA) with three-dimensional electrodes. Cerebellar slices are marked by high levels of spontaneous neuronal activity, probably originating from Purkinje neurons.[18] As can be seen in Figure 5d, neuronal firing was increased upon irradiation with 480 nm but decreased markedly once the light was turned off. Although the effects are not large, they are reversible and reproducible. They are probably limited by the low solubility of PhENAQ in buffer solution, which makes it difficult to deliver uniformly in brain slices. Figure 5e shows an example of a single cerebellar neuron whose activity was strongly photomodulated. As a control, we checked that light itself has no effect on the activity of naïve cerebellar slices (Supporting Information Figure 2).

■ CONCLUSION

Following a general paradigm for tuning azobenzene photoswitches, we have developed compounds that function as red-shifted photochromic blockers of potassium channels, which turn themselves off automatically in the dark. The lessons learned during this study could be applied to other types of photoswitches, including photochromic versions of the neurotransmitter glutamate[19,20] and covalently tethered blockers, agonists, and antagonists of neural receptor proteins (so-called photochromic tethered ligands, or PTLs).[12,21−24]

One of our most advanced compounds, DENAQ, is a blocker of $K_v3.1$ channels that is active in its dark-adapted *trans* state. By contrast, PhENAQ is a *cis*-blocker that becomes active upon irradiation with blue light, which makes it an attractive molecule for the optical regulation of neuronal excitability. A photochromic *cis*-blocker of Shaker channels has been previously observed, but it was neither red-shifted nor thermally instable and it proved to be too toxic to be of any practical use.[7] Although tonic blockers have performed remarkably well in complex neural systems, *cis*-blockers such as PhENAQ could have advantages where a minimum of perturbation upon addition of the compound is desirable. Both DENAQ and PhENAQ revert thermally, that is, in the dark, to their default *trans* states within hundreds of milliseconds to seconds.

The use of these compounds in the photopharmacological control of electrical activity with visible light in neural tissue such as the retina is currently under investigation. Their effects on other voltage-gated ion channels, such as Na_v and Ca_v channels, are also under study in our laboratories. Finally, the incorporation of red-shifted, thermally destabilized azobenzenes into other soluble and tethered photochromic ligands is under active investigation and will be reported in due course.

■ METHODS

Synthesis. See the Supporting Information.

Spectroscopic Analysis. UV/Vis spectra were measured at room temperature using a SmartSpec Plus photometer (Biorad). UV/Vis spectra of thermally unstable compounds were measured on a Nano-Drop 2000c (Thermo Scientific) instrument at concentrations of approximately 1 mM in DMSO solvent. Photoisomerization was achieved by directly illuminating a 1 μL sample on the pedestal with 473 nm light from a 200 μm, 0.22 NA fiber optic cable placed perpendicular to the optical path such that the sample was at the focal point of the fiber tip. 150 mW was delivered to the sample from a 200 mW DPSS blue 473 nm laser (MBL-III-473, Opto Engine).

Cell Culture. HEK 293 cells were grown in Dulbecco's modified Eagle's medium (DMEM) containing 10% fetal bovine serum (FBS). Cells were plated on 12 mm diameter poly-L-lysine coated glass coverslips at a density of 20 000 cells/cm^2. Transfection was performed using the calcium phosphate method, as already described.[9] We transfected cells either with Shaker-IR (Inactivation Removed)[25] or rat $K_v3.1$ cDNA, using a bicistronic GFP-expression vector (pIRES). Cells were recorded 12−48 h after transfection. Primary cultures of neonatal rat hippocampal neurons were performed using standard procedures, as previously described.[9] Recordings were performed 2−3 weeks after plating.

Cerebellar Slice Preparation. Sagittal cerebellar slices were prepared from 13−17 day-old Sprague−Dawley rats. Briefly, the animal was decapitated under isoflurane anesthesia and the brain was quickly removed. Sagittal slices (340 μm thick) were cut with a microtome (Leica VT1000S; Leica Microsystems, Wetzlar, Germany) in an ice-cold artificial cerebrospinal fluid (ACSF) and then placed in an incubating chamber for 30 min at 34 °C. Thereafter, slices were kept at room temperature. Bicarbonate-buffered ACSF was used as the slicing, storage, and recording solution; composition in mM: NaCl 126, KCl 2.5, NaHCO$_3$ 26, NaH$_2$PO$_4$ 1.25, CaCl$_2$ 2.5, MgSO$_4$ 1.3, and glucose 10, saturated with O$_2$/CO$_2$ (95/5%).

Animal care and experimental protocols were approved by the University of California Berkeley Animal Care and Use Committee.

Electrophysiology. Cells were incubated with 10 μM to 1 mM (as indicated) photoswitch for 15 min in the cell incubator (37 °C, 7% CO$_2$, dark). The photoswitch was diluted in extracellular solution (contains in mM: NaCl 138, KCl 1.5, MgCl$_2$ 1.2, CaCl$_2$ 2.5, HEPES free acid 5, and glucose 10, pH 7.4). Final DMSO content was always $\leq$1% vol/vol. Cells were then washed twice with 500 μL of extracellular solution and directly used for electrophysiological recordings. Whole-cell recordings were performed using an PC-505B amplifier (Warner Instruments, CT) linked to a personal computer equipped with pClamp8 (Molecular Devices). Patch pipettes had resistances between 3 and 4 MΩ and were filled with intracellular solution (contains in mM: NaCl 10, K$^+$ gluconate 135, HEPES free acid 10, MgCl$_2$ 2, MgATP 2, EGTA 1, pH 7.4). For neuronal recordings only, synaptic transmission was blocked using 25 μM DNQX and 20 μM biccuculine, and voltage-gated sodium channels were blocked using 1 μM tetrodotoxin in the extracellular solution (in voltage-clamp mode only). To measure voltage-gated K$^+$ current from HEK cells or neurons, the holding membrane potential was set to −60 mV and stepped to +40 mV (unless otherwise indicated) for 200 ms at 0.5 or 1 Hz. In current clamp mode, injection of current was used to depolarize the cell and induce action potential firing. For illumination, we used a monochromator (Polychrome V, Till photonics) controlled using Clampex and connected to the back of the microscope using a UV/Vis quartz fiber. Light output measured using a hand-held power meter (Newport 840-C) and through a 20× objective was 4−7 mW/mm^2. Data were filtered at 2 kHz and acquired at a sampling frequency of 10 kHz.

Multielectrode Array (MEA) Recordings. Experiments were performed at room temperature in ACSF saturated with O$_2$/CO$_2$. Slices

were incubated with 50 μM PhENAQ (DMSO concentration 0.5% vol/vol) for 15 min at room temperature and then washed 5 min prior to recording. Slices were then placed on a tridimensional microarray made of 60 pyramid-shape microelectrodes (MEA60 200 3D GND, Ayanda Biosystems SA, Lausanne, Switzerland). Recordings were acquired with an MEA-1060 amplifier board (gain 1200, sampling frequency 20 kHz, Butterworth second order highpass filter 300 Hz, Multi Channel Systems, Reutlingen, Germany) positioned on the stage of an inverted microscope (Olympus IX71). Principal component analysis of spike waveforms was used for sorting spikes generated by individual cells (Offline Sorter; Plexon, Denton, TX). Light was delivered using the 100 W halogen lamp of the microscope and a 480/40 bandpass filter, and was focused on the slice using a 4× objective (Olympus UPLanFL N, NA 0.13). Light was computer-controlled using a filter-wheel controller (Lambda 10-3, Sutter Instruments) and an ultrafast shutter (Uniblitz VCM-D1, Vincent Associates). Light intensity measured at the back of the 4× objective and through the MEA was 17−28 mW/mm^2. Slices were continuously superfused during recording with fresh ACSF.

Statistics and Data Analysis. Data were analyzed using Clampfit 10 (Molecular Devices, Sunnyvale, CA), MC Rack (Multi Channel Systems, Reutlingen, Germany), Offline Sorter (Plexon, Denton, TX), and Origin (OriginLab, Northampton, MA) software. Statistical analysis was performed using Origin. All values reported are mean ± SEM except when stated.

■ ASSOCIATED CONTENT

ⓢ Supporting Information. Additional figures and experimental procedures, and general experimental details. This material is available free of charge via the Internet at http://pubs.acs.org.

■ AUTHOR INFORMATION

Corresponding Author
*E-mail: dirk.trauner@lmu.de.

Author Contributions
‖These authors contributed equally to this work.

■ ACKNOWLEDGMENT

■ REFERENCES

(1) Banghart, M. R., Volgraf, M., and Trauner, D. (2006) Engineering light-gated ion channels. *Biochemistry 45* (51), 15129–15141.

(2) Gorostiza, P., and Isacoff, E. Y. (2008) Optical switches for remote and noninvasive control of cell signaling. *Science 322* (5900), 395–399.

(3) Kramer, R. H., Fortin, D. L., and Trauner, D. (2009) New photochemical tools for controlling neuronal activity. *Curr. Opin. Neurobiol. 19* (5), 544–552.

(4) Mayer, G., and Heckel, A. (2006) Biologically active molecules with a "light switch. *Angew. Chem., Int. Ed. 45* (30), 4900–4921.

(5) Deisseroth, K. (2011) Optogenetics. *Nat. Methods 8* (1), 26–29.

(6) Hegemann, P., and Moglich, A. (2011) Channelrhodopsin engineering and exploration of new optogenetic tools. *Nat. Methods 8* (1), 39–42.

(7) Banghart, M. R., Mourot, A., Fortin, D. L., Yao, J. Z., Kramer, R. H., and Trauner, D. (2009) Photochromic blockers of voltage-gated potassium channels. *Angew. Chem., Int. Ed. 48* (48), 9097–9101.

(8) Bartels, E., Wassermann, N. H., and Erlanger, B. F. (1971) Photochromic activators of the acetylcholine receptor. *Proc. Natl. Acad. Sci. U.S.A. 68* (8), 1820–1823.

(9) Fortin, D. L., Banghart, M. R., Dunn, T. W., Borges, K., Wagenaar, D. A., Gaudry, Q., Karakossian, M. H., Otis, T. S., Kristan, W. B., Trauner, D., and Kramer, R. H. (2008) Photochemical control of endogenous ion channels and cellular excitability. *Nat. Methods 5* (4), 331–338.

(10) Lester, H. A., and Chang, H. W. (1977) Response of acetylcholine receptors to rapid photochemically produced increases in agonist concentration. *Nature 266* (5600), 373–374.

(11) Knoll, H. Photoisomerization of Azobenzenes. In *CRC Handbook of Organic Photochemistry and Photobiology*; Horspool, W. M., Lenci, F., Eds.; CRC Press: Boca Raton, FL, 1996, 2nd ed., pp 89.1−89.16.

(12) Gorostiza, P., Volgraf, M., Numano, R., Szobota, S., Trauner, D., and Isacoff, E. Y. (2007) Mechanisms of photoswitch conjugation and light activation of an ionotropic glutamate receptor. *Proc. Natl. Acad. Sci. U.S.A. 104* (26), 10865–10870.

(13) Sadovski, O., Beharry, A. A., Zhang, F., and Woolley, G. A. (2009) Spectral tuning of azobenzene photoswitches for biological applications. *Angew. Chem., Int. Ed. 48* (8), 1484–1486.

(14) Schanze, K. S., Mattox, T. F., and Whitten, D. G. (1983) Solvent Effects upon the Thermal Cis-Trans Isomerization and Charge-Transfer Absorption of 4-(Diethylamino)-4′-nitrobenzene. *J. Org. Chem. 48* (17), 2808–2813.

(15) Whitten, D. G., Wildes, P. D., Pacifici, J. G., and Irick, G., Jr. (1971) Solvent and substituent on the thermal isomerization of substituted azobenzenes. Flash spectroscopic study. *J. Am. Chem. Soc. 93* (8), 2004–2008.

(16) Kamei, T., Kudo, M., Akiyama, H., Wada, M., Nagasawa, J., Funahashi, M., Tamaoki, N., and Uyeda, T. Q. P. (2007) Visible-Light Photoresponsivity of a 4-(Dimethylamino)azobenzene Unit Incorporated into Single-Stranded DNA: Demonstration of a Large Spectral Change Accompanying Isomerization in DMSO and Detection of Rapid (Z)-to-(E) Isomerization in Aqueous Solution. *Eur. J. Org. Chem. 2007* (11), 1846–1853.

(17) Kamei, T., Akiyama, H., Morii, H., Tamaoki, N., and Uyeda, T. Q. (2009) Visible-light photocontrol of (E)/(Z) isomerization of the 4-(dimethylamino)azobenzene pseudo-nucleotide unit incorporated into an oligonucleotide and DNA hybridization in aqueous media. *Nucleosides, Nucleotides Nucleic Acids 28* (1), 12–28.

(18) Kessler, M., Kiliman, B., Humes, C., and Arai, A. C. (2008) Spontaneous activity in Purkinje cells: multi-electrode recording from organotypic cerebellar slice cultures. *Brain Res. 1218*, 54–69.

(19) Volgraf, M., Gorostiza, P., Szobota, S., Helix, M. R., Isacoff, E. Y., and Trauner, D. (2007) Reversibly caged glutamate: a photochromic agonist of ionotropic glutamate receptors. *J. Am. Chem. Soc. 129* (2), 260–261.

(20) Abrams, Z. R., Warrier, A., Trauner, D., and Zhang, X. (2010) A Signal Processing Analysis of Purkinje Cells in vitro. *Front. Neural Circuits 4*, 13.

(21) Banghart, M., Borges, K., Isacoff, E., Trauner, D., and Kramer, R. H. (2004) Light-activated ion channels for remote control of neuronal firing. *Nat. Neurosci. 7* (12), 1381–1386.

(22) Chambers, J. J., Banghart, M. R., Trauner, D., and Kramer, R. H. (2006) Light-induced depolarization of neurons using a modified Shaker K(+) channel and a molecular photoswitch. *J. Neurophysiol. 96* (5), 2792–2796.

(23) Szobota, S., Gorostiza, P., Del Bene, F., Wyart, C., Fortin, D. L., Kolstad, K. D., Tulyathan, O., Volgraf, M., Numano, R., Aaron, H. L., Scott, E. K., Kramer, R. H., Flannery, J., Baier, H., Trauner, D., and

542

dx.doi.org/10.1021/cn200037p |*ACS Chem. Neurosci.* 2011, 2, 536–543

86

Isacoff, E. Y. (2007) Remote control of neuronal activity with a light-gated glutamate receptor. *Neuron 54* (4), 535–545.

(24) Volgraf, M., Gorostiza, P., Numano, R., Kramer, R. H., Isacoff, E. Y., and Trauner, D. (2006) Allosteric control of an ionotropic glutamate receptor with an optical switch. *Nat. Chem. Biol. 2* (1), 47–52.

(25) Hoshi, T., Zagotta, W. N., and Aldrich, R. W. (1990) Biophysical and molecular mechanisms of Shaker potassium channel inactivation. *Science 250* (4980), 533–538.

Author Contributions

M.R.B., A.M., and D.T. designed the research. A.M. and D.T. wrote the paper. M.A.K., M.S., and F.M.E.H. synthesized the compounds. A.M. and T.F. carried out the biological investigations.

543

dx.doi.org/10.1021/cn200037p |*ACS Chem. Neurosci.* 2011, 2, 536–543

87

Tuning Photochromic Ion Channel Blockers

*Alexandre Mourot, * Michael A. Kienzler,* Matthew R. Banghart, Timm Fehrentz,*

Florian M. E. Huber , Marco Stein, Richard H. Kramer and Dirk Trauner

Supplementary Information

Supplementary Figure 1: Photoisomerization of **DENAQ** and **PhENAQ** in DMSO solution. UV/VIS spectra of a) **DENAQ** and b) **PhENAQ** in the dark adapted, presumably all *trans* state (black) and at the photostationary states produced under constant 473 nm laser illumination (blue).
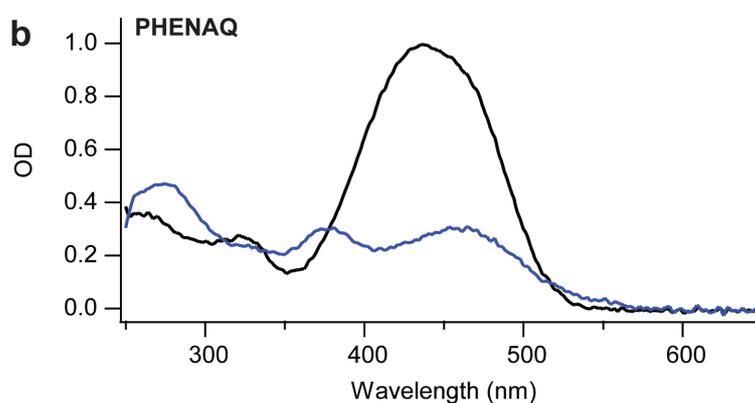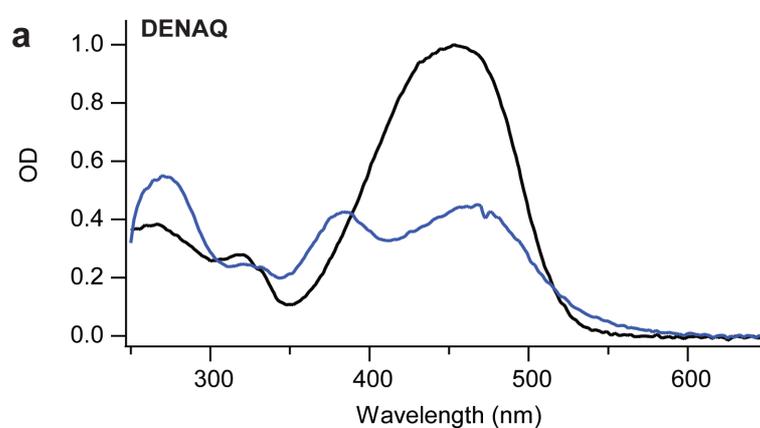
Supplementary Figure 2: Multi-electrode array recording from acute rat cerebellar slices. Condensed firing rate (average firing rate calculated in 100 ms time bins, 10 cycles of 480 nm / dark averaged) for a) a slice treated with 50 μM **PhENAQ** (same slice as in Figure 5d) and b) a control slice.
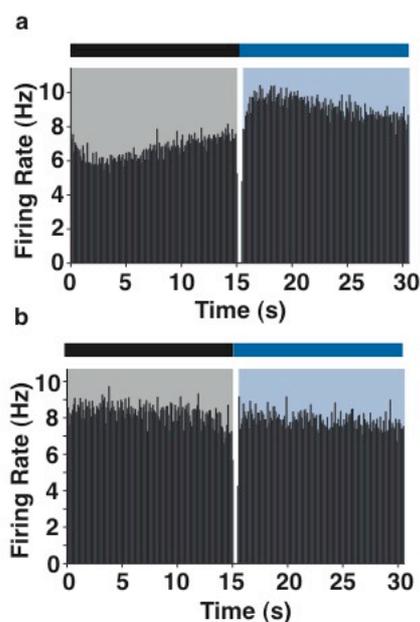
General Experimental Details. Unless otherwise noted, all reagents were purchased from commercial suppliers and used without further purification. Unless otherwise noted, all reaction mixtures were magnetically stirred in oven-dried glassware under a nitrogen atmosphere. External bath temperatures were used to record all reaction mixture temperatures. Analytical thin layer chromatography (TLC) was carried out on Merck silica gel 60 F_{254} TLC plates. TLC visualization was accomplished using 254 nm UV light, 0.1% HCl in MeOH or a charring solution of ceric ammonium molybdenate. All aqueous solutions were saturated unless otherwise noted. Normal phase flash chromatography was performed on Dynamic Adsorbents Silica Gel (40–63 μm particle size) using a forced flow of eluant at 1.3–1.5 bar pressure. Reverse-phase chromatography was carried out

with Waters Preparative C18 Silica Gel WAT010001 125 Å. Yields refer to chromatographically and spectroscopically (^{1}H NMR and ^{13}C NMR) homogenous material. ^{1}H, ^{13}C, and ^{19}F NMR spectra were recorded on Varian ARX 200, AC 300, WH 400, or AMX 600 instruments. Chemical shifts (δ) are reported in ppm with the solvent resonance employed as the internal standard (CDCl$_3$ at δ = 7.26 and 77.0 ppm; DMSO-d$_6$ at δ = 2.50 and 39.5 ppm; Acetone-d$_6$ at δ = 2.05 and 206.3/29.8 ppm; Methanol-d$_4$ at δ = 3.31 and 49.0 ppm; THF-d$_8$ at δ = 3.58/1.73 and 67.4/25.2 ppm; D$_2$O at δ = 4.80/4.81 ppm). Chemical shifts of ^{19}F NMR spectra were calibrated to δ = 0 ppm using CFCl$_3$ as internal standard. The following abbreviations are used to explain the multiplicities: s = singlet, d = doublet, t = triplet, q = quartet, m = multiplet, br = broad. Coupling constants (J_H and J_F) are reported in Hz. Infrared spectra were recorded in the of 4000–400 cm^{-1} on a Perkin Elmer BY FT-IR spectrometer using a Smiths Detection Dura Sample IR II Diamond ATR sensor for detection. Samples were prepared as neat film. UV/Visible spectra were recorded on a Varian Cary 50 Bio UV-Visible Spectrophotometer using Starna 29/B/12 quartz cuvettes with 10 mm section thickness. High resolution mass spectroscopy (HRMS) data was recorded using a Varian MAT 711 instrument by electrospray ionization (ESI) or using a Varian MAT CH 7A by electron impact (EI) techniques.

Experimental Procedures.
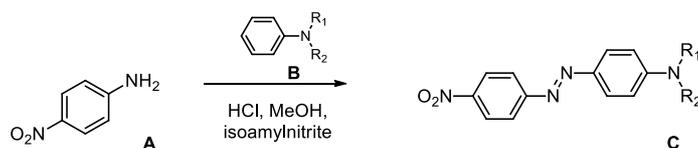
Standard Procedure 1: Azo coupling of a *p*-nitroaniline (**A**) with an aniline (**B**) to form the corresponding azobenzene derivatives (**C**).

1.0 Eq. of *p*-nitroaniline (**A**) was dissolved in methanol and cooled in an ice bath to 0 °C, at which point 12M HCl was added. The resulting solution was stirred for five minutes, and then 1.0 eq. of isoamyl nitrite was added over a period of five minutes. The reaction was stirred for one hour at 0 °C. Meanwhile, 1.0 eq. of aniline **B** was dissolved in water or methanol, depending on solubility, and 12M HCl and cooled to 0 °C. To this solution, the diazonium salt was added over a period of ten minutes. The solution turned deep red and was stirred for another 1.5 hours at 0 °C. Once all starting material was consumed as gauged by TLC, the reaction mixture was poured on an ice-cooled saturated solution of NaHCO$_3$. The crude product was extracted three times with ethyl acetate and, if red/orange color remained in the aqueous layer, twice with dichloromethane. The combined organic layers were washed with brine, dried over MgSO$_4$, and concentrated *in vacuo*.
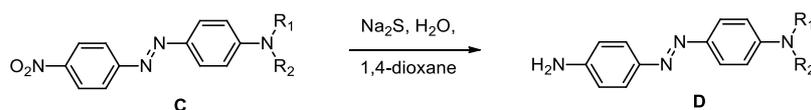
Standard Procedure 2: Reduction of an aromatic nitro group to the corresponding amine in the presence of an azobenzene group using sodium sulfide.

1.0 Eq. of *p*-nitroazobenzene **C** was dissolved in a 10:1 mixture of 1,4-dioxane and water. To this solution 1.0 eq. of sodium sulfide was added, and the reaction mixture was heated to 90 °C for one hour. The reaction was monitored by TLC, and after every hour that starting material **C** was observed, another eq. of sodium sulfide was added. When all starting material was consumed, the solution was poured on a saturated solution of NaHCO$_3$. The crude product was extracted three times with dichloromethane and the combined organic layers were washed with brine, dried over MgSO$_4$, and concentrated *in vacuo*.
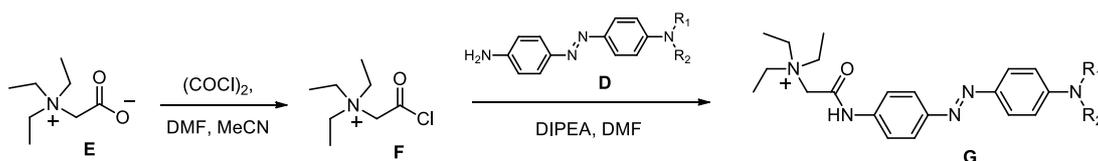
Standard Procedure 3: Amide bond formation between an azoaniline (**D**) and betaine (**E**) to form the corresponding azobenzene quaternary ammonium derivatives (**G**).

According to Fortin et al.[1] 5.0 eq. of betaine **E** were dissolved in acetonitrile. To this solution, 3 drops of DMF and 5.05 eq. of oxalyl chloride were added and the solution was stirred for 45 minutes at room temperature. The solvent then was removed *in vacuo* until all residual HCl had faded. The acid chloride **F** thus generated was partially dissolved in a 1:1 mixture of acetonitrile and DMF. This suspension was then was added dropwise to a flask containing 1.0 eq. of azoaniline **D** and 5.0 eq. of DIPEA in DMF at 0 °C over a period of ten minutes. The reaction was warmed to room temperature, stirred overnight, and then concentrated *in vacuo*.

S1
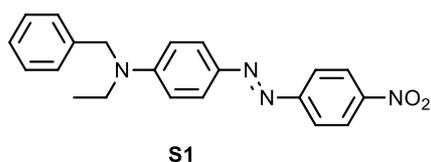
Nitroazobenzene S1. Following **standard procedure 1**, 1.38 g (10 mmol) of *p*-nitroaniline dissolved in 20 mL of MeOH and 5 mL of 12M HCl first reacted with 1.4 mL (10 mmol) of isoamylnitrite to form a diazonium salt, which then further reacted with 2.07 mL (10 mmol) of *N*-benzyl-*N*-ethylaniline dissolved in 20 mL of MeOH and 5 mL of 12M HCl. Column chromatography on silica gel (hexanes/EtOAc, 20:1 then 9:1) gave 1.45 g (87%) of nitroazobenzene **S1** as a deep red, glassy solid. R_f(EtOAc/hexanes, 3:10) = 0.7; ^{1}H NMR (CDCl$_3$, 600 MHz): δ = 8.31 (d, ^3J = 9.0 Hz, 2H), 7.92–7.85 (m 4H), 7.35 (t, ^3J = 7.5 Hz, 2H), 7.30–7.25 (m, 2H), 7.23 (d, ^3J = 7.6 Hz, 2H), 6.78 (d, ^3J = 9.1 Hz, 2H), 4.67 (s, 2H), 3.61 (q, ^3J = 7.1 Hz, 2H), 1.31 ppm (t, ^3J = 7.1 Hz, 3H); ^{13}C NMR (CDCl$_3$, 150 MHz): δ = 156.8, 152.0, 147.4, 143.8, 137.5, 131.5, 128.8, 124.9, 124.0, 123.3, 122.6, 111.7, 53.8, 45.8, 12.3 ppm; IR: 3427, 3049, 2971, 2924, 2254, 1734, 1598, 1512, 1451, 1423, 1392, 1357, 1339, 1281, 1246, 1197, 1177, 1156, 1140, 1104 cm^{-1}; HRMS (ESI), *m/z* calcd. for C$_{21}$H$_{21}$N$_4$O$_2$ [MH]$^+$: 361.1659, found [MH]$^+$: 361.1649.

4
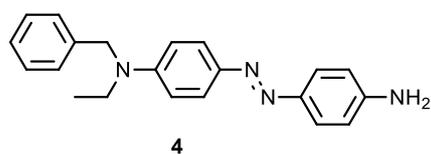
Aminoazobenzene 4. Following **standard procedure 2**, 350 mg (0.97 mmol) of nitrobenzene **S1** in 20 mL of 1,4-dioxane and 1 mL of water was reduced by three separate additions of 76 mg (0.97 mmol) of sodium sulfide. Purification of the crude product by column chromatography on silica gel (hexanes/EtOAc, 9:1→1:1) gave 280 mg (88%) of aminoazobenzene **4** as a deep red, glassy solid. R_f(hexanes/EtOAc, 10:3) = 0.3;

6

^{1}H NMR (CDCl$_3$, 400 MHz): δ = 7.80–7.69 (m, 4H), 7.36–7.20 (m, 5H), 6.80–6.65 (m, 4H), 4.60 (s, 2H), 3.90 (s, 2H), 3.54 (q, ^3J = 7.1 Hz, 2H), 1.32–1.21 ppm (m, 3H); ^{13}C NMR (CDCl$_3$, 100 MHz): δ = 146.1, 144.2, 142.1, 139.9, 134.4, 122.4, 120.4, 120.3, 120.0, 100.9, 110.7, 107.7, 49.9, 41.6, 8.4 ppm; IR: 3452, 3378, 2965, 2923, 2853, 1618, 1595, 1511, 1450, 1394, 1355, 1293, 1275, 1242, 1198, 1178, 1151, 1125, 1073 cm^{-1}; HRMS (ESI), m/z calcd. for C$_{21}$H$_{23}$N$_4$ [MH]$^+$: 331.1917, found [MH]$^+$: 331.1907.
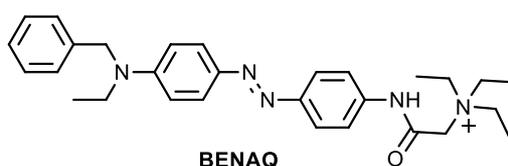
BENAQ

BENAQ. Following **standard procedure 3**, 96.4 mg (0.61 mmol) of betaine **E** dissolved in 5 mL of acetonitrile were reacted with 0.32 mL (2M solution in CH$_2$Cl$_2$, 0.64 mmol) of oxalyl chloride to form acid chloride **F**, which was further reacted with 100 mg (0.30 mmol) of aminoazobenzene **4** dissolved in 3 mL of DMF and 0.11 mL (3.0 mmol) of DIPEA. The crude product was purified by column chromatography on reversed-phase silica gel (0.1% formic acid in water/methanol, 1:0→2:3) to yield 105 mg (67%) **BENAQ** formate salt as a red-orange, glassy solid. ^{1}H NMR (CD$_3$OD, 600 MHz): δ = 8.40 (s, 1H), 7.84–7.69 (m, 6H), 7.30–7.23 (m, 2H), 7.23–7.14 (m, 3H), 6.79–6.68 (m, 2H), 4.58 (s, 2H), 4.22 (s, 2H), 3.60 (q, ^3J = 6.9 Hz, 6H), 3.53 (q, ^3J = 7.0 Hz, 2H), 1.33 (t, ^3J = 6.9Hz, 9H), 1.19 ppm (t, ^3J = 7.0 Hz, 3H); ^{13}C NMR (CD$_3$OD, 151 MHz): δ = 167.9, 163.2, 152.5, 151.4, 144.8, 140.1, 139.8, 129.8, 128.1, 127.7, 126.2, 124.0, 121.7, 112.9, 57.8, 55.9, 54.8, 46.8, 12.8, 8.1 ppm; IR: 3189, 3028, 2958, 2928, 2854, 2684, 1691, 1585, 1557, 1502, 1479, 1464, 1447, 1374, 1343, 1320, 1304, 1255, 1223, 1158, 1095, 1074, 1042 cm^{-1};

HRMS (ESI), *m/z* calcd. for $C_{29}H_{38}N_5O^+$ [M]$^+$: 506.2681, found: 472.3070; UV/Vis (DPBS, pH = 7.4): λ_{max} = 459 nm.

S2
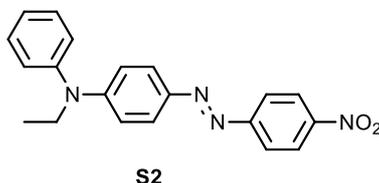
Nitroazobenzene S2. Following **standard procedure 1**, 385 mg (2.8 mmol) of *p*-nitroaniline in 50 mL of MeOH and 5 mL of 12M HCl first reacted with 0.375 mL (2.8 mmol) of isoamylnitrite to form a diazonium salt, which then further reacted with 0.27 mL (2.8 mmol) of freshly prepared *N*-ethyl-*N*-phenylaniline[2] in 50 mL of MeOH and 5 mL of 12M HCl. Column chromatography on silica gel (CH$_2$Cl$_2$/hexanes, 1:1) gave 763 mg (79%) of nitroazobenzene **S2** as a red solid. R$_f$(hexanes/EtOAc, 5:2) = 0.9; ^{1}H NMR (acetone-d$_6$, 400 MHz): δ = 8.37 (d, ^3J = 9.2 Hz, 2H), 7.98 (d, ^3J = 9.2 Hz, 2H), 7.85 (d, ^3J = 9.2 Hz, 2H), 7.50 (t, ^3J = 7.2 Hz, 3H), 7.33 (t, ^3J = 8.0 Hz, 3H), 6.85 (d, ^3J = 9.2 Hz, 2H), 3.92 (q, ^3J = 7.2 Hz, 2H), 1.27 ppm (t, ^3J = 7.2 Hz, 3H); ^{13}C NMR (acetone-d$_6$, 100 MHz): δ = 156.6, 152.2, 147.7, 145.6, 144.5, 130.1, 127.4, 126.4, 125.6, 124.7, 122.6, 114.0, 46.8, 11.9 ppm; IR: 3454, 3016, 2969, 2361, 2338, 1738n, 1602, 1584, 1513, 1490, 1477, 1448, 1425, 1372, 1230, 1217, 1155, 1143, 1132, 1091 cm^{-1}; HRMS (ESI), *m/z* calcd. for $C_{20}H_{18}N_4O_2$ [MH]$^+$: 346.38, found [MH]$^+$: 347.1504.

5
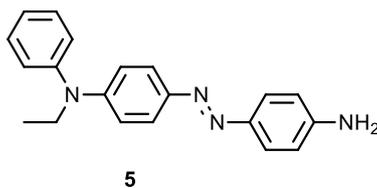
Aminoazobenzene 5. Following **standard procedure 2**, 763 mg (2.2 mmol) of nitrobenzene **S2** in 30 mL of 1,4-dioxane was reduced by two separate additions of 1.05 g (13.2 mmol) and 516 mg (6.6 mmol) of sodium sulfide. Purification of the crude product by column chromatography on silica gel (hexanes/EtOAc, 9:1→4:1) gave 291 mg (42%) of aminoazobenzene **5** as a red solid. R_f(hexanes/EtOAc, 5:1) = 0.3; ^{1}H NMR (CD$_3$OD, 400 MHz): δ = 7.65 (dd, [3]J = 8.6 Hz, 2H), 7.61 (dd, [3]J = 8.6 Hz, 2H), 7.38 (t, [3]J = 9.2 Hz, 2H), 7.17 (m, 3H), 6.85 (dd, [3]J = 8.6 Hz, 2H), 6.73 (dd, [3]J = 8.6 Hz, 2H), 3.84 (q, [3]J = 7.2 Hz, 2H), 1.21 ppm (m, 3H); ^{13}C NMR (CD$_3$OD, 100 MHz): δ = 150.8, 149.6, 146.6, 145.2, 144.6, 129.4, 125.4, 124.3, 123.9, 123.2, 115.5, 114.0, 46.3, 11.6 ppm; IR: 3464, 3379, 3213, 3037, 2974, 2536, 2361, 2339, 1618, 1599, 1586, 1504, 1493, 1372, 1375, 1347, 1269, 1245, 1151, 1132, 1090 cm^{-1}; HRMS (ESI), m/z calcd. for C$_{20}$H$_{21}$N$_4$ [MH]$^+$: 317.1761, found [MH]$^+$: 317.1760.
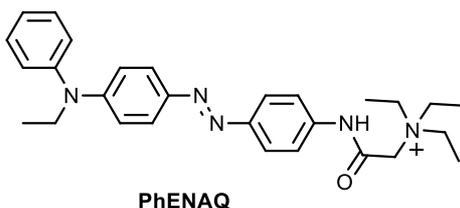
PhENAQ

PhENAQ. Following **standard procedure 3**, 73 mg (0.46 mmol) of betaine **E** in 5 mL of MeCN reacted with 0.24 mL (2M solution in DCM, 0.48 mmol) of oxalyl chloride to form acid chloride **F**, which was further reacted with 143 mg (0.45 mmol) of aminoazo-benzene **5** in 10 mL of DMF and 0.1 mL (10.0 mmol) of DIPEA over the course of two days. The crude product was purified by column chromatography on reversed-phase

silica gel (0.1% formic acid in water/MeOH, 1:0→1:1) to yield 149 mg (66%) **PhENAQ** formate salt as a red solid. R_f(0.1% formic acid in water/MeOH, 1:1) = 0.1; ^{1}H NMR (CD$_3$OD, 200 MHz): δ = 8.53 (s, 1H), 7.79 (d, ^3J = 8.8 Hz, 2H), 7.72 (m, 4H), 7.40 (t, ^3J = 7.6 Hz, 2H), 7.21 (m, 3H), 6.79 (d, ^3J = 9.2 Hz, 2H), 4.19 (s, 2H), 3.83 (q, ^3J = 7.2 Hz, 2H), 3.63 (q, ^3J = 7.2 Hz 6H), 1.35 (t, ^3J = 7.2 Hz, 9H), 1.22 ppm (t, ^3J = 7.2 Hz, 3H); ^{13}C NMR (CD$_3$OD, 100 MHz): δ = 168.3, 161.7, 150.9, 149.8, 146.1, 144.5, 138.8, 129.6, 129.4, 126.5, 125.4, 125.3, 124.2, 123.9, 122.6, 120.1, 114.4, 56.2, 54.4, 46.4, 11.5, 6.6 ppm; IR: 3500–3200, 3030, 2980, 2660, 1678, 1585, 1556, 1506, 1461, 1385, 1345, 1320, 1276, 1135, 1089, cm^{-1}; HRMS (ESI), m/z calcd. for C$_{28}$H$_{36}$N$_5$O [M]$^+$: 458.2914, found [M]$^+$: 358.2912; UV/Vis (H$_2$O): λ_{max} = 463 nm.

S3
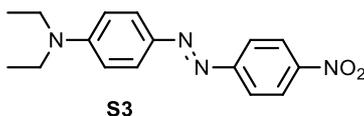
Nitroazobenzene S3. Following **standard procedure 1**, 1.38 g (10 mmol) of *p*-nitroaniline dissolved in 20 mL of MeOH and 5 mL of 12M HCl first reacted with 1.4 mL (10 mmol) of isoamylnitrite to form a diazonium salt, which then further reacted with 1.66 g (10 mmol) of diethylaniline in 20 mL of MeOH and 5 mL of 12M HCl. Column chromatography on silica gel (hexanes/EtOAc, 10:3 then 2:1) gave 1.85 g (62%) of nitroazobenzene **S3** as a red-brown solid. R_f(hexanes/EtOAc, 10:3) = 0.7; ^{1}H NMR (600 MHz, CDCl$_3$): δ = 8.32–8.29 (m, 2H), 7.92–7.86 (m, 4H), 6.75–6.71 (m, 2H), 3.48 (q, ^3J = 7.1 Hz, 4H), 1.25 ppm (t, ^3J = 7.1 Hz, 6H); ^{13}C NMR (150 MHz, CDCl$_3$): δ = 157.0, 151.3, 147.2, 143.3, 126.4, 124.7, 122.5, 111.0, 44.9, 12.7 ppm; IR: 3427, 2965, 2926, 1937, 1600, 1587, 1518, 1504, 1444, 1425, 1408, 1391, 1341, 1324, 1274, 1258, 1194,

10

1139, 1103, 1076 cm^{-1}; HRMS (ESI), *m/z* calcd. for C$_{16}$H$_{19}$N$_4$O$_2$ [MH]$^+$: 299.1503, found [MH]$^+$: 299.1492.

6
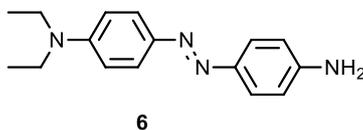
Aminoazobenzene 6. Following **standard procedure 2**, 1.8 g (6.0 mmol) of nitrobenzene **S3** in 90 mL of 1,4-dioxane and 9 mL of water was reduced by three separate additions of 0.47 g (6.0 mmol) of sodium sulfide. Purification of the crude product by column chromatography on silica gel (hexanes/EtOAc, 7:3) gave 1.41 g (88%) of aminoazobenzene **6** as a deep red, glassy solid. R$_f$(EtOAc/hexanes, 3:10) = 0.3; ^{1}H NMR (400 MHz, DMSO-d$_6$): δ = 7.62–7.57 (m, 2H), 7.53–7.47 (m, 2H), 6.73–6.68 (m, 2H), 6.62–6.57 (m, 2H), 5.68 (m, 2H), 3.38 (q, ^3J = 7.0 Hz, 4H), 1.10 ppm (t, ^3J = 7.0 Hz, 6H); ^{13}C NMR (100 MHz, DMSO-d$_6$): δ = 162.7, 151.4, 149.1, 143.7, 142.8, 124.2, 113.9, 111.4, 44.4, 13.0 ppm; IR: 3440, 3323, 2972, 2252, 1896, 1669, 1623, 1590, 1557, 1512, 1450, 1403, 1386, 1374, 1350, 1307, 1271, 1250, 1196, 1166, 1148, 1095 cm^{-1}; HRMS (ESI), *m/z* calcd. for C$_{16}$H$_{21}$N$_4$ [MH]$^+$: 269.1761, found [MH]$^+$: 269.1751.
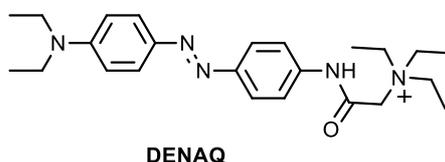
DENAQ

DENAQ. Following **standard procedure 3**, 478 mg (3.0 mmol) of betaine **E** dissolved in 10 mL of acetonitrile was reacted with 1.5 mL (2M solution in DCM, 3.0 mmol) of oxalyl chloride to form the acid chloride **F**, which was further reacted with 161 mg (0.6 mmol) of aniline **6** dissolved in 20 mL of DMF and 0.51 mL (3.0 mmol) of DIPEA. The crude product

was purified by column chromatography on reversed-phase silica gel (0.1% formic acid in water/acetonitrile, 1:0→17:3) to yield 250 mg (92%) of **DENAQ** formate salt as a deep red, glassy solid. ^{1}H NMR (CD$_3$OD, 400 MHz): δ = 8.48 (s, 1H), 7.79–7.67 (m, 6H), 6.74–6.62 (m, 2H), 4.23–4.12 (m, 2H), 3.64–3.48 (m, 6H), 3.43–3.31 (m, 4H), 1.37–1.24 (m, 9H), 1.18–1.05 ppm (m, 6H); ^{13}C NMR (CD$_3$OD, 100 MHz): δ = 167.2, 161.7, 150.3, 149.9, 142.7, 138.6, 125.0, 122.4, 120.2, 110.8, 56.3, 54.4, 44.2, 11.7, 6.7 ppm; IR: 2972, 1688, 1630, 1597, 1547, 1514, 1448, 1394, 1351, 1249, 1194, 1154, 1138, 1076 cm^{-1}; HRMS (ESI), m/z calcd. for C$_{24}$H$_{36}$N$_5$O [MH]$^+$: 410.2914, found [MH]$^+$: 410.2899; UV/Vis (H$_2$O): λ_{max} = 470 nm.

S4
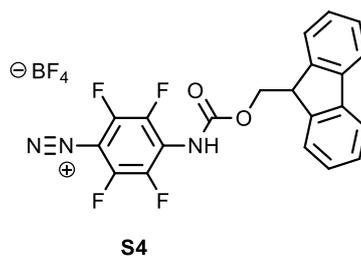
Diazonium tetrafluoroborate S4. Under argon atmosphere a solution of 100 mg (0.25 mmol) of 4-{*N*-[(9-fluorenylmethoxy)carbonyl]amino}tetrafluoroaniline (synthesized following the procedures of Chehade et al.[3]) in 1 mL of dry THF was added dropwise to 47.2 µL (0.37 mmol) of boron trifluoride etherate at −40 °C. The resulting solution was stirred for 5 minutes and 41.8 µL isoamyl nitrite (0.31 mmol, 1.25 eq) was subsequently added dropwise. The reaction mixture was warmed to −5 °C over 3 hours, causing a color change to orange. The crude diazonium salt was precipitated by addition of 15 mL of cold pentane. The supernatant was transfused and when necessary centrifuged at 4 °C. The orange and solid diazonium tetrafluoroborate **S4** was dried *in vacuo* at −5 °C for one hour and employed for further reaction without additional purification. ^{1}H NMR

(DMSO-d$_6$, 200 MHz): δ = 9.96 (s, br, 1H), 7.90–7.80 (m, 2H), 7.72–7.63 (m, 2H), 7.44–7.27 (m, 4H), 4.58–4.56 (m, ^3J = 6.8 Hz, 2H), 4.35–4.25 ppm (m, 1H).

8
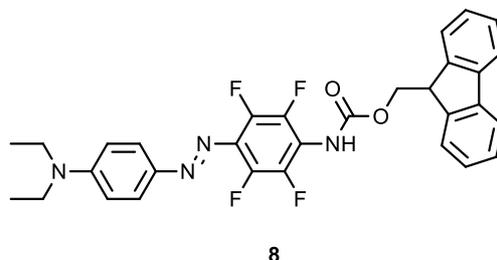
Tetrafluoroazobenzene 8. 601 mg (1.20 mmol) of freshly prepared diazonium tetrafluoroborate **S4** was dissolved in 6 mL of dry THF under argon atmosphere. To this solution, 0.23 mL (1.44 mmol) of *N,N*-diethylanilin and 98 mg (1.44 mmol) of sodium acetate were added at 0 °C. The dark red reaction mixture was allowed to warm to room temperature and stirred overnight. Then the mixture was poured into 100 mL of EtOAc and washed with saturated bicarbonate solution, water, and brine. The organic phase was dried over Na$_2$SO$_4$ and concentrated *in vacuo*. Purification by column chromatography (hexanes/EtOAc = 20:1→8:1) yielded 246 mg (36%) of carbamate **8** as a red-orange solid. R$_f$(hexanes/EtOAc = 7:3) = 0.42. ^{1}H NMR (THF-d$_8$, 400 MHz): δ = 8.90 (s, br, 1H), 7.83–7.75 (m, 4H), 7.64 (d, ^3J = 7.4 Hz, 2H), 7.38–7.33 (m, 2H), 7.28 (td, ^3J = 7.4 Hz, 2H), 6.81–6.76 (m, 2H), 4.52 (d, ^3J = 6.6 Hz, 2H), 4.27 (t, ^3J = 6.6 Hz, 1H), 3.51 (q, ^3J = 7.1 Hz, 4H), 1.21 ppm (t, ^3J = 7.1 Hz, 6H). ^{13}C NMR (THF-d$_8$, 100 MHz): δ = 155.0, 153.4, 146.2–146.0 (m), 145.9, 145.8, 143.8–143.5 (m), 143.2, 141.3–143.0 (m), 132.9–132.7 (m), 129.2, 126.8, 127.7, 126.6, 121.5, 117.7, 112.7, 49.0, 46.3, 13.7 ppm. ^{19}F NMR (THF-d$_8$, 376 MHz): δ = −147.93 (dd, ^3J = 20.6 Hz, ^4J = 9.3 Hz, 2F), −153.09 ppm (dd, ^3J = 20.6 Hz, ^4J = 9.3 Hz, 2F). IR: 3255, 2976, 1703, 1602, 1527, 1498, 1473, 1406, 1383,

1353, 1305, 1273, 1231, 1195, 1144, 1104, 1077, 1023 cm^{-1}. HRMS (ESI), *m/z* calcd. for C$_{31}$H$_{27}$F$_4$N$_4$O$_2$ [MH]$^+$: 563.2065, found [MH]$^+$: 563.2061. UV/Vis (EtOH): λ_{max} = 446 nm.

S5
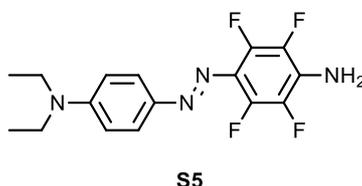
Tetrafluoroazobenzene S5. 243 mg of freshly prepared FMOC-protected azo-benzene **8** (0.43 mmol) was suspended in 9 mL of degassed diethyl ether under argon atmosphere and cooled to 0 °C. After addition of 0.9 mL (774 mmol) of piperidine, the mixture was warmed to room temperature, stirred for 3 hours, subsequently diluted with 100mL of diethyl ether , and washed with HCl (1M), water, and brine. The organic layer was dried over Na$_2$SO$_4$ and concentrated *in vacuo*. Purification by column chromatography (CH$_2$Cl$_2$/hexanes= 1:4→2:3) yielded 125 mg (85%) of tetrafluoroaniline **S5** as red crystals. R$_f$(hexanes/EtOAc = 7:3) = 0.64. ^{1}H NMR (Acetone-d$_6$, 400 MHz, 27 °C): δ = 7.77–7.70 (m, 2H), 6.84–6.78 (m, 2H), 5.72 (s, br, 2H), 3.52 (q, ^3J = 7.1 Hz, 4H), 1.21 ppm (t, ^3J = 7.1 Hz, 6H). ^{13}C NMR (Acetone-d$_6$, 100 MHz, 27 °C) δ = 150.6, 143.9, 143.0–142.9 (m), 140.6–140.4 (m), 137.8–137.5 (m), 135.3135.1 (m), 124.9, 110.9, 44.3, 12.0 ppm. ^{19}F NMR (Acetone-d$_6$, 376 MHz, 27 °C): δ = −155.12– −155.30 (m, 2F), −165.55– −165.74 ppm (m, 2F). IR: 3500, 3397, 2972, 2926, 1654, 1596, 1559, 1515, 1501, 1455, 1399, 1351, 1296, 1273, 1238, 1196, 1138, 1095, 1080, 1058, 1012, 1000 cm^{-1}. HRMS (ESI), *m/z* calcd. for C$_{16}$H$_{17}$F$_4$N$_4$ [MH]$^+$: 341.1384, found [MH]$^+$: 341.1381. UV/Vis (EtOH): λ_{max} = 430, 458 nm.
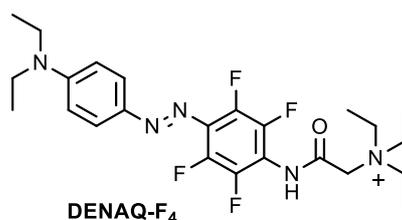
DENAQ-F$_4$

DENAQ-F$_4$. Following **Standard Procedure 3**, 125 mg (0.37 mmol) of tetrafluoro-aniline **S5** and 0.32 mL (1.83 mmol) of DIPEA were dissolved in 7 mL of dry DMF. To this solution, 390 mg (1.83 mmol) of betaine acid chloride **F** dissolved in 10 mL of dry DMF was added. The resulting mixture was allowed to warm to room temperature, stirred overnight, and DMF was subsequently removed *in vacuo*. Reversed phase column chromatography (0.1% formic acid in water/methanol, 9:1→1:1) yielded 74.1 mg (38%) of **DENAQ-F$_4$** formate salt as a deep red hygroscopic solid. R$_f$(0.1% formic acid in water/methanol = 1:1) = 0.20. ^{1}H NMR (CD$_3$OD, 400 MHz): δ = 8.51 (s, 1H) 7.84–7.72 (m, 2H), 6.84–6.70 (m, 2H), 4.36 (s, 2H), 3.64 (q, ^3J = 7.2 Hz, 6H), 3.49 (q, ^3J = 7.1 Hz, 4H), 1.38 (t, ^3J = 7.2 Hz, 9H), 1.20 ppm (t, ^3J = 7.1 Hz, 6H). ^{13}C NMR (CD$_3$OD, 100 MHz) δ = 167.6 (br), 162.6, 152.0, 144.2–143.9 (m), 143.7, 141.8–141.4 (m), 139.3–139.1 (m), 132.1–131.9 (m), 126.0, 110.8, 55.6, 54.5, 44.4, 11.5, 6.6 ppm. ^{19}F NMR (CD$_3$OD, 376 MHz): δ = −148.72 (dd, ^3J = 19.2 Hz, ^4J = 8.5 Hz, 2F), −155.15 ppm (dd, ^3J = 19.2 Hz, ^4J = 8.5 Hz, 2F). IR: 3406, 3186, 2978, 1673, 1597, 1555, 1519, 1494, 1380, 1352, 1307, 1274, 1246, 1200, 1150, 1116, 1076, 1008 cm^{-1}. HRMS (ESI), *m/z* calcd. for C$_{24}$H$_{32}$F$_4$N$_5$O [M]$^+$: 482.2537, found [M]$^+$: 482.2533. UV/Vis (DPBS, pH = 7.4): λ_{max} = 487 nm.
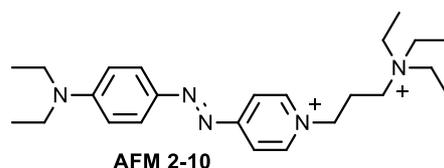
AFM 2-10

AFM 2-10. In a 10 mL Schlenk flask equipped with a reflux condenser, 100 mg (0.39 mmol) of 4-(4-diethylaminophenylazo)pyridine and 358 mg (1.18 mmol) of (3-bromopropyl)triethylammonium bromide (see Jeon et al.[4]) were dissolved in 8 mL of dry DMF under argon atmosphere. The reaction mixture was stirred at 80 °C for 30 hours, cooled to room temperature, and subsequently dried *in vacuo*. Purification by reversed phase column chromatography (0.1% formic acid in water/methanol, 1:0→50:1) had to be performed two times, yielding 180 mg (92%) **AFM 2-10** as deep purple hygroscopic solid bisformate salt. ^{1}H and ^{13}C NMR samples were taken from the corresponding trifluoroacetate salt, which was obtained by further purification using reversed phase HPLC. R_f(0.1% formic acid in water/methanol, 1:10) = 0.05. ^{1}H NMR (D_2O, 400 MHz): $\delta =$ 8.48 (d, ^3J = 7.4 Hz, 2H), 7.77 (m, br, 4H), 7.31 (s, br, 2H), 4.40 (t, ^3J = 7.6 Hz, 2H), 3.90 (q, ^3J = 7.2 Hz, 4H), 3.21–3.16 (m, 8H), 2.29 (m,2H), 1.29 (t, ^3J = 7.2 Hz, 6H), 1.13 ppm (t, ^3J = 7.2, 9H). ^{13}C NMR (D_2O, 100 MHz): $\delta =$ 162.7 (q), 160.2, 154.1, 144.4, 141.9, 126 (br), 126.5 (br), 116.2 (q), 112.7, 56.1, 52.9, 52.6, 49.4, 23.0, 12.8, 6.5 ppm. IR: 3390, 2977, 1650, 1634, 1593, 1543, 1513, 1502, 1476, 1418, 1395, 1370, 1343, 1318, 1300, 1266, 1189, 1164, 1115, 1071, 1025, 1006 cm^{-1}. HRMS (ESI), *m/z* calcd. for $C_{24}H_{39}N_5$ [M]$^{2+}$: 198.6597, found [M]$^{2+}$: 198.6596. UV/Vis (DPBS, pH = 7.4): λ_{max} = 580 nm.

References:

1. Fortin, D. L.; Banghart, M. R.; Dunn, T. W.; Borges, K.; Awagenaar, D.; Gaudry, Q.; Karakossian, M. H.; Otis, T. S.; Kristan, W. B.; Trauner, D.; Kramer, R. H., *Nature Methods* **2008,** *5*(4), 331–338.

2. Haga, K.; Oohashi, M.; Kaneko, R., *Bulletin of the Chemical Society of Japan* **1984,** *57*(6), 1586–1590.

3. Chehade, K. A. H.; Spielmann, H. P., *Journal of Organic Chemistry* **2000,** *65*(16), 4949–4953.

4. Jeon, W. S.; Kim, E.; Ko, Y. H.; Hwang, I. H.; Lee, J. W.; Kim, S. Y.; Kim, H. J.; Kim, K., *Angewandte Chemie International Edition* **2005,** *44*(1), 87–91.

BENAQ

S2

PhENAQ

DENAQ

DENAQ-F₄

AFM 2-10
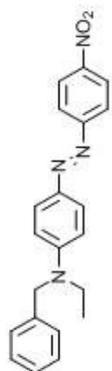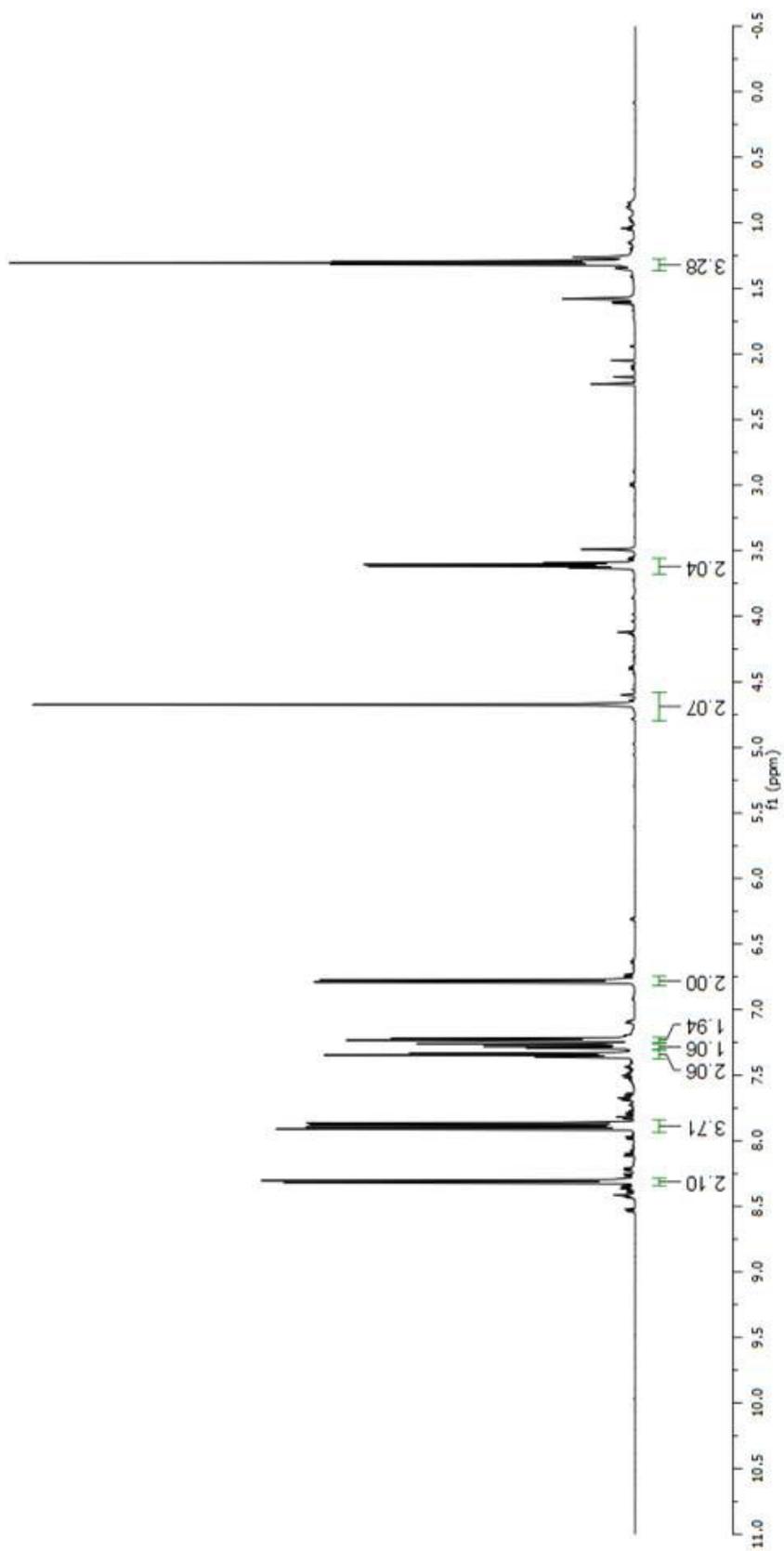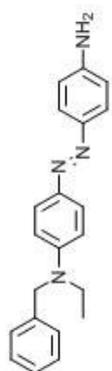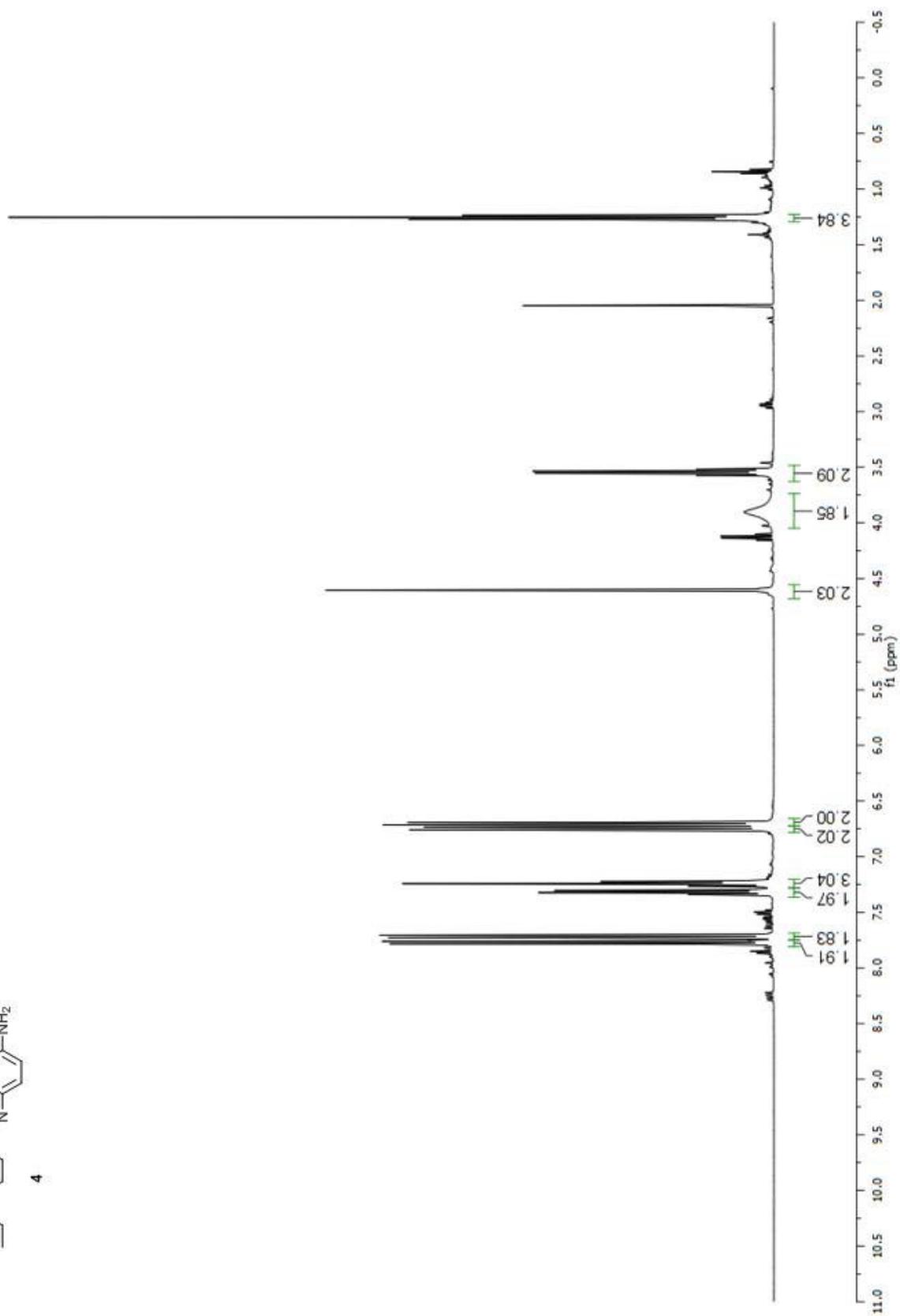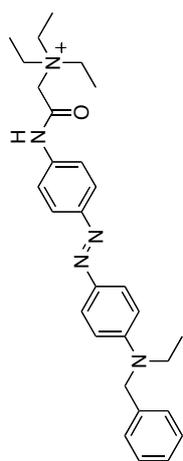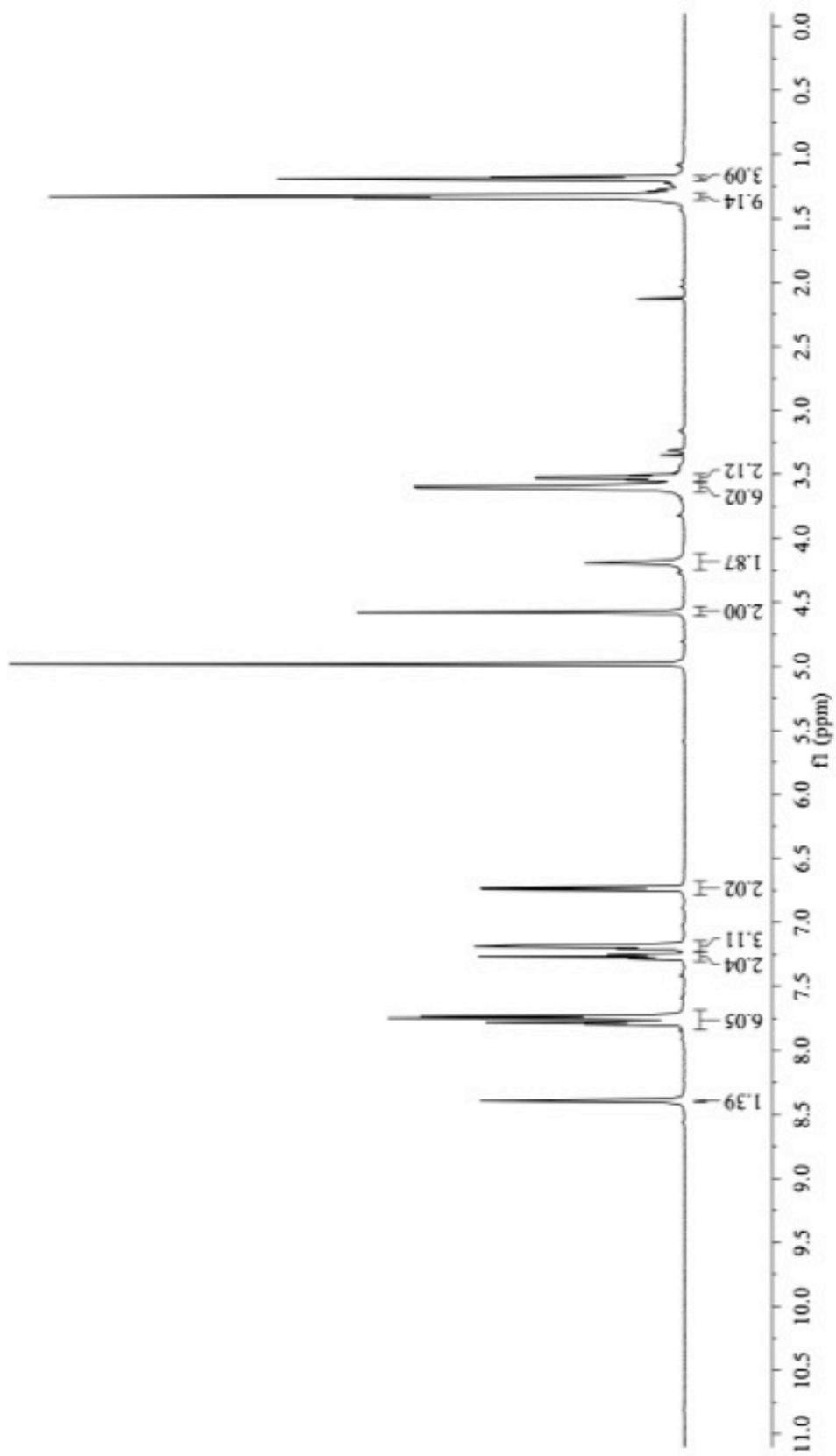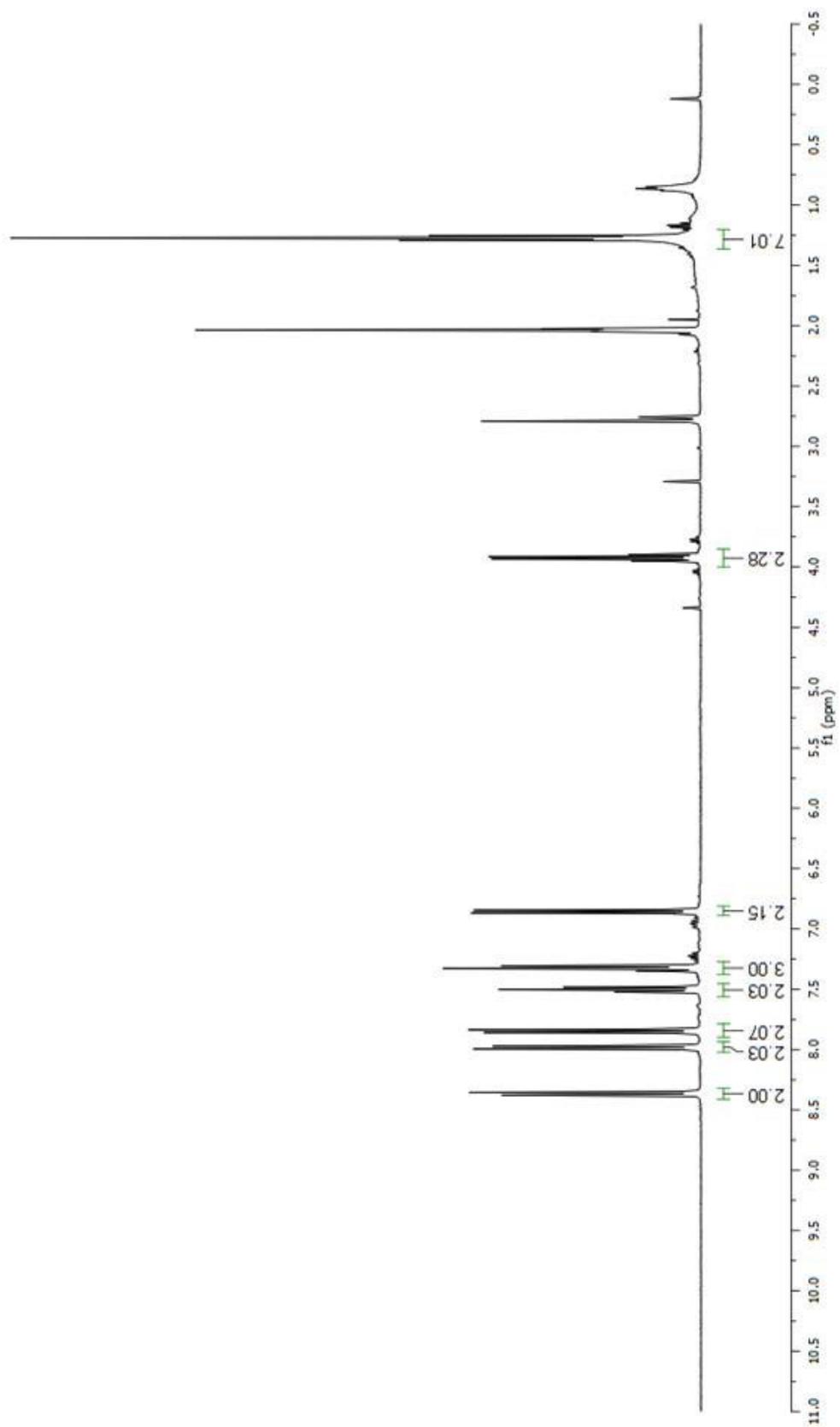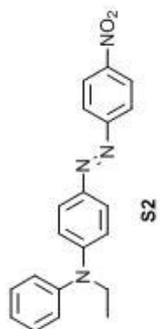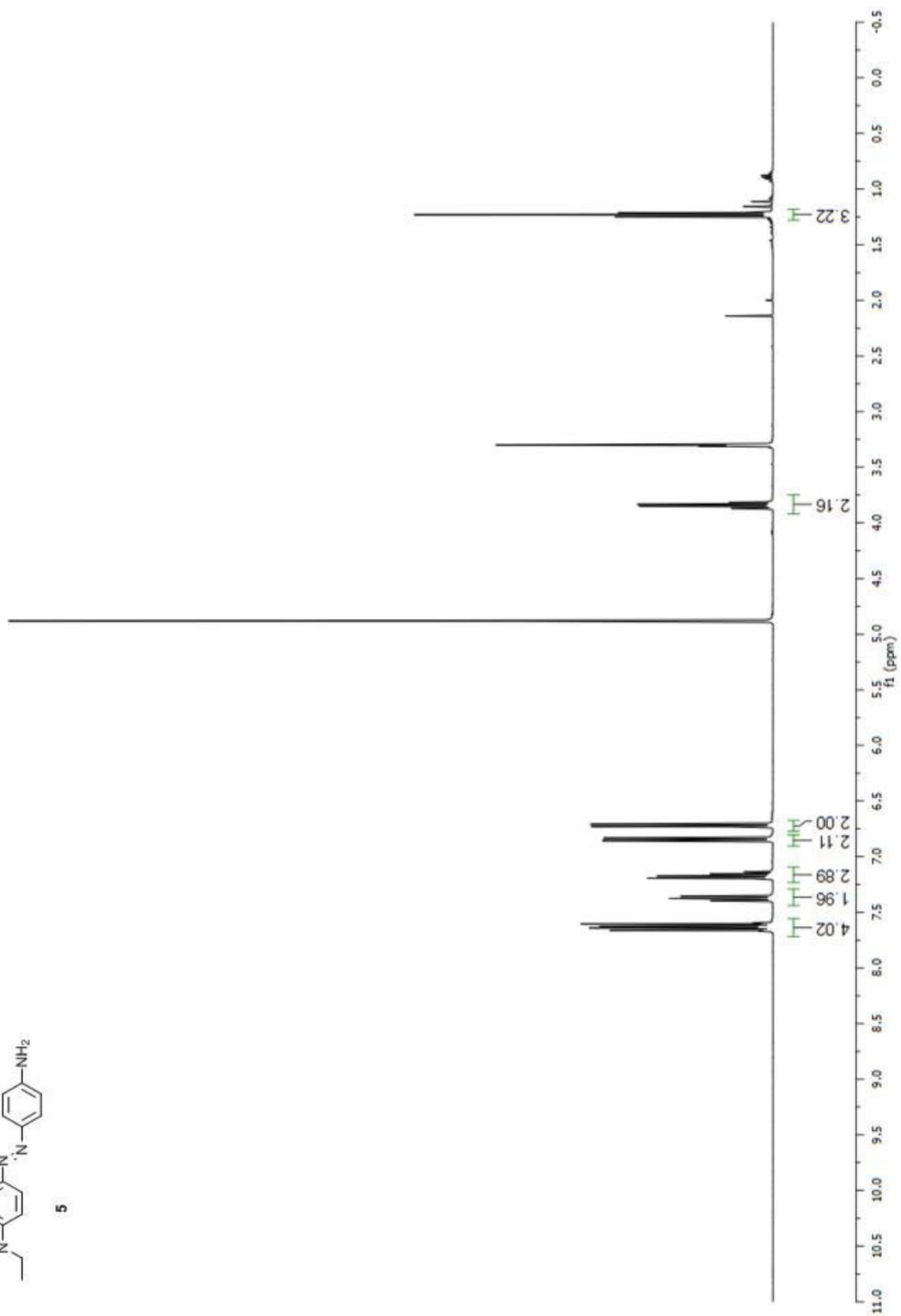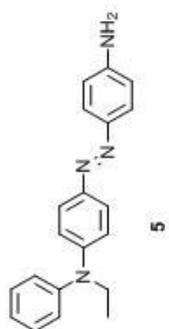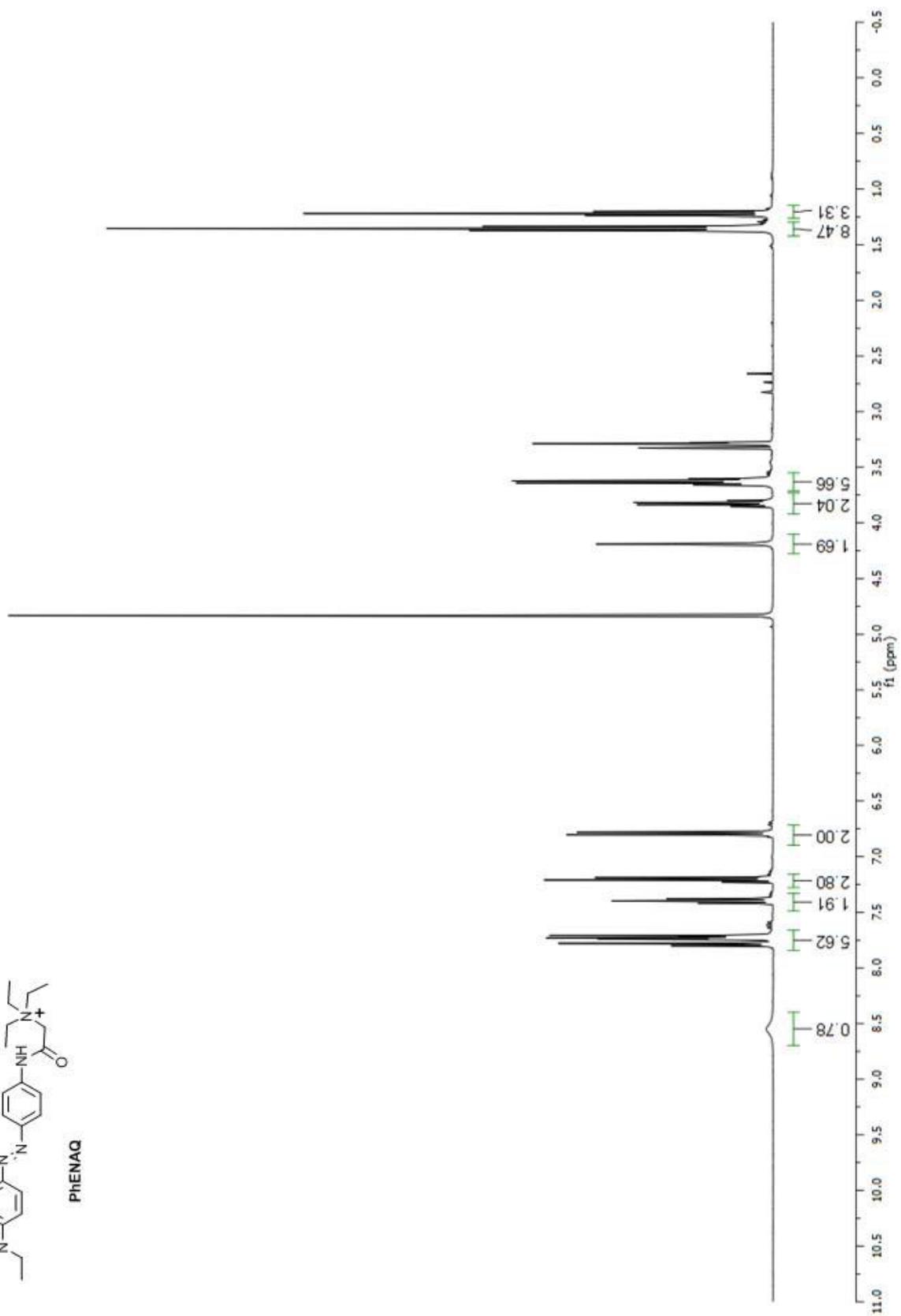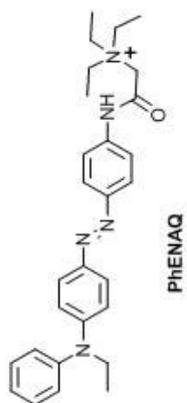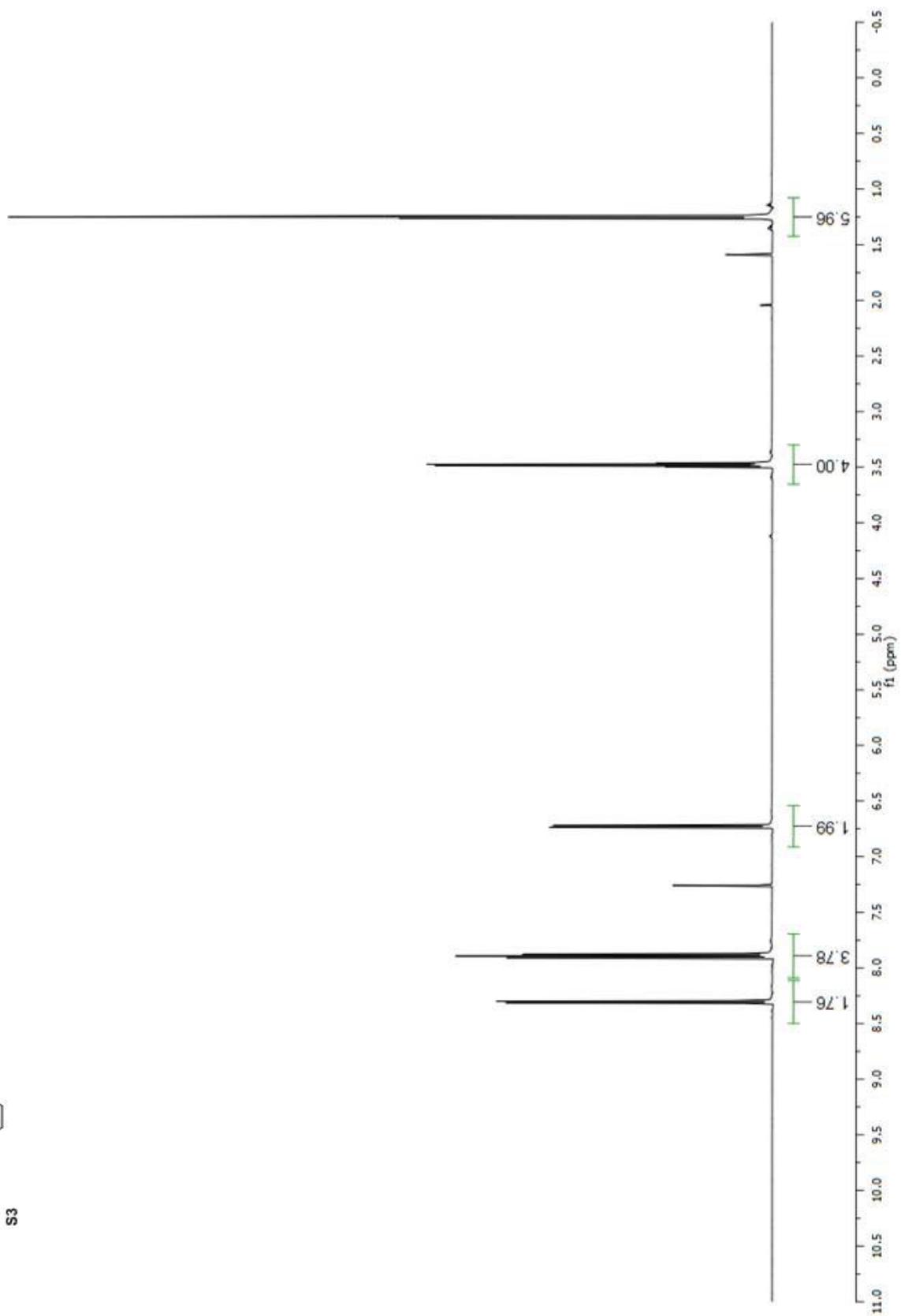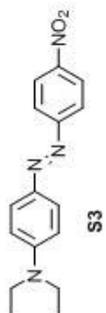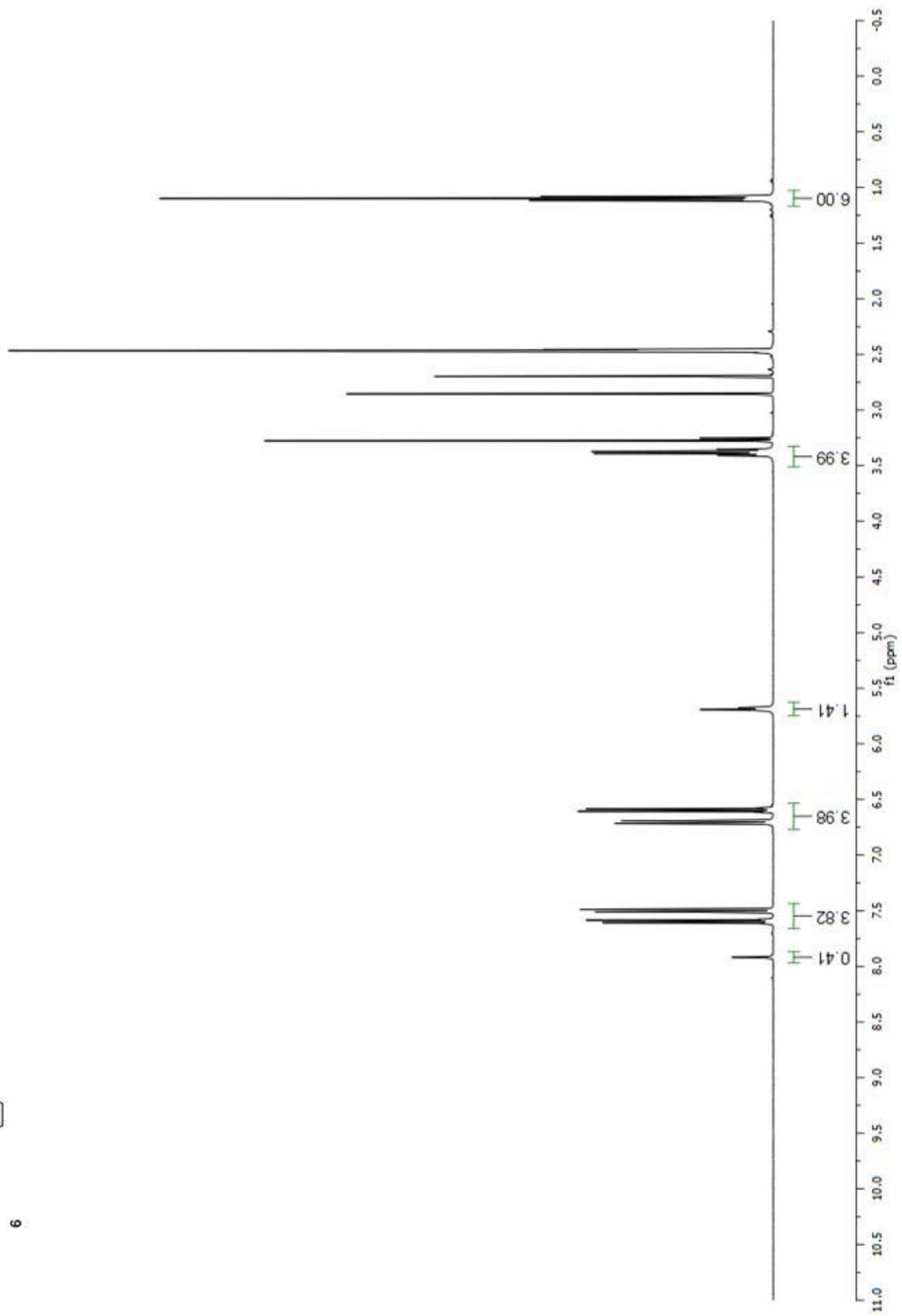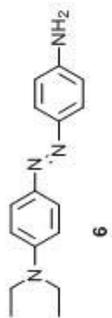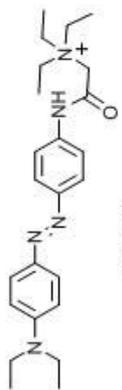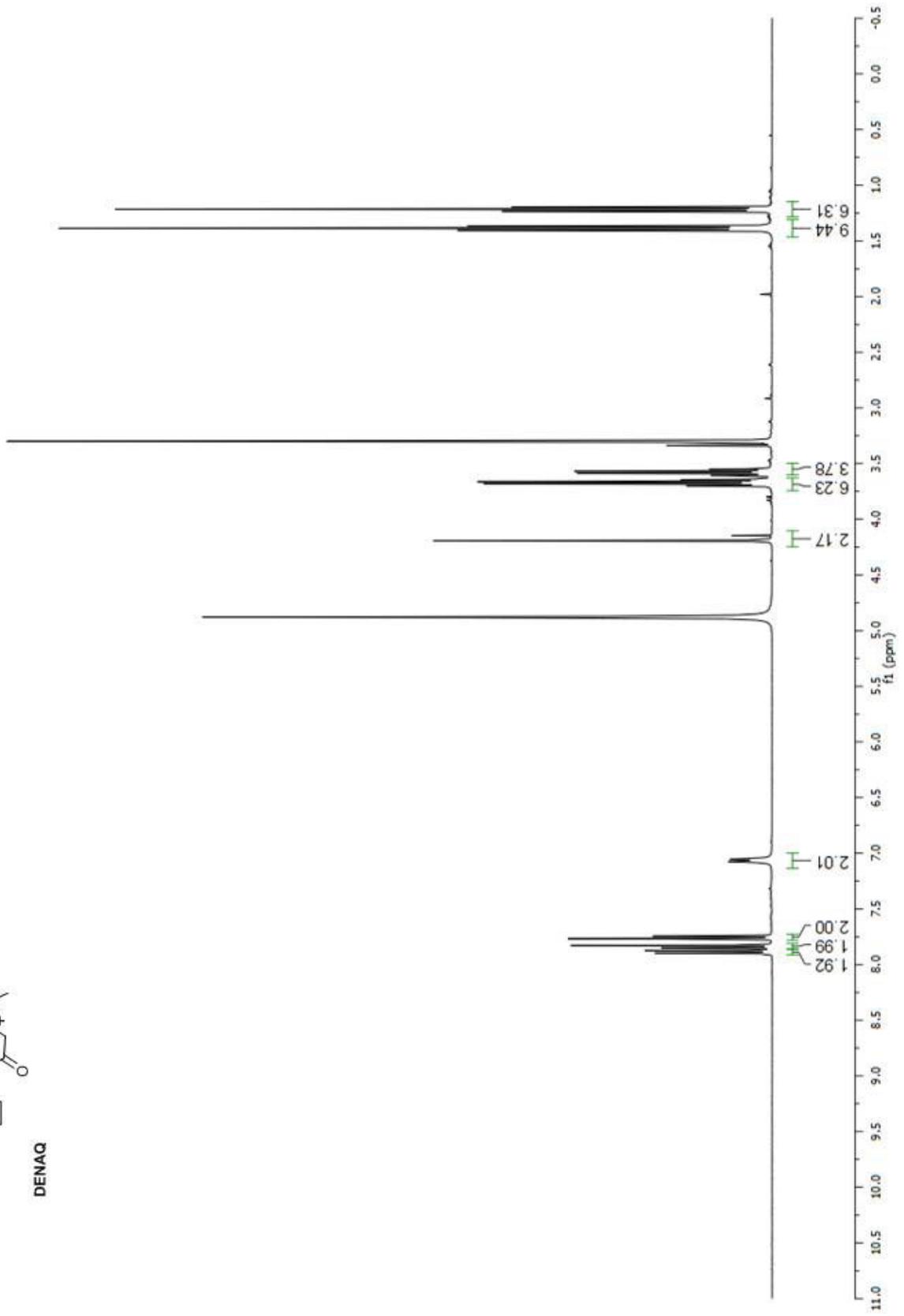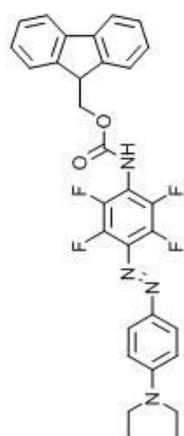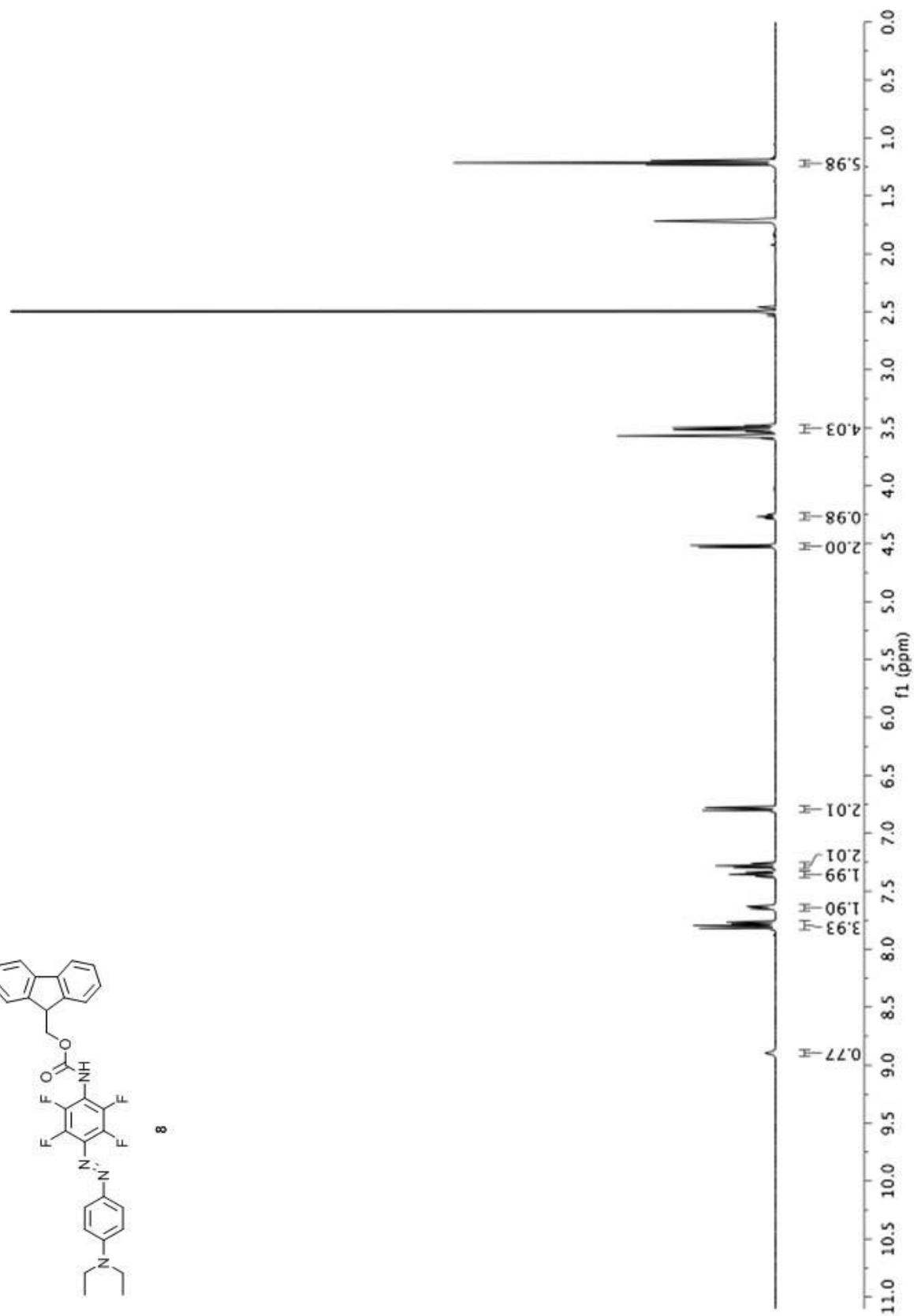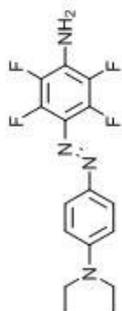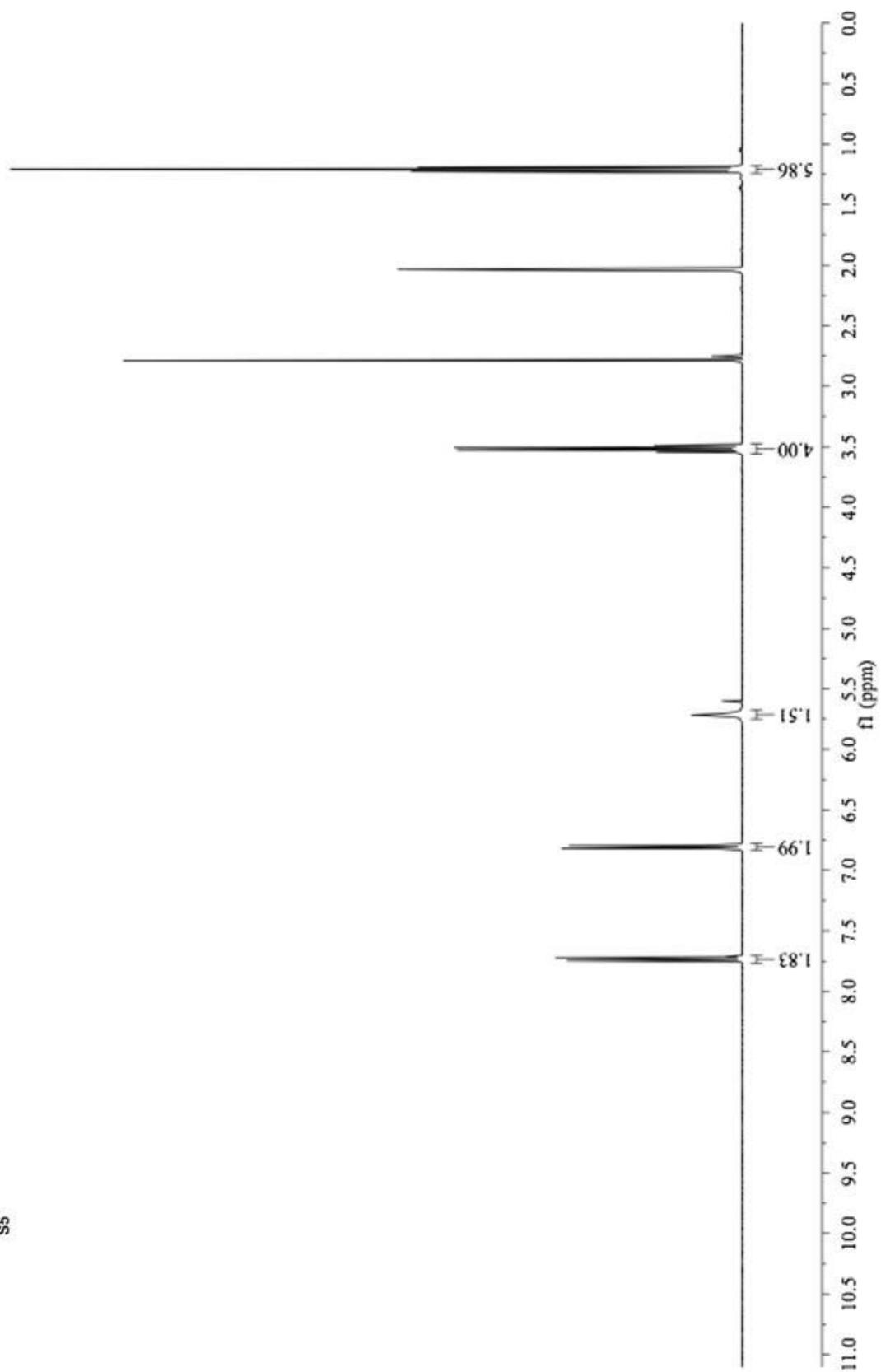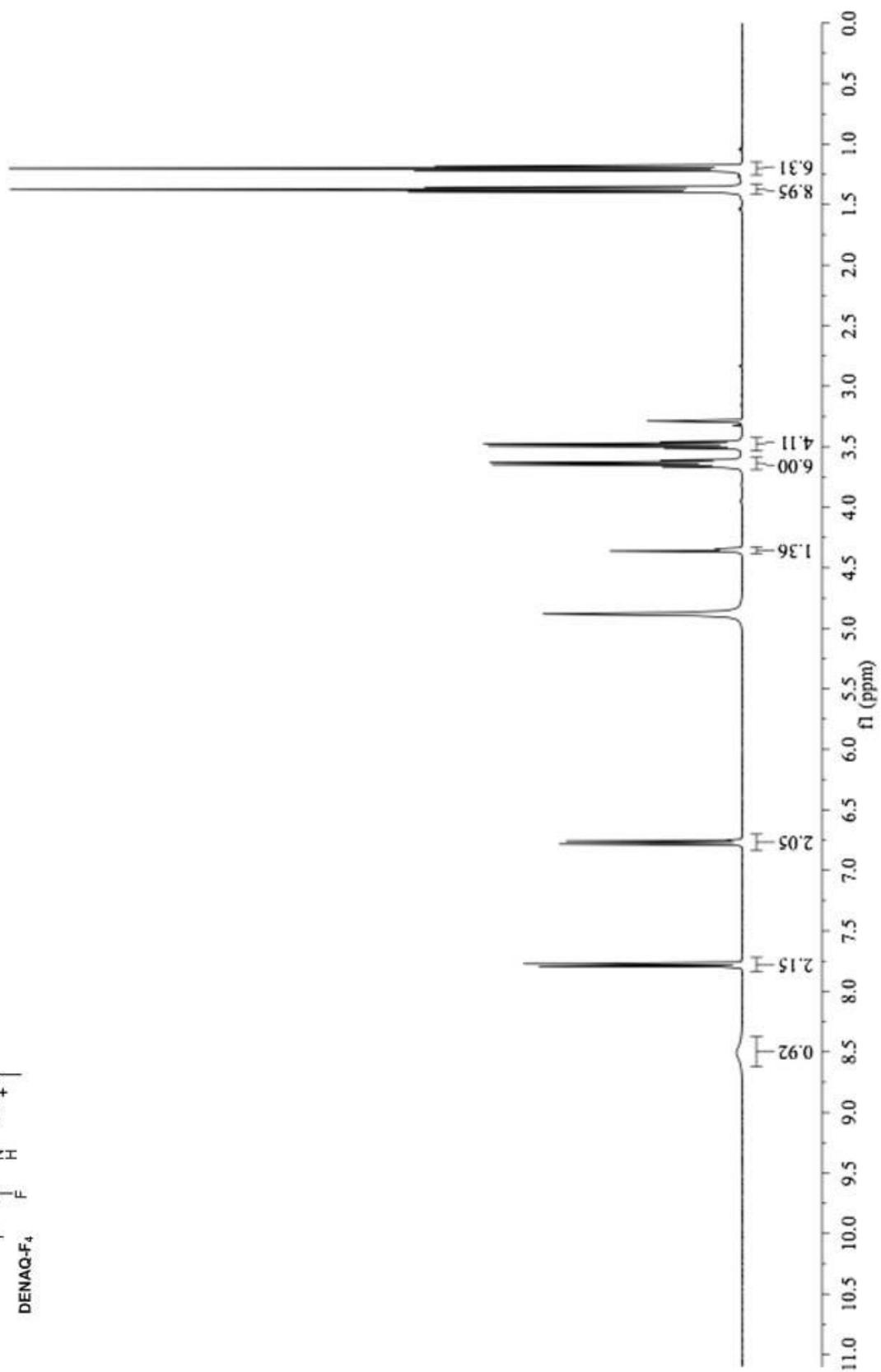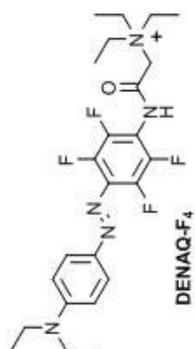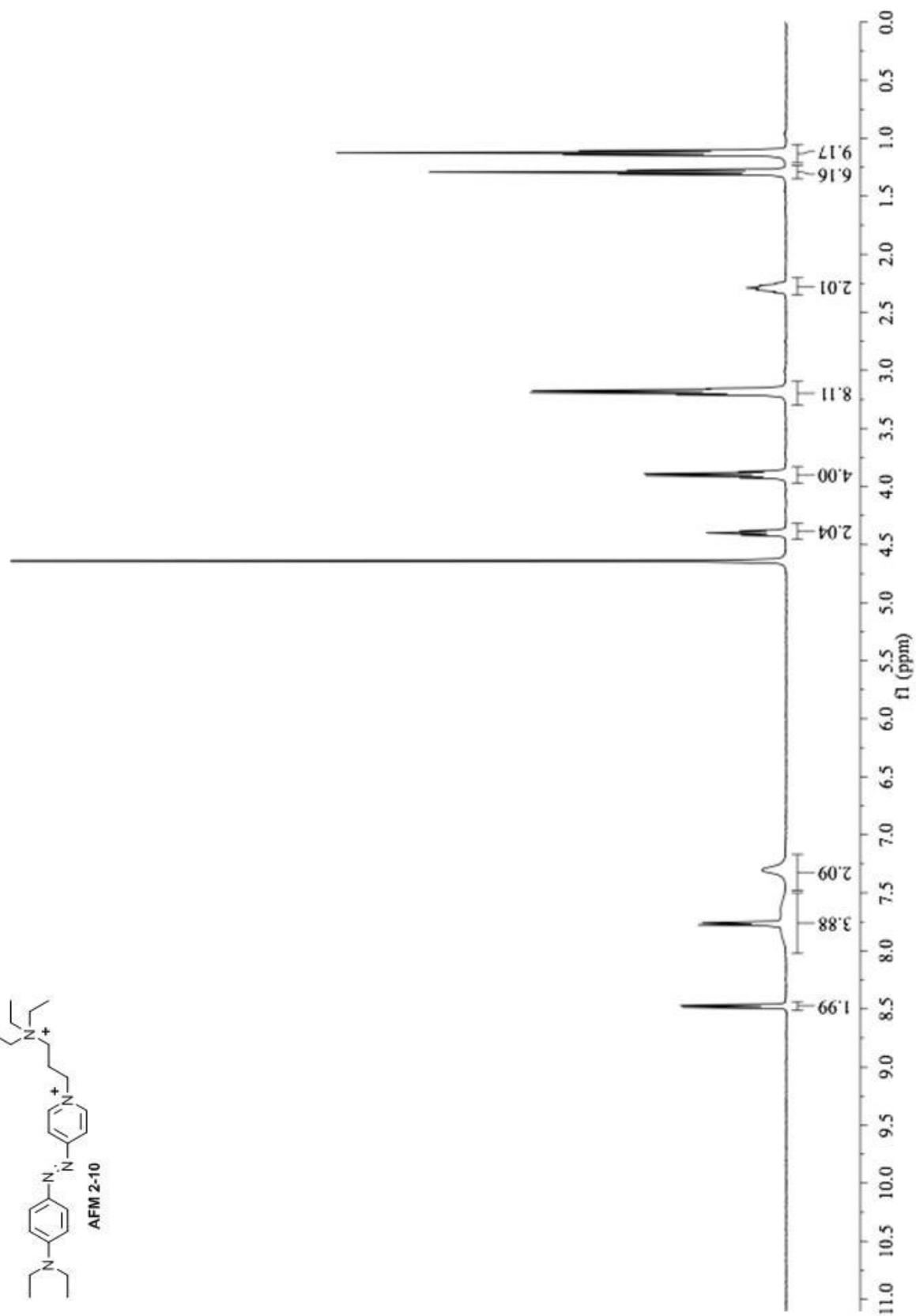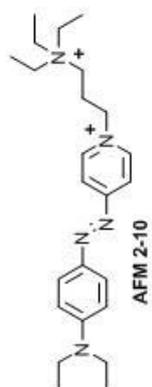
4) L-type calcium channels as potential targets for PCLs

Calcium ions represent a key second messenger in the intracellular communication of cells, which is crucial for adaptations to environmental changes.[1] In neurons for instance, the difference between internal and external Ca^{2+} concentration, which is about 10000 fold, allows for a precise temporal control of intracellular processes.[1] Voltage-gated calcium (Ca_v) channels are opened by a depolarization of the membrane, which leads to internal Ca^{2+} elevation in a defined space and triggers further downstream signaling.[2,3] These processes are involved in neuronal regulation of gene expression and neurotransmitter release at presynapses, which is important for dendritic differentiation and neuronal communication, respectively.[3]

4.1) Calcium as a second messenger

In a neuronal context, the class of L-type calcium channels (LTCCs), which are voltage-gated, have been extensively studied in terms of their influence on gene regulation.[3] Different LTCCs related second messenger pathways trigger the phosphorylation of the cAMP response element-binding protein (CREB) at Serine 133.[3] The phosphorylated state of CREB represents the active form of a transcription factor, which is for instance crucial in the gene expression of neutrophins. An example of this class is BDNF, which has an important influence on dendritic growth and synaptic development.[3]

A rather slow second messenger pathway, initiated by LTCCs, includes the Ras/MAP kinase pathway.[4] Here, calmodulin (CaM) is associated with the internal side of a LTCC and coordinates Ca^{2+} upon channel opening, thereby triggering the RAS/MAP kinase cascade, which leads to the phosphorylation of CREB. This pathway reaches its maximal activity after 30-60 min.[4]

Another second messenger pathway starts with the Ca^{2+} influx through LTCCs and the binding of Ca^{2+} to closely located CaM.[5] Activated Ca^{2+}/CaM units directly translocate to the cell nucleus, where they control CaMKIV dependent CREB

phosphorylation. This process happens within 1-3 minutes and represents a rather fast pathway.[5]

A third LTCCs initiated CREB phosphorylation pathway, which shows maximal activity in a timescale of minutes, involves CaMKII.[6] Ca^{2+} entering via LTCCs binds to apoCaM, which then coordinates to CaMKII. The second messengers that follow this process and finally phosphorylate CREB are still under investigation.

A)

B)
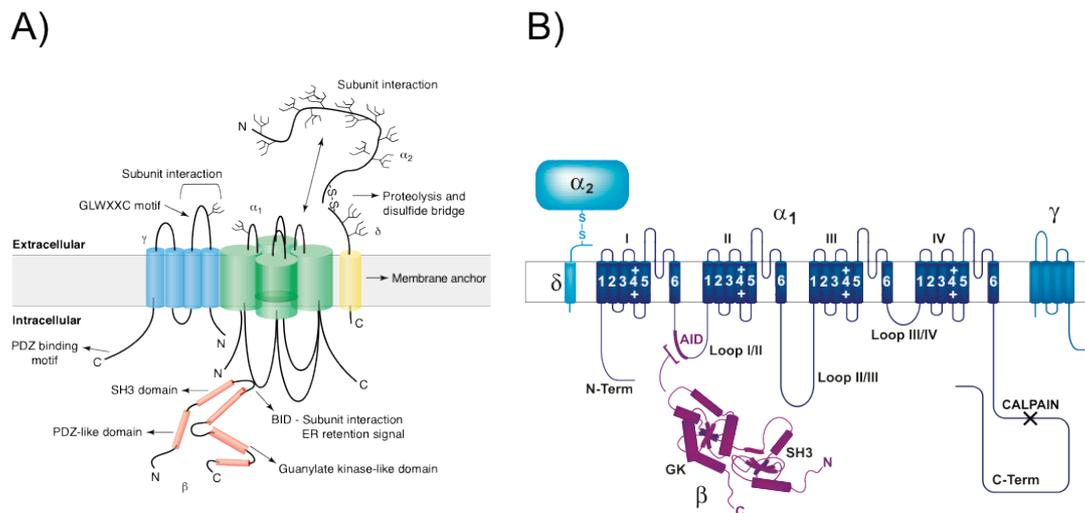
Figure 2. Two schematic depictions of a LTCC including the α-subunit co-assembled with β, $α_2δ$ and γ auxiliary subunits. **A)** A spatial representation of a LTCC arrangement (modified from publication[7]). **B)** A detailed presentation of the α -subunit homologue domains I-IV and their transmembrane domains 1-6 (modified from publication[8]).

4.2) Molecular composition of Ca_v channels.

The core of Ca_v channels includes a central α-subunit with a mass of about 200 kDa, which forms an ion-conducting pore (Fig. 2). Several α-subunit families exist and are divided in Ca_v1 (LTCC/L-type), Ca_v2 (P/Q-, N-, R-type), Ca_v3 (T-type) channels.[8,9] So far 10 α -subunits have been identified.[10] The α -subunit co-assembles with the auxiliary subunits β, $α_2δ$ and γ (Fig. 2). These auxiliary subunits modulate biophysical properties of the channel and have an influence on the surface expression.[7,8,9]

The α-subunit contains four homologue domains, I-IV, whereat each domain has six transmembrane domains, 1-6 (Fig. 2).[7,8,9]

The β-subunit is located in the cytosol and contains two main protein-protein interaction domains, a SH3 domain and a GK domain (Fig. 2).[7,8,9] Four different β-subunits, β_1-β_4, have been identified. Additionally, alternative splicing events increase the number of β-subunits. The main interaction site of the α- and β-subunit lies for the α-subunit on the connecting loop between domains I/II and for the β-subunit on the GK domain.[8]

The $\alpha_2\delta$-subunit consists of two polypeptides, α_2 and δ, which are connected by a disulfide bond. Four different isoforms have been identified, $\alpha_2\delta$-1 - $\alpha_2\delta$-4.[7,8,9] Although the polypeptides are separated, they were originally found as one transcript, which is separated by proteolytic cleavage.[7,8,9] The $\alpha_2\delta$-subunits have only a minor influence on the biophysical properties of the Ca_v channels. These subunits seem to be upregulated in certain parts of the brain, during development of physiological dependence on drugs of abuse.[11]

The γ-subunit is a glycoprotein with four transmembrane segments. So far, eight genes encoding γ_1-γ_8 have been characterized, whereat the N- and C-terminus are both located in the cytosol.[7,8,9]

4.3) Subtypes and physiological role of LTCC α-subunits

The human genome encodes four LTCC α-subunit genes, known as Ca_v1.1-1.4.[8,9,10] Ca_v1.1 is mainly expressed in skeletal muscle. The channel has influence on intracellular calcium release by activating the ryandine receptor in the sacroplasmic reticulum.[10] Ca_v1.2 is expressed in diverse tissue like ventricular cardiac muscle, pancreatic cells and neurons. An important role of Ca_v1.2 channel lies in the initiation of cardiac muscle contraction, by the influx of calcium during channel opening.[10] Ca_v1.2 channels expressed in neurons play an important role in intracellular downstream signaling.

$Ca_v1.3$ and $Ca_v1.2$ channels have similar expression patterns and subcellular localizations in different tissue. In neurons, $Ca_v1.2$ and $Ca_v1.3$ channels are present in the dendritic region.[10,13] Activity of $Ca_v1.3$ compared to $Ca_v1.2$ channels initiate a stronger phosphorylation of CREB, via second messenger pathways.[13] In heart tissue, $Ca_v1.3$ is not expressed in ventricular muscle but in atrial tissue. Here the channel influences the pacemaking of heart contraction.[10] $Ca_v1.3$ compared to $Ca_v1.2$ channels, start to open at a membrane potential which is approximately 20 mV more hyperpolarized.[10,12]

$Ca_v1.4$ represents a member of LTCCs with unusual characteristics. The expression of the channel is almost limited to the synaptic terminals of rod photoreceptors and bipolar cells within the retina.[10,14] $Ca_v1.4$ compared to other LTCCs does not show calcium dependent inactivation, which is due to an autoinhibitory domain within the C terminus.[14] This characteristic of $Ca_v1.4$ can be interpreted as a functional need of rod photoreceptors and bipolar cells to adapt to certain variations of input signals, which is important in the vision process.[14]

4.4) Pharmacology of LTCCs

As LTCCs play for instance a central role in controlling the activity of the mammalian heart, by linking cardiac membrane depolarization to contraction, they have been intensively studied as pharmacological targets. From an historical point of view, the influence of calcium on the contraction of heart muscle was first described by Sir Sidney Ringer, in the year 1882. He discovered that in calcium free medium contractility of the heart muscle is quickly lost.[15] Later Albrecht Fleckenstein demonstrated that contractility was prevented by applying random drugs including nifedipine (**12**), verapamil (**13**) and diltiazem (**14**) on the muscle in calcium containing medium (Fig. 3).[15] He concluded that these drugs have an antagonistic effect on calcium.[15] In the year 1975 4-Aryl-1,4,dihydropyridine-3,5-dicarboxylic diesters of the nifedipine type (Adalat®) (**12**) have been introduced for treatment of coronary diseases in Germany.[16] Soon after the discovery of 1,4-dihydropyridines (DHPs) effects on cardiovascular properties, certain LTCCs were identified as main protein

targets of DHPs.[15,16] Here they act as blockers, preventing influx of calcium through LTCCs.

A)

Nifedipine (12)   Felodipine (20)   (S)-Nimodipine (17)

(S)-BK-10 (19)   (S)-Bay K 8644 (15)   boat conformation 18

B)

FPL 64176 (16)   (S)-Verapamil (13)   Diltiazem (14)
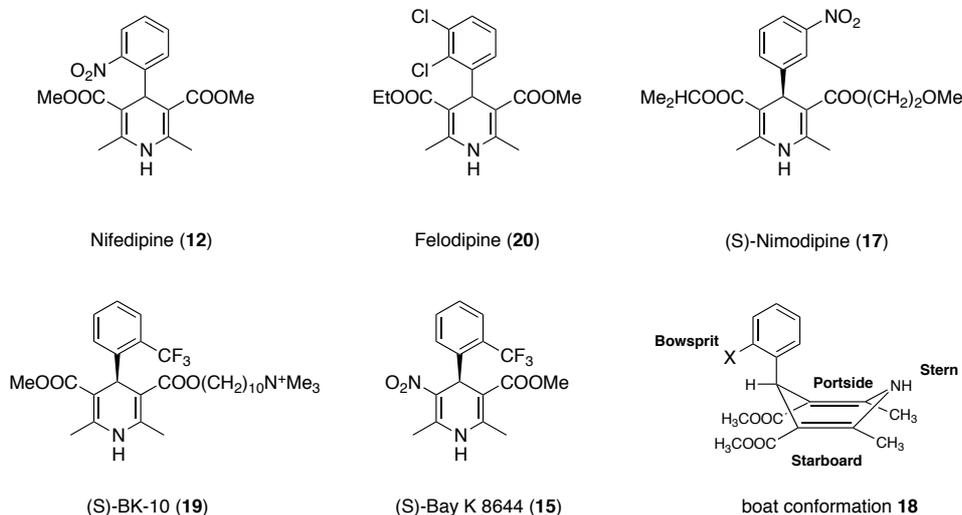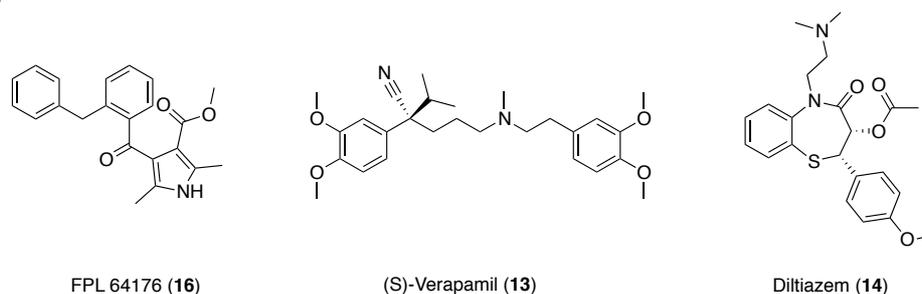
Figure 3 . A) Representation of different DHP LTCC agonists, antagonist and the energetically preferred DHP boat conformation (aryl axial). **B**) Structures of the activator FPL-64176 (**16**)**,** the antagonists (S)-verapamil (**13**) and diltiazem (**14**).

Most DHPs act as antagonists, whereas few examples, such as BAY K 8644 (**15**), act as agonists.[16,17] The classes of phenylalkylamines (PAAs) and benz(othi)azepines (BTZs) were additional indentified as LTCC blockers, whereat verapamil (**13**) and diltiazem (**14**) represent members of PAAs and BTZs with clinical application, respectively (Fig. 3).[15] Many DHPs, PAAs and BTZs do not, or only to a small extent, affect T-, Q-, R-, N- and P-type Ca$_v$ channels, which makes them useful pharmacological tools. All three LTCC antagonists bind to overlapping binding sites within the α -subunits.[15] FPL-64174 (**16**) represents a LTCC activator**,** which

increases macroscopic inward current and has frequently been used to answer scientific questions.[6,18]
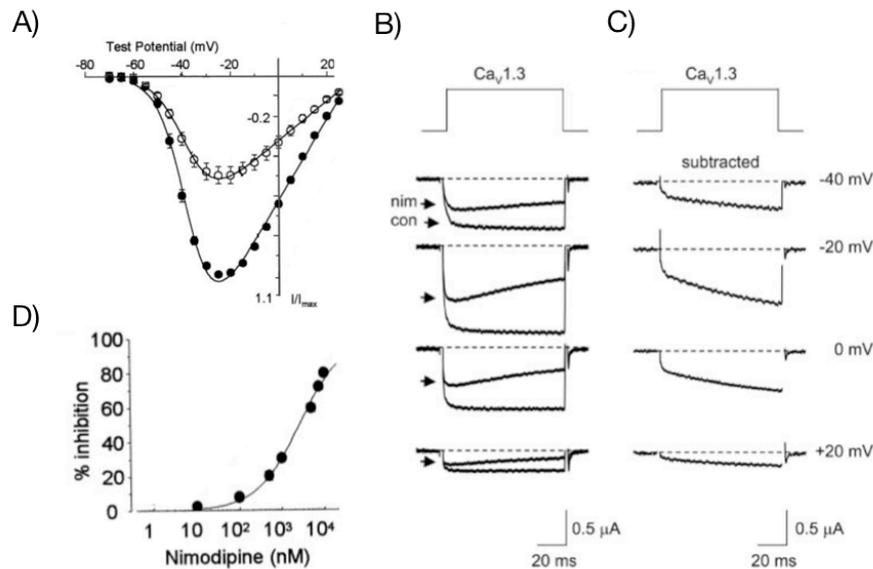
Figure 4 . A) A current-voltage (I-V) curve of $Ca_v1.3\alpha_1$ under normal conditions (•) and under nimodipine influence (o). **B**) Single current traces reveal the amount of block induced by nimodipine at indicated voltage. **C**) DHPs block late phase of the current initiated by a depolarizing pulse. **D**) Dose-response curve of nimodipine block (**A**)-**D**) modified from publication[12]) .

4.5) DHPs on $Ca_v1.3$ and $Ca_v1.2$ channels

Subtypes of LTCCs own different binding affinities towards DHPs. $Ca_v1.3$ and $Ca_v1.4$ channels are significantly less sensitive to DHPs than $Ca_v1.2$ channels.[10,12] Nimodipine, like other DHPs, blocks mainly the late phase of the Ca^{2+} current, elicited by depolarization of the membrane. Based on a dose-response curve, the half maximal inhibitory concentration (IC_{50}) of nimodipine (**17**) on $Ca_v1.3$ channel was calculated to be $IC_{50} = 2.7\ \mu M\ \pm\ 0.3\ \mu M$ (Fig. 4).[10,12] Typical DHP antagonist concentrations that inhibit $Ca_v1.2$ and $Ca_v1.3$ currents lie in the range of $IC_{50} = 1\ nM - 10\ \mu M$.

4.6) Theoretical models of Ca_v channel gating

Simplified biophysical description of Ca_v channel gating resulted in two main kinetic models. One is based on a gating scheme of the Shaker K_v channel, introduced by Zagotta and Aldrich. Here multiple closed states of a channel are connected by voltage-dependent transitions followed by a final voltage-independent opening state.[19] Another model presented by Marks and Jones describes multiple open states in parallel with closed states, which account for binding effects of some DHP agonists.[19] In a simplified, but intuitive model, only three channel-states are considered, whereat from each state both other states can be kinetically entered. Here a closed, occupied at rest, an open and an inactivated channel-state are connected in a triangle. After depolarization, occupation of the open state is kinetically faster compared to the inactive state.[19] In equilibrium however, the inactivated state is higher populated.[19] In absence of a DHP, the channel interconverts between the states. DHPs prefer to bind to the inactivated state of the channel.[19] The probability of the channel to rest in its inactivated state increases with less negative cell membrane potential. Based on this, DHPs act as voltage-dependent blockers.[15]

4.7) Molecular interaction site of DHPs and LTCCs

Several investigations have been performed to localize the binding site of DHPs on LTCCs and the amino acids involved in the direct ligand-receptor interaction. A rather rough estimation of the DHP binding position as well as the access route of DHPs toward their binding site has been determined by an approach of molecular tape measurements.[20,21]

(S)-BK-n (**19**), a series of DHPs with long alkyl chains of different length at their starboard side and a positively charged quaternary ammonium group at the end allowed to estimate how distant the DHP binding site is from the external and the cytosolic side of the receptor (Fig. 3). (S)-BK-n (**19**) with an n>2 were shown to have access to the binding site from the external side via the "sidewalk", but not from the internal side. Based on the ligand with the highest efficacy on LTCCs, (S)-BK-10

(**19**), the length from extracellular side to the DHP binding side was estimated to be 11-14 Å.[20,21]

The exact position of the DHP binding side and the molecular surrounding of ligand, have been revealed by antibody mapping, photoaffinity labeling, chimeric $Ca_v\alpha_1$ subunits and site-directed mutagenesis.[15] The binding site is located below the selectivity filter of LTCCs and interacting amino acids are located in transmembrane segments IIIS5, IIIS6, IVS6 as well as in the pore helix IIIP.[15] DHP antagonists have been shown to stabilize the impermeable state of LTCCs with only one calcium ion bound to the selectivity filter, which is associated with a direct interaction of an antagonist with calcium ion occupancy.[22]

Until today, the mode of action of DHP agonists is unclear and highlights the need for a LTCC crystal structure in coordination with DHPs.

4.8) Chemical structure of DHPs

Unsubstituted DHP rings have an almost planar conformation. Introduction of an Aryl group into 4 position shifts the energetically preferred structure into a flattened boat form **18** (Fig. 3) with the Aryl ring in pseudoaxial position.[16] This conformation has been confirmed by several crystal structures and calculations.[16] Pharmacological effective DHPs have an H-bond donor on their stern and H-bond acceptor at their bowsprit, portside and starboard side (Fig. 3).[22] Modeling of DHP binding site interactions proposed the portside substituents to induce block of LTCCs.[22]

4.9) Design of photoswitchable LTCC ligands

The influence of LTCCs on gene regulation motivated to design photoswitchable agonists and antagonists.[3] Light gated LTCCs should in principle improve the understanding of the temporal and spatial relation of LTCC activity and CREB phosphorylation.

Different PCLs were designed that potentially could bestow light sensitivity on LTCCs currents. The successfully applied molecular tape measurements and the number of DHPs with bulky substituents on the starboard and portside positions (Fig. 5),[23,24] indicate that these positions are well suited for the attachment of an azobenzene.

Efonidipine (21)

compound 22

compound 23

compound 24
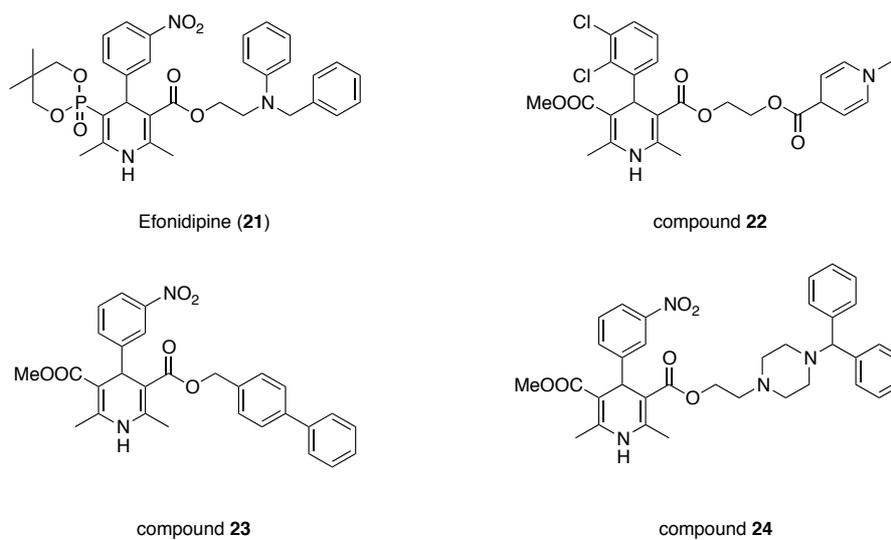
Figure 5. Chemical structures of Efonidipine (**21**),[25] DHP derivative **22**,[24] **23**,[23] and **24**.[16] These DHPs exhibit bulky substituents at their portside and starboard sides, indicating potential tolerance towards azobenzenes.

Nifedipine (**1**) and other DHPs are sensitive towards 200-450 nm light.[26,27] Irradiation oxidizes the 1,4-Dihydropyridine structure yielding pyridines, which have no antagonistic effect on LTCCs. This sensitivity was even transformed into an approach called "light-flash physiology", which allows to delete nifedipine (**12**) induced LTCCs block with high temporal and spatial precision.[28] One study on the light sensitivity of DHPs revealed Felodipine (**20**), a LTCC antagonists, to be stable for some hours under irradiation with 300-800 nm light.[29] Based on this finding, Felodipine (**20**) was chosen as the DHP core of LTCC PCLs. Furthermore, compound **20** was shown to exhibit an $IC_{50} = 14.9$ nM on Ca_v channels.[30]
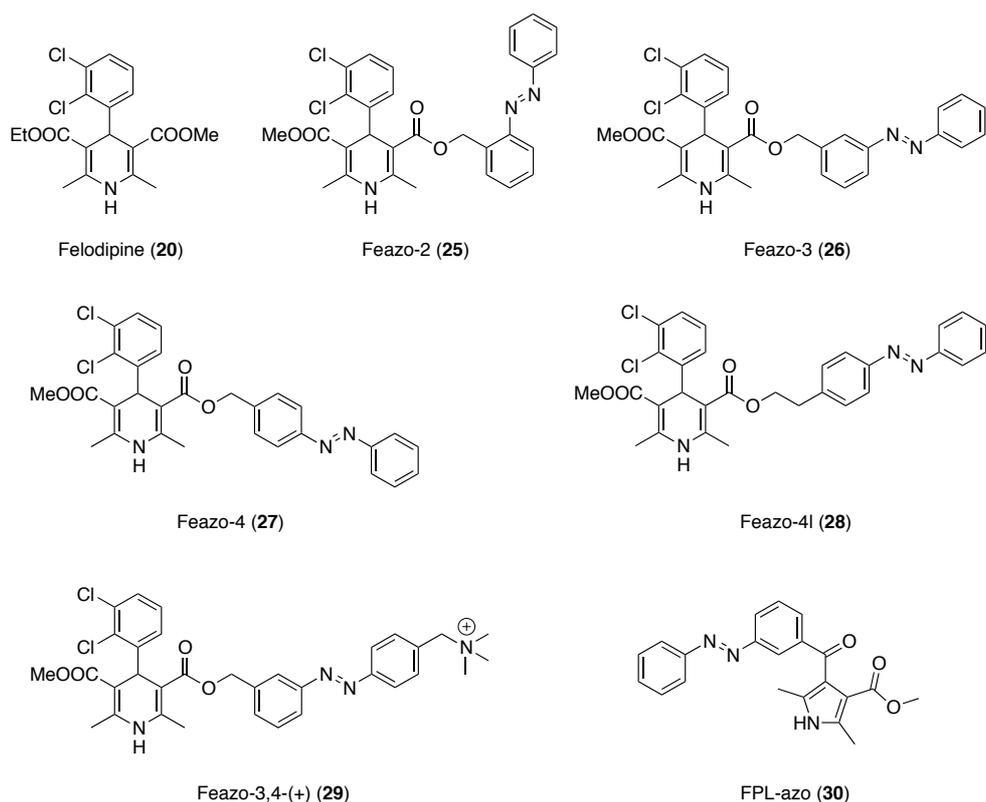
Figure 6. Chemical structures of potential antagonistic and agonistic LTCC PCLs.

Several neutral derivatives of Felodipine (**20**) coupled to an azobenzene were designed and named Feazo-x. It was hypothesized that the transition between the *cis* and *trans* state of the azobenzene and the associated change in polarity of about 2-3 debye,[31] could result in different efficacies of Feazo-x towards its binding site. The spacer length between the portside ester and the azobenzene and the substitution pattern of the azo group within the azobenzene was varied to give Feazo-2 (**25**), Feazo-3 (**26**), Feazo-4 (**27**), Feazo-4l (**28**) (Fig. 6).

Another strategy to generate an antagonistic PCL for LTCCs aimed to hitchhike the tape measurement approach of (S)-BK-n (**19**).[20,21,32] It was reasoned that a positive charge positioned at the azobenzene end of a Feazo-x derivative would selectively allow the elongated *trans* state to reach the DHP binding site, resembling the length of (S)-BK-10 (**19**). Thereby, channel blocking would be installed. The shortened *cis* state would locate the DHP in proximity to the membrane surface and release block. By switching between the two states reversible light control of LTCCs should be possible. Together this considerations lead to the design of Feazo-3,4-(+) (**29**).

To generate a PCL activator for LTCCs, FPL-64176 (**16**) was chosen as a lead structure (Fig. 3).[18,33,34] Here the diphenylmethane part was replaced by an azobenzene. Compared to the parent molecule a carbonyl bridge between the pyrrole and the azobenzene was installed in the 3' instead of the 2' position, yielding FPL-azo (**30**).

4.10) DHP synthesis

4.10.1) Synthesis of Feazo-x

The synthesis of Feazo-x **25**-**28** commenced with coupling of substituted benzylalcohols **31**-**34** with nitrosobenzene to give diazene **35**-**38**, *via* Mills reaction.[35] In the following step, diketone **39**-**42** was furnished by nucleophilic attack of compound **35**-**39** on in situ formed ketene. Finally, compound **39**-**42** was converted into the desired 1,4-dihydropyridine called Feazo-x **25**-**28**, *via* Hantzsch reaction.
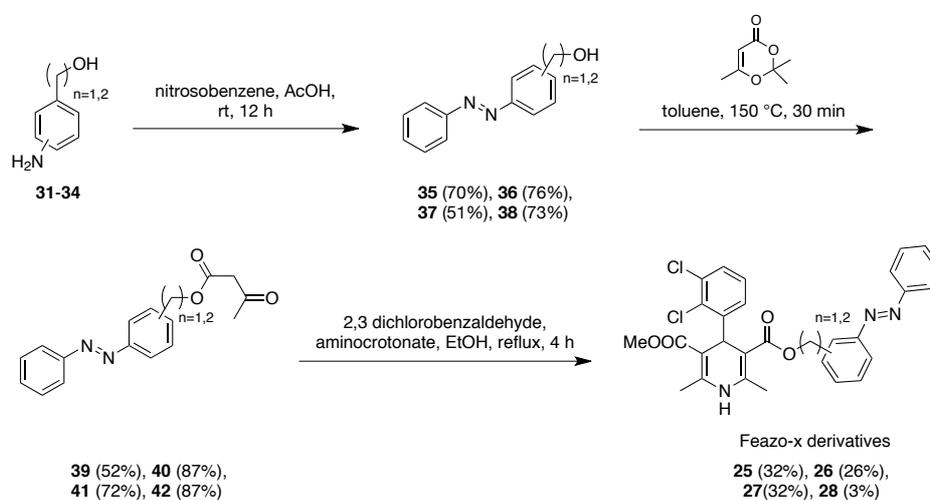
Scheme 1. Synthesis of Feazo-x derivatives **25**-**28**

4.10.2) Synthesis of Feazo-3,4 (**48**)

4-Aminobenzylamine **43** was reacted with Boc$_2$O to give *tert*-butyl 4-aminobenzylcarbamate **44**. Oxidation of the latter using Oxon® yielded carbamate **45**. 3-Aminobenzylalcohol was coupled to compound **45** *via* Mills reaction,[35] resulting in

diazene **46**. This was reacted with an in situ formed ketene to give diketone **47**. Finally, a Hantzsch reaction of **47** with aminocrotonate and 2,3-dichlorbenzaldehyd yielded Feazo-3,4 (**48**).

Acidic treatment of compound **48** with a saturated solution of HCl in EtOAc effected the removal of the Boc-protecting group to yield free amine. Since the latter could not be purified, it was directly methylated using methyl iodide. However, this reaction afforded a inseparable mixture of different products and even the attempted purification by reverse phase column chromatography or HPLC failed to give clean Feazo-3,4-(+). Therefore, Feazo-3,4 (**48**) was pharmacologically characterized on LTCCs.
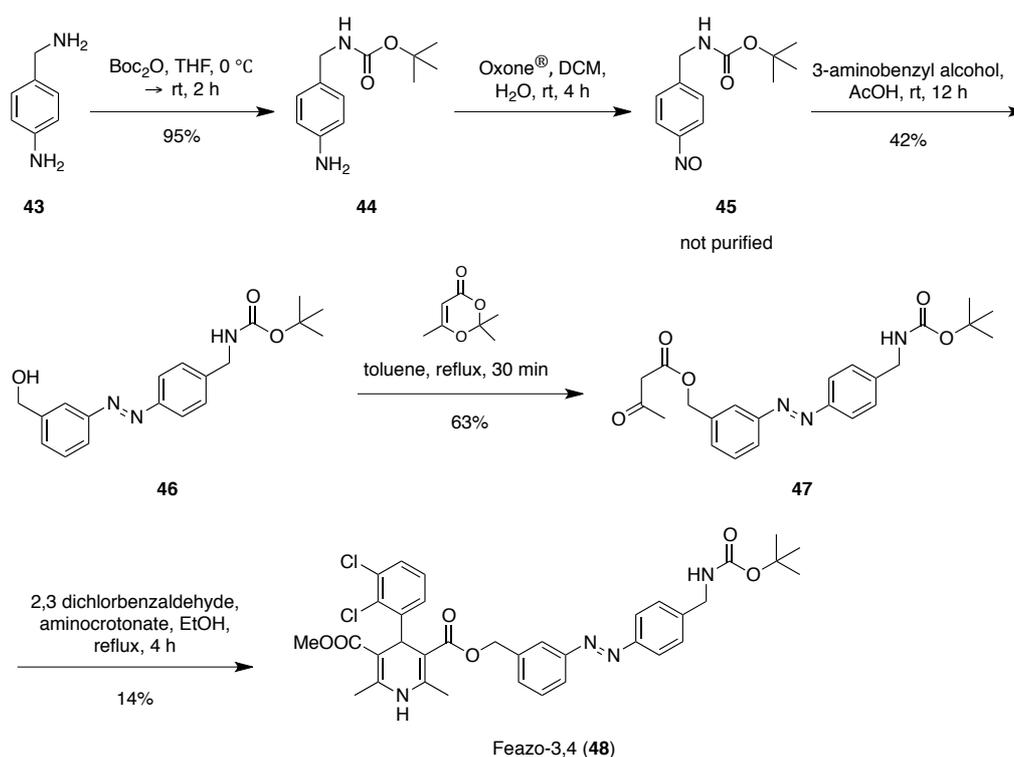
Scheme 2. Synthesis of Feazo-3,4 (**48**)

4.10.3) Synthesis of FPL-azo (**30**)

The synthesis of FPL-azo (**30**) started with coupling of anthranilic acid (**49**) with nitrosobenzene to yield diazene **50** *via* Mills reaction.[35] This was next treated with oxalyl chloride to generate benzoyl chloride **51**. Friedel crafts acylation of pyrrole **52** with benzoyl chloride **51** resulted in the formation of FPL-azo (**30**).[33]
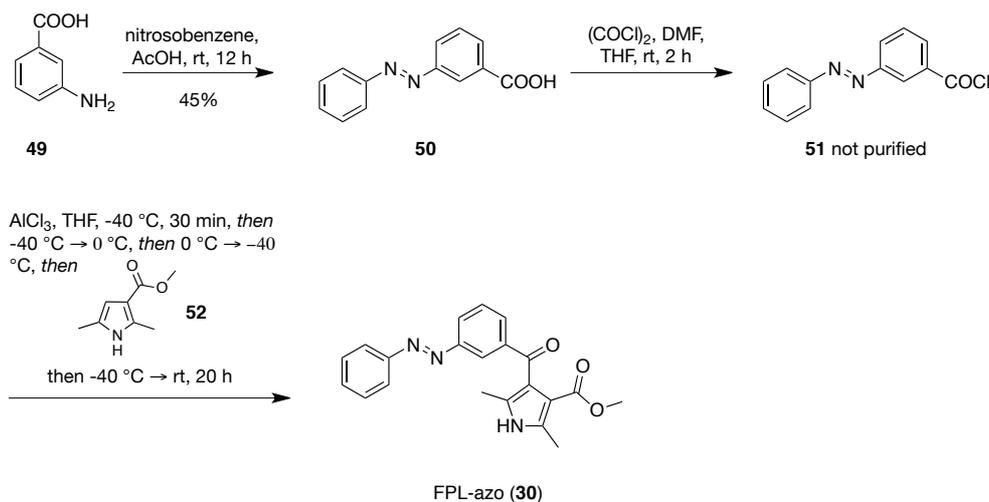
Scheme 3. Synthesis of FPL-azo (**30**)

4.11) Characterization of Feazo-x on LTCCs

The first question was whether Feazo-x derivatives would induce block of LTCC current in the dark. Therefore, derivatives were characterized on $Ca_v1.3\alpha_1$ channels, co-expressed with the auxilary subunits $Ca_v\beta_3$ and $Ca_v\alpha_2\delta$ in HEK293T cells. The electrophysiological protocol is described in Ref. 12.[12] During experiments LTCCs typically lose current strength, which is called rundown.[28] This process is often difficult to distinguish from antagonist induced current reduction. Thus, control measurements were performed to quantify the amount of rundown. The quantification of Felodipine (**20**) block on the $Ca_v1.3\alpha_1$ channel, established the fundament to determine the block of Feazo-x derivatives (Fig. 7).
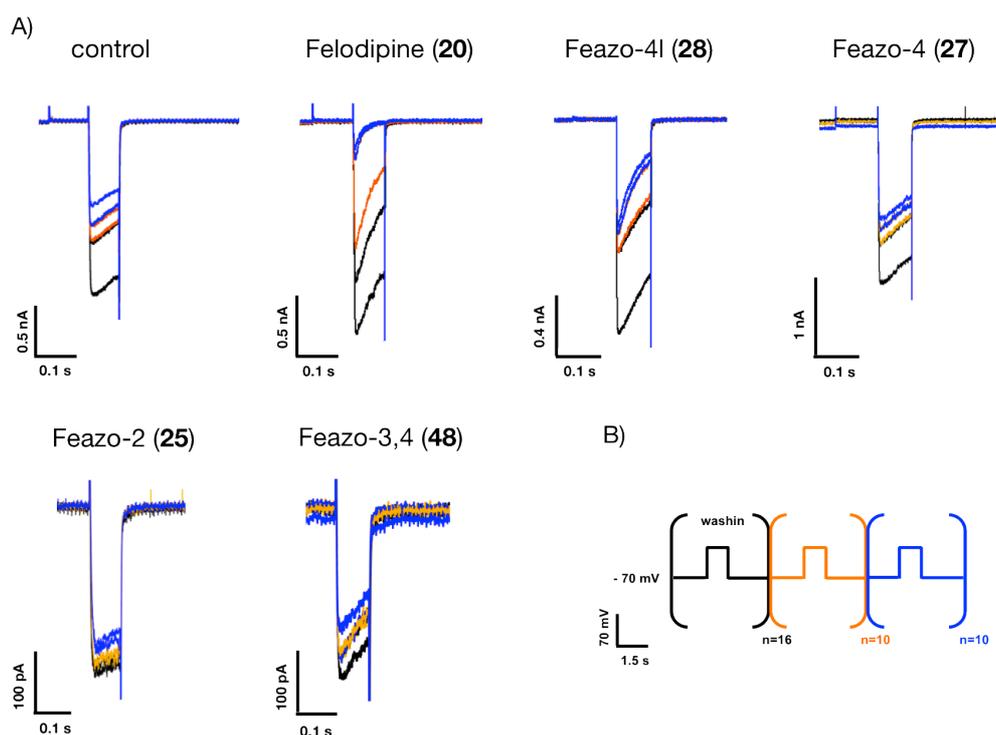
Figure 7. A) Determination of Felodipine (**20**) and Feazo-x block on $Ca_v1.3\alpha_1$, co-expressed with auxilary subunits $Ca_v\beta_3$ and $Ca_v\alpha_2\delta$ in HEK293T cells. Current traces, of each single compound, were superimposed to visualize the temporal course of current reduction. Black, orange and blue traces represent the wash-in period, second recording period and third recording period, respectively. The first and last current trace of all three periods are shown. Based on temporal lack of the $Ca_v\beta_3$ clone, Feazo-2 (**25**) and Feazo-3,4 (**48**) were recorded without co-transfection of $Ca_v\beta_3$. **B)** Sequence of 36 protocol-cycles, used to study LTCCs in the dark.

HEK293T cells expressing $Ca_v1.3\alpha_1$ were depolarized from a holding potential of -70 mV to -10/0 mV for 80 ms, with a frequency of 0.25 Hz (Fig. 7). The complete measurement contained 36 protocol-cycles. During the initial 16 cycles a blocker was perfused on cells, whereas in control experiments only external solution was applied. Within the following 20 protocol-cycles, block accumulation was continued to be recorded.

The physiological function of the $Ca_v1.3\alpha_1$ channel, to conduct Ca^{2+} ions, goes along with Ca^{2+} dependent inactivation of the channel current. This inhibitory process hampers to study antagonist induced channel blocking. To prevent and reduce this unrequested effect, Ca^{2+} was replaced by Ba^{2+} in the external recording solution.[12]
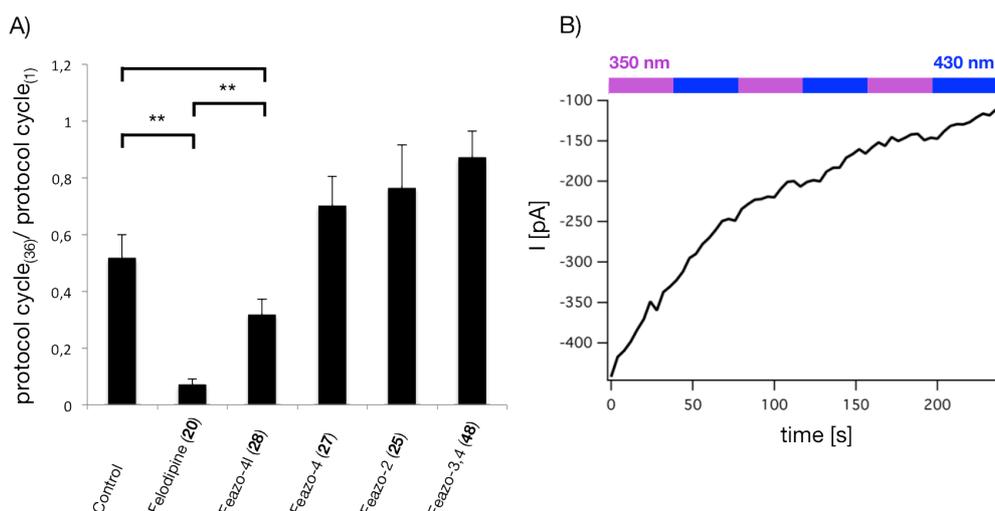
Figure 8. A) Quantification of Feazo-x induced blocking on $Ca_v1.3\alpha_1$ channel current. $Ca_v\beta_3$ was not present for Feazo-2 (**25**) and Feazo-3,4 (**48**) recordings. Error bars, ± s.e.m.; Student *t*-test; *$P < 0.05$, **$P < 0.01$. **B)** Current trace of representative Feazo-3,4 (**48**) photoswitching on $Ca_v1.3\alpha_1$ channel. Data indicate that photoswitching has no influence on current size. The trace was recorded after the 36 protocol-cycles in the dark.

To quantify the block, the current size of the first and last elicited depolarization were compared, using the given equation protocol-cycle$_{(36)}$/protocol-cylce$_{(1)}$. For control experiments, the statistics on the latter equation revealed a rundown to 51.7% ± 15.6% of the initial Ba^{2+} current (n = 11 cells) (Fig. 8). Application of the antagonist Felodipine resulted in a strong reduction of the LTCC current. Only 7% ± 2.4% (n = 9 cells, 10 µM) of current remained after 36 protocol-cycles, indicating, that the system applied to study the blocking of the DHP-derivatives is reliable. The compound Feazo-4l (**28**) showed no statistically significant block compared to Felodipine (**20**) and control experiments (Fig. 8). Application of the compound decreased the current strength to 31.8% ± 12.0% (n = 7 cells, 30 µM). Feazo-4 (**27**) did not induce clear block, which was even less than for control experiments. The measurement resulted in a current strength of 70.2% ± 35.1% (n = 4 cells). Application of Feazo-2 (**25**) and Feazo-3,4 (**48**) resulted in 76.6% ± 12.0% (n = 3 cells, 30 µM) and 87.2% ± 50.0% (n = 3 cells, 20 µM) current strength, respectively. All Feazo-derivatives were applied at maximal solubility in external solution. Once the sequence of protocols to determine Feazo-x block was completed in the dark, additional protocol-cycles were performed. Here, every 10 protocol-cycles irradiation was alternated between 350 nm and 430 nm light. The wavelengths were

chosen based on UV/VIS spectra of the compounds (see Appendix UV/VIS spectra). These recordings revealed no photocontrol of LTCC current, see representative current trace in Fig. 8.
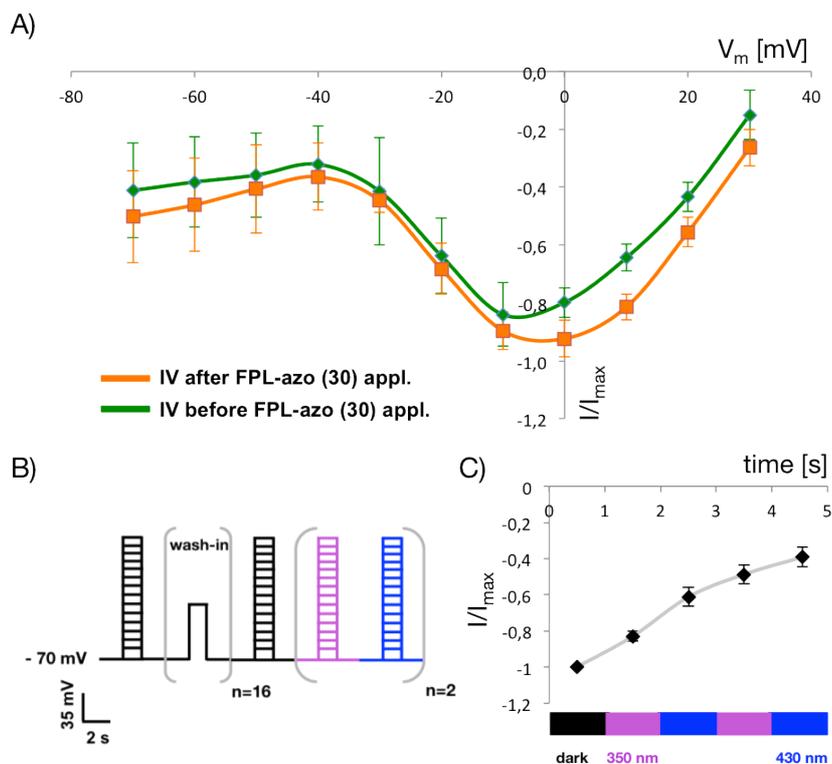
Figure 9. A) Comparison of I-V before (green) and after (orange) FPL-azo (**30**) application on $Ca_v1.3\alpha_1$ channel in the dark (n = 3 cells, error bars, ± s.e.m.). **B)** Sequence of protocols used to determine FPL-azo (**30**) effect on $Ca_v1.3\alpha_1$. **C)** Current elicit at 0 mV of I-Vs recorded after FPL-azo (**30**) application (wash-in). The first I-V was recorded in the dark and afterwards under changing irradiation wavelengths. Error bars, ± s.e.m..

FPL-azo (**30**) was characterized on $Ca_v1.3\alpha_1$ channels, co-expressed with the auxilary subunit $Ca_v\alpha_2\delta$. A single I-V curve was recorded before and after the wash-in of FPL-azo (**30**), which was applied at a concentration of 10 µM. The protocol applied to record the I-V relationship depolarized cells from a holding potential of - 70 mV up to + 70 mV in 10 mV intervals (Fig. 9). The depolarization lasted 80 ms with a frequency of 0.25 Hz. The protocol to wash-in FPL-azo (**30**) was taken from Feazo-x experiments including 16 cycles of depolarization. The I-Vs recorded (n = 3 cells) in the dark showed a small increase in current strength, raising the possibility of a modest agonistic effect of FPL-azo (**30**) (Fig. 9). After the processes of wash-in and I-V recording in the dark were completed, I-V protocols with alternating

irradiation of 350 nm and 430 nm light were applied (Fig. 9). Analysis of the current at 0 mV of all I-Vs recorded, after the wash-in period, revealed no light induced influence on the current strength (Fig. 9).

4.12) Discussion

The data presented here indicate, that Feazo-2 (**25**), Feazo-3 (**26**), Feazo-4 (**27**), Feazo-4l (**28**) did not induce block on the $Ca_v1.3\alpha_1$ channel. The reasons for this finding may be associated with the size of the azobenzene as a substituent. To answer this question a series of Feazo-x derivatives, with benzene instead of azobenzene, could be synthesized and characterized on the $Ca_v1.3\alpha_1$ channel. Here, one would expect to generate DHP antagonists with less sterical hindrance. However, DHP derivatives presented in Fig. 5 suggested that a certain tolerance towards bulky substituents at the starboard and portside position is given. Furthermore, Felodipine derivatives with huge substituents, e.g. compound **22** were reported (Fig. 5),[24] which still exhibit a high affinity towards Ca_v channels. Light control of Feazo-x states did not result in modulation of $Ca_v1.3\alpha_1$ current size. To improve chances to generate an active DHP photoswitch, other structures than Felodipine could be considered. To form Feazo-3,4-(+) (**29**) or similar derivatives, other synthetic strategies could be considered.

FPL-azo (**30**) showed a slight increase of $Ca_v1.3\alpha_1$ current strength. An effect that hampers the determination of the agonistic effect lies in the presence of current rundown, which acts opposed to the increasing effect. However, changing wavelength between 350 nm and 430 nm light did not alter the current strength.

To increase chances to create a photoswitchable PCL for LTCCs, combinations of phenylalkylamines and benz(othi)azepines with azobenzenes could be designed and tested.

[1]   D. E. Clapham, *Cell* **2007**, *131*, 1047-1058.
[2]   M. J. Berridge, *Cell Calcium* **2006**, *40*, 405-412.
[3]   P. L. Greer, M. E. Greenberg, *Neuron* **2008**, *59*, 846-860.

[4]   R. E. Dolmetsch, U. Pajvani, K. Fife, J. M. Spotts, M. E. Greenberg, *Science* **2001**, *294*, 333-339.

[5]   K. Deisseroth, E. K. Heist, R. W. Tsien, *Nature* **1998**, *392*, 198-202.

[6]   D. G. Wheeler, C. F. Barrett, R. D. Groth, P. Safa, R. W. Tsien, *J. Cell Biol.* **2008**, *183*, 849-863.

[7]   J. Arikkath, K. P. Campbell, *Curr. Opi. Neurobio.* **2003**, *13*, 298-307.

[8]   S. Dai, D. D. Hall, J. W. Hell, *Physiol Rev* **2009**, *89*, 411-452.

[9]   W. A. Catterall, *Annu. Rev. Cell Dev. Biol.* **2000**, *16*, 521-555.

[10]   D. Lipscombe, T. D. Helton, W. Xu, *J. Neurophysiol.* **2004**, *92*, 2633-2641.

[11]   M. Shibasaki, K. Kurokawa, S. Ohkuma, *Neuroscience* **2009**, *163*, 731-734.

[12]   W. Xu, D. Lipscombe, *J. Neurosci.* **2001**, *21*, 5944-5951.

[13]   H. Zhang, Y. Fu, C. Altier, J. Platzer, D. J. Surmeier, I. Bezprozvanny, *Eur. J. Neurosci.* **2006**, *23*, 2297-2310.

[14]   C. Wahl-Schott, L. Baumann, H. Cuny, C. Eckert, K. Griessmeier, M. Biel, *Proc. Nat. Acad. Sci.USA* **2006**, *103*, 15657-15662.

[15]   J. Striessnig, *Cell Physio.l Biochem.* **1999**, *9*, 242-269.

[16]   S. J. Goldmann S., *Angew. Chem. Int. Ed.* **1991**, *30*, 1559-1578.

[17]   P. Hess, R. W. Tsien, *Nature* **1984**, *309*, 453-456.

[18]   W. Zheng, D. Rampe, D. J. Triggle, *Mol. Pharm.* **1991**, *40*, 734-741.

[19]   S. I. McDonough, Y. Mori, B. P. Bean, *Biophy. J.* **2005**, *88*, 211-223.

[20]   N. Baindur, A. Rutledge, D. J. Triggle, *J. Med. Chem.* **1993**, *36*, 3743-3745.

[21]   R. Bangalore, N. Baindur, A. Rutledge, D. J. Triggle, R. S. Kass, *Mol. Pharm.* **1994**, *46*, 660-666.

[22]   D. B. Tikhonov, B. S. Zhorov, *J. Biol. Chem.* **2009**, *284*, 19006-19017.

[23]   C. C. Chang, S. Cao, S. Kang, L. Kai, X. Tian, P. Pandey, S. F. Dunne, C. H. Luan, D. J. Surmeier, R. B. Silverman, *Bioorg. & Med. Chem.* **2010**, *18*, 3147-3158.

[24]   S. Yiu, E. E. Knaus, *J. Med. Chem.* **1996**, *39*, 4576-4582.

[25]   H. Masumiya, T. Shijuku, H. Tanaka, K. Shigenobu, *Eur. J. Pharmacology* **1998**, *349*, 351-357.

[26]   H. de Vries, G. M. Beijersbergen van Henegouwen, *J. Photochem. Photobio.* **1998**, *43*, 217-221.

[27]   E. Fasani, D. Dondi, A. Ricci, A. Albini, *Photochem. Photobiol.* **2006**, *82*, 225-230

[28]   A. M. Gurney, H. A. Lester, *Physiol. Rev.* **1987**, *67*, 583-617.

[29]   D. L. M. Ioele G., Oliverio F., Ragno G., *Talanta* **2009**, *79*, 1418-1424.

[30]   D. Vo, W. C. Matowe, M. Ramesh, N. Iqbal, M. W. Wolowyk, S. E. Howlett, E. E. Knaus, *J. Med. Chem.* **1995**, *38*, 2851-2859.

[31]   T. Fehrentz, M. Schönberger, D. Trauner, *Angew. Chem. Int. Ed.* **2011**, *50*, 12156-12182.

[32]   R. S. Kass, J. P. Arena, S. Chin, *J. Gen. Physiol.* **1991**, *98*, 63-75.

[33]   A. J. Baxter, J. Dixon, F. Ince, C. N. Manners, S. J. Teague, *J. Med. Chem.* **1993**, *36*, 2739-2744.

[34]   D. C. R. Kane J.M., Velayo N.L., Rampe D., *Bioorg. Med. Chem.y* **1995**, *5*, 873-876.

[35]   F. Hamon, F. Djedaini-Pilard, F. Barbot, C. Len, *Tetrahedron* **2009**, *65*, 10105-10123.

4.13) General experimental details

General experimental details were carried out as reported beforehand in reference.[1] In brief, unless stated otherwise, all reactions were carried out in oven-dried glassware under a nitrogen or argon atmosphere. Solvents for flash column chromatography extraction and some reactions were distilled under reduced pressure. Tetrahydrofuran (THF) was distilled from benzophenone and sodium prior to use. Flash column chromatography was performed as described by Still *et al.*[2] using Merck silica gel (SiO_2; 60 Å, 40-63 μm) or for reversed phase column chromatography waters C18 (C18; 55-105 μm, 125 Å). 1.3-1.5 bar have been applied to force flow of eluant. Reactions were monitored by analytical thin-layer chromatography (TLC) using E. Merck 0.25 mm silica gel 60 F_{254} precoated glass plates. Chemicals on TLC plates were detected by exposure to ultraviolet light.

4.14) Instrumentation

Instrumentation was carried out as reported beforehand in reference[1]. In brief, all presented proton (^{1}H) and carbon (^{13}C) NMR spectra were recorded with Varian VNMRS 300, VNMRS 400, INOVA 400 or VNMRS 600 spectrometers. ^{1}H spectra were measured at 300 MHz, 400 MHz or 600 MHz. ^{13}C NMR spectra have been detected by 50 MHz, 75 MHz, 150 MHz. For ^{1}H spectra shifts were presented as parts per million (δ), signals arising from residual non-deuterated solvent were used as the internal standard and the solvent shifts reported were used as references.[3] Data for ^{1}H NMR spectra are reported as follows: chemical shift (δ ppm) (multiplicity, coupling constant (Hz), integration). Multiplicities are reported as follows: s = singlet, d = doublet, t = triplet, q = quartet, m = multiplet, m_c = centrosymmetric multiplet, *br* = broad, or combinations thereof. ^{13}C spectra shifts are presented as parts per million (δ), signals arising from residual non-deuterated solvent were used as the internal standard and the solvent shifts reported were used as references.[3]

[1] T. Fehrentz, C. A. Kutruff, Florian M. E. Huber, Michael A. Kienzler, Peter Mayer, Dirk Trauner, *under revision.*

[2] W.C. Still, M. Kahn, A. Mitra, *J. Org. Chem*. **1978**, *43*, 2923–2925.

[3] G. R. Fulmer, A. J. M. Miller, N. H. Sherden, H. E. Gottlieb, A. Nudelman, B. M. Stoltz, J. E. Bercaw, K. I. Goldberg, *Organometallics* **2010,** *29,* 2176–2179.
P. Stawski, M. Sumser, D. Trauner, *Angew. Chem. Int. Ed.* **2012**, *51*, 5748-5751.

Mass spectrometry was performed with a Thermo Finnigan MAT 95 (EI), a Thermo Finnigan LTQ FT (ESI) apparatus. Melting points (mp) were detected using a Standford Research Systems MPA apparatus. IR spectra were obtained using a Perkin-Elmar BXII-FTIR spectrometer equipped with an ATR unit. UV/Vis spectra were recorded with a Varian Cary50 Scan Systems MPA120 instrument and STARNA 29/B/12 quartz cuvettes (10 mm light path). Absorption spectra, which were recorded under an additional perpendicular illumination to the UV/VIS light beam, were pre-irradiated for 5 minutes.

4.15) Electrophysiology and cell culture

HEK293T cells (tsA-201 cells, large T-antigen transformed HEK293 cells) have been grown in DMEM (Biochrom, Dulbeco's MEM, Cat. No. FG0445, F0445) 95% and 5% (FBS, Biochrom) with a final concentration of 2mM L-Gln. Cells wer splitted once confluency was reached. Between 20000 to 25000 cells were plated on a single coverslip, coated with poly L-lysine. HEK293T cells were transfected with 1µg $Ca_v1.3\alpha_1$, $Ca_v\beta_3$ and $Ca_v\alpha_2\delta$ in a molar ratio of 1:1:1.[4] To simplify the detection of transfected cells, eGFP was co-transfected. Transient transfection was carried out using the calcium phosphat method. Before recordings were performed, transfected cells were incubated at 37 °C for 12 hours, followed by period at 32 °C for 48 hours.

Patch clamp recordings and analysis have been performed with a standard electrophysiological setup, including an inverse microscope, a HEKA Patch Clamp EPC10 USB amplifier and patch master software. Measurements have been recorded in whole cell mode. Pipette (Science Products GB200-F-8P with filament) resistence varied between 4-8 MΩ. Irradiation of samples has been performed through a Nicon Fluor 60x/1.00w objective, with a TILL Photonics Polychrome 5000 monochromator as light source.[5]

---

[4] W. Xu, D. Lipscombe, *J. Neurosci.* **2001**, *21*, 5944-5951.

[5] A. Mourot, T. Fehrentz, Y. Le Feuvre, C. M. Smith, C. Herold, D. Dalkara, F. Nagy, D. Trauner, R. H. Kramer, *Nat. Methods* **2012**, *9*, 396-402.

External barium current recording solution contained in mM: 82 NaCl, 30 $BaCl_2$, 5.4 CsCl, 1 $MgCl_2$, 5 HEPES free acid, 10 glucose and pH was ajusted to 7.4. Internal barium current recording solution contained in mM: 112 CsCl, 3 $MgCl_2$, 5 HEPES free acid, 3 $MgCl_2$, 3 MgATP, 10 EGTA and pH was ajusted to 7.4 using CsOH. Photoswitches were solved in external bath solution to give the final working concentrations. DMSO concentration was below 0.1%.

The voltage clamp protocol used to record antagonist/Feazo-x block of $Ca_v1.3\alpha_1$ channel current, depolarized the membrane from its holding potential of -70 mV to -10/0 mV for 80 ms, with a frequency of 0.25 Hz (Fig. 7). This protocol was looped and within the first 16 cycles of the recording, external solution containing an antagonist was perfused on cells. In total 36 cycles were performed in the dark (Fig. 7). Afterwards, irradiation was altered between 350 nm and 430 nm light every ten protocol cycles.

To study the FPL-azo (**30**) effect on $Ca_v1.3\alpha_1$ channels, a current-voltage (I-V) protocol was followed by a wash-in sequence of the agonist, before an additional I-V was recorded in the dark. Further I-Vs were recorded under alternating 350 nm or 430 nm light irradiation (Fig. 9). To record I-V curves of $Ca_v1.3\alpha_1$ channels, cells were hold at -70 mV and depolarized in a loop sequence to values between -70 mV and +70 mV, in 10 mV intervals at 0.25 Hz. For the wash-in of FPL-azo (**30**), the protocol for the detection of Feazo-x block was coppied (Fig. 9).

4.16) Synthetic procedures

Procedure 1
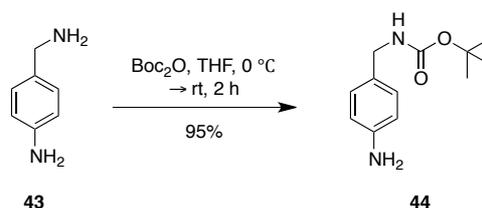
4-aminobenzylamin (**43**) (1.00 g, 8.19 mmol, 1.00 eq) was dissolved in THF (10 mL) and the mixture was cooled to 0 °C. Di-*tert*-butyldicarbonat (1.965 g, 9.00 mmol, 1.1 eq) in THF (2 mL) was slowly added to the reaction mixture. The reaction mixture was stirred at 0 °C for 40 minutes and an additional hour at rt. The reaction was stopped after TLC monitoring showed no starting material. The reaction mixture was concentrated and the crude material was purified by flash column chromatography (silica, EtOAc: hexanes = 1:3) to yield the title compound **44**.

Procedure 2
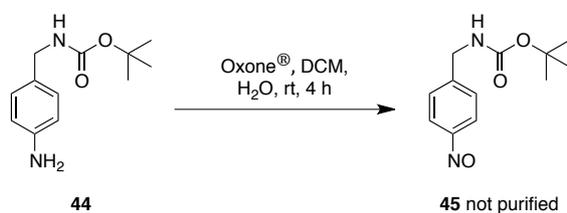
A solution of aniline **44** (1.00 g, 4.50 mmol, 1.00 eq) in dichlormethan (250 mL) was treated with an aqueous solution of Oxone® (8.62 g, 22.5 mmol, 5.0 eq). The mixture was stirred at rt for four hours, while the colour of the solution turned green. The organic phase was separated and the aqueous phase was extracted four times with DCM (100 mL). The combined organic phases were washed with aqueous HCl (150 mL, 1M), aqueous saturated $NaHCO_3$ solution (150 mL) and a 10% aqueous NaCl solution (150 mL). The organic phase was dried over Na_2SO_4 and the solvent was concentrated under reduced pressure. Due to volatility of the title compound **45** no further purification was carried out and the nitrosoarene **45** was directly added to next reaction.

Procedure 3

31-34, **49** → **35** (70%), **36** (76%), **37** (51%), **38** (73%), **46** (42%), **51** (45%)
yield over two steps

X = $\overset{OH}{\underset{n=1,2}{\text{, }}}$ COOH

Y = H , NHBoc
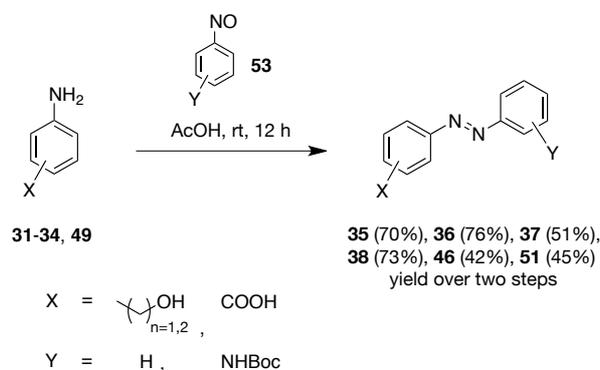
Nitrosoarene **53** (1.0 eq) was dissolved in glacial acid (3.8 mL/mmol$_{nitrosoarene}$). To this solution aniline **31-34**, **49** (0.83 eq) was added and the reaction mixture was stirred at rt. The colour of the reaction mixture turned red. The reaction was stopped after TLC monitoring did not show any more presence of aniline **31-34**, **49**. The solution was pured on an aqueous saturated NaHCO$_3$ solution (46 mL/mmol$_{nitrosoarene}$, CO$_2$ release). The product was extracted four times with EtOAc (23 mL/mmol$_{nitrosoarene}$). The combined organic phases were dried over Na$_2$SO$_4$ and the solvent was removed under reduced pressure. The crude product was purified by flash column chromatography (silica, EtOAc: hexanes = 1:4) to yield title compounds **35-38**, **46**, **51**.

Procedure 4

35-38, **46** → **39** (52%), **40** (87%), **41** (72%), **42** (87%), **47** (63%)

X$_1$ = $\overset{OH}{\underset{n=1,2}{}}$

Y = H , NHBoc

X$_2$ = $\underset{n=1,2}{}$
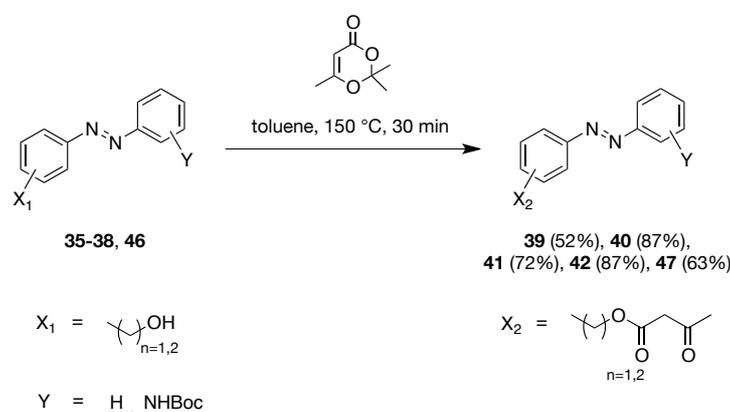
To a solution of toluene (1.06 mL/mmol$_{alcohol}$) and alcohol **35-38**, **46** (1.0 eq) was added 2,2,6-trimethyl-4H-1,3-dioxin-4-one (1.0 eq). Under vigorously stiring the mixture was heated to 160 °C under strong gas release. The reaction was stopped after TLC monitoring did not show any more starting material. The reaction mixture was concentrated and the crude product was purified by flash column chromatography (silica, EtOAc: hexanes = 1:4-1:7) to yield the title compound **39-42**, **47**.

Procedure 5

39-42, **47**

2,3 dichlorobenzaldehyde,
aminocrotonate, EtOH, reflux, 4 h

25 (32%**), 26 (**26%**), 27** (32%), **28 (**3%**), 48 (**42)%

X =

Y = H , NHBoc
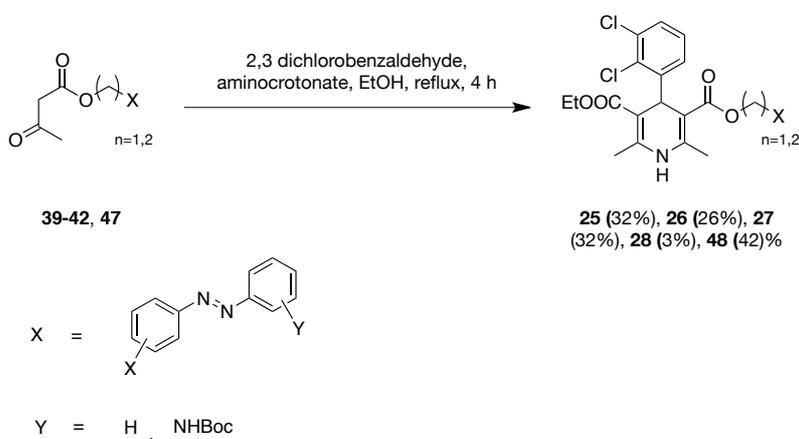
A solution of aminocrotonate (1.0 eq), 2,3 dichlorobenzaldehyd (1.0 eq) and diketone **39-42, 47** (1.0 eq) dissolved in ethanol (1 mL/mmol$_{39-42, 47}$) was refluxed. The reaction was stopped after TLC monitoring did not show any more presence of the diketone. The reaction mixture was concentrated and the crude product was purified by flash column chromatography (silica, EtOAc: hexanes = 1:2-1:6) to yield the title compound **25-28**, **48**.

Procedure 6

methyl acetoacetate,
NH$_3$, rt, 17h

14%

54

52
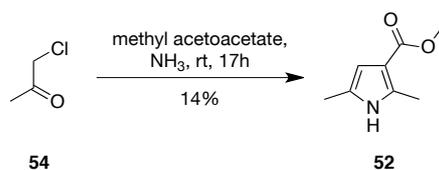
A solution of methyl actoacetate (5.2 mL, 48 mmol, 1.0 eq), ammonia (25 mL), and H$_2$O (25 mL) was treated with chloracetone **54** (4.0 mL, 50 mmol, 1.0 eq). The reaction mixture was stirred at rt for 17 hours and the colour turned into red. The product was extracted five times with EtOAc (25 mL). The combined organic phases were washed with 10% aqueous NaOH (10 mL) and 5% aqueous HCL solution (10 mL). Organic solvent was removed under reduced pressure and the resulting solid was purified by flash column chromatography (silica, EtOAc: Hexanes = 1:5) to yield Methyl *N*-(*tert*-Butoxycarbonyl)-2,5-dimethylpyrrole-3-carboxylate (**52**).

Procedure 7
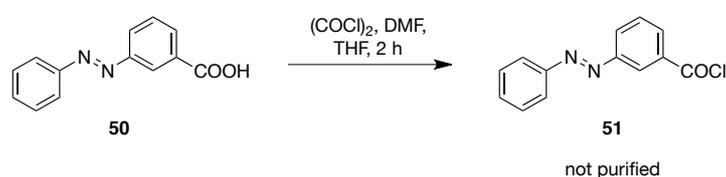
In a schlenk flask 3-(phenyldiazenyl)benzoic acid (**50**) (50.0 mg, 0.22 mmol, 1.00 eq) and oxalylchlorid (22.2 mL, 0.26 mmol, 1.20 eq) were dissolved in THF (3 mL) under a nitrogen atmosphere. The reaction was initiated by adding three drops of DMF. The solvent was evaporated, after TLC monitoring did not show any more starting material. Product **51** was not further purified and directly added to the next reaction.

Procedure 8
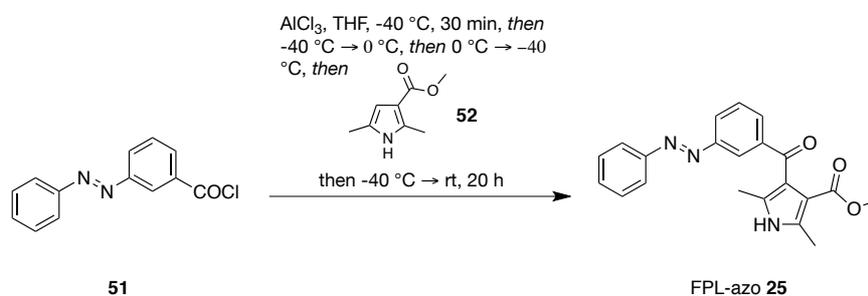
Methyl *N*-(tert-Butoxycarbonyl)-2,5-dimethylpyrrol-3-carboxylat (**52**) (38.0 mg, 0.25 mmol, 1.12 eq) and AlCl$_3$ (104 mg, 0.78 mmol, 3.56 eq) were dissolved in THF (2 mL) under Argon atmosphere. The mixture was cooled to -40 °C and kept at the

temperature for 20 minutes. The reaction was allowed to warm up to rt and recooled to -40 °C. Reactant **51** was added and the reaction mixture was kept at -40 °C for 45 minutes.[6] The reaction mixture was allowed to warm up to rt and stirred for 20 hours. The reaction mixture was poored on water followed by addition of saturated NaHCO$_3$ solution (20 mL, gas release). Under reduced pressure THF was removed and the product was extracted five times with EtOAc (10 mL). The combined organic phases were dried over Na$_2$SO$_4$ and the solvent was removed under reduced pressure. The resulting brown oil was purified by silica column chromatography (silica, EtOAc:hexanes = 3:4) to yield FPL-azo (**25**).

Feazo-2 (25), 3-methyl 5 -(2-(phenyldiazenyl)benzyl) 4 -(2,3-dichlorophenyl)-2,6-dimethyl-1,4-dihydropyridine-3,5-dicarboxylate

25
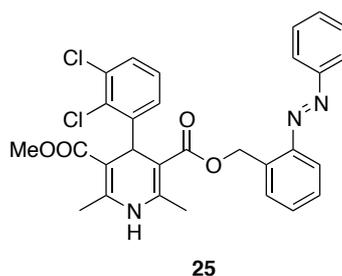
The synthesis was carried out according to general *Procedure 4.* Utilizing 2-(phenyldiazenyl)benzyl 3-oxobutanoate (**39**) (200 mg, 0.50 mmol, 1.00 eq), 2,3-dichlorobenzaldehyde (118 mg, 0.67 mmol, 1.34 eq) and methyl 3-aminobut-2-enoate (78.0 mg, 0.50 mmol, 1.00 eq) yielded the desired product Feazo-2 (**25**) (117 mg, 0.21 mmol) as an orange solid and as a 1:4.8 mixture of (E)/(Z) isomers.

Yield = 32%.

R$_f$ = 0.19 (hexanes: EtOAc = 6:1).

Melting point = oil.

NMR spectroscopic data for major isomer:

---

[6] A. J. Baxter, J. Dixon, F. Ince, C. N. Manners, S. J. Teague, *J. Med. Chem.* **1993**, *36*, 2739-2744.

¹H NMR (CDCl₃, 600 MHz): δ = 7.84 (m$_c$, 2H), 7.69 (m$_c$, 1H), 7.47 (m$_c$, 3H), 7.38 (m$_c$, 2H), 7.23 - 7.13 (m, 3H), 6.9 (m$_c$, 1H), 5.78 (d, J = 13.0 Hz, 1H), 5.63 (s, 1H), 5.57 (d, J = 12.6 Hz, 1H), 5.46 (s, 1H), 3.54 (s, 3H), 2.31 (s, 3H), 2.27 (s, 3H) ppm.

¹³C NMR (CDCl₃, 150 MHz): δ = 167.9, 167.2, 152.8, 149.8, 147.8, 145.0, 144.0, 135.8, 133.0, 131.2*, 131.2*, 129.8, 129.3, 129.1, 128.8, 128.7, 128.3, 127.0, 123.3, 115.6, 103.7, 103.4, 61.9, 51.0, 38.9, 19.9, 19.6 ppm.

* represents different signals

ESI-MS for H₂₆C₂₉Cl₂N₃O₄ [(M + H)⁺]:

calcd.   550.1300

found   550.1294.

IR (ATR): $\tilde{\nu}$/cm⁻¹ = 3335, 2947, 2361, 1735, 1681, 1617, 1488. 1446, 1431, 1418, 1378, 1301, 1274, 1206, 1138, 1113, 1090, 1042, 1017, 864, 799, 773, 750, 734, 686.

UV-Vis (DMSO): λ_{max} = 333.9 nm.

Feazo-3 (26), 3-methyl 5 -(3-(phenyldiazenyl)benzyl) 4 -(2,3-dichlorophenyl)-2,6-dimethyl-1,4-dihydropyridine-3,5-dicarboxylate
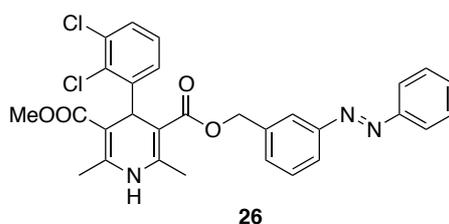
The synthesis was carried out according to general *Procedure 5.* Utilizing 3-(phenyldiazenyl)benzyl 3-oxobutanoate (**40**) (148 mg, 0.50 mmol, 1.00 eq), 2,3-dichlorobenzaldehyde (87.5 mg, 0.50 mmol, 1.00 eq) and aminocrotonate (57.5 mg, 0.50 mmol, 1.00 eq) yielded the desired product 3-methyl Feazo-3 (**26**) (73.0 mg, 0.13 mmol) as an oil and as a 1:2 mixture of (E)/(Z) isomers.

Yield = 26%.

R$_f$ = 0.21 (hexanes: EtOAc = 2:1).

Melting point = oil.

NMR spectroscopic data for major isomer:

¹H NMR (CDCl₃, 600 MHz): δ = 7.94–7.88 (m, 2H), 7.84–7.71 (m, 2H), 7.55–7.35 (m, 5H), 7.28–7.23 (m, 3H), 5.76 (s, 1H), 5.49 (s, 1H), 5.21 (d, J = 13 Hz, 1H), 5.12 (d, J = 13 Hz, 1H), 3.57 (s, 2H), 2.32 (s, 3H), 2.28 (s, 3H) ppm.

¹³C NMR (CDCl₃, 150 MHz): δ = 167.9, 167.1, 152.7*, 152.7*, 148.0, 145.3, 144.1, 137.8, 137.7, 131.2*, 131.2*, 130.7, 129.9, 129.2, 128.8, 128.4, 127.1, 123.0, 122.8, 122.3, 103.8, 103.2, 65.8, 51.1, 38.8, 19.9, 19.6 ppm.

* represents different signals

ESI-MS for $H_{26}C_{29}Cl_2N_3O_4$ [(M + H)⁺]:   calcd.   550.1300

found   500.1292.

IR (ATR): $\tilde{v}$/cm⁻¹ = 3338, 3060, 2947, 1681, 1648, 1616, 1516, 1487, 1446, 1431, 1418, 1380, 1301, 1274, 1206, 1138, 1114, 1096, 1043, 1017, 923, 888, 865, 843, 796, 775, 732, 692.

UV-Vis (DMSO): λ_{max} = 326.0 nm.

Feazo-4 (27), 3-methyl 5 -(4-(phenyldiazenyl)benzyl) 4 -(2,3-dichlorophenyl)-2,6-dimethyl-1,4-dihydropyridine-3,5-dicarboxylate

27

The synthesis was carried out according to general *Procedure 5.* Utilizing 4-(phenyldiazenyl)benzyl 3-oxobutanoate (**41**) (296 mg, 1.00 mmol, 1.00 eq), 2,3-dichlorobenzaldehyde (175 mg, 1.00 mmol, 1.00 eq) and methyl 3-aminobut-2-enoate (115 mg, 1.00 mmol, 1.00 eq) yielded the desired product Feazo-4 (**27**) (177 mg, 0.32 mmol) as an orange solid and as a 1:5.5 mixture of (E)/(Z) isomers.

Yield = 32%.

R$_f$ = 0.2 (hexanes: EtOAc = 2:1).

Melting point = 68.4 °C.

NMR spectroscopic data for major isomer:

^{1}H NMR (CDCl$_3$, 600 MHz): δ = 7.92–7.90 (m, 2H), 7.84–7.80 (m, 2H), 7.53–7.45 (m, 3H), 7.30–7.26 (m, 5H), 7.05–7.01 (m, 1H), 5.87 (s, 1H), 5.50 (s, 1H), 5.18 (d, J = 15.41 Hz, 1H), 5.10 (d, J = 13.03 Hz, 1H), 3.60 (s, 3H), 2.30 (s, 1H), 2.28 (s, 1H) ppm.

^{13}C NMR (CDCl$_3$, 150 MHz): δ = 167.9, 167.1, 152.7, 152.2, 148.2, 145.4, 144.1, 139.6, 133.0, 131.1, 129.8, 129.2, 128.8, 128.4, 127.2, 123.0, 120.7, 120.6, 103.8, 103.2, 65.1, 51.0, 38.8, 19.8, 19.5 ppm.

ESI-MS for H$_{26}$C$_{29}$Cl$_2$N$_3$O$_4$ [(M + H)$^+$]: 　　calcd. 　550.1300

　　　　　　　　　　　　　　　　　　　　　found 　550.1292.

IR (ATR): $\tilde{v}$/cm^{-1} = 3338, 2948, 2250, 1682, 1649, 1617, 1486, 1432, 1418, 1380, 1301, 1276, 1208, 1138, 1114, 1094, 1044, 1015, 907, 726, 687.

UV-Vis (DMSO): λ_{max} = 333.9 nm.

Feazo-4l (28), (3-methyl 5-(4-(phenyldiazenyl)phenethyl) 4-(2,3-dichlorophenyl)-2,6-dimethyl-1,4-dihydropyridine-3,5-dicarboxylate
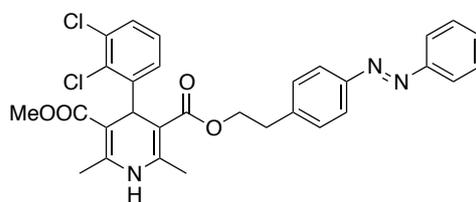
28

The synthesis was carried out according to general *Procedure 5.* Utilizing 4-(phenyldiazenyl)phenethyl 3-oxobutanoate (**42**) (2.00 g, 6.45 mmol, 1.00 eq), 2,3-dichlorobenzaldehyde (822 mg, 4.70 mmol, 0.72 eq) and methyl 3-aminobut-2-

enoate (541 mg, 4.7 mmol, 0.72 eq) yielded the desired Feazo-4l (**28**) (96.0 mg, 0.17 mmol) as an orange solid.

Yield = 2.6%.

R_f = 0.23 (hexanes: EtOAc = 3:1).

Melting point = 81.4 °C.

NMR spectroscopic data for major isomer:

^{1}H NMR (CDCl$_3$, 600 MHz): δ = 7.92–7.87 (m, 2H), 7.82–7.78 (m, 2H), 7.54–7.44 (m, 4H), 7.26–7.22 (m, 3H), 7.06–7.02 (m, 2H), 5.64 (s, 1H), 5.44 (s, 1H), 4.31 (t, J = 7 Hz, 2H), 3.61 (s, 3H), 3.01–2.89 (m, 2H), 2.3 (s, 3H), 2.26 (s, 3H) ppm.

^{13}C NMR (CDCl$_3$, 150 MHz): δ = 167.9, 167.2, 152.8, 151.4, 148.1, 144.8, 144.2, 141.7, 133.0, 131.0, 129.7, 129.2, 128.5, 127.2, 123.1, 122.9, 121.1, 120.5, 103.9, 103.7, 64.1, 51.0, 38.9, 35.2, 19.8, 19.6 ppm.

ESI-MS for H$_{28}$C$_{30}$Cl$_2$N$_3$O$_4$ [(M + H)$^+$]:   calcd.   564.1457

                                                        found   564.1461.

IR (ATR): $\tilde{v}$/cm^{-1} = 3342, 2956, 1681, 1618, 1487, 1446, 1432, 1418, 1380, 1302, 1276, 1210, 1139, 1099, 1043, 1017, 925, 837, 797, 768, 734, 687.

UV-Vis (DMSO): λ_{max} = 337.0 nm.

FPL-azo (30), Methyl 2,5 -dimethyl-4-(3-(phenyldiazenyl)benzoyl)-1H-pyrrole-3-carboxylate
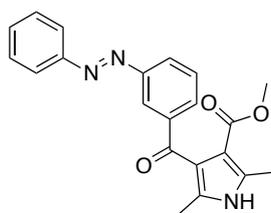
30

The synthesis was carried out according to general *Procedure 8.* Utilizing Methyl N-(tert-Butoxycarbonyl)-2,5-dimethylpyrrol-3-carboxylat (**52**), AlCl$_3$ and 3-

(phenyldiazenyl)benzoyl chloride (**51**) yielded the desired product FPL-azo (**30**) as an orange solid and as a 1:4.4 mixture of (E)/(Z) isomers

Yield = unknown

$\mathbf{R}_f$ = 0.24 (hexanes: EtOAc = 4:3).

Melting point = 75 °C.

NMR spectroscopic data for major isomer:

¹H NMR (DMSO, 400 MHz): δ = 8.76 (s, 1H), 8.33 (m, 1H), 8.03 (m, 2H), 7.92 (m, 1H), 7.88 (m, 1H), 7.52 (m, 4H) ppm.

¹³C NMR (DMSO, 100.5 MHz): δ = 193.6, 165.2, 152.7, 152.6, 141.5, 134.5, 131.4, 131.1, 129.3, 129.1, 125.3, 124.0, 123.1, 120.7, 120.6, 112.1, 50.6, 12.8, 12.0 ppm.

ESI-MS for $H_{19}C_{21}N_3O_3$ [(M - H)⁺]: calcd. 360.1348

  found 360.1351.

IR (ATR): $\tilde{\nu}$/cm⁻¹ = 3278, 1676, 1635, 1533, 1436, 1381, 1338, 1299, 1234, 1203, 1170, 1153, 1088, 1020, 908, 809, 766, 690.

UV-Vis (DMSO): λ_{max} = 320.0 nm.

(2-(phenyldiazenyl)phenyl)methanol (35)
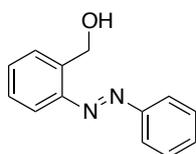
35

The synthesis was carried out according to general *Procedure 3*. Utilizing nitrosobenzene (700 mg, 6.53 mmol, 1.20 eq) and (2-aminophenyl)methanol (670 mg, 5.44 mmol, 1.00 eq) yielded the desired product (2-(phenyldiazenyl)phenyl)methanol (**35**) (806 mg, 3.80 mmol) as an orange solid and as a 1:23 mixture of (E)/(Z) isomers.

Yield = 70%.

R$_f$ = 0.2 (hexanes: EtOAc = 4:1).

Melting point = 74.7–75.1 °C.

NMR spectroscopic data for major isomer:

¹H NMR (CDCl$_3$, 300 MHz): δ = 7.90 (m, 2H), 7.82 (m, 1H), 7.52 (m, 6H), 5.05 (s, 2H), 3.16 (br, 1H) ppm.

¹³C NMR (CDCl$_3$, 75.5 MHz): δ = 152.7, 150.5, 138.6, 131.6, 131.5, 129.4, 129.4, 128.6, 123.1, 118.5, 63.4 ppm.

ESI-MS for H$_{13}$C$_{13}$N$_2$O [(M + H)$^+$]: calcd.   213.1022
found   213.1024.

IR (ATR): $\tilde{v}$/cm^{-1} = 3250, 1571,1471, 1451, 1356, 1130, 1239, 1219, 1185, 1145, 1101, 1069, 1042, 986, 948, 936, 924, 833, 768, 706, 685.

(3-(phenyldiazenyl)phenyl)methanol (36)
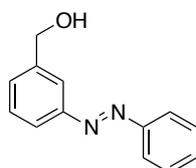
36

The synthesis was carried out according to general *Procedure 2.* Utilizing nitrosobenzene (700 mg, 6.53 mmol, 1.20 eq) and (3-aminophenyl)methanol (670 mg, 5.44 mmol, 1.00 eq) yielded the desired product (3-(phenyldiazenyl)phenyl)methanol (**36**) (880 mg, 4.10 mmol) as an orange solid, whereat only the Z isomers was detected in the ¹H NMR measurement.

Yield = 76%.

R$_f$ = 0.13 (hexanes: EtOAc = 4:1).

Melting point = 38.2–38.6 °C.

NMR spectroscopic data for major isomer:

¹H NMR (CDCl₃, 600 MHz): δ = 7.95–7.90 (m, 3H), 7.86 (m_c, 1H), 7.56–7.45 (m, 5H), 4.81 (s, 2H), 1.89 (s, 1H) ppm.

¹³C NMR (CDCl₃, 150 MHz): δ = 153.0, 152.8, 142.2, 131.2, 129.5, 129.4, 129.2, 123.0, 122.8, 120.7, 65.1 ppm.

ESI-MS for $H_{13}C_{13}N_2O$ [(M + H)⁺]:   calcd.   213.1022

found   213.1023.

IR (ATR): $\tilde{v}$/cm⁻¹ = 3287, 3051, 2926, 2870, 2362, 2341, 1954, 1684, 1587, 1491, 1471, 1446, 1406, 1307, 1243, 1194, 1162, 1144, 1119, 1087, 1071, 1039, 1012, 991, 948, 918, 896, 872, 807, 793, 768, 669.

(4-(phenyldiazenyl)phenyl)methanol (37)
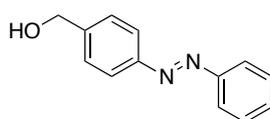
37

The synthesis was carried out according to general *Procedure 3.* Utilizing nitrosobenzene (700 mg, 6.53 mmol, 1.20 eq) and (4-aminophenyl)methanol (670 mg, 5.44 mmol, 1.00 eq) yielded the desired product (4-(phenyldiazenyl)phenyl)methanol (**37**) (588 mg, 2.80 mmol) as an orange solid, whereat only the Z isomers was detected in the ¹H NMR measurement.

Yield = 51%.

R_f = 0.21 (hexanes: EtOAc = 4:1).

Melting point = 143 °C.

NMR spectroscopic data for major isomer:

¹H NMR (CDCl₃, 600 MHz): δ = 7.95–7.91 (m, 4H), 7.54–7.46 (m, 5H), 4.79 (s, 2H), 1.84 (s, 1H) ppm.

¹³C-NMR (CDCl₃, 150 MHz): δ = 152.8, 152.3, 144.0, 131.1, 129.2, 127.6, 123.2, 123.0, 65.0 ppm.

ESI-MS for $H_{13}C_{13}N_2O$ $[(M + H)^+]$: calcd. 213.1028

found 213.1022.

IR (ATR): $\tilde{v}/cm^{-1} = 3200, 1440, 1346, 1302, 1148, 1018, 848, 829, 762, 682.$

2-(4-(phenyldiazenyl)phenyl)ethanol (38)

38

The synthesis was carried out according to general *Procedure 3.* Utilizing nitrosobenzene (1.874 g, 17.49 mmol, 1.20 eq) and (4-aminophenyl)ethanol (2.000 g, 14.58 mmol, 1.00 eq) yielded the desired product (4-(phenyldiazenyl)phenyl)ethanol (**38**) (2.870 mg, 12.69 mmol) as an orange solid and as a 1:13 mixture of (E)/(Z) isomers.

Yield = 73%.

R$_f$ = 0.16 (hexanes: EtOAc = 4:1).

Melting point = 85.6–85.8 °C.

NMR spectroscopic data for major isomer:

^{1}H NMR (CDCl$_3$, 300 MHz): δ = 7.93–7.86 (m, 4H), 7.55–7.45 (m, 3H), 7.4–7.35 (m, 2H), 3.92 (q, J = 5.84 Hz, 2H), 2.95 (tri, J = 6.26 Hz, 2H), 1.54 (tri, J = 5.58 Hz, 1H).

^{13}C NMR (CDCl$_3$, 75 MHz): δ = 152.8, 151.6, 142.1, 131.0, 129.9, 129.2, 123.2, 122.9, 63.6, 39.2 ppm.

EI-MS for $H_{14}C_{14}N_2O$ $[M^+]$: calcd. 226.1106

found 226.1100.

IR (ATR): $\tilde{v}/cm^{-1}$ = 3314, 2862, 1601, 1500, 1466, 1441, 1412, 1364, 1302, 1219, 1151, 1106, 1056, 1037, 1010, 921, 840, 822, 795, 763, 727, 683.

2-(phenyldiazenyl)benzyl 3-oxobutanoate (39)

39

The synthesis was carried out according to general *Procedure 4.* Utilizing (2-(phenyldiazenyl)phenyl)methanol (**35**) (700 mg, 3.30 mmol, 1.00 eq) and 2,2,6-trimethyl-4*H*-1,3-dioxin-4-one (472 mg, 3.32 mmol, 1.00 eq) yielded the desired product 2-(phenyldiazenyl)benzyl 3-oxobutanoate (**39**) (507 mg, 1.70 mmol) as an orange solid and as a 1:4.2 mixture of (E)/(Z) isomers.

Yield = 52%.

R_f = 0.2 (hexanes: EtOAc = 7:1).

Melting point = 65.7–66.2 °C.

NMR spectroscopic data for major isomer:

^{1}H NMR (CDCl$_3$, 400 MHz): δ = 7.93–7.91 (m, 2H), 7.75–7.73 (m, 1H), 7.59–7.57 (m, 1H), 7.55–7.42 (m, 5H), 5.79 (s, 2H), 3.49 (s, 2H), 2.21(s, 3H) ppm.

^{13}C NMR (CDCl$_3$, 150 MHz): δ = 200.4, 167.0, 152.8, 150.0, 134.5, 131.5, 131.3, 129.7, 129.4, 129.3, 120.9, 115.9, 63.4, 50.2, 30.3 ppm.

ESI-MS for H$_{17}$C$_{17}$N$_2$O$_3$ [(M + H)$^+$]:   calcd.   297.1239

                                                                              found   297.1234.

IR (ATR): $\tilde{v}$/cm^{-1} = 1742, 1718, 1404, 1360, 1312, 1296, 1264, 1221, 1169, 1150, 1037, 981, 957, 922, 772, 747, 705, 684.

3-(phenyldiazenyl)benzyl 3-oxobutanoate (40)
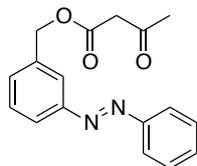
40

The synthesis was carried out according to general *Procedure 4.* Utilizing (3-(phenyldiazenyl)phenyl)methanol (**36**) (100 mg, 0.47 mmol, 1.00 eq) and 2,2,6-trimethyl-4*H*-1,3-dioxin-4-one (67.5 mg, 0.47 mmol, 1.00 eq) yielded the desired product 3-(phenyldiazenyl)benzyl 3-oxobutanoate (**40**) (121 mg, 0.41 mmol) as an orange solid and as a 1:15.5 mixture of (E)/(Z) isomers.

Yield = 87%.

R$_f$ = 0.18 (hexanes: EtOAc = 4:1).

Melting point = oil.

NMR spectroscopic data for major isomer:

^{1}H NMR (CDCl$_3$, 400 MHz): δ = 7.95–7.87 (m, 4H), 7,56–7,46 (m, 5H), 5.28 (s, 2H), 3.54 (s, 2H), 2.27 (s, 3H) ppm.

^{13}C NMR (CDCl$_3$, 100 MHz): δ = 200.4, 167.0, 152.9, 152.6, 136.5, 131.4, 130.7, 129.5, 129.2, 123.3, 123.0, 122.0, 66.8, 50.1, 30.3 ppm.

ESI-MS for H$_{17}$C$_{17}$N$_2$O$_3$ [(M + H)$^+$]:   calcd.   297.1239

                                                found   297.1240.

IR (ATR): $\tilde{v}$/cm^{-1} = 3063, 2960, 2363, 1742, 1715, 1651, 1586, 1448, 1408, 1360, 1312, 1227, 1146, 1086, 1071, 1030, 1000, 972, 924, 892, 796, 765, 692.

4-(phenyldiazenyl)benzyl 3-oxobutanoate (41)
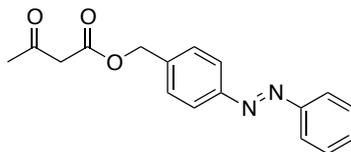
41

The synthesis was carried out according to general *Procedure 4.* Utilizing (4-(phenyldiazenyl)phenyl)methanol (**37**) (400 mg, 1.90 mmol, 1.00 eq) and 2,2,6-trimethyl-4*H*-1,3-dioxin-4-one (0.27 g, 1.90 mmol, 1.00 eq) yielded the desired product 4-(phenyldiazenyl)benzyl 3-oxobutanoate (**41**) (397 mg, 1.34 mmol) as an orange solid and as a 1:8 mixture of (E)/(Z) isomers.

Yield = 72%.

R$_f$ = 0.2 (hexanes: EtOAc = 7:1).

Melting point = 70.8–71.5 °C.

NMR spectroscopic data for major isomer:

^{1}H NMR (CD$_2$Cl$_2$, 400 MHz): δ = 7.95–7.92 (m, 4H), 7.57–7.48 (m, 5H), 5.25 (s, 2H), 3.55 (s, 2H), 2.25 (s, 3H) ppm.

^{13}C NMR (CD$_2$Cl$_2$, 100 MHz): δ = 200.3, 167.0, 152.7, 152.5, 138.6, 131.3, 129.2, 128.9, 123.0, 122.9, 66.4, 50.0, 30.1 ppm.

ESI-MS for H$_{17}$C$_{17}$N$_2$O$_3$ [(M + H)$^+$]: calcd. 297.1239

found 297.1232.

IR (ATR): $\tilde{v}$/cm^{-1} = 2926, 2360, 1738, 1701, 1484, 1411, 1362, 1311, 1265, 1145, 1030, 1000, 962, 828, 768, 724, 689.

4-(phenyldiazenyl)phenethyl 3-oxobutanoate (42)
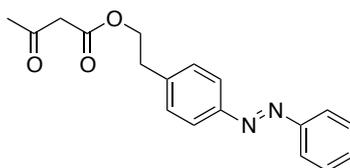
42

The synthesis was carried out according to general *Procedure 4.* Utilizing (4-(phenyldiazenyl)phenyl)ethanol (**38**) (2.000 g, 8.84 mmol, 1.84 eq) and 2,2,6-trimethyl-4*H*-1,3-dioxin-4-one (68.00 mg, 4.74 mmol, 1.00 eq) yielded the desired product 4-(phenyldiazenyl)phenethyl 3-oxobutanoate (**42**) (2.397 g, 7.73 mmol) as an orange solid and as a 1:12 mixture of (E)/(Z) isomers.

Yield = 87%.

R$_f$ = 0.26 (hexanes: EtOAc = 4:1).

Melting point = 85.9–86.4 °C.

NMR spectroscopic data for major isomer:

^{1}H NMR (CDCl$_3$, 400 MHz): δ = 7.92–7.86 (m, 4H), 7.55–7.45 (m, 3H), 7.39–7.35 (m, 2H), 4.42 (t, *J* = 7 Hz, 2H), 3.45 (s, 2H), 3.05 (t, *J* = 6.93 Hz, 2H), 2.2 (s, 3H) ppm.

^{13}C NMR (CDCl$_3$, 100 MHz): δ = 200.5, 167.1, 152.8, 151.7, 140.9, 131.1, 129.8, 129.2, 123.2, 122.9, 65.5, 50.2, 35.0, 30.3 ppm.

EI-MS for H$_{18}$C$_{18}$N$_2$O$_3$ [M$^+$]:   calcd.   310.1317

   found   310.1316.

IR (ATR): $\tilde{v}$/cm^{-1} = 2960, 2937, 2866, 1732, 1712, 1648, 1630, 1602, 1499, 1464, 1474, 1446, 1416, 1362, 1316, 1284, 1270, 1238, 1177, 1157, 1109, 1070, 1040, 1006, 971, 928, 847, 835, 771, 726, 688.

Tert-butyl 4-aminobenzylcarbamate (44)

44
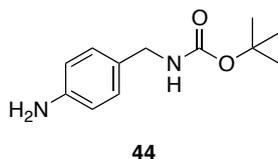
The synthesis was carried out according to general *Procedure 1.* Utilizing 4-aminobenzylamine (1.000 g, 8.19 mmol, 1.0 eq) and di-*tert*-butyl dicarbonate (1.965 g, 9.0 mmol, 1.1 eq) yielded the desired product *tert*-butyl 4-aminobenzylcarbamate (**44**) (1.73 g, 7.78 mmol) as a white solid.

Yield = 95%.

R$_f$ = 0.23 (hexanes: EtOAc = 3:1).

Melting point = 80.8 °C.

NMR spectroscopic data:

^{1}H NMR (CDCl$_3$, 400 MHz): δ = 7.05 (d, J = 8.09 Hz, 2H), 6.62 (d, J = 8.82 Hz, 2H), 4.80 (brs, 1H), 4.17 (d, J = 5.42 Hz, 2H), 3.61 (brs, 1H), 1.45 (s, 9H) ppm.

^{13}C NMR (CDCl$_3$, 100 MHz): δ = 155.9, 145.8, 128.9, 128.8, 115.2, 79.3, 44.4, 28.5 ppm.

EI-MS for H$_{18}$C$_{12}$N$_2$O$_2$ [M$^+$]:

calcd. 222.1368

found 222.1355.

IR (ATR): $\tilde{\nu}$/cm^{-1} = 3901, 3854, 3745, 3711, 3676, 3367, 2360, 2341, 1684, 1653, 1576, 1559, 1540, 1507, 1457, 1394, 1363, 1246, 1162, 1048, 1027, 930, 865, 821 668.

Tert-butyl 4-((3-(hydroxymethyl)phenyl)diazenyl)benzylcarbamate (46)

46
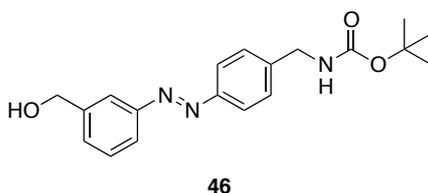
The synthesis was carried out according to general *Procedure 3.* Utilizing *tert*-butyl 4-nitrosobenzylcarbamate (**45**) (unknown, estimated to be 1 g, see *Procedure 1*) and 3 aminophenyl)methanol (1 g, 8.12 mmol) yielded the desired *tert*-butyl 4-((3-(hydroxymethyl)phenyl)diazenyl)benzylcarbamate (**46**) (1.16 g, 3.4 mmol) as an orange solid and as a 1:15 mixture of (E)/(Z) isomers.

Yield = about 42%.

R$_f$ = 0.2 (hexanes: EtOAc = 2:1).

Melting point = 114.7–115 °C.

NMR spectroscopic data for major isomer:

^{1}H NMR (CDCl$_3$, 600 MHz): δ = 7.79 (s, 1H), 7.86 (d, *J* = 9.11 Hz, 2H), 7.82 (d, *J* = 7.51 Hz, 1H), 7.51-7.46 (m, 2H), 7.40 (d, *J* = 8.06 Hz, 2H), 4.99 (brs, 1H), 4.78 (s, 2H), 4.37 (d, *J* = 5.23 Hz, 2H), 2.26 (brs, 1H), 1.47 (s, 9H) ppm.

^{13}C NMR (CDCl$_3$, 150 MHz): δ = 156.1, 152.9, 152.0, 142.3, 129.4, 129.4, 128.1, 127.6, 123.3, 122.7, 120.7, 79.9, 65, 44.5, 28.5 ppm.

ESI-MS for H$_{24}$C$_{19}$N$_3$O$_3$ [M+H$^+$]: calcd. 342.1817

  found 342.1811.

IR (ATR): $\tilde{v}$/cm^{-1} = 3351, 2358, 1678, 1503, 1364, 1245, 1167, 1050, 1020, 847, 800, 692.

3-((4-(((*tert*-butoxycarbonyl)amino)methyl)phenyl)diazenyl)benzyl 3-oxobutanoate (47)
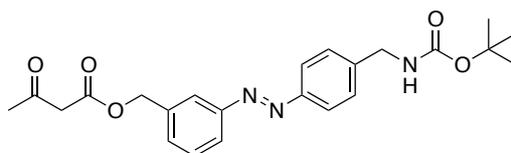
47

The synthesis was carried out according to general *Procedure 4.* *tert*-butyl 4-((3-(hydroxymethyl)phenyl)diazenyl)benzylcarbamate (**46**) (1.00 g, 2.93 mmol, 1.00 eq)

and 2,2,6-trimethyl-4*H*-1,3-dioxin-4-one (342 mg, 2.41 mmol, 1.20 eq) yielded the desired product 3-((4-(((*tert*-butoxycarbonyl)amino)methyl)phenyl)diazenyl)benzyl 3-oxobutanoate (**47**) (651 mg, 1.53 mmol) as an orange solid and as a 1:5 mixture of (E)/(Z) isomers.

Yield = 63%.

R$_f$ = 0.23 (hexanes: EtOAc = 3:1).

Melting point = 101.2 °C.

NMR spectroscopic data for major isomer:

^{1}H NMR (CDCl$_3$, 400 MHz): δ = 7.91–7.87 (m, 1H), 7.54–7.51 (t, *J* = 7.50 Hz, 1H), 7.47 (d, *J* = 7.43 Hz, 1H), 7.43 (d, *J* = 8.34 Hz, 2H), 5.28 (s, 2H), 4.40 (d, *J* = 5.41 Hz, 2H), 3.54 (s, 2H), 2.27 (s, 3H), 1.48 (s, 9H) ppm.

^{13}C NMR (CDCl$_3$, 100 MHz): δ = 200.4, 167.0, 152.9, 152.0, 136.6, 130.7, 129.6, 128.2, 127.8, 127.1, 123.4, 123.3, 122.4, 121.1, 66.8, 50.2, 44.5, 30.4, 28.6 ppm.

ESI-MS for H$_{28}$C$_{23}$N$_3$O$_5$ [M+H$^+$]:　　　　calcd.　426.4855

　　　　　　　　　　　　　　　　　　　　found　426.2021.

IR (ATR): $\tilde{\nu}$/cm^{-1} = 3364, 2975, 1738, 1720, 1678, 1500, 1465, 1412, 1365, 1312, 1244, 1149, 1049, 1028, 1013, 965, 920, 871, 850, 798, 781, 727, 690.

Feazo-3,4 (48), 3-methyl 5-(3-(phenyldiazenyl)benzyl) 4-(2,3-dichlorophenyl)-2,6-dimethyl-1,4-dihydropyridine-3,5-dicarboxylate
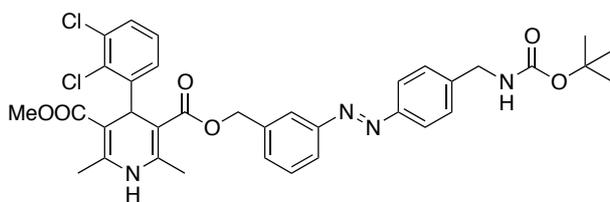
48

The synthesis was carried out according to general *Procedure 5.* Utilizing 3-((4-(((*tert*-butoxycarbonyl)amino)methyl)phenyl)diazenyl)benzyl 3-oxobutanoate (**47**) (700 mg, 1.64 mmol, 1.00 eq), 2,3-dichlorobenzaldehyde (288 mg, 1.64 mmol, 1.00 eq) and methyl 3-aminobut-2-enoate (189 mg, 1.64 mmol, 1.00 eq) yielded the desired Feazo-3,4 (**48**) (152 mg, 0.22 mmol) as an orange solid and as a 1:7 mixture of (E)/(Z) isomers.

Yield = 14%.

R_f = 0.11 (hexanes: EtOAc = 2:1).

Melting point = 89.1 °C.

NMR spectroscopic data for major isomer:

¹H NMR (CDCl$_3$, 600 MHz): δ = 7.88 (d, J = 8.78 Hz, 2H), 7.80 (d, J = 7.68 Hz, 1H), 7.72 (s, 1H), 7.44–7.39 (m, 3H), 7.26–7.24 (m, 2H), 7.18–7.16 (m, 1H), 6.99 (t, J = 7.74 Hz, 1H), 5.80 (s, 1H), 5.49 (s, 1H), 5.21 (d, J = 12.43 Hz, 1H), 5.11 (d, J = 13.06 Hz, 1H), 4.40 (d, J = 5.63 Hz, 2H), 3.57 (s, 3H), 2.31 (s, 3H), 2.28 (s, 3H), 1.48 (s, 9H) ppm.

¹³C NMR (CDCl$_3$, 150 MHz): δ = 167.9, 167.1, 156.1, 152.7, 152.0, 148.0, 145.3, 144.1, 142.2, 137.8, 133.0, 131.3, 130.7, 129.9, 129.2, 128.4, 128.1, 127.1, 123.3, 122.8, 122.3, 103.8, 103.3, 79.9, 65.3, 51.0, 44.5, 38.8, 28.6, 19.9, 19.6 ppm.

ESI-MS for H$_{37}$C$_{35}$Cl$_2$N$_4$O$_6$ [(M + H)$^+$]:   calcd.   679.2090

                                                                                                      found   679.2083.

IR (ATR): $\tilde{v}$/cm^{-1} = 3337, 2979, 1683, 1618, 1491, 1446, 1432, 1419, 1380, 1366, 1301, 1274, 1208, 1163, 1138, 1115, 1098, 1044, 1017, 935, 864, 798, 749, 690, 666.

UV-Vis (DMSO): λ_{max} = 337.0 nm.

3-(phenyldiazenyl)benzoic acid (51)
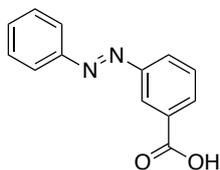
51

The synthesis was carried out according to general *Procedure 3.* Utilizing nitrosobenzene (700 mg, 6.53 mmol, 1.20 eq) and Anthranilic acid (746 mg, 5.44 mmol, 1.00 eq) yielded the desired product (**51**) (0.55 g, 2.43 mmol) as an orange solid, whereat only the Z isomer was detected in the ^{1}H NMR measurement.

Yield = 45%.

R$_f$ = 0.2 (DCM, 1% acetic acid).

Melting point = 171.8 °C.

NMR spectroscopic data for major isomer:

^{1}H NMR (DMSO, 300 MHz): δ = 13.31 (br, 1H), 8.38 (m, 1H), 8.13 (m, 2H), 7.93 (m, 2H), 7.74 (m, 1H), 7.6 (m, 3H) ppm.

^{13}C NMR (DMSO, 75.45 MHz): δ = 166.6, 151.8*, 151.8*, 132.1, 131.9, 131.8, 129.9, 129.5, 127.3, 122.7, 122.3 ppm.

* represents different signals

ESI-MS for $H_9C_{13}N_2O_2$ [(M - H)$^+$]:   calcd.   225.0664

                                                          found   225.0671.

IR (ATR): $\tilde{v}$/cm^{-1} = 3051, 2359, 1684, 1586, 1470, 1448, 1431, 1394, 1236, 1208, 1175, 1156, 1080, 1018, 998, 923, 852, 819, 765, 686.

Methyl N-(*tert*-Butoxycarbonyl)-2,5-dimethylpyrrole-3-carboxylate (52)

52
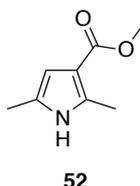
The synthesis was carried out according to general *Procedure 6.* Utilizing methyl acetoacetate (5.2 mL, 48 mmol, 1.0 eq) ammonia (50 mL) and chloracetone (4.0 mL, 50 mmol, 1.0 eq) yielded the desired product Methyl N-(*tert*-Butoxycarbonyl)-2,5-dimethylpyrrole-3-carboxylate (**52**) (1.1 g, 7.1 mmol) as a yellow solid.

Yield = 14%.

R$_f$ = 0.2 (hexanes: EtOAc = 5:1).

Melting point = 106.4 °C.

NMR spectroscopic data:

^{1}H NMR (CDCl$_3$, 400 MHz): δ = 8.16 (br, 1H), 6.18 (d, J = 1.8 Hz, 1H), 3.78 (s, 3H), 2.47 (s, 3H), 2.19 (s, 3H) ppm.

^{13}C NMR (CDCl$_3$, 100,55 MHz): δ = 166.4, 134.6, 125.8, 111.4, 107.5, 50.8, 13.2, 12.7 ppm.

EI-MS for H$_{11}$C$_8$N$_1$O$_2$ [(M)$^+$]:   calcd.   153.0790

                                                                found   153.0781.

IR (ATR): $\tilde{v}$/cm^{-1} = 3300, 3192, 2949, 1666, 1599, 1518, 1452, 1387, 1327, 1265, 1222, 1188, 1130, 1089, 1005, 958, 806, 779, 744, 718.

4.17) Appendix: NMR spectra

¹H NMR:
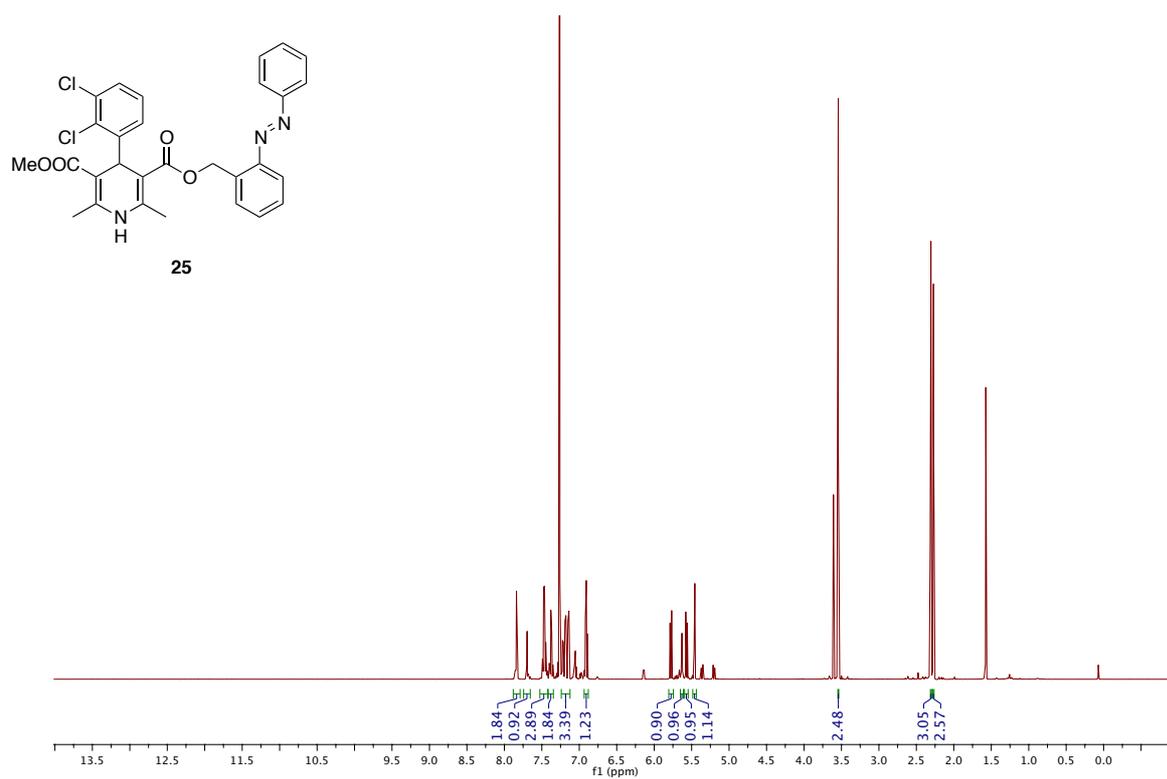
¹³C NMR:
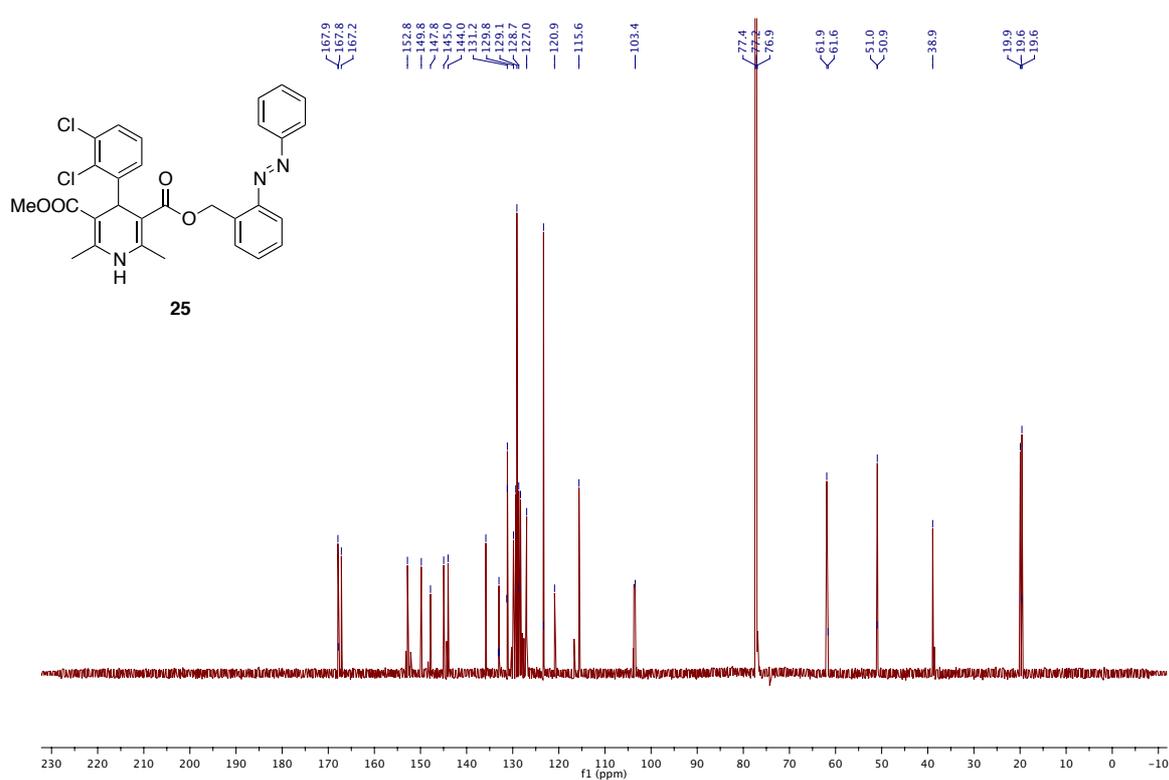
¹H NMR:
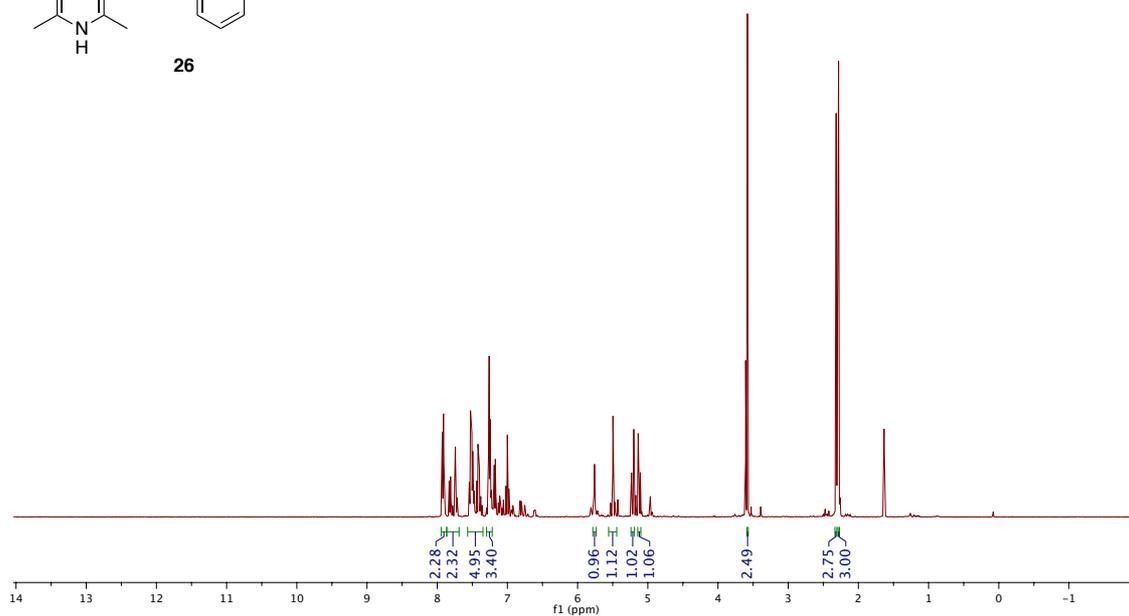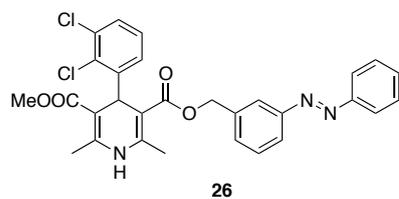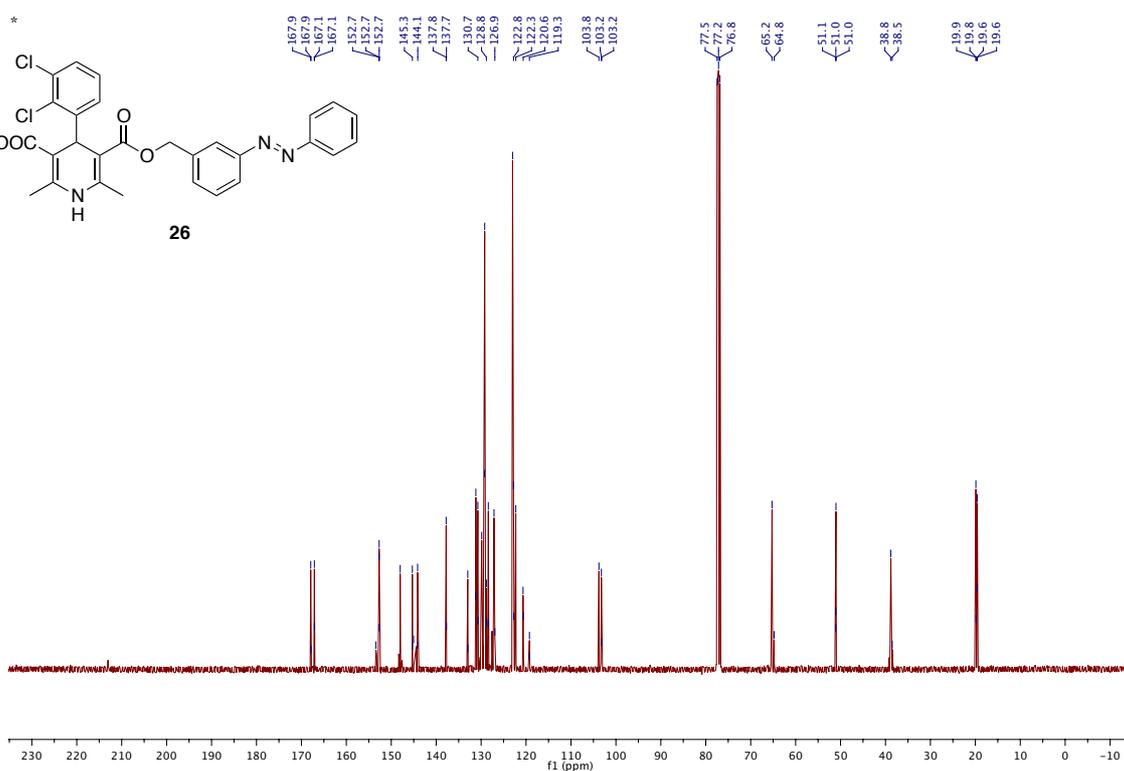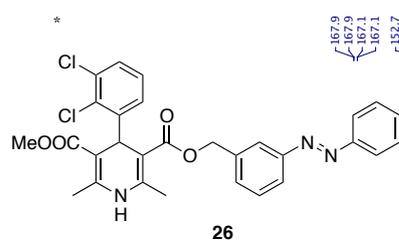
¹³CNMR:

^{1}H NMR:

27

^{13}CNMR:

27

165
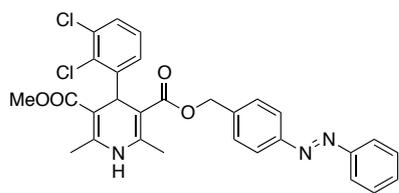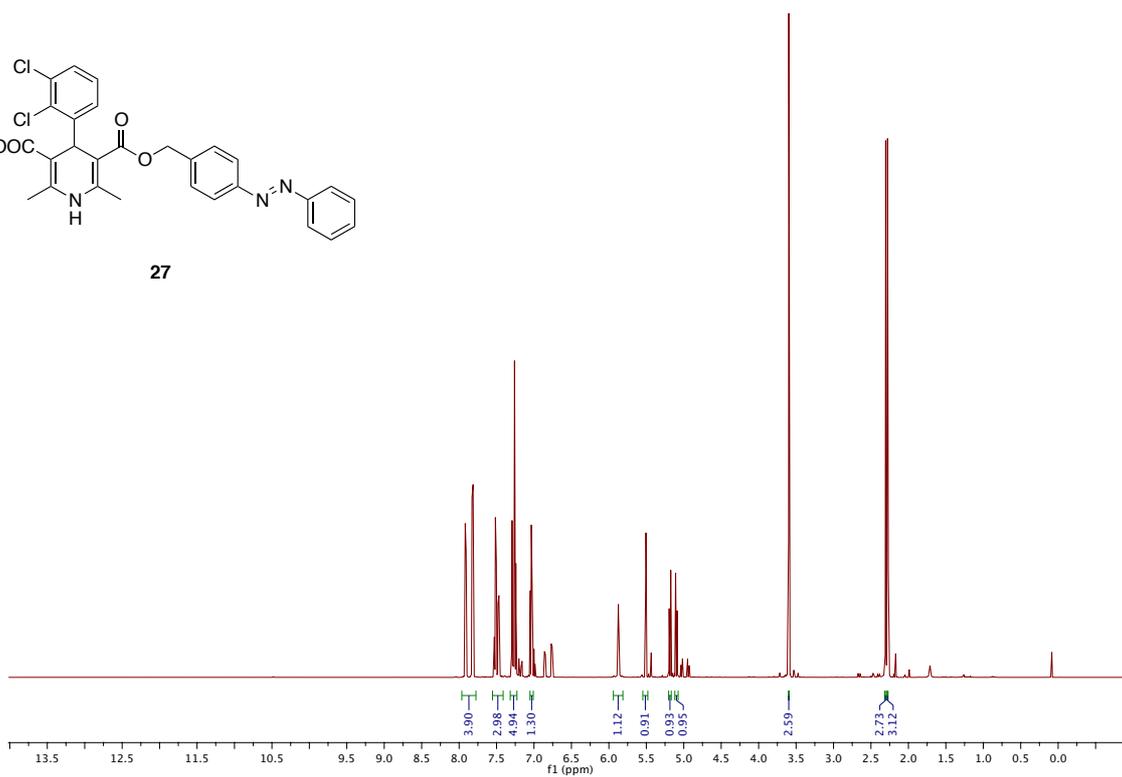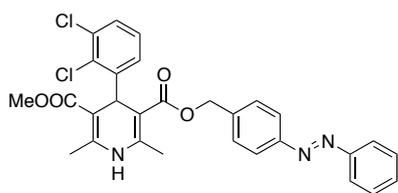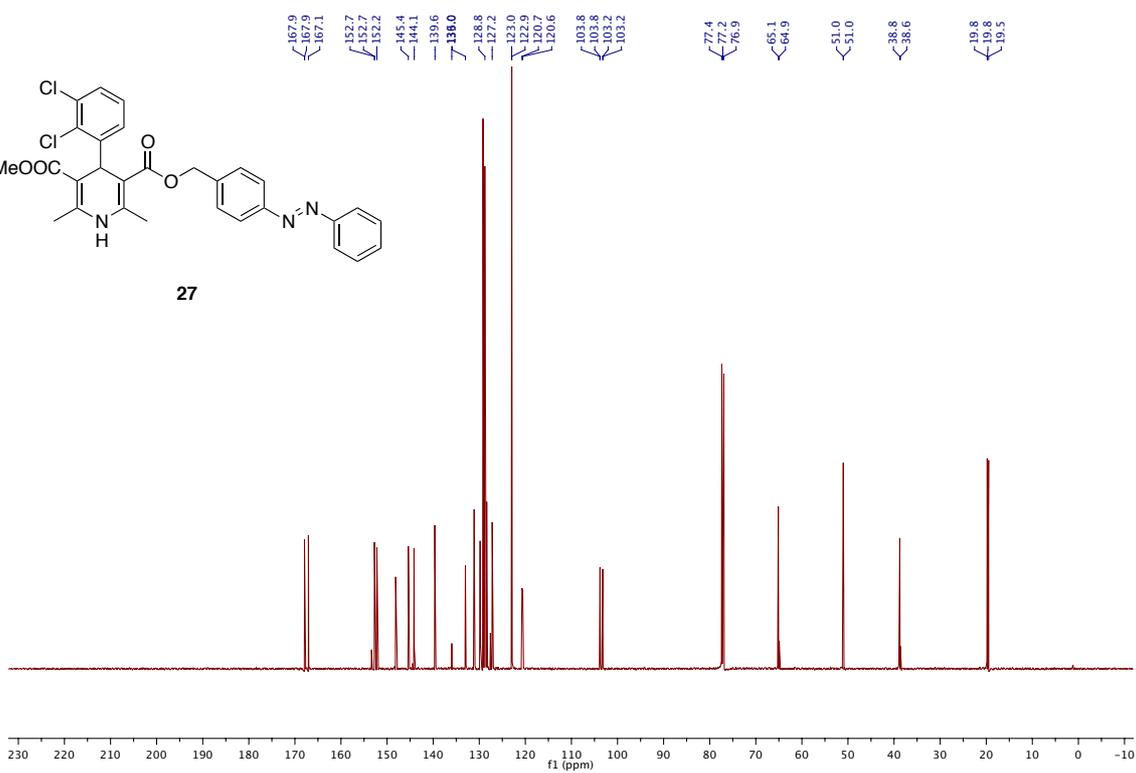
¹H NMR:

28

¹³CNMR:

28

^{1}H NMR:

30

^{13}CNMR:

30

^{1}H NMR:

35

^{13}CNMR:

35

¹H NMR:

36

¹³CNMR:

36
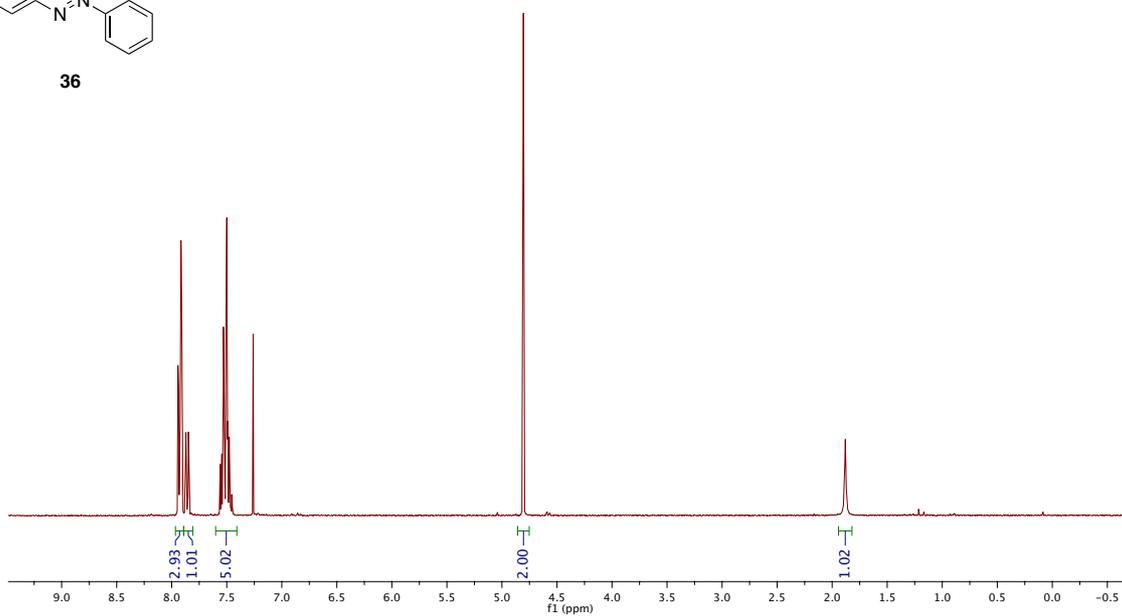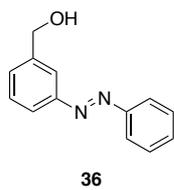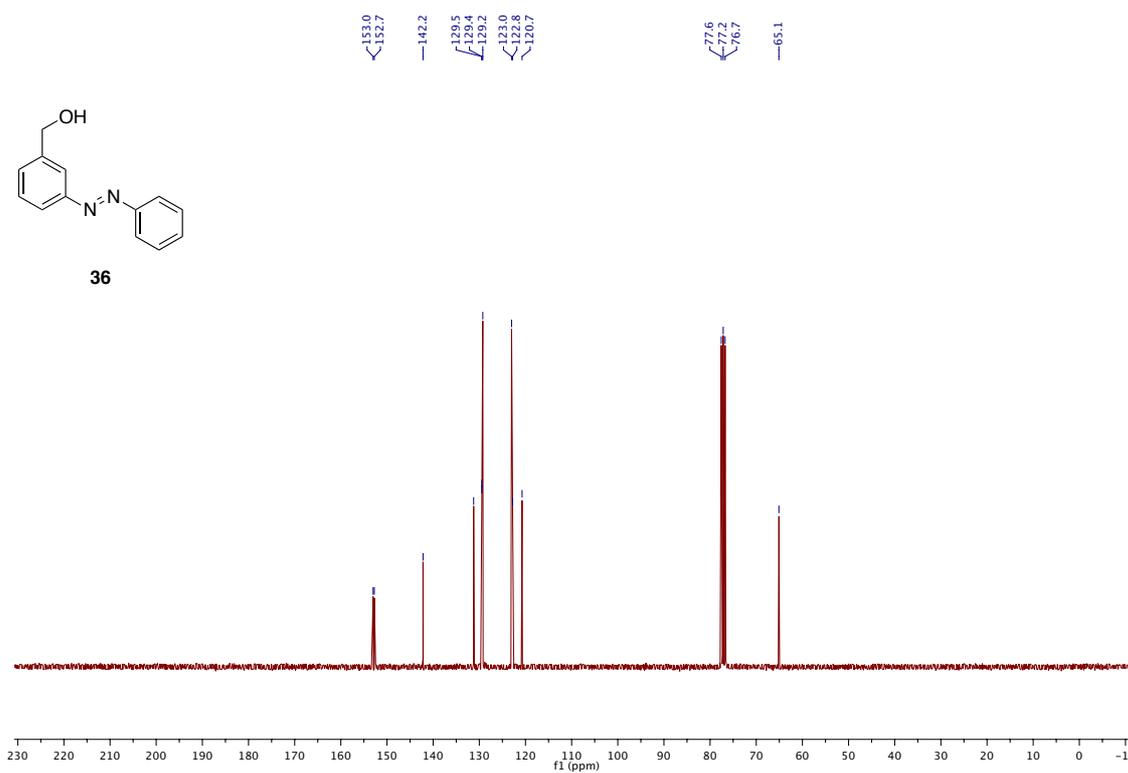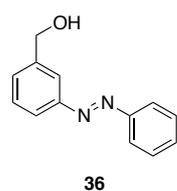
^{1}H NMR:

37

^{13}CNMR:

37

¹H NMR:

¹³CNMR:

^{1}H NMR:

39

^{13}CNMR:

39

172
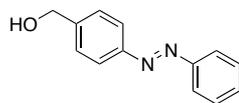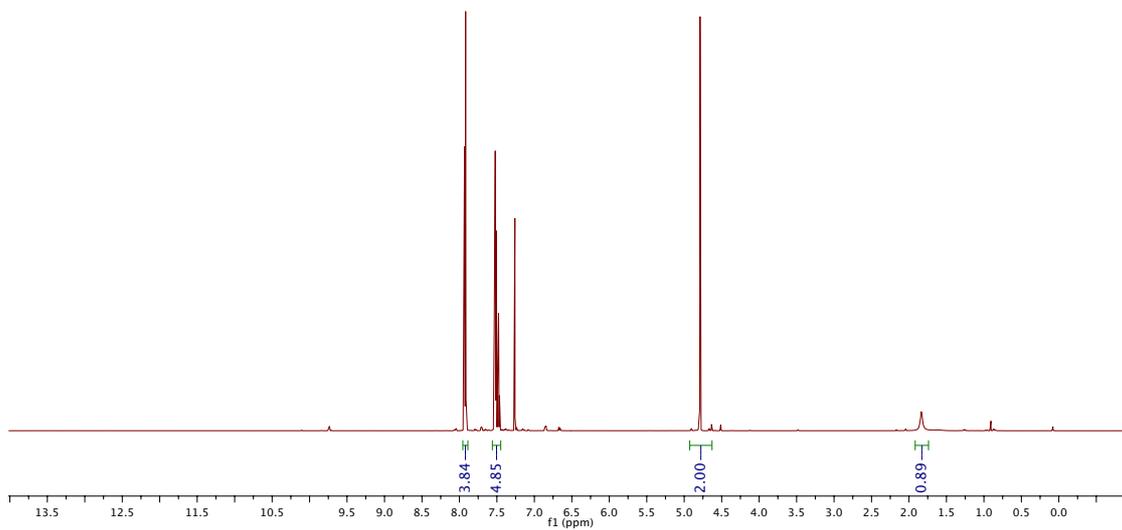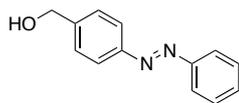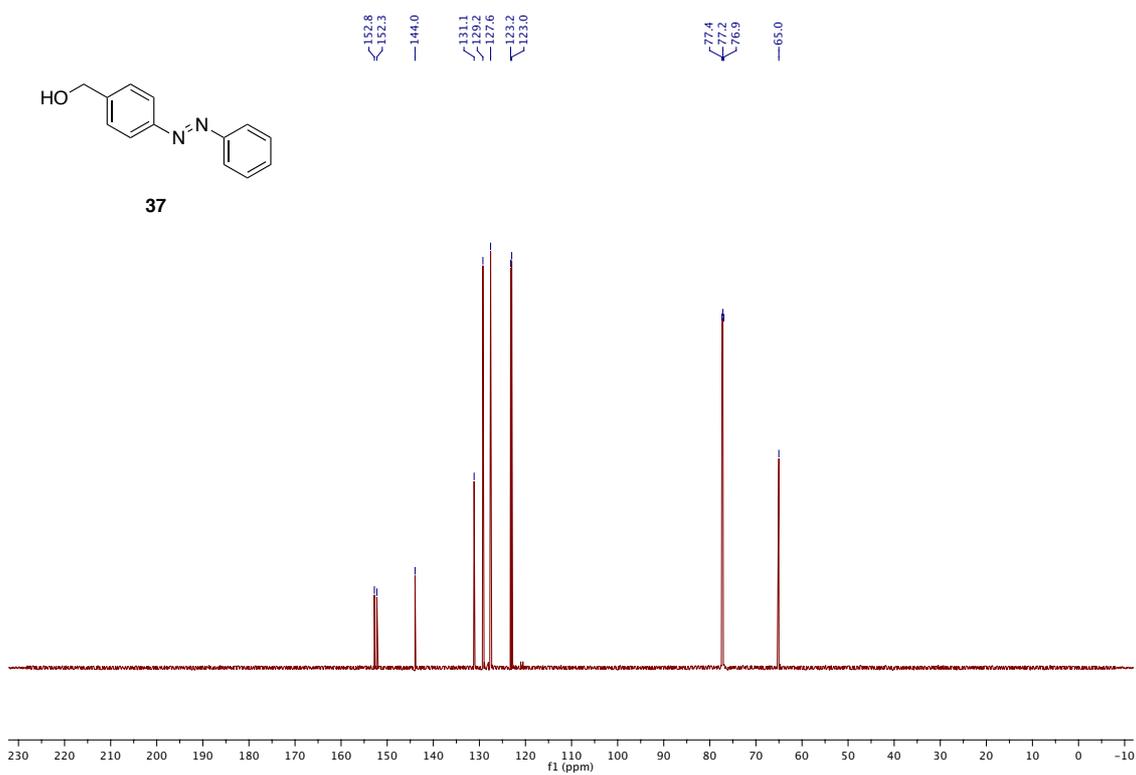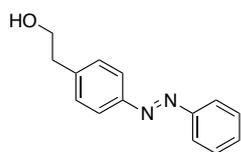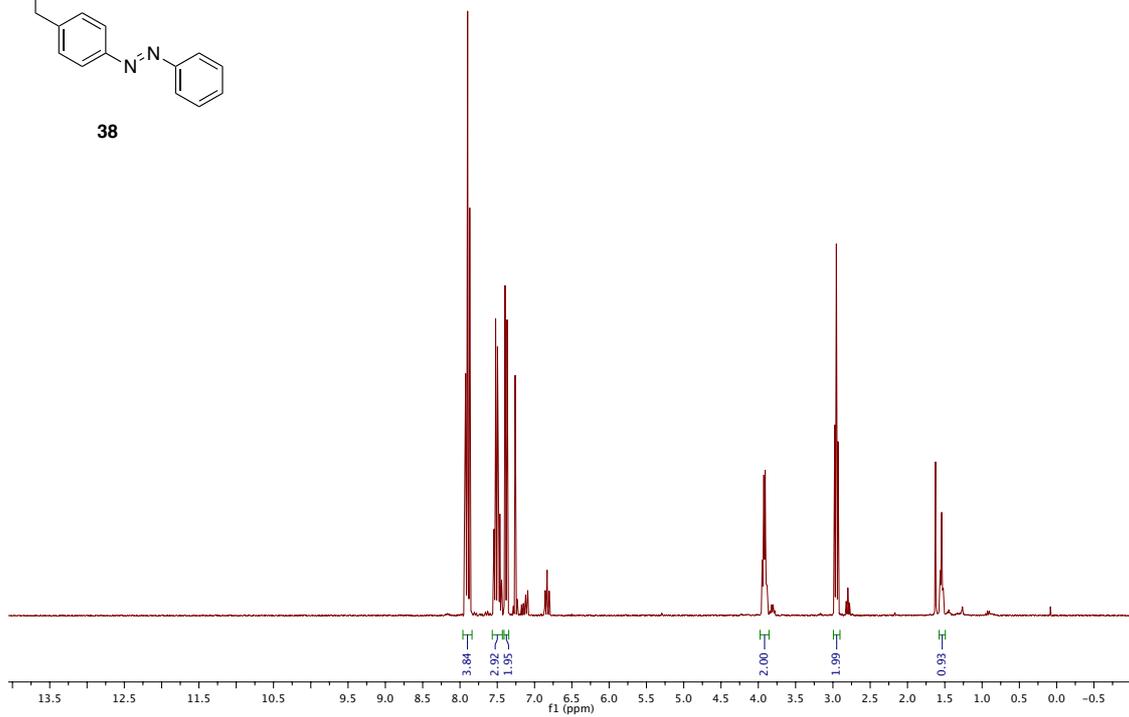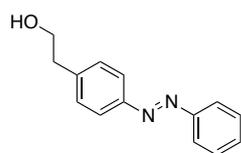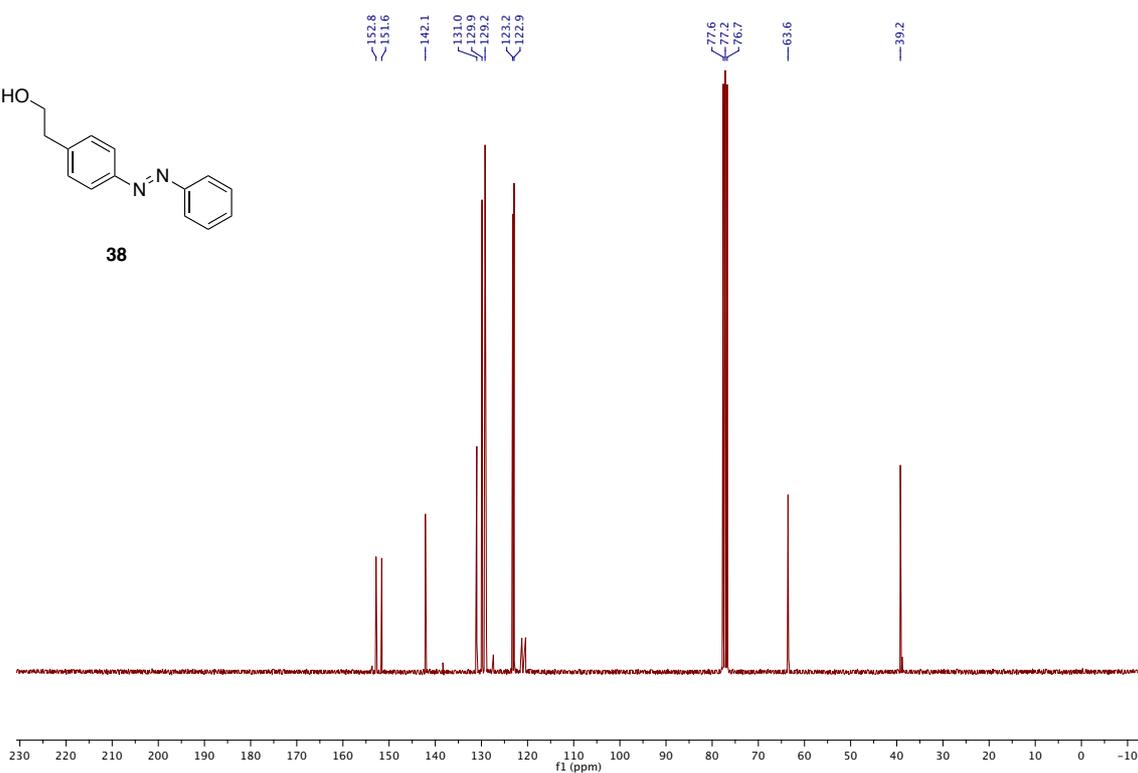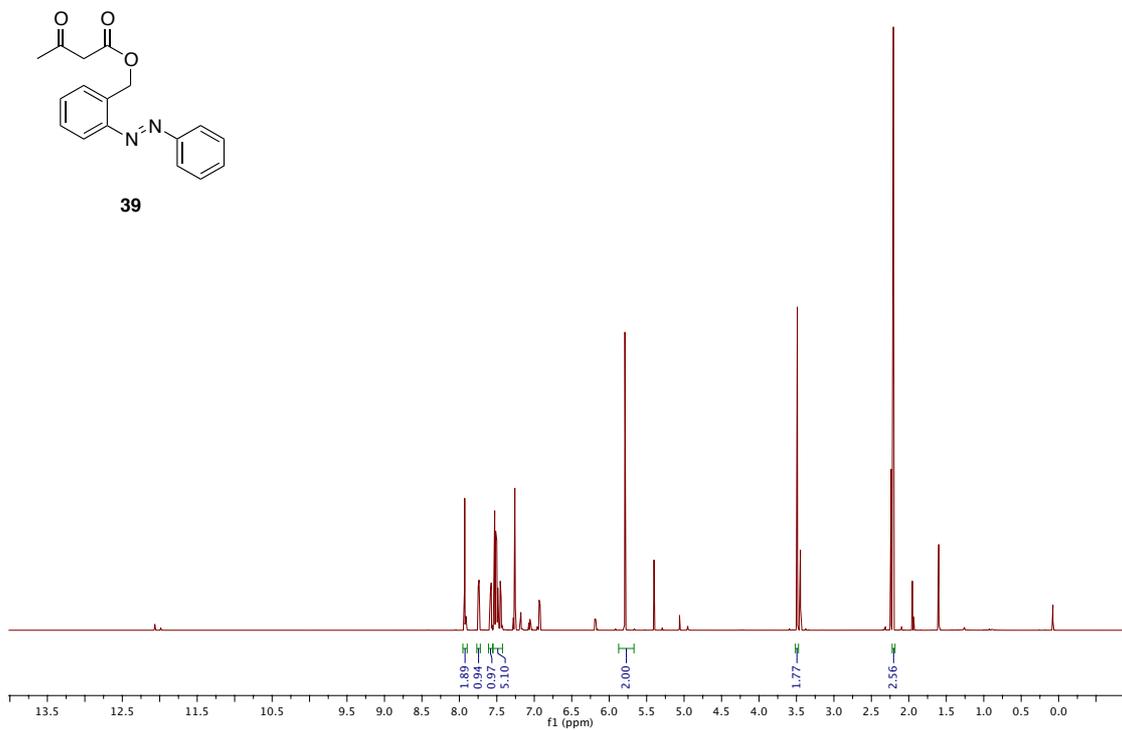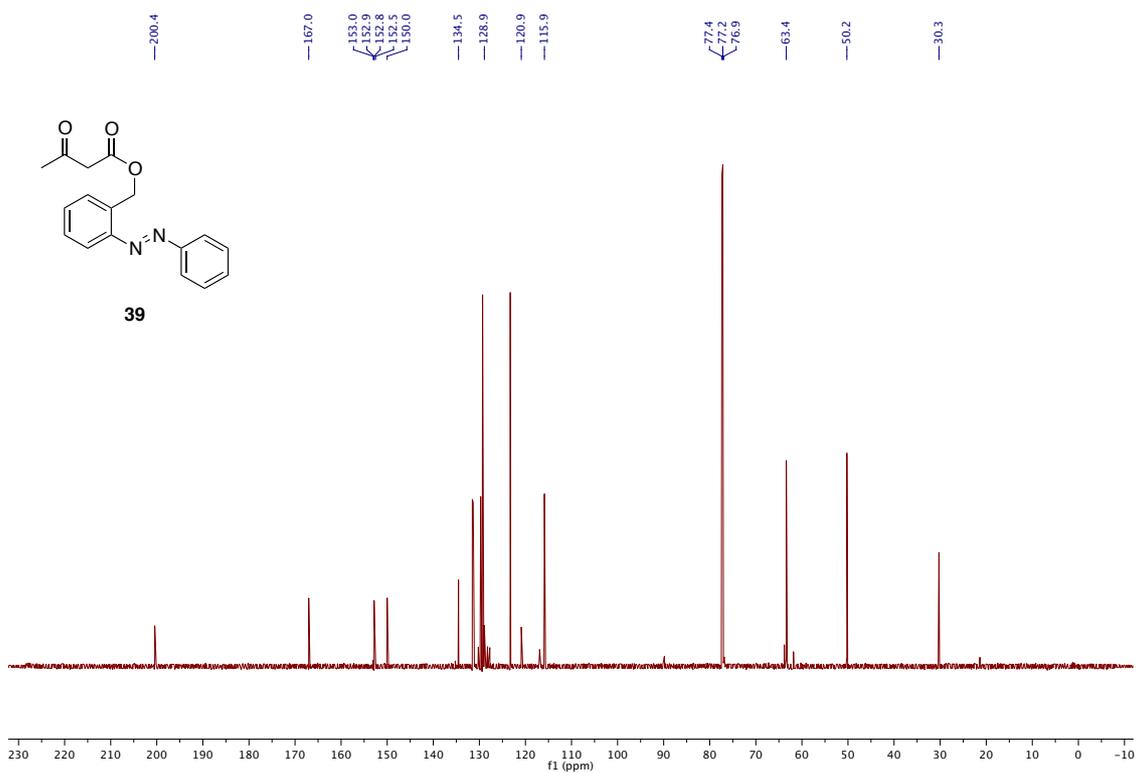
¹H NMR:

40

¹³CNMR:

40

173
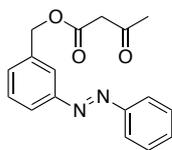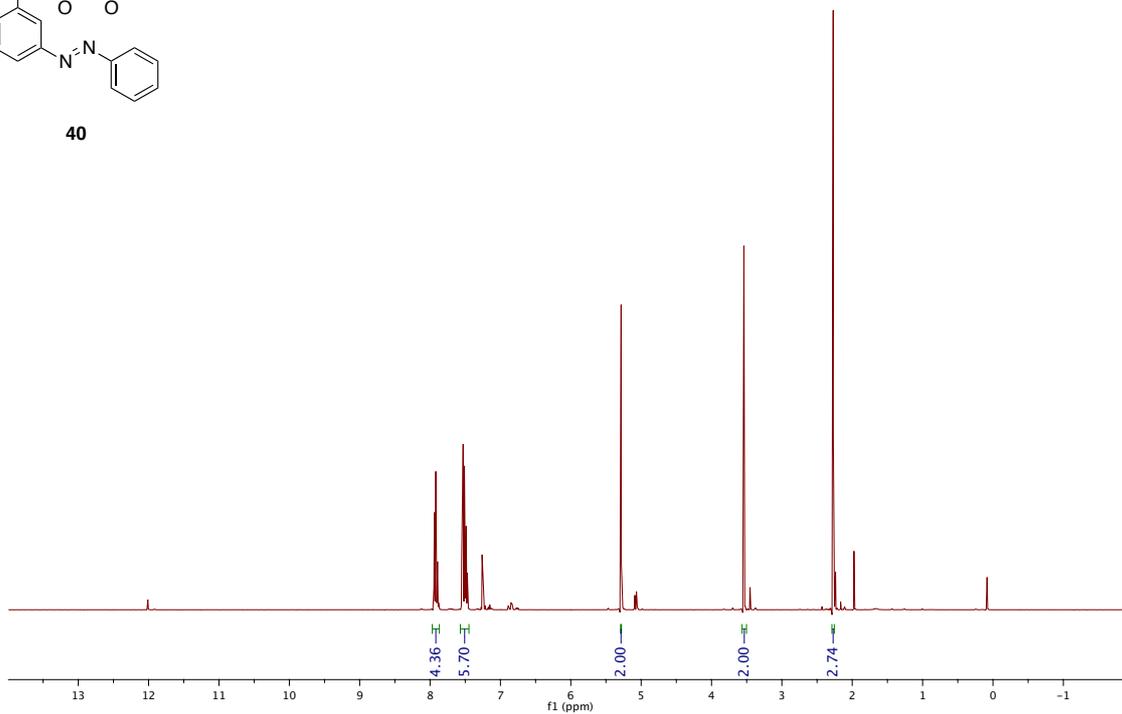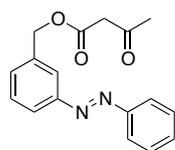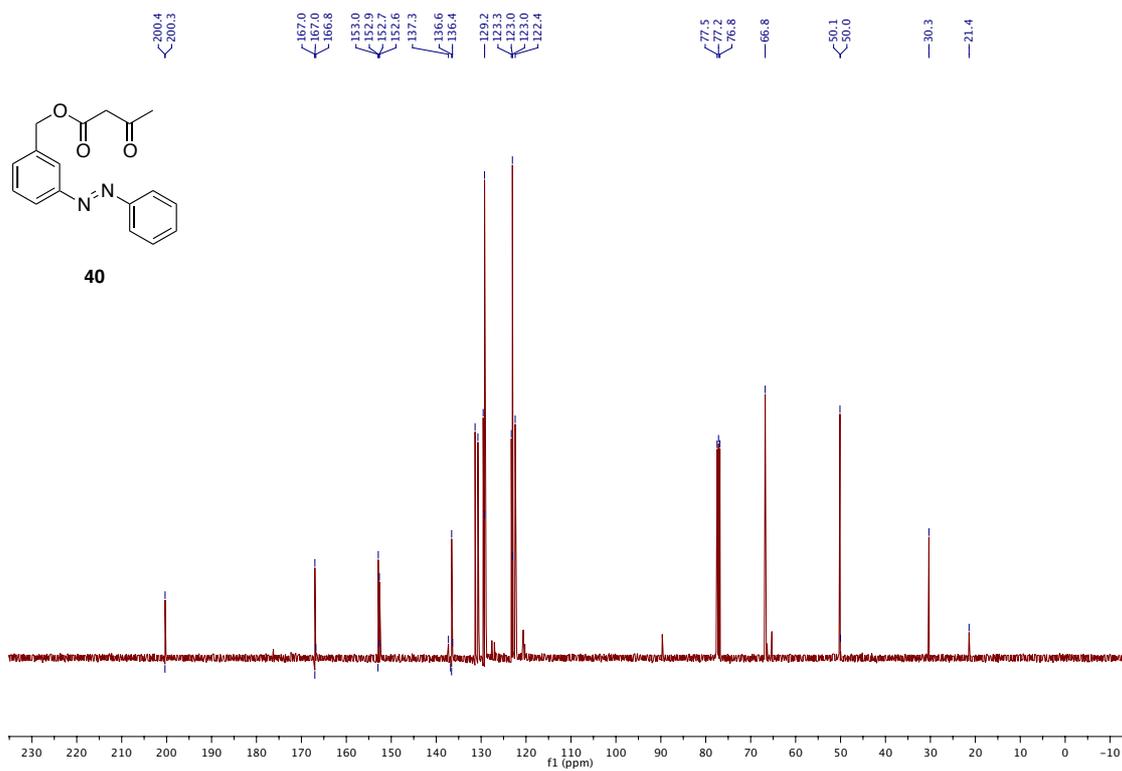
¹H NMR:

41

¹³CNMR:

41

174

¹H NMR:

42

¹³CNMR:

42
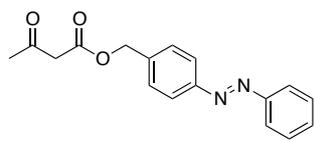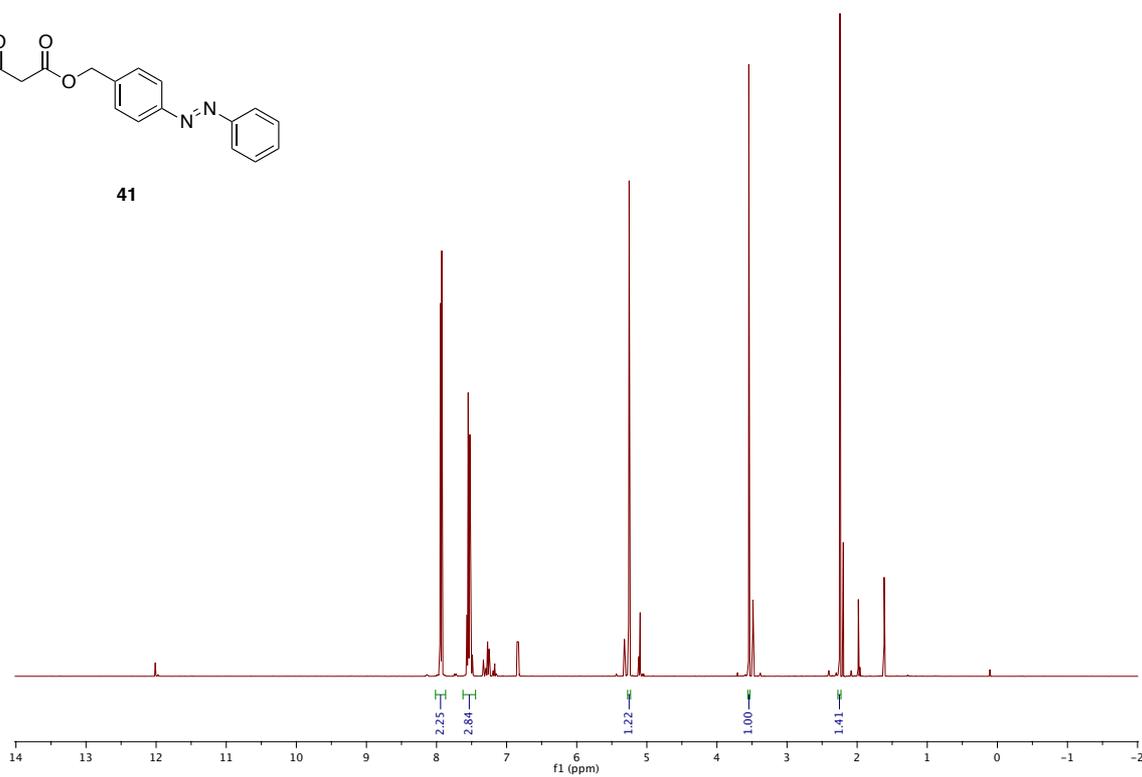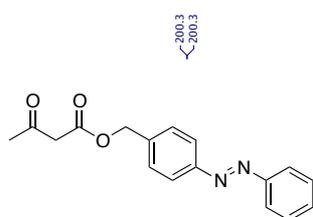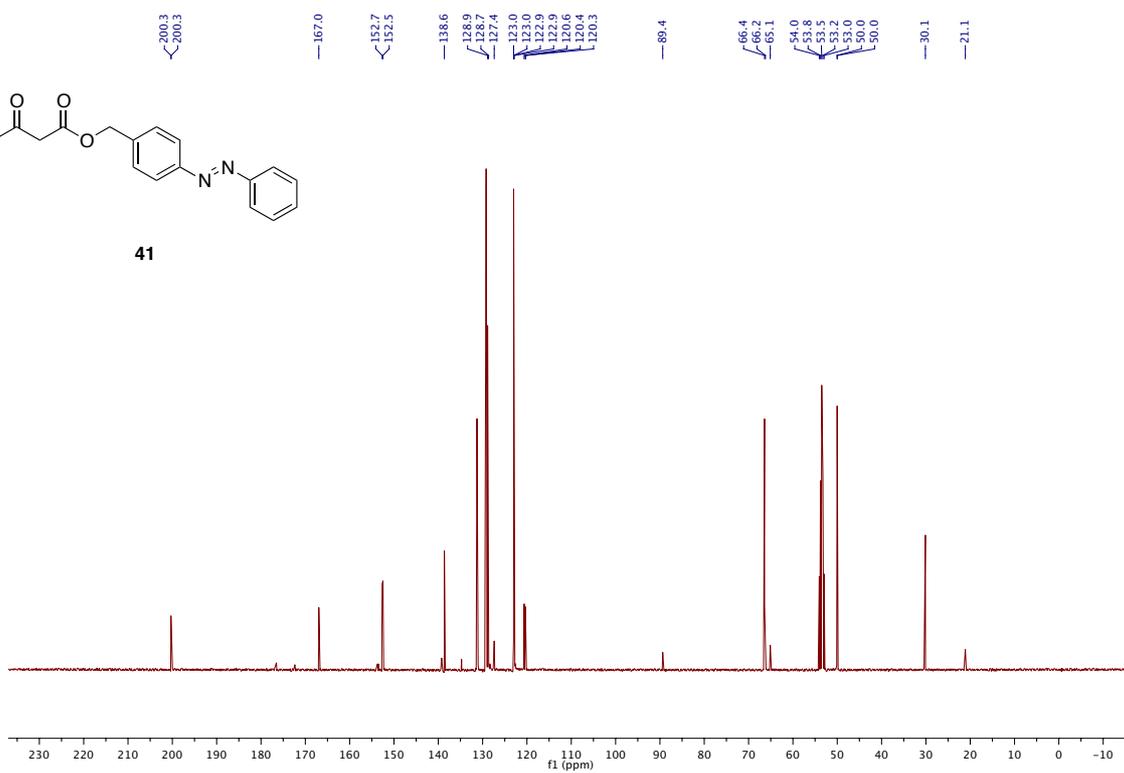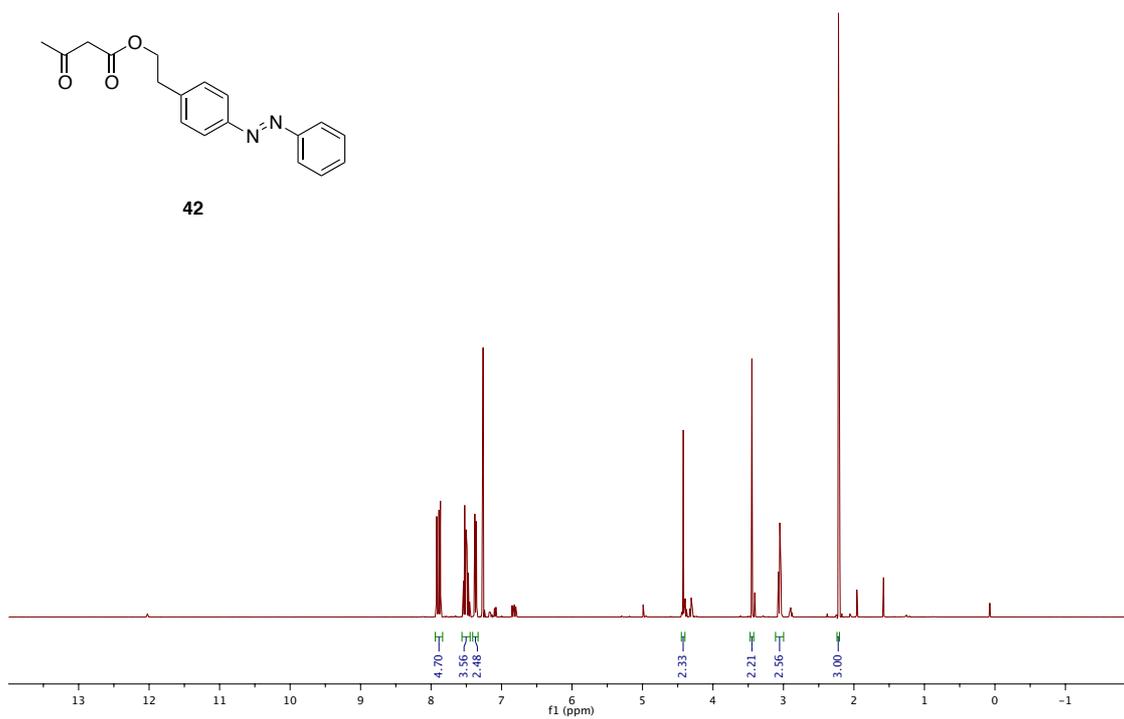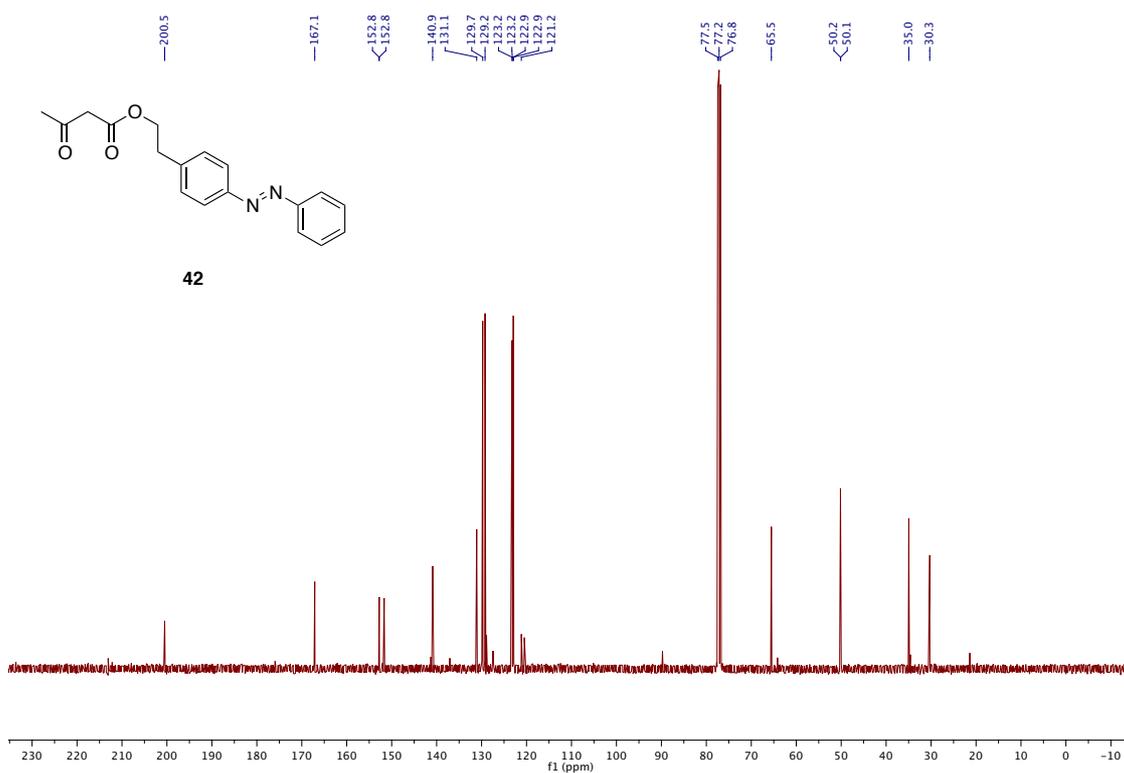
¹H NMR:

44

¹³CNMR:

44

¹H NMR:

¹³CNMR:

¹H NMR:

¹³CNMR:

178

¹H NMR:

48

¹³CNMR:

48

179

¹H NMR:

51

¹³CNMR:

51

180
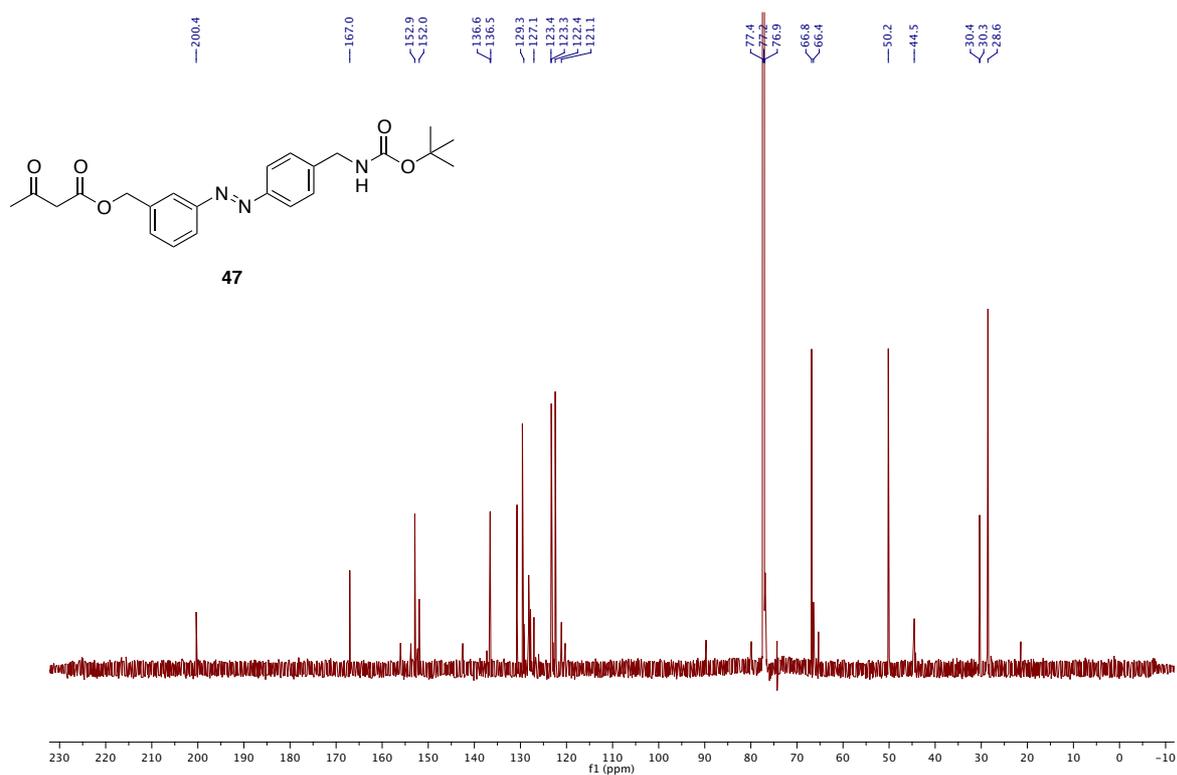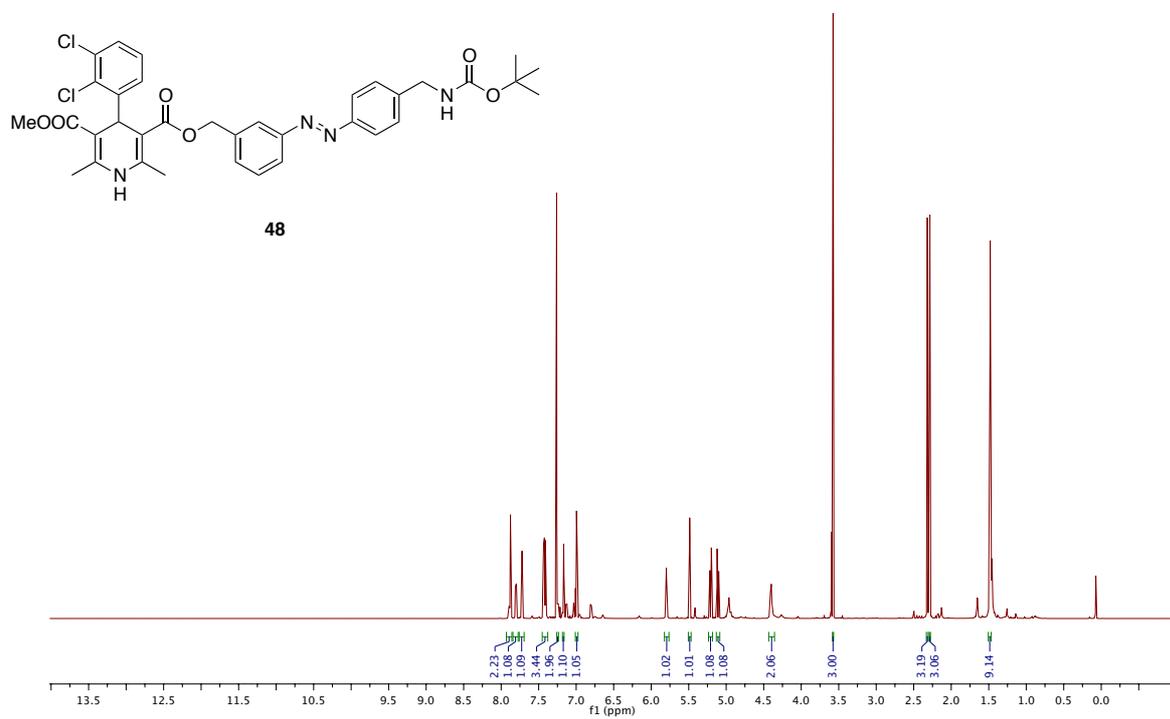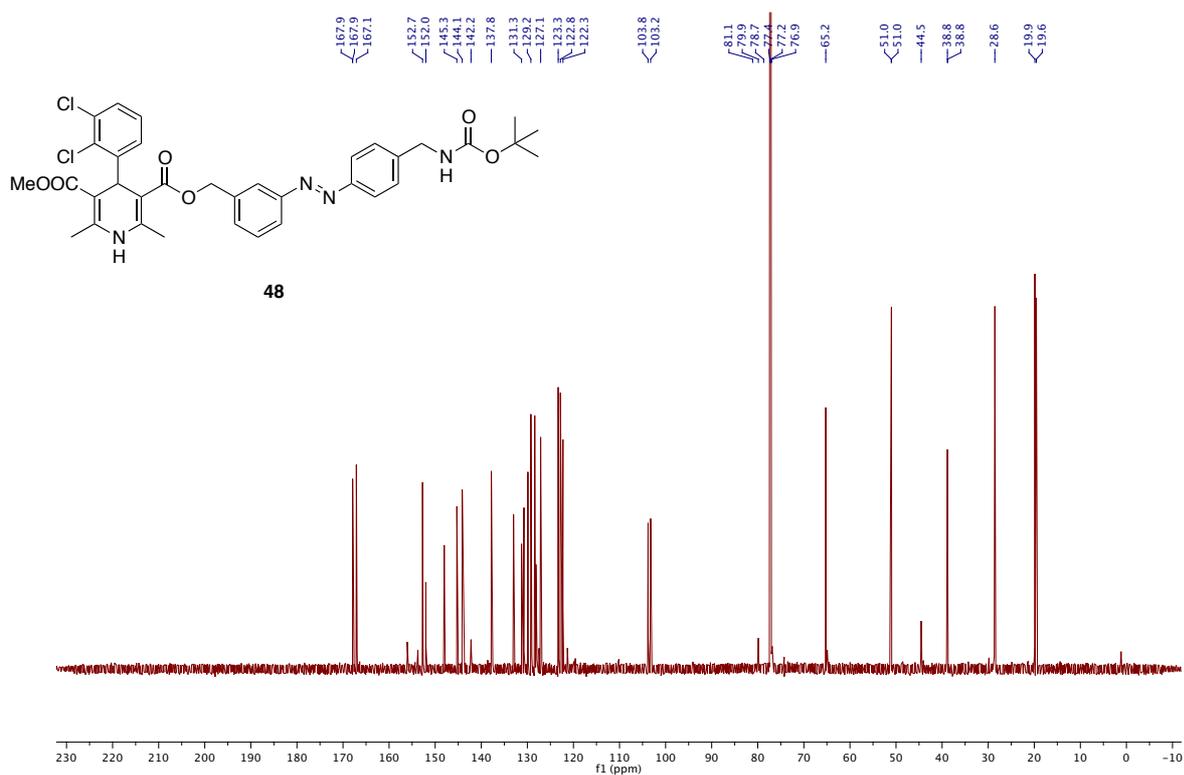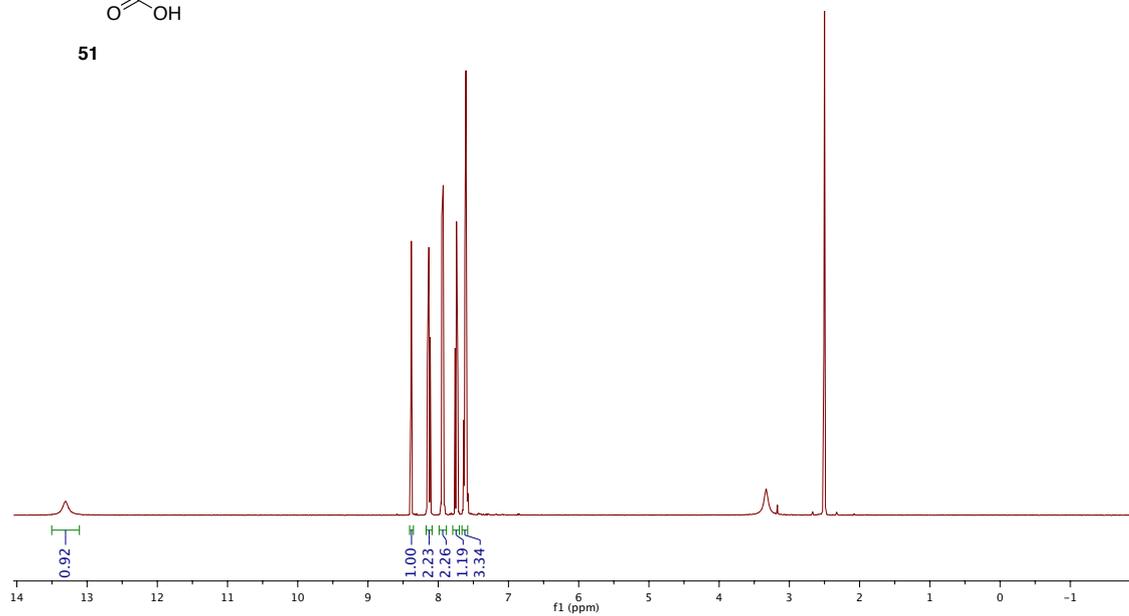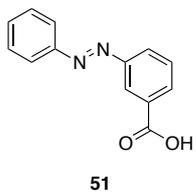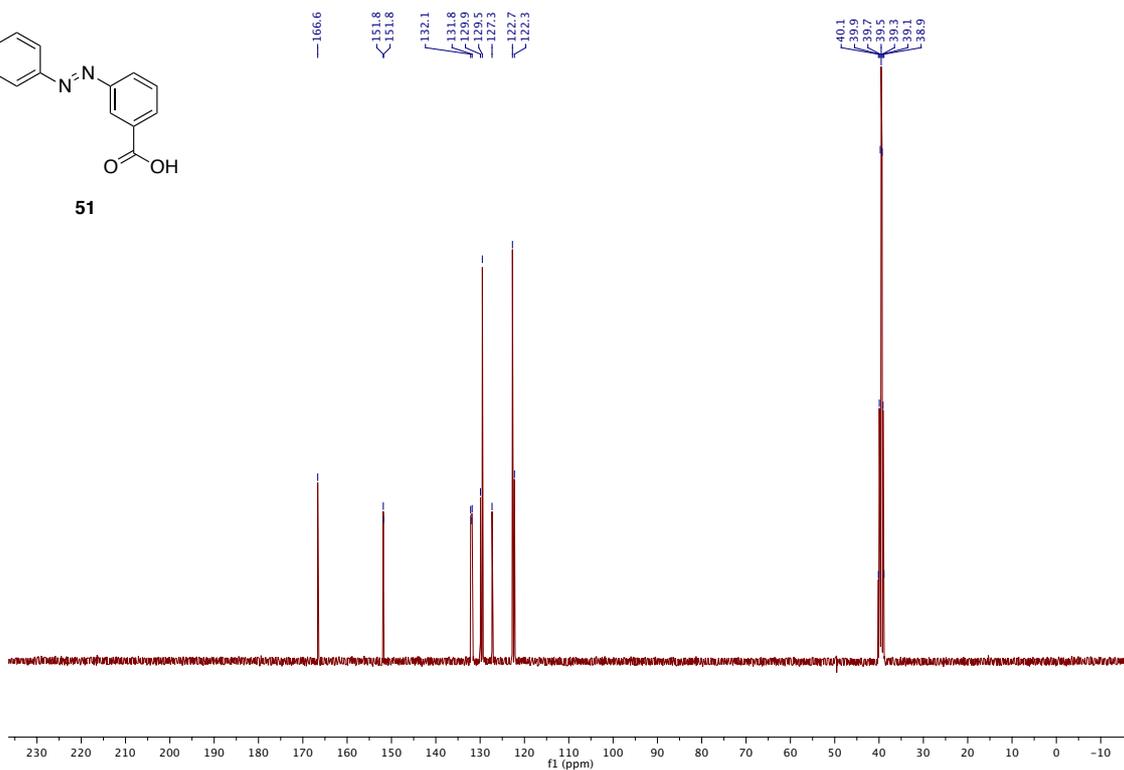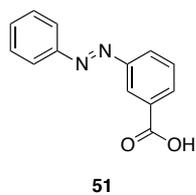
¹H NMR:
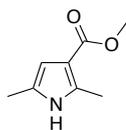
52
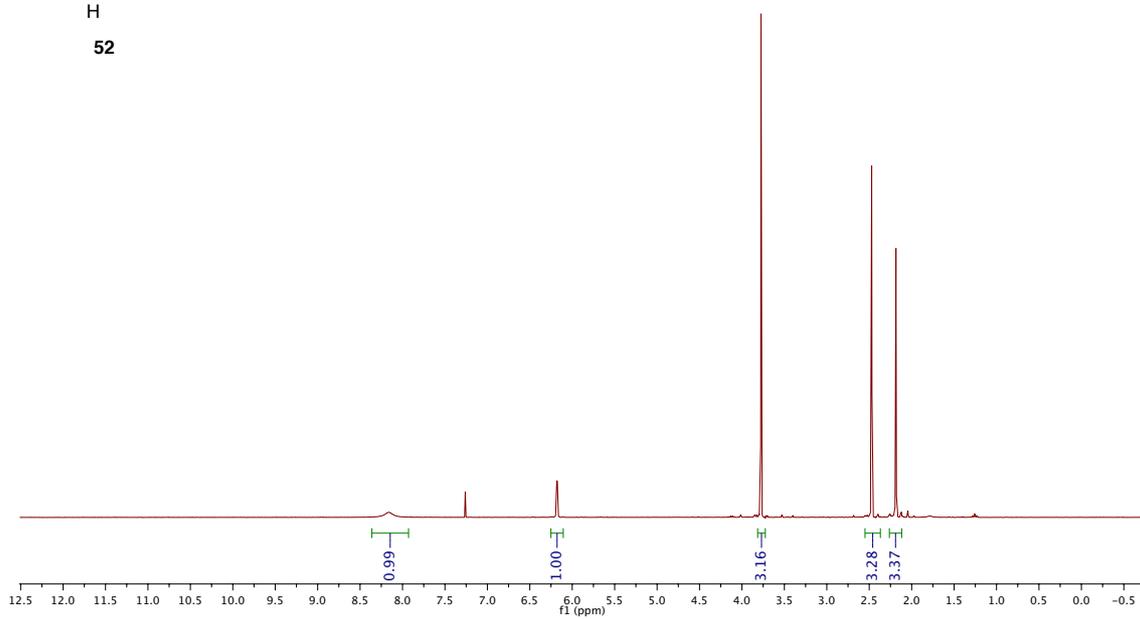
¹³CNMR:
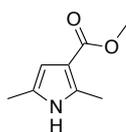
52
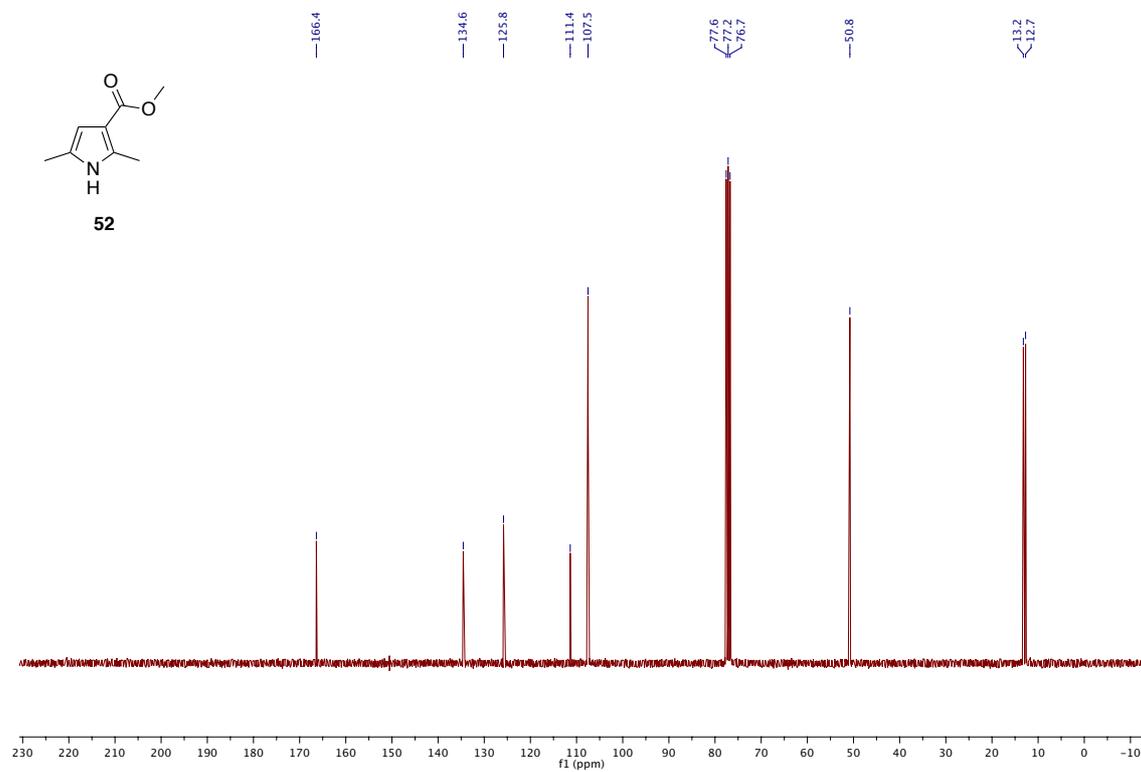
4.18) Appendix: UV/VIS spectra

Feazo-2 **25**

Feazo-3 **26**

Feazo-4 **27**

1) see footnote

Feazo-4I **28**

---
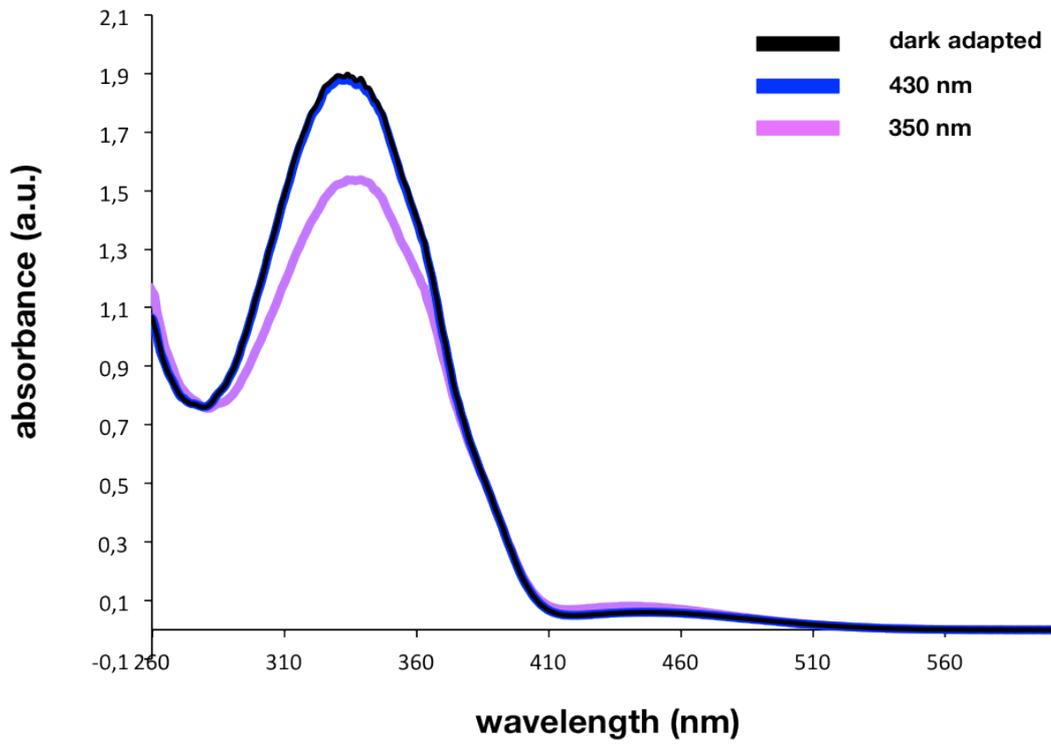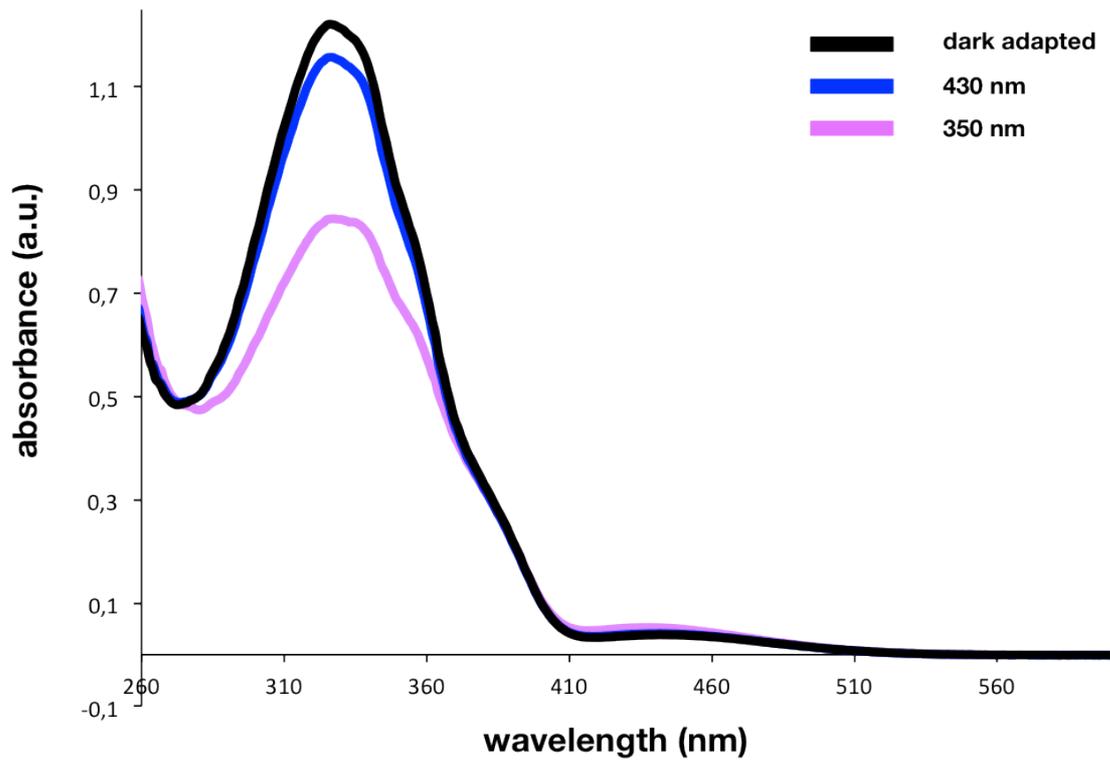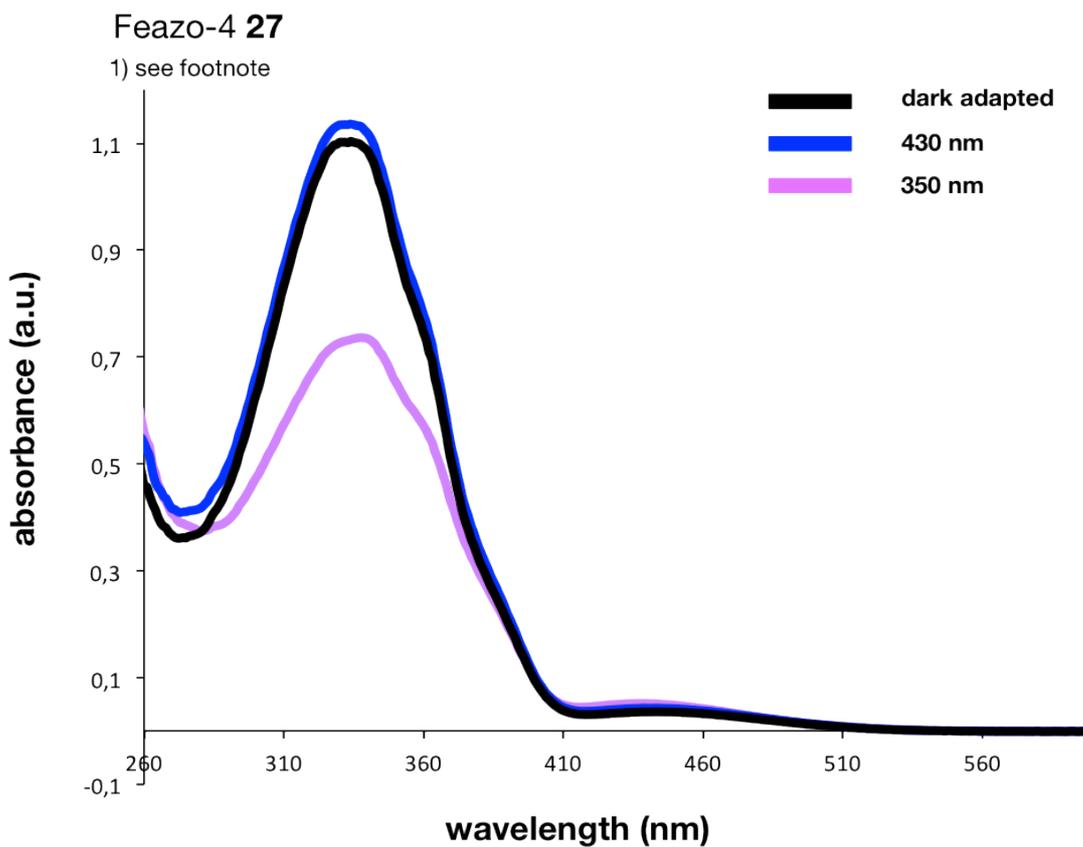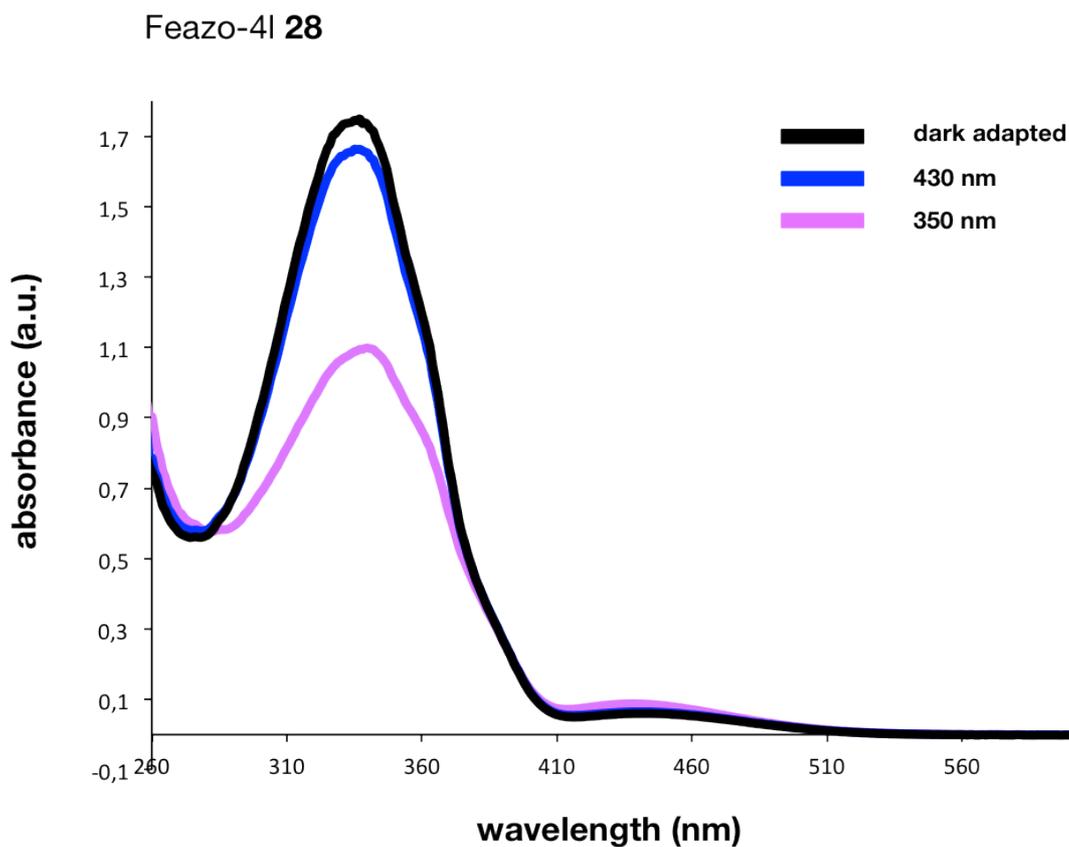
[1] The fact that the UV/VIS spectrum recorded under 430 nm light shows stronger absorbance than the UV/VIS spectrum recorded in the dark, might be due to a not completely established equilibrium between the *cis* and *trans* compound in the dark, before recording.

FPL-azo **30**
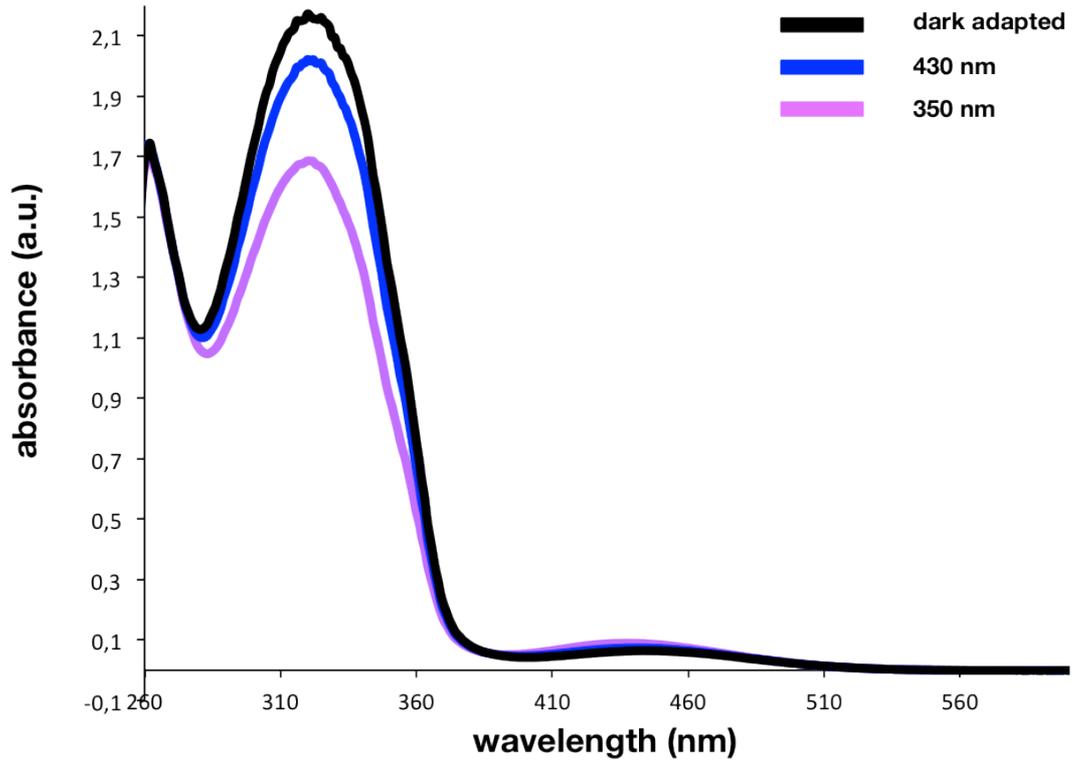
Feazo-3,4 **48**

5) Acknowledgements